Evaluation of Aniline formaldehyde condensate polymer in two different forms for heavy metals and anionic dyes adsorption from wastewater

A Thesis

Submitted in Partial

Fulfillment of the Requirements for the Degree of

Doctor of Philosophy

By

Praisy Terangpi

Centre for the Environment
Indian Institute of Technology Guwahati
Guwahati – 781039, Assam, India

November, 2018

Dedicated

To

Almighty GOD,

my family

and

my mentors

Centre for the Environment

Indian Institute of Technology Guwahati

India-781039

STATEMENT

I do hereby declare that the matter embedded in this thesis is the result of investigations conducted by me in the Centre for the Environment, Indian Institute of Technology Guwahati, Guwahati, Assam, India, under the supervision of Prof. S. Chakraborty, Department of Civil Engineering and Prof. M. Ray, Department of Chemistry, Indian Institute of Technology Guwahati, Guwahati, Assam, India.

In keeping with the general practice of reporting scientific observations, due acknowledgement has been made wherever the work described is based on the findings of other investigators.

November, 2018
I.I.T.Guwahati

Praisy Terangpi
Roll no. 11615204
Centre for the Environment
Indian Institute of Technology Guwahati
Guwahati-781039

Centre for the Environment

Indian Institute of Technology Guwahati

India-781039

CERTIFICATE

It is certified that the work contained in this thesis entitled **"Evaluation of Aniline formaldehyde condensate polymer in two different forms for heavy metals and anionic dyes adsorption from wastewater"** submitted by **Ms. Praisy Terangpi** (Roll no. 11615204) for the award of the degree of Doctor of Philosophy has been carried out in Centre for the Environment, Indian Institute of Technology Guwahati under our supervision and this work has not been submitted elsewhere for the award of any other degree or diploma and has reached the standard fulfilling the requirements for the award of the degree of Doctor of Philosophy in accordance with the regulations of the institute.

(Dr. S. Chakraborty)
Professor
Department of Civil Engineering
Indian Institute of Technology Guwahati
Guwahati-781039

(Dr. M. Ray)
Professor
Department of Chemistry
Indian Institute of Technology Guwahati
Guwahati-781039

November, 2018

Acknowledgements

I would like to take this opportunity to express my heart-felt gratitude to them, whose contribution has made this thesis possible.

In particular, the foremost appreciation goes to my supervisors Prof. S. Chakraborty and Prof. M. Ray for their valuable guidance throughout the research work. I thank them for their encouragement, guidance and moral support throughout, which enabled to pursue my academic skills under their precious guidance and expertise. I would like to acknowledge my sincere gratitude to my doctoral committee members, Prof. Sreedeep S., Prof. S. Gokhale and Dr. S. Dutta for their valuable suggestion and effort which made my thesis successful. I am also grateful to my present and former HOC's and Staffs of Centre for the Environment for providing me necessary facilities.

I would also like to extend my sincere thanks to the Department of Civil Engineering for permitting me to use the facilities of the laboratory. I would also like to convey my sincere thanks to the Head of Central Instruments Facility (CIF), IIT Guwahati, for providing me the analytical facilities of CIF.

I extend my sincere thanks to Mr. Partha Protim Bakal, Mr. Payodhar Pathak, Ms Jonali Saikia, Mr. Chitta Ranjan Medhi, and Mr. Rajiv Kumar Gogoi for their constant help and motivation.

I am indebted to the selfless help and co-operation from Anaiah G., Subrat, Sachin, Yagom, Ebria, Jhumrik and Dipti and also for their friendly support and helping nature during my stay in IITG.

I am also thankful to all the Research Scholars of Centre for the Environment for their constant help and motivation.

I would also like to express my gratitude to my beloved parents, brother for showering their love and care. Finally, I would like to thank my beloved husband Reswel for his constant support and encouragement right from the beginning of my research work. I owe everything to him, without his everlasting love, motivation and sacrifice, this thesis would have never been completed.

Thank you all.

Praisy Terangpi

Table of contents

List of Figures

List of Tables

Nomenclature

AFC : Aniline formaldehyde condensate

PANI : Polyaniline

C_o :Initial concentration ofadsorbate (mg/L or meq/L)

EDX : Energy dispersive X-ray

FTIR : Fourier transform infrared spectrometer

BET :Brunauer-Emmett-Teller

FESEM :Field emission scanning electron microscope

TGA :Thermo gravimetric analyzer

PSD : Pore size distribution

pH_{zpc} : Point of zero charge

R^2 : Coefficient of determination

RMSE : Root mean square error

SSE : Sum of squared error

ARE : Average relative error

χ^2 : Chi square error

q_t : Amount of adsorbate adsorbed per unit weight of adsorbent

C_{des} : Final concentration of adsorbate after desorption

rpm : Revolution per minute

T : Absolute temperature (K)

$\Delta H°$: Change in enthalpy

$\Delta S°$: Change in entropy

$\Delta G°$: Change in Gibb's free energy

WHO : World Health Organization

Q_o : Maximum monolayer coverage capacity (mg/g)

K_L : Langmuir isotherm constant (L/mg)

K_f : Freundlich adsorption capacity (mg/g)

A_T : Temkin isotherm binding constant (L/mg)

b_T : Temkin isotherm constant

K_{ad} : Dubinin-Radhuskevich isotherm constant (mol^2/kJ^2)

K_{HA} : Halsay isotherm constant

Q_{max} : Sips maximum adsorption capacity (mg/g)

Ks : Sips model isotherm constant

n : Sips model exponent

C.I. : Colour index number

M.W. : Molecular weight (g/mol)

λ_{max} : maximum wavelength (nm)

IUPAC : Internation Union of Pure and Applied Chemistry

BJH : Barrett-Joyner-Halenda

k_f : external mass transfer coefficient (m/min)

BIS : Bureau of Indian Standard

AAS : Atomic absorption spectroscopy

meq : Milliequivalent

ABSTRACT

Adsorption technique for wastewater treatment is considered to be the most economically feasible method. Various literatures reported the removal of dyes, heavy metals, etc., by adsorbents such as activated carbon, fly ash, fruit peels, polymeric adsorbents, clay materials, etc. Removal of metal ions and dyes by functionalized polymer has become an important option in the integrated approach to wastewater treatment. Functional groups, which are responsible for binding metal ions and dyes are amines, carboxylates, ethers etc. Amine groups have been found to be one of the most efficient functional groups for adsorption in which the mechanisms have generally been attributed to the formation of complexes between the amine groups present on the adsorbents and the adsorbates to be removed.

The objective of the thesis work was to investigate anionic dyes removal by two amine coated polymer – i) aniline formaldehyde coated silica gel (AFC-silica) and ii) short-chain polyaniline coated jute fiber (PANI-jute) and to synthesize a new supportless amine based polymer (modified-AFC) with detail characterization and study the removal conditions of heavy metals from very dilute solution. During the interaction with the anionic dyes both the polymers achieved maximum adsorption in acidic pH. Electrostatic attraction with protonated amine group and hydrophobic–hydrophobic interaction and hydrogen bonding were responsible for dye uptake besides which dye molecular weight was also found to play an important role. The supportless amine polymer (modified-AFC) was powdered mesoporous material with BET surface area was 6.88 m^2/g and average pore diameter of 10.46 nm. Batch adsorption experiments of Cr(VI) and Hg(II) in single system and Pb(II), Cu(II) and Cr(III) in multicomponent system were carried out from aqueous solution under various operating parameters. Ion exchange as well as redox interaction between chromate ion and protonated amine group of polymer was found to be the key factor for adsorption

of chromium. The residual concentration of total chromium (1.74 mg/L) from initial concentration 10 mg/L was found within the discharge limit (2mg/L) of wastewater which supports the adsorbent application in real wastewater. Similarly, it was observed that ion exchange between protonated amine group ($-NH_3^+$) and anionic species of mercury was the main removal mechanism. The adsorption experiment was also further carried out in multicomponent system comprising of three heavy metals – Pb(II), Cu(II) and Cr(III). Adsorption due to the coordination bond between metal ions and nitrogen present in amine ($-NH_2$) group of modified-AFC was the main factor for the removal of mixed metals. It was also observed that it followed the Hard and Soft acid base theory in single system whereas in binary and ternary system competitive adsorption between the metals was observed. Sips isotherm model fitted very well with the experimental data suggesting heterogeneous adsorption. In multicomponent system, chromium adsorption was highly affected by the presence of other ions either lead or copper or both.

Finally, the results obtained from this research work gave an insight view of an efficient amine based polymer with and without any supporting material as a high potential adsorbent to remove toxic anionic azo dyes and heavy metals both in single as well as multicomponent system from aqueous solution.

Keywords: Amine functional groups; AFC-silca; PANI-jute; Modified-AFC; Anionic azo dyes; Mesoporous; Protonated amine group; Sips isotherm.

CHAPTER 1

INTRODUCTION

1.1 Background

Rapid development of industrialization and population growth has led to the spread of wide range of contaminants in surface water as well as in ground water leading to very critical issue worldwide. Unfortunately, large range of industries such as printing, textile, dyestuff, paper, plastic, cosmetic and other products (Babae et al., 2017; Bayramoglu et al., 2017) discharge toxic pollutants into the water bodies causing serious environmental issues as small amount of dye adds color in water, which is aesthetically displeasing and affect the aquatic life cycle since it depletes the dissolved oxygen and reduces the sunlight penetration. Also, heavy metals contaminated water bodies has led to serious threat to aquatic living organisms and human life due to their tendency of accumulating in living organisms as well as being relatively toxic even in very low concentration. The water bodies are contaminated by heavy metals coming from anthropogenic sources from industries such as mining, electroplating, tanning, textile industry and agricultural plants that lack environment-friendly techniques and also from natural forces such as volcanoes, earthquakes or storms etc. (Abdelhadi et al., 2017; Kettum et al., 2018). It was only when the catastrophe of Minamata in 1952, that led public awareness on the toxicity of metals and its after effects. This prompted the regulation on the maximum permissible limit of toxic metals in drinking water and restrictions on the discharge of effluents into the waterbodies. Since then researchers have given more emphasis on the removal methods of these pollutants from wastewater to prevent the harmful effects on living organisms.

The various treatment processes involved in the removal methods are- adsorption, membrane separation, coagulation-flocculation, advanced oxidation, reverse osmosis etc., (Gogulothu et al., 2017; Yavari et al., 2016; Zhang et al., 2015). Amongst all the method, adsorption is considered to be the most simple and convenient method for the removal of the pollutants from wastewater. Activated carbon is one of the most widely used adsorbents but fails to be cost effective due to its costly regeneration. In order to overcome the mentioned drawbacks, research works have been focused on the preparation of adsorbent in terms of feasibility, cost effectiveness and easy availability. Most of the adsorbents are easily available and low-cost but they have some disadvantages such as heat resistance and relatively limited adsorption capacity. Thus, researchers are interested to focus on modification (treatment) of adsorbents to improve the performance.

In the recent years, polymeric adsorbents have gain significant recognition as a potential alternative to activated carbon due to its vast surface area, perfectly mechanical rigidity, adjustable surface chemistry, pore size distribution and feasible regeneration under mild conditions. Polymeric adsorbents can effectively trap many of the ubiquitous organic pollutants namely phenolic compounds, organic acids, aromatic or polyaromatic hydrocarbons, alkanes and their derivatives (Chanda and Rempel, 1995; Kumar et al., 2007a,b; Elwakeel et al., 2012; Ahmad and Kumar, 2010; etc). Adsorption capacity of a polymeric adsorbent toward pollutants can be improved using monomers, which have functional groups such as amino group, due to the specific interaction of functional groups bound to the polymeric matrixes with the target pollutants.

Previous research work found out the successful application of amine based polymer in the removal of heavy metals from aqueous solution (Kumar et al., 2007a,b; Kumar et al., 2008; Kumar et al., 2009). The adsorbents named – aniline formaldehyde condensate coated on silica gel (AFC-silica) and short chain polyaniline coated onto jute fiber (PANI-jute) were synthesized, and

employed for the removal of trivalent and hexavalent chromium and copper. Kumar et al., 2007a,b, 2008, 2009 stated that the above adsorbents were found to be very effective in the adsorption of hexavalent chromium (500 times more toxic than trivalent chromium) from concentrated aqueous solution in acidic medium where the main mechanism responsible for adsorption of hexavalent chromium was anion exchange between the cationic form of the polymer functional groups (NH_3^+) and anionic form of chromium $HCrO_4^-$ by both the above stated polymers (AFC-silica and PANI-jute).

In the present research work emphasis was given to investigate the application of anionic azo dyes removal by amine coated polymers and removal heavy metals from aqueous solution by a supportless amine based polymer and also to improve the properties of the polymer. The entire research work in the thesis has been divided into seven chapters. Chapter 1 consists of an introduction to the research work carried out with reviews of up-date literature on heavy metals and anionic azo dyes. Thorough survey was carried out on its definition, source, toxicity, available treatment techniques and its merits, demerits, complete details were analyzed on the literature findings, and scope of the research work was developed. Chapter 2 presents the elaborative adsorption batch studies carried out during the adsorption of anionic dyes onto amine based polymer coated adsorbents (AFC coated silica gel and Polyaniline coated jute fiber). Chapter 3 provides the details of the preliminary synthesis and performance evaluation test of the new polymers to improve the efficiency properties by synthesizing without using any support material. After optimization, the polymer (modified-AFC) with the best efficiency properties was considered for further studies. Chapter 4 presents the detailed investigation carried out on the adsorption of chromium onto the modified–AFC polymer adsorbent from aqueous solution. Similarly, chapter 5 consists of a detailed investigation on the removal mercury another toxic

heavy metal in dilute concentration with modified-AFC polymer adsorbent. Chapter 6 also consists of results and discussion for removal of heavy metals – Pb(II), Cu(II) and Cr(III) in single and multicomponent systems from aqueous solution. Chapter 7 presents the summary of the thesis work and the conclusion drawn from the research work. Future scope of the present work was also provided in the chapter.

1.2 Literature review

1.2.1 Dye pollutants

Dye is a colored organic compound, which have a property of imparting color to any material of which it becomes an integral part. Dye molecules comprise of two key components: the chromophores - responsible for producing the color, and the auxochromes - which can not only supplement the chromophore but also render molecule soluble in water and give enhanced affinity (to attach) toward the fibers. Thousands of dyes are used in industries such as textile, paper, rubber, plastics, paints, printing, inks, art and craft, leather, food, medical and cosmetics. It is estimated that around 10–15% of dyes are wasted into the environment upon completion of their use in the dyeing unit. One of the most important industries using dyes is the textile industry, which generates a strongly colored wastewater, typically with a concentration in the range of 10–200 mg/L (Moussavi et al., 2009). Generally, the volume of discharged wastewater from each step of a textile operation is approximately at a high rate of between 40 L/kg and 65 L/kg of the product (Mezohegyi et al., 2012). Azo dyes are the most widely used dyes that accounts 65-70 % of the total dyes produced and are used in industries because of their ease and cost effectiveness in synthesis compared to natural dyes and constitute the largest group over thousands of commercial dyestuffs and are commonly used for textiles dyeing, paper printing, food and cosmetic coloring (Qureshi et al., 2017; Long et al., 2017; Ayati et al., 2016; Sarvajitha et al., 2018).

1.2.1.1 Types of dyes

The classification of dyes are based on many factors such as- the chemical structure system, different applications, particle charge, dissolution in water and its origin. But the complexities of the color nomenclature from their chemical structure system led to the ease in classification of dyes based on their particle charge upon dissolution in water such as - i) cationic (all basic dyes), ii) anionic (direct, acid and reactive dyes) and non-ionic (dispersed dyes) (Salleh et al., 2011; Yagub et al., 2014). Table 1.1 represents the different types of dyes along with their applications.

Table 1.1: Application of different type of dyes

Dyes	Description	Applications
Acid	Water-soluble anionic compounds	Wool, Silk, Nylon (Polyamide) Polyurethane fibers
Basic	Water-soluble, applied in weakly acidic dyebaths; very bright dyes	Polyester, Wool, Silk Mod-acrylic nylon
Direct	Water-soluble, anionic compounds; can be applied directly to cellulosics without mordants (or metals like chromium and copper)	Cotton, Wool, Flax silk Leather in (alkaline or netural bath)
Disperse	Not water-soluble	Polyamide fibers, Polyesters Nylon, polyacrylonitriles
Reactive	Water-soluble, anionic compounds; largest dye class	Cellulosic fibers Wool Polyamide
Sulfur	Organic compounds containing sulfur or sodium sulfide	Cellulose fibers, staple fibers and yarn
Vat	Water-insoluble; oldest dyes; more chemically complex	Wool Flax, Wool Rayon fibers

Source: Seow et al., 2016; Yagub et al., 2014; Dawood et al., 2014

Besides these classification there are other classes like azo groups, fluorescent brighteners, etc. and more than 100,000 commercial dyes are estimated to be known with an annual production of more than 7×10^5 tonnes per year. Amongst all azo derivatives are the major class of dyes that are used in the industry today.

1.2.1.2 Sources and toxicity of dyes

The source of dyes can be obtained from natural resources such as derivatives from plants, invertebrates or minerals. The majority of natural dyes comes from vegetable dyes derived from plants sources such as leaves (Mongkholrattanasit et al., 2010; Mongkholrattanasit et al., 2013), bark (Ali et al., 2007; Naz et al., 2011), berries, roots, wood, etc., extracts from eucalyptus processing (Shahid-ul-Islam et al., 2013). But at present synthetic dyes are widely used compared to natural dyes due to economical reasons, property of having color fastness, wide variety of color and greater reproducibility (Bulut and Akar, 2012; Leitner et al., 2012). The synthetic dyes, can be named according to the chemical structure of their particular chromophoric group. Synthetic dyes has the potential to generate toxic effluents that can adversely affect the aquatic ecosystem and causing serious health effects towards human being carcinogenic, mutagenic, toxicological properties, dermatitis etc. (Bulut and Akar, 2012; Malinauskiene et al., 2012; Shahid-ul-Islam et al., 2013; Sinha et al., 2012). Amongst the synthetic dyes, acid dyes are anionic dyes that are water soluble and consists a negative ion. Anionic dyes removal is the most challenging task as they produced very bright colors in water and show acidic properties. But amongst them azo dyes are the most toxic because of the presence of toxic amines in the effluent and can be carcinogenic upon degradation. Basic dyes too are high brilliance colors and can be visible even at lower concentration. The complex dyes are generally chromium based, which is carcinogenic in nature. Similarly, anthraquinone based dyes are most resistant to degradation and remains color for a large

time in effluents. Therefore focuses on specific removal methods and technologies of dyes from wastewater streams are of significant importance.

Dye is one of the important class of pollutant. Once they enter the water it is no longer good and sometimes difficult to treat as the dyes have a synthetic origin and a complex molecular structure which makes them more stable and difficult to be biodegraded (Rai et al., 2005). Low concentration of dye (less than 1 mg/L for some dyes) in water is easily visible and can reduce photosynthetic activities in aquatic environments by preventing the penetration of light and oxygen (Crini, 2006). Since dyes are stable, recalcitrant, colorant, and even potentially carcinogenic and toxic, their release into the environment poses serious environmental aesthetical and health problems. Thus, industrial dye-laden effluents are an increasingly major concern and need to be effectively treated before being discharged into the environment in order to prevent these potential hazards.

1.2.1.3 Guidelines

Over 92% of some 4461 commercially available dyes tested in ETDA (Ecological and Toxicological Association of the dyestuff) survey had LD_{50} (is a standard measurement of acute toxicity that is stated in milligrams (mg) of pesticide per kilogram (kg) of body weight) values greater than 2000 mg/kg. Based on the ETDA tests made for 3000 commonly used dyes in 27 cases, the registered LC_{50} (Lethal Dose50) values were of the order 0.05 mg/L (Wawrzkiewicz et al., 2017).The new drinking water prescribed by the Bureau of Indian Standards (BIS) set the color standards at five color units as the desirable limit and extended to 15 color units as the desirable limit in the absence of alternate source. With the permissible limit of dye discharge effluent being regulated the problem lies in the removal of dyes from aqueous solution as it seems a very difficult

one. Thus there is a need to optimize the removal techniques used for dye removal which meets with the permissible limit.

1.2.1.4 Removal techniques

Till date various removal techniques were used such as ion exchange, precipitation, biodegradation, membrane technology, coagulation, oxidation or ozonation, flocculation and adsorption (Abdi et al., 2014; de Luna et al., 2017; Umukoro et al., 2017; Salam et al., 2018). Advantages and disadvantages of dye removal are listed in Table 1.2. The removal methods have been categorized in three categories, which are chemical, biological, physical and acoustical, radiation, and electrical processes.

Table 1.2: Advantages and disadvantages of dye removal methods

Removal methods	Advantages	Disadvantages	References
Oxidative process	Ease of application	(H_2O_2) agent needs to be activated by some means	Hassaan et al., 2017
H_2O_2 + Fe(II) salts (Fenton's reagent)	Suitable chemical means	Sludge generation	Ertugay et al., 2017 Kuo W, 1992 Barbusiński et al., 2003
Ozonation	Applied in its gaseous state and no increase in the volume of wastewater and sludge	Short half-life (20 min)	Wijannarong et al., 2013 Muthukumar et al., 2004
Sodium hypochlorite (NaOCl)	Initiates and accelerates azo-bond cleavage	Release of aromatic amines	Thasilu et al., 2016
Electrochemical destruction	No consumption of chemicals and no sludge buildup	Relatively high flow rates affects dye removal	Singh et al., 2016 Kariyajjanavar et al., 2011
Photochemical	No sludge production	Formation of by-products	Rahmani et al., 2012
Decolourisation by white-rot fungi	White-rot fungi are able to degrade dyes using enzymes	Enzyme production has also been shown to be unreliable	Kirby et al., 2000 Anastasi et al., 2011
Other microbial cultures (mixed bacterial)	Decolorised in 24–30 h	Under aerobic conditions azo dyes are not readily metabolised	Cetin et al., 2006 Przystaś et al., 2017
Adsorption by living/dead microbial biomass	Specific dyes have a particular affinity for binding with microbial species	Not effective for all dyes	Ali et al., 2012 Archna et al., 2012
Anaerobic textile–dye bioremediation systems	Allows azo and other water-soluble dyes to be decolorised	Anaerobic breakdown yields methane and hydrogen sulphide	Buthelezi et al., 2012 Ghosh et al., 2017
Adsorption by activated carbon	Good removal of wide variety of dyes	Very expensive	Ferreira et al., 2017 Giannakoudakis et al., 2016
Membrane filtration	Removes all dye types	Concentrated sludge production, expensive	Mansourpanah et al., 2017
Ion exchange	Regeneration: no adsorbent loss	Not effective for all dyes	Saruchi et al., 2016
Irradiation	Effective oxidation at lab scale	Requires a lot of dissolved O_2	Rehman Bhuiyan et al., 2015
Electrokinetic coagulation	Economically feasible	High sludge production	Pirkarami et al., 2017

1.2.1.4.1 Chemical methods

The most common method of decolorizing is by chemical treatment. Hydrogen peroxide (H_2O_2) is used as the oxidizing agent for chemical-oxidation of dyes by oxidizing the aromatic rings present in the dye molecule thereby removing the dye molecules. Fentons reagent is also another suitable chemical means of treating wastewaters which are resistant to biological treatment or is poisonous to live biomass (Slokar and LeMarechal, 1998; Son et al., 2018; Babaei et al., 2017; Sohrabi et al., 2017). Ozone is a strong oxidizing gas and it reacts with inorganic and organic compounds directly or indirectly by the formation of hydroxyl radicals. It preferentially oxidizes electronrich molecules containing carbon–carbon double bonds and aromatics.The ozone treatment splits the long-chain compounds making them biodegradable. Ozonation is used to decolourise dyes or peroxidation to enhance the biodegradability or to reduce inert COD fractions and toxicity removal and post treatment of textile industry wastewater (Shawaqfah et al., 2012). Photochemical methods degrade dye molecules to CO_2 and H_2O by UV treatment in the presence of H_2O_2 (Peralta-Zamora et al., 1999; Soares et al., 2017; Conceição et al., 2015). Whereas, Sodium hypochloride (NaOCl) method, attacks the amino goup of the dye by the chloride ions (Slokar and Marechal, 1997; Gupta et al., 2009). It initiates and accelerates azo bond cleavage. But the use of Cl ions for dye removal is becoming less frequent due to the negative effects such as release into waterways in the form of aromatic rings which are toxic and carcinogenic. Electrochemical method also have been successfully applied for the dye wastewater treatment and it shows efficient and economical removal of dyes and a high efficiency for color removal and degradation of recalcitrant pollutants (Pelegrini et al., 1999; Nidheesh et al., 2018). But the disadvantage is the relatively high flow rates causing a direct decrease in dye removal rate and moreover the cost of electricity used is comparable to the price of chemicals.

1.2.1.4.2 Biological methods

Biological methods is the most widely used technique for the removal of dyes from aqueous solution. This method is less expensive and the end products are non-toxic. White-rot fungi are able to degrade dyes using enzymes, such as lignin peroxides (LiP) or Manganese dependent peroxidases (MnP), H_2O_2-producing enzymes (Kirby, 1997; Mishra et al., 2011; Kunjadia et al., 2016). Mixed bacterial cultures from a wide variety of habitats have also shown to decolorize the diazo linked chromospheres of dye molecules in 15 days (Kamal et al., 2015; Chen et al., 2003; Wang et al., 2009). Dead bacteria, yeast and fungi have all been used for the purpose of decolorizing dye-containing effluents. The use of biomass has its advantages, especially if the dye-containing effluent is very toxic. Biomass adsorption is effective when conditions are not always favorable for the growth and maintenance of the microbial population (Przyśtas et al., 2017; da Fontoura et al., 2017; Angelova et al., 2016; Jia et al., 2017). Anaerobic system, apart from the decolorization of soluble dyes, can produce biogas, which can be reused to provide heat and power to reduce energy cost (Katal et al., 2014). Moreover, azo groups are also microbiologically reduced to corresponding amines with simultaneous disappearance of color under anaerobic/anoxic conditions (Delee et al., 1998; Xiao et al., 2018; Venkatesh et al., 2017; Olivo-Alanis et al., 2018). Though some efforts in the recent past to decolorize dyes under aerobic conditions have met with success the general perception of non-biodegradability of most azo dyes in conventional aerobic systems still persists. (Krishnan et al., 2017; Mullai et al., 2017; Gnanapragasam et al., 2011).

1.2.1.4.3 Physical methods

Adsorption is one of the widely applied technique for wastewater treatment for dye removal and the process is economically feasible and produces high quality product (Anandkumar et al., 2011). The term adsorption refers to a process where a material gets adhered at a solid surface from its

liquid or gaseous surroundings. The adsorption of dyes occurs in two ways – physical adsorption and chemical adsorption. In physical adsorption the attractive forces between adsorbed molecules and the solid surface are van der Waals forces and they being weak in nature result in reversible adsorption. On the other hand if the attraction forces are due to chemical bonding, the adsorption process is called chemisorption. In view of the higher strength of the bonding in chemisorption, it is difficult to remove chemisorbed species from the solid surface. Several adsorbents have been experienced on the possibility to remove dye from wastewaters (Fabryanty et al., 2017; Zhao et al., 2017; Sham.et al., 2018; Belbachir et al., 2017; Salam et al., 2018; Munagapati et al., 2017; Salzano de Luna et al., 2017; Mahmoodi et al., 2014). For obtaining high-performance adsorbent, it is crucial to select the more efficient and cheaper adsorbents by higher adsorption ability. Ion exchange is basically a reversible chemical process where an ion from solution is exchanged for a similarly charged ion attached to an immobile solid particle (Saruchi et al., 2016; Makhoukhi et al., 2015; Constantin et al., 2013; Kaith et al., 2015; El-Moselhy et al., 2018). The advantage include no loss of adsorbent on regeneration but the disadvantage is the cost.

Membrane separation technique has the ability to clarify, concentrate and separate dye continuously from effluent (Wang et al., 2017; Li et al., 2017; Zhao et al., 2017; Liu et al., 2017; Karim et al., 2014; Puspasari et al., 2016). This method of filtration is suitable for water recycling within a textile dye plant if the effluent contains low concentration of dyes but membrane clogging, high cost membrane, etc., makes water reuse a difficult task. Electrocoagulation method utilizes direct current to produce sacrificial electrode ions, which removes undesirable contaminants either by chemical reactions and precipitation or by causing colloidal materials to coalesce (Khemila et al., 2018; Pajootan et al., 2012; Khorram et al., 2018; Fajardo et al., 2017; Wei et al., 2012).

Adsorption removal techniques for dyes seems to be a very effective process after thorough analyzing and comparing with various other removal methods due to its cost effectiveness, easy recovery and possible regeneration of the adsorbents, no sludge production and also ease in the operating cost. But the adsorbents used during the adsorption process plays a very important role and thus various types of adsorbents have been reported and used in wastewater treatment till date (Yagub et al., 2014). Adsorbents from natural materials such as waste biopolymers, waste materials from industry, agricultural by-products, and biomass based activated carbon, clay minerals, polymeric adsorbents, biosorbents, etc. in the removal of various dyes has been economically advantageous to the water treatment as well as locally available.

i) Removal of dyes by various adsorbents

Reports by many researchers observed the common mechanism involved in the adsorption of metal ions was the interaction with the functional groups present in the various adsorbents. Daoud et al., 2017 reported the adsorption of reactive dye BEZAKTIV Red S-MAX (BRSM) by commercial activated carbon (CAC) and activated carbons prepared from date palm rachis (RPK) and jujube stones (NJK), by-product agricultural wastes. Two different trends of pH effects were observed for the adsorption of BRSM onto the tested activated carbons. On the one hand, a decrease in the adsorption capacity of NJK and CAC with the increase in the pH from 2 to 4 and then an increase with the increasing pH from 4 to 10 indicate that the electrostatic mechanism and the availability of adsorption sites were not the only mechanism for dye adsorption in this system due to the neutral protonated groups of activated carbons which are mainly phenolic group (OH^+) and carboxylic ($COOH^+$), while there are positive groups (SO_3H^+) or partially positive charges of dye which interact with the (OH^-) of the solution. On the other hand, the adsorption capacity of RPK rises progressively when the pH range was between 2 and 8 reaching its maximum, and decreases at pH

> 8. The adsorption capacities were found to be 128.21 mg/g, 28.49 mg/g and 45.66 mg/g (Langmuir parameter) using RPK, NJK and CAC, respectively. Jiang et al., 2018 synthesized a complex chitosan/β-cyclodextrin polymer by bridging with maleoyl chains followed by cross-linking with glutaraldehyde to investigate the removal of methyl orange (MO) from aqueous solution. The maximum adsorption capacity for MO was 392 mg/g for initial concentration 50 mg/L. The adsorption mechanism could be explained by the synergistic effect of electrostatic attraction of amino groups from chitosan and host-guest interaction from β-cyclodextrin and also demonstrated high selectivity towards MO due to the unique structure of cross-linked chitosan/β-cyclodextrin polymer that are complementary to that of MO molecule. Subramani et al., 2017 analyzed the capability of malachite Green (MG), reactive Red (RR) and direct Yellow (DY) dyes adsorption onto chitosan synthesized from prawn shells. The adsorption capacities of the synthesized chitosan was 166 mg/g for dye MG, 1250 mg/g for dye RR and 250 mg/g for dye DY at pH 3.0 and the adsorption mechanism was based on the electrostatic attraction between the dye molecules and the synthesized chitosan. Munagapati et al., 2018 investigated the adsorption characteristics of reactive black 5 (RB5) and cong Red (CR) onto banana peel powder (BPP). The maximum monolayer adsorption capacities of RB5 and CR on BPP calculated from Langmuir isotherm model were 49.2 and 164.6 mg/g at pH 3.0 and 298 K. Acidic conditions were favorable for the adsorption between two dyes and the adsorbent, because a significantly high electrostatic force of attraction exists between the positively charged surfaces of the adsorbent and the negative charged anionic dye under acidic conditions (RB5 and CR are anionic dyes in solution for SO_3^- group in their structure). Some literatures are reported for dye adsorption by various adsorbents are listed in Table 1.3.

Table 1.3: Literature reported various adsorbents for dye adsorption

Adsorbents	Dye	pH	Equilibrium time	Adsorption capacity (mg/g)	References
Fermented peanut shell	Crystal violet	7	4 hours for initial concentration of 50 mg/L	256.0	Liu et al., 2018
Cement kiln dust	Basic Blue 69 (BB69) Acid Red 114 (AR114)	-	30 mins for initial concentration of 500 mg/L	2119.0 2125.0	Magdy et al., 2018
Graphitic magnetic mesoporous nanocomposite	Acid black 1(AB 1)	3	15 mins for initial concentration of 300 mg/L	361.7 304.5	Dai et al., 2018
Non-living cells of *Nannochloropsis oceanica*	Reactive Violet 5 (RV5)	8	72 hours for initial concentration of 600 mg/L	75.9	Zuorro et al., 2017
Modified immobilized activated alumina (MIAA)	Maxilon blue GRL Direct yellow DY 12	7	90 mins for initial concentration of 400 mg/L	25.0	Wasti et al., 2016
Apricot stones Commercial activated carbon	Methylene blue (MB) Methyl orange (MO) Methylene blue (MB) Methyl orange (MO)	4.85 4.87 4.85 4.87	130 mins for initial concentration of 10 mg/L 120 mins for initial concentration of 10 mg/L 60 mins for initial concentration of 10 mg/L 180 mins for initial concentration of 10 mg/L	36.68 32.25 199.60 35.43	Djilani et al., 2015

ii) Amine based adsorbents

Functionalized polymers containing amine groups are generally considered as a potential adsorbent due to its high binding properties with the target pollutants. Amine groups have been found to be one of the most efficient functional groups for dye removal (Gupta et al., 2004; Goscianska et al., 2017; Aliabadi et al., 2018; Ahmed et al., 2016). Sharma et al., 2016 synthesized a nanoporous hypercrosslinked polyaniline (HCPANI) with specific surface area of 1083 m^2/ g which was used as an efficient adsorbent to remove both cationic (crystal violet, CV) and anionic (methyl orange, MO) dyes in the aqueous solution. Both the dyes showed adsorption capacity that reaches up to 245 mg/g and 220 mg/g for CV and MO, respectively. Strong interaction of cationic dye (CV) and anionic dye (MO) at higher side and lower side of pH 7.3 (point of zero charge) respectively. The adsorption of CV on HCPANI was due to π-π interaction and adsorption of MO was due to the combined effect of π-π interaction, Lewis acid-Lewis base interaction and H-bonding interaction. Mahmoodi et al., 2013 synthesized poly (amidoamine-co-acrylic acid) copolymer (PAC) and investigated its removal ability of acid dyes (direct red 31, direct red 80 and acid blue 25). The maximum dye adsorption capacity (Langmuir parameter) of PAC was 3400 mg/g, 3448 mg/g and 3500 mg/g for direct red 31, direct red 80 and acid blue 25, respectively for initial dye concentration of 300 mg/L. Maximum adsorption of anionic dyes occurs at acidic pH (pH 2.0) due to the electrostatic attraction as well as the organic property and structure of dye molecules and PAC played very important roles in dye adsorption onto PAC. Janaki et al., 2012 investigated the removal of congo Red, coomassie brilliant blue, remazol brilliant blue R, and methylene blue from aqueous solution by eco-friendly polymer/biopolymer composite (polyaniline/chitosan). Equilibrium time condition for CR, CBB and RBBR was about 60 mins respectively and the optimum pH was pH 3.0 with maximum adsorption capacity of CR, CBB and

RBBR - 322.58 mg/g, 357.14 mg/g and 303.03 mg/g (Langmuir parameter), respectively. The main removal mechanism was electrostatic interaction between the dye anion and positively charged sites of polyaniline backbone could be possible in acidic pH. He et al., 2017 prepared an adsorbent functionalized triptycene-based 3D polymer (TPP-NH_2) as a novel adsorbent for the removal of organic dyes. The maximum adsorption capacity was 204.9 mg/g and 213.2 mg/g for MEB and MO, respectively. The pH had no obvious effect on the adsorption of MEB and MO and in addition, the TPP-NH_2 can adsorb up to 33 times its own weight in organic solvents while wiping off the water. The high surface area, hierarchical porosity and π-π stacking interactions between the aromatic rings of MEB and MO and the aromatic rings of 3D TPP-NH_2 were the main mechanism responsible for the efficient adsorption. List of the effect of polymeric amine based adsorbents for dye adsorption is given in Table 1.4.

Table 1.4: Literature reported polymeric amine based adsorbents for dye adsorption

Adsorbents	Dyes	Initial concentration (mmol/L)	Adsorption capacity (mmol/g)	pH	References
Polyaminoimide homopolymer	Direct Red 31 Direct Red 23 Direct Black 22 Acid Blue 25	0.420 0.368 0.276 0.720	9.342 6.826 8.385 14.126	2	Mahmoodi et al., 2011
Pentaethylene Hexamine functionalized SBA-3	Acid blue 113 Acid red 114 Acid green 28 Acid yellow 127 Acid orange 67	0.146 0.120 0.135 0.154 0.165	0.108 0.082 0.057 0.080 0.080	3	Anbia and Salehi (2012)
p-toluene sulfonic acid (PTSA) doped PANI	Orange G, Coomassie Brilliant Blue R-250, Remazol Brilliant Blue R, Alizarine cyanine Green	0.884 0.484 0.638 0.642	0.000756 0.000250 0.000272 0.000152	3.9	Mahanta et al., 2009
Amine-functionalized silica nanoparticle	Acid Red 14 Acid Black 1 Acid Blue 25	0.099 0.081 0.120	0.863 0.405 0.401	2	Mahmoodi et al., 2011
CS/Q-NFC composite cryogels	Acid red 88	0.1998	0.939	7	Chen et al., 2017
Poly-melamine-formaldehyde polymer	Methyl orange Orange II sodium salt Congo red	0.305 0.285 0.143	0.248 0.255 0.125	4-8	Wang et al., 2016
Microgel based on nanocellulose and polyvinylamine	Congo red 4BS Acid red GR Reactive light yellow K-4G	0.143 0.179 0.110	1.247 2.247 1.622	3.5	Jin et al., 2015
Chitosan-montmorillonite beads (KSF-CTS-25%)	Remazol Blue	0.798	0.497	3	Pereira et al., 2017
Nanopolyaniline	Acid red 14	0.547	0.529	4	Ahmed et al., 2016
Nanoporous hypercrosslinked polyaniline	Methyl orange	0.305	0.672	3	Sharma et al., 2016

1.2.2 Heavy metals pollutants

Heavy metals are elements from the fourth period of the periodic table and having atomic weights between 63.5 and 200.6 with a specific gravity greater than 5.0 (Srivastava and Majumder, 2008). Heavy metals (Co, Cu, Fe, Mn, Mo, V, Sr, and Zn) in trace amounts are essential (metabolic activites, etc.) for living organisms but their excessive levels can be harmful to living organisms (Barakat, 2011). Some heavy metals (Hg, Cr, Cd, As, Pb, Sr, etc.) are non-essential and considered to be great threat to aquatic life (end of aquatic life, oxygen insufficiency and algal blooms, etc.) as well as other living organisms (cancer, nervous system damage, and kidney failures, etc.). Heavy metals are naturally found in the environment but with the rapid development of industries such as metal plating, mining operations, fertilizer industries, tanneries, batteries, paper industries and pesticides, etc., heavy metals are directly or indirectly discharged into the environment increasingly, especially in developing countries producing toxic wastewater. Unlike, organic contaminants, heavy metals are not biodegradable and tend to accumulate in living organisms and many heavy metal ions are known to be toxic or carcinogenic even at very low concentration (Dincer et al., 2015). Generally it is observed that anthropogenic sources contaminates the environment compared to natural sources in high alarming rate leading to serious concerns (Figure 1.1). Heavy metals in wastewater are a major problem in the environment, because the toxic metals can remain either in chemical form or mixed form, thus it is difficult to remove from the wastewater. When they are discharge into the rivers, the heavy metals get converted into hydrated ions which are highly toxic than the metal atoms and the hydrated ions disrupt the enzymatic process as well as the absorption is faster in it (Namieśnik et al., 2010). To reduce the water pollution level, World Health Organization (WHO) and Environmental Protection Agency (EPA) have set the most admissible discharge level of heavy metal into the environment.

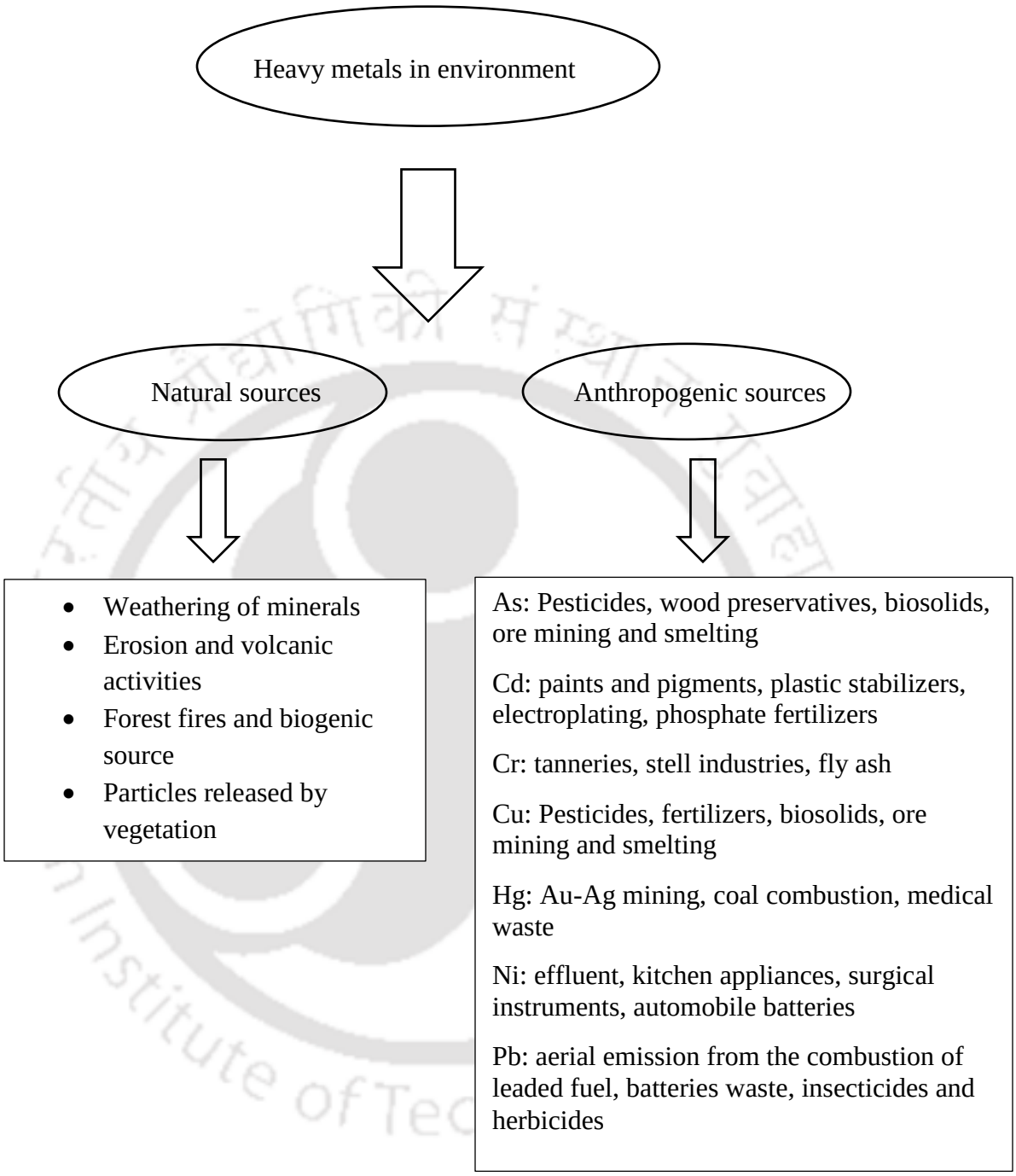

Figure 1.1: Various natural and anthropogenic sources of metal contamination in the environment (Das et al., 2017)

1.2.2.1 Sources and toxicity

Environmental pollution from hazardous metals and minerals arise from natural as well as anthropogenic sources. Natural sources for heavy metals occurs – seepage from rocks into water, volcanic activity, forest fires, etc. Anthropogenic sources of heavy metals are industrial activities such as electroplating, mining, refinery, printing, dyeing and tanning discharge effluents containing heavy metals and other recalcitrant organic pollutants (Majumdar et al., 2008; Yin et al., 2008; Fu et al., 2011; Lee et al., 2018; Abdelhadi et al., 2017). Other sources such as landfill leachate, municipal wastewater, agricultural activities and urban runoff contribute significant heavy metal to the environment. The essential heavy metals exert biochemical and physiological functions in plants and animals. They are important constituents of several key enzymes and play important roles in various oxidation-reduction reactions. However, excess an excess amount of such metals produces cellular and tissue damage leading to a variety of adverse effects and human diseases.

From among various metal ions, lead, mercury, cadmium and hexavalent chromium (VI) are at the top on the toxicity list (Volesky, 1994; Ballesteros et al., 2016). Several studies have demonstrated that reactive oxygen species (ROS) production and oxidative stress play a key role in the toxicity and carcinogenicity of metals such as arsenic, cadmium, chromium, lead, and mercury. Because of their high degree of toxicity, these five elements rank among the priority metals that are of great public health significance. They are all systemic toxicants that are known to induce multiple organ damage, even at lower levels of exposure. Due to non-biodegradability, metal ions accumulate and their amounts are increased along the food chain. Hence, their toxic effects are more pronounced in the animals at higher trophic levels. According to the United States Environmental Protection Agency (USEPA), and the International Agency for Research on Cancer (IARC), these metals are

also classified as either “known” or “probable” human carcinogens based on epidemiological and experimental studies showing an association between exposure and cancer incidence in humans and animals. A list of toxic effects of heavy metals on human health is given in Table 1.5.

Table 1.5: Toxic effects of heavy metals on human health

Heavy metals	Toxic effects	References
Cadmium	Renal failure, human carcinogen, Osteomalacia, itai–itai disease, weakens the bone, respiratory disease, gastrointestinal diseases, birth defects, anemia, inhibits the calcium control in biological systems	Huang et al., 2018 Xu et al., 2017
Chromium	Genotoxic, alopecia	Tahar et al., 2018 Kan et al., 2017
Copper	Liver illness, cancer in respiratory tract, lack of blood, stomach and intestinal irritation	Rani et al., 2018 Hu et al., 2017
Lead	Damages the developing infant brain, kidney failure, affects the sense organs and circulatory system, loss of voluntary muscle function	Heraldy et al., 2018 Cataldo et al., 2018
Mercury	Affects the joints in the human body, kidney disease, affects the muscle movements, death, unconsciousness, abortion, skin cell death in humans, inflammation of gums, painful extremities, nervousness, affects the vision, memory loss	Elhami et al., 2016 Nouri et al., 2017
Nickel	Anaphylaxis, lung cancer, hair loss, destroys red blood cells, cause liver diseases, nephrotoxic	Vieira et al., 2010 Raval et al. 2016
Zinc	Creates dizziness, depression	Cristian et al., 2015 Sarkar et al., 2018

1.2.2.2 Guidelines

Considering the health risks associated with the exposure to these toxic heavy metals, even at low concentrations, and unless properly treated, their ingestion at levels that exceed regulatory standards causing serious health disorders. Thus, the need for their removal from water and wastewater is currently a major regulatory and academic concern. Considering the health effects associated with these heavy metals, a number of organizations, including the World Health Organization (WHO) and the Bureau of Indian Standards (BIS) have defined maximum contamination levels for some metals (Table 1.6).

Table 1.6: Guidelines for some heavy metals in drinking water and wastewater effluent

Metals	Drinking water (mg/L)	Wastewater (mg/L) (BIS)		
	WHO	Inland surface water	Public Sewers	Marine coastal areas
Arsenic	0.01	0.2	0.2	0.2
Copper	1.0	3.0	3.0	3.0
Cadmium	0.005	2.0	1.0	2.0
Hexavalent chromium	0.05	0.1	2.0	1.0
Total chromium	0.05	2.0	2.0	2.0
Lead	0.005	0.1	1.0	2.0
Mercury	0.001	0.01	0.01	0.01
Nickel	-	3.0	3.0	5.0
Selenium	0.01	0.05	0.05	0.05
Zinc	5.0	5.0	15.0	15.0

*WHO =World Health Organization, BIS = Bureau of Indian Standards (Vunain et al., 2016; BIS 2012)

1.2.2.3 Removal techniques

The removal of heavy metals include methods like coagulation, chemical precipitation, electrodialysis, evaporative recovery, floatation, flocculation, ion exchange, nanofiltration, reverse osmosis, ultrafiltration etc. The use of polymer in water treatment as a coagulant is an old practice Coagulation–flocculation technique can also be employed to treat wastewater laden with heavy metals wherein the coagulation process destabilizes colloidal particles by adding a chemical agent (coagulant) and results in sedimentation (Wang et al., 2004). The membrane filtration technique used different types of membranes for removal of various heavy metals in aqueous solution. This technique also removes oils, suspended solids, heavy metals, and organic and inorganic materials (Barakat, 2011; Fu and Wang, 2011). The nature of the electrochemical process is the applying of electricity to pass a current through an aqueous metal bearing solution, which also contains a cathode plate and an insoluble anode. The treatment is the precipitation of the heavy metals in a weakly acidic or neutralized electrolyte as hydroxides (Tran et al., 2017). Ion exchange method involves ion exchange resin, either natural or synthetic resin which has the ability to exchange the cations with the metals in the wastewater. Ionic charge also plays an important role in ion-exchange process (Tavakoli et al., 2017). Biological treatment of heavy metals involves the adsorption of the soil or reduction of the metal by microorganism (Jacob et al., 2018). Oxidizing agents such as fenton's reagent, chemical oxidation, etc., oxidize or reduce metals (insoluble form or metal hydroxides) to non toxic form (Yoo et al., 2017). Although effective, the disadvantages of these methods are usually expensive due to high energy and reagent requirements. Moreover, they generate large amount of toxic sludges and byproducts, which pollutes the environment. The advantages and disadvantages of the metals removal methods are given in Table 1.7.

Table 1.7: The advantages and disadvantages associated with the removal methods of heavy metals

Removal methods	Advantages	Disadvantages	Heavy Metals	References
Coagulation	Cost effective, Dewatering qualities	Generation of sludge, Utilization of chemicals is high	Cu(II), Pb(II), Cr(III)	Yao et al., 2017
Membrane filtration	High removal of heavy metals, lower space requirement	Very expensive, membrane fouling, complex process.	Cu(II), Fe(III), Cd(II)	Feng et al., 2018 Abdi et al., 2018
Adsorption	Easy operation, less sludge production, utilization of low cost adsorbents	Depends of adsorbent type and adsorbent require regeneration	Cd(II), Cu(II), Ni(II), Pb(II)	Peng et al., 2018 Lee et al., 2018
Electrochemical treatment	Efficient for the removal of important metal ions, low chemical usage	Initial investment is high, need high electrical supply	Cd(II),Cu(II), Hg(II),Ni(II), Pb(II), Zn(II)	Ya et al., 2018 Zhou et al., 2017
Electrodialysis	High segregation of metals	Clogging and energy loss	Ag(II), Cd(II) Cu(II), Zn(II), Pt(II)	Frioui et al., 2017
Ion exchange	High transformation of components	Removes only limited metal ions, operational cost is high	Cu(II), Zn(II) Cd(II), Pb(II)	Tavakoli et al., 2017
Photocatalysis	Eliminates both the metal ions and organic pollutants concurrently	It takes prolonged time to remove the metals	Cu(II), Cd(II), Cr(VI), Pb(II)	Zhang et al., 2012 Wahyuni et al., 2015
Biological treatment	This technology is beneficial in removing heavy metals	Need to be developed	Cd(II), Ni(II), Zn(II)	Fang et al., 2016 Ge et al. 2017
Oxidation	No need of electricity	Rusting occurs in the system due to the usage of oxidation	Cu(II), Pb(II)	Yoo et al., 2017

i) Removal of metals by various adsorbents

Adsorbents such as – industrial byproducts, agricultural waste, biomass, polymeric materials etc., makes adsorption an economically favorable method for wastewater treatment. Lee et al. 2018 investigated the removal of lead, copper and cadmium using waste biomass adsorbent, persimmon leaves, in an aqueous solution. Persimmon leaves are biomaterials having a large number of hydroxyl groups and are highly suitable heavy metals removal. The optimum pH for Cd was pH 5 whereas for Cu and Pb was pH 6. The point of zero charge played an important role on the removal mechanism of metal from the solution. The maximum adsorption capacity of Cu, Pb, and Cd was determined to be 19.42 mg/g, 22.59 mg/g, and 18.26 mg/g, respectively. Abou El-Reash et al., 2016 prepared cross-linked chitosan magnetic beads modified with cysteine-glutaraldehyde schiff's base (Chi-CG) adsorbent for the elimination of Cu(II) and Cr(VI) from aqueous solutions. The adsorption equilibrium was achieved after almost 90 min in case of Cu(II) and 110 min in case of Cr(VI). The maximum adsorption capacities for Cu(II) and Cr(VI) were 156.49 and 138.53 mg/g, respectively. In case of Cr(VI) adsorption maximum was achieved at pH 2 due to the protonation of both nitrogen percentage in form of non-substituted NH_2 and (CN) of Chi-CG, which leads to an electrostatic interaction with the anionic CrO_4^{2-} and $HCrO_4^-$ from the Cr(VI) solution. Whereas, the adsorption of Cu(II) reaches its maximum at pH 5 which is due to the presence of free lone pair of electrons on nitrogen atoms of (NH_2 and CN) and easiness deprotonation of both carboxylic and SH groups which facilitates the coordination with Cu(II) ions on Chi-CG and formation of an inner-sphere complex via surface chelation ion exchange rather than electrostatic interaction. Table 1.8 reported the list of few different adsorbents for heavy metal removal from aqueous solution.

Table 1.8: Comparison on the removal of heavy metals by different adsorbents

Metals	Equilibrium time	Adsorbents	pH	Adsorption capacity (mg/g)	Reference
Cu(II) Cr(III) Fe(II)	180 mins 300 mins 360 mins for initial concentration of 10 mg/L for each metals	Clinoptilolite zeolite	4	ND 2.5 1.8	Zanina et al., 2017
Pb(II)	90 min for initial concentration of 100 mg/L 60 min for initial concentration of 100 mg/L	Tomato waste Apple juice residue	4	152 108	Heraldy et al., 2018
Cd(II) Pb(II)	9 hours for initial concentration of 100 mg/L	Forest biowastes, chestnut bur	4	34.77 74.35	Kim et al., 2015
Cu(II) Co(II) Fe(III)	240 mins for the initial concentration of 500 mg/L	Rice husk Palm leaf Water hyacinth	9	285.7; 256.4; 192.3 217.4; 303.0; 263.2 181.8; 222.2; 294.1	Sadeek et al., 2015
Cu(II) Cr(VI) Ni(II)	4 hours for initial concentration of 1500 mg/L	Boronic acid-functionalized carbon-based adsorbent	3 2 7	255 285 270	Kettum et al., 2018
Cu(II) Cd(II) Pb(II) Zn(II)	180 mins for initial concentration of 50 mg/L	Multi-metal binding biosorbent	5.5	41.06 31.73 76.25 26.63	Abdolali et al., 2016
Cu(II) Cd(II)	12 hours for initial concentration 250 mg/L	Alginate-based attapulgite foams	4 6	119 160	Wang et al., 2018

ii) Removal by Amine based adsorbents

Nitrogen atom in compounds of amine derivative makes coordinate bond with positive charge of metals due to the presence of electron in sp3 orbital of nitrogen (Kumar et al., 2008). Amine groups could affect the adsorptive property by providing electrostatic attraction, ion exchange, coordinate bond, chelation, etc. In particular, adsorbents with amino group have been proved to be one of the efficacious groups for heavy metals removal. Kumar et al., 2007 synthesized aniline formaldehyde condensate coated on silica gel and studied the adsorption of chromium. The study suggested that total chromium removal was acombinations of electrostatic attraction of acid chromate ion by protonated AFC, reduction of Cr(VI) to Cr(III) and bond formation of Cr(III) with nitrogen atom of AFC. Kong et al., 2011 carried out batch adsorption experiments to remove heavy metal ions such as Cu(II), Ni(II), Cd(II), and Cr(VI) from single-metal solutions using a polyaniline/palygorskite (PP) composite. The adsorption capacity calculated were 114 mg/g Cu(II), 84 mg/g Ni(II), 56 mg/g Cd (II), and 198 mg/g Cr (VI). Three removal mechanism was involved in the adsorption process - chelation, ion exchange, and electrostatic attraction simultaneously when the PP composite was used as an adsorbent. Lin et al., 2017 prepared polyethersulfone (PES) beads with diameter of around 2.5 mm, in which nanosized amine-rich polymer spheres (APSs) with particle size of ~400 nm are immobilized, are fabricated via phase inversion route. The cooperative attributing of the hierarchical structure and APSs demonstrates enhanced Cr(VI) adsorption efficiency by the synergistic contribution of electrostatic attraction and reduction process. Table 1.9 reported the list of some amine based adsorbents for the adsorption of heavy metals.

Table 1.9: List of various amine based adsorbents used for heavy metals removal

Metals	Initial concentration (mg/L)	Adsorbents	pH	Adsorption capacity (mg/g)	Reference
Cr(VI)	100	Nanosized amine-rich spheres embedded polymeric beads	2	243.9	Lin et al., 2017
Pb(II) Cr(VI)	250	Modified Nylon Fibers with Amino Chelating Groups	4	51.81 49.75	Racho et al., 2017
Cu(II)	10	Amine-functionalized Kaolin	7.1	20.54	Huang et al., 2016
Cr(VI) Hg(II) Ni(II) Cd(II) Mn(VII)	100	Carboxymethyl chitosan–hemicellulose resin	4	6.1 6.6 36.4 30.8 6.4	Wu et al., 2017
Cr(III)	50	Amine-based polymer aniline formaldehyde condensate	6	17	Kumar et al., 2009
Zn(II) Pb(II) Cd(II)	100	Ethyl acrylate grafted chitosan	6	653 613 573	Maleki et al., 2015
Cu(II)	4	Amine functionalized carbon nanotubes	7	29.85	Zhang et al., 2015
As(V) Cr(VI)	100	Amine based p(TAEA-co-GDE) microgels	4	98.72 160.62	Rahman et al., 2017
Cr(VI)	100	PANI-jute	3	62.9	Kumar et al., 2008
Hg(II)	41.59	Amine-modified activated carbon	6	8.12	Zhu et al., 2009

Xu et al., 2011 prepared an adsorbent by cross-linking the amine groups to wheat straw. The adsorption capacity of AC-WS for Cr(VI) was 5.68 mmol/g. The adsorption mechanism suggested for chromium (VI) onto AC-WS was the complicated interactions including complexation and electrostatic force.Wang et al., (2010) investigated on amino-functionalized Fe_3O_4@SiO_2 nano adsorbent and found out that it exhibited high adsorption affinity for aqueous Cu(II), Pb(II), and Cd(II) ions, resulting from complexation of the metal ions by surface amino groups. Fan et al., 2012 synthesized 3-[2-(2-aminoethylamino) ethylamino] propyl-trimethoxysilane (AAAPTS) functionalized silica gel (AAAPTS/SiO2). It was found that As(V) could be selectively adsorbed on AAAPTS/SiO_2 adsorbent within pH of 2.7–9.2, while As(III) could not be absorbed in the studied pH range. Adsorption occurred mainly via electrostatic effect between As(V) and available active sites in synthesized adsorbent within pH of 2.7–9.2. The adsorption behavior of AAAPTS/SiO_2 adsorbent for As(V) mostly belonged to monolayer chemical sorption or chemisorption.

1.2.3 Theoretical Background for adsorption

1.2.3.1 Adsorption kinetics

It is important to investigate adsorption kinetics because it can predict the rate at which a pollutant is removed from aqueous solutions and provides valuable data for understanding the mechanism of adsorption reactions. Adsorption kinetic models correlate the adsorbate uptake rate with bulk concentration of the adsorbate.

i) Pseudo-first order adsorption model

The Pseudo-first order kinetic model is represented as (Lagergren, 1898), the differential equation which can be generally expressed as follows (Kumar et al., 2012):

$$\frac{dq_1}{dt} = k_1(q_e - q_t) \quad (1.1)$$

Where k_1 is the rate constant of pseudo-first-order adsorption and q_e represents the adsorption capacity (i.e., the amount of adsorbed corresponding to monolayer coverage). After definite integration by applying the initial conditions t=0 to t and q_t= 0 to q_t , Eq. (1.1) becomes:

$$log(q_e - q_t) = logq_e - \frac{k_1 t}{2.303} \quad (1.2)$$

Where q_e and q_t are the amount of adsorbate adsorbed (mg/g) at equilibrium and at any time t, k_1 is the rate constant (mins). The plot of log (q_e-q_t) versus t gives a straight line for the pseudo-first-order sorption kinetic. The value of the pseudo-first-order rate constant k_1 was obtained from the slopes of the straight lines. Further, equation (1.2) can be expressed as a function of time as

$$q_t = q_e(1 - e^{-k_1 t}) \quad (1.3)$$

The modeling of pseudo-first order kinetics was done by the method of least squares or the Fujimoto method as described in Wastewater Engineering (Metcalf and Eddy, 2003).

ii) Pseudo-second order adsorption model

The pseudo-second order kinetic equation as (Lagergren, 1989):

$$\frac{dq_t}{dt} = k_2(q_e - q_t)^2 \quad (1.4)$$

Where, q_e and q_t are the amounts of adsorbed on adsorbent (mg/g) at equilibrium and at time t, and k_2 (g/mg.min) is the rate constant of the second order adsorption. Integrating equation (1.4) for the boundary conditions t=0 to t=t and q_t=0 to q_t = 0 to q_t =q_e leads to

$$\frac{1}{q_e - q_t} - \frac{1}{q_e} = k_2 t \quad (1.5)$$

Or,

$$q_t = q_e \frac{q_e k_2 t}{1 + q_e k_2 t} \quad (1.6)$$

Or,

$$\frac{t}{q_t} = \frac{1}{k_2 q_e^2} + \frac{t}{q_e} \quad (1.7)$$

In order to select the best fit kinetic model, Chi-square (χ^2) (Kumar et al., 2008) and Root mean square error (RMSE) tests were done.

$$\chi^2 = \frac{\sum(q_t - q_{tm})^2}{q_{tm}} \quad (1.8)$$

Where, q_t and q_{tm} (mg/g) are dye/metal adsorption capacity at time t calculated using experimental data and model respectively.

$$RMSE = \sqrt{\frac{\sum_{i=0}^{n}(q_t - q_{tm})^2}{n}} \quad (1.9)$$

iii) Intra-particle diffusion model

The structure of the solid and its interaction with the diffusion substance influences the rate of transport. Adsorbent may be in the form of porous barriers and solute movement by diffusion from one fluid body to the other by virtue of concentration gradient (Shrihari et al., 2005). Intra-particle diffusion is a transport process involving movement of species from the bulk of the solution to the solid phase. In a well stirred batch adsorption system, the intra-particle diffusion model has been used to describe the adsorption process occurring on a porous adsorbent. A plot of the amount of adsorbate adsorbed, q_t (mg/g) and the square root of the time, gives the rate constant (slope of the plot). It is calculated by using the intra-particle diffusion model given as equation (1.10) (Robati et al., 2013).

The intra-particle diffusion equation is the following:

$$q_t = k_i t^{0.5} + C_i \quad (1.10)$$

Where, k_i is the intra-particle diffusion rate constant, mg/g.min$^{0.5}$ and C_i is the intra-particle diffusion constant i.e. intercept of the line (mg/g). It is directly proportional to the boundary layer thickness

A functional relationship common to most treatments of intra-particle diffusion is that uptake varies almost proportionately with the half power of time, $t^{0.5}$, nearly linear variation of the quantity adsorbed with $t^{0.5}$ is predicted for a large initial fraction of reactions controlled by rates of intra-particle diffusion. Good linearization of the data is observed for the initial phase of the reaction in accordance with expected behavior if intra-particle diffusion is the rate-limiting step.

iv)Boyd model

Boyd model is applied to check whether adsorption proceeds via film diffusion or intraparticle diffusion mechanism (Nethaji et al., 2013). The model can be expressed in the following form:

$$F = 1 - \frac{6}{\pi^2}\sum_{n=1}^{\infty}\frac{1}{n^2}exp\left(-\frac{n^2 D_s \pi^2 t}{R^2}\right) \quad (1.11a)$$

$$F = 1 - \frac{6}{\pi^2}\sum_{n=1}^{\infty}\frac{1}{n^2}exp(n^2 Bt) \quad (1.11b)$$

Where, $B = \frac{\pi^2 D_S}{R^2}$, F is fractional uptake at any time t (min) and F=q_t/q_e,q_t and q_e are the uptakes at time t and equilibrium, respectively, Bt is a mathematical function of F and D_s is the effective diffusion coefficient (cm^2/min), n is an integer that defines the infinite series solution.

The values of Bt for each value of F was calculated as proposed by Reinchenberg (1953) and given below:

F values <0.85, $Bt = 6.28318 - 3.2899F - 6.28318(1 - 1.0470F)^{1/2}$

F values > 0.85, $Bt = -0.4997 - \ln(1 - F)$

If the plot of Bt vs t is linear and passes through the origin, it suggests that adsorption is governed by particle diffusion, otherwise it is controlled by film diffusion.

B) Thermodynamics properties

The effect of temperature study is also an important phenomenon as the rate of diffusion of the dye molecules is a temperature controlled process, variation in temperature alters the equilibrium capacity of the adsorbent for a particular adsorbate. The experimental data obtained from batch adsorption studies at varying temperatures, can be analyzed by using the thermodynamic equations (Fosso-Kankeu et al., 2017) as expressed by equation (1.12)

$$\Delta G^\circ = -RTlnk_L \tag{1.12}$$

$$lnk_L = \frac{\Delta S^\circ}{R} - \frac{\Delta H^\circ}{RT} \tag{1.13}$$

Where, R is the universal gas constant (8.314 J/(mol.K)), T is temperature (K) and k_L is the distribution coefficient. Gibbs free energy change of adsorption was calculated using ln k_L values for different temperatures. The k_L values were calculated using following equation (1.14):

$$k_L = \frac{q_e}{C_e} \tag{1.14}$$

Where, C_e is the equilibrium concentration of dye, q_e is the amount of dye adsorbed per unit weight of adsorbent at equilibrium concentration (mg/g). The enthalpy change (ΔH) and entropy change (ΔS) of adsorption were estimated from the following equation (1.15):

$$log\frac{q_e}{C_e} = \frac{\Delta S^\circ}{2.303R} + \frac{-\Delta H^\circ}{2.303RT} \tag{1.15}$$

According to Eq. (1.15), ΔS° and ΔH° parameters can be calculated from the slope and intercept of the plot of ln k_L versus 1/T, respectively. The negative ΔH° suggests that the adsorption process is exothermic process and positive indicates endothermic process. The negative values of Gibbs

free energy ΔG° suggest spontaneous adsorption process while positive value suggests non-spontaneous process.

1.2.3.2 Adsorption isotherm

A) Two parameters adsorption isotherm model

i) Langmuir adsorption isotherm

This describes the formation of a monolayer adsorbate on the outer surface of the adsorbent, and after that no further adsorption takes place. The Langmuir isotherm (Kumar et al., 2010) is valid for monolayer adsorption onto a surface containing a finite number of identical sites. The model assumes uniform energies of adsorption onto the surface and no transmigration of adsorbate in the plane of the surface. Based upon these assumptions, Langmuir represented the following equation

$$q_e = \frac{Q_o K_L C_e}{1 + K_L C_e} \tag{1.16}$$

Langmuir adsorption parameters were determined by transforming the Langmuir equation (1.17) into linear form:

$$\frac{1}{q_e} = \frac{1}{Q_o} + \frac{1}{Q_o K_L C_e} \tag{1.17}$$

Where, C_e= the equilibrium concentration of adsorbate (mg/L), q_e = the amount of metal adsorbed per gram of the adsorbent at equilibrium (mg/g), Q_o = maximum monolayer coverage capacity (mg/g) and K_L = Langmuir isotherm constant (L/mg).

The values of Q_o and $K_L$were computed from the slope and intercept of the Langmuir plot. The essential features of the Langmuir isotherm may be expressed in terms of equilibrium parameter R_L, which is a dimensionless constant referred to as separation factor or equilibrium parameter.

$$R_L = \frac{1}{(1 + K_L C_o)} \quad (1.18)$$

Where: C_o = initial concentration, K_L = the constant related to the energy of adsorption (Langmuir Constant). R_L value indicates the adsorption nature to be either unfavourable if R_L>1, linear if R_L =1, favourable if 0< R_L<1 and irreversible if R_L =0.

ii) Freundlich adsorption isotherm

This is commonly used to describe the adsorption characteristics for the heterogeneous surface. These data often fit the empirical equation proposed by Freundlich:

$$Q_e = K_f C_e^{\frac{1}{n}} \quad (1.19)$$

Where, K_f= Freundlich isotherm constant (mg/g), n = adsorption intensity, C_e = the equilibrium concentration of adsorbate (mg/L) and Q_e = the amount of metal adsorbed per gram of the adsorbent at equilibrium (mg/g).

Linearizing equation (1.19) (Desta, 2013), we have:

$$logQ_e = logK_f + \frac{1}{n} logC_e \quad (1.20)$$

The constant K_f is an approximate indicator of adsorption capacity, while 1/n is a function of the strength of adsorption in the adsorption process.

iii) Temkin adsorption isotherm

This isotherm contains a factor that explicitly taking into the account of adsorbent–adsorbate interactions. As implied in the equation, its derivation is characterized by a uniform distribution of binding energies (up to some maximum binding energy) was carried out by plotting the quantity

adsorbed q_e against ln C_e and the constants were determined from the slope and intercept. The model is given by the following equation (1.21) (Dada et al., 2012):

$$q_e = \frac{RT}{b} ln(A_T C_e) \quad (1.21)$$

$$q_e = \frac{RT}{b} lnA_T + \left(\frac{RT}{b}\right) lnC_e \quad (1.22)$$

$$B = \frac{RT}{b_T}$$

$$q_e = BlnA_T + BlnC_e \quad (1.23)$$

Where, A_T=Temkin isotherm equilibrium binding constant (L/g); b_T = Temkin isotherm constant; R= universal gas constant (8.314J/mol/K); T= Temperature at 298K; B = Constant related to heat of sorption (J/mol).

iv) Dubinin- Radhuskevich adsorption isotherm

Dubinin–Radushkevich adsorption isotherm is generally applied to express the adsorption mechanism with a Gaussian energy distribution onto a heterogeneous surface. The model has often successfully fitted high solute activities and the intermediate range of concentrations data well (Inyinbor et al., 2016).

$$q_e = (q_s) exp(-K_{ad}\varepsilon^2) \quad (1.24)$$

$$lnq_e = ln(q_s) - (K_{ad}\varepsilon^2) \quad (1.25)$$

Where, q_e = amount of adsorbate in the adsorbent at equilibrium (mg/g), q_s = theoretical isotherm saturation capacity (mg/g), K_{ad} = Dubinin–Radushkevich isotherm constant (mol^2/kJ^2) and ε = Dubinin–Radushkevich isotherm constant. The approach was usually applied to distinguish the physical and chemical adsorption of dye ion with its mean free energy, E per molecule of adsorbate

(for removing a molecule from its location in the sorption space to the infinity) can be computed by the relationship

$$E = \left| \frac{1}{\sqrt{2K_{ad}}} \right| \tag{1.26}$$

$$\varepsilon = RTln\left[1 + \frac{1}{C_e}\right] \tag{1.27}$$

Where, R, T and Ce represent the gas constant (8.314 J/mol K), absolute temperature (298 K) and adsorbate equilibrium concentration (mg/L), respectively.

v) BET adsorption isotherm

The BET equation (equation 1.28), which is the most widely used model in food systems, was first proposed by Brunauer, Emmett and Teller (Sumithra et al., 2018). It represents a fundamental milestone in the interpretation of multi-layer sorption isotherms, particularly the types II and III. It is also an effective method for estimating the amount of bound water in specific polar sites of dehydrated food systems

$$q_e = \frac{Q_m B C_e}{(C_s - C_e)[1 + (B-1)\left(\frac{C_e}{C_s}\right)]} \tag{1.28}$$

Where. Q_m is the amount adsorbed in a complete monolayer, B is equilibrium constant and C_s is the saturation concentration of adsorbate in water.

vi) Halsay adsorption isotherm

This model provides an expression for the condensation of multilayers at a relatively large distance from the surface, assuming that the potential energy of a molecule varies as the inverse n^{th} power

of its distance from the surface (Amin et al., 2015). This equation is a good representation of adsorption data regarding isotherms type I, II, or III.

The Halsay adsorption isotherm can be given as

$$q_e = exp\left(\frac{lnK_{HA} - lnC_e}{n_{HA}}\right) \quad (1.29)$$

Where, K_{Ha} (mg/L) and n_{Ha} are the Halsay isotherm constants. A plot of lnq_e Vs lnC_e enables the determination of n_{Ha} and K_{Ha} from the slope and intercept. This equation is suitable for multilayer adsorption and the fitting of the experimental data to this equation attest to the heteroporous nature of adsorbent. The experimental data and the model predictions based on the non-linear form of the Halsay models.

vii) Hill adsorption isotherm

Hill's equation was postulated to explain the binding of various species onto homogeneous substrates. The model assumes that adsorption is a cooperative phenomenon, with the ligand binding ability at one site on the macromolecule, may influence different binding sites on the same macromolecule (Yousef et al., 2016) given in equation (1.30).

$$q_e = \frac{Q_H C_e n_H}{KD + C_e n_H} \quad (1.30)$$

Where, KD, n_H, and Q_H are constants.

viii) Smith adsorption isotherm

In 1947, Smith developed an empirical model to describe the final curved portion of water sorption isotherm of high molecular weight biopolymers. In this model, the adsorbed amount on the surface

is subdivided into a bound and a normally condensed fraction. The bound fraction of adsorbate is on the inner or outer surface of the solid adsorbent by forces in excess of the normal forces for condensation. The normally condensed fraction may also have more than one condensed layer of adsorbate. The equation (1.31) describes Smith isotherm equation (D. Andrade P. et al., 2011):

$$q_e = W_b - Wln(1 - C_e) \tag{1.31}$$

Where W and W_b are the constant parameters for the isotherm equation.

B) Three parameters adsorption isotherm

ix) Koble-Corrigan adsorption isotherm

Koble-Corrigan isotherm is a three-parameter equation which incorporated both Langmuir and Freundlich isotherm models for representing the equilibrium adsorption data (Salarirad et al., 2011). The isotherm has an exponential dependence on concentration in the numerator and denominator. It is usually used with heterogeneous adsorption surfaces. The equation (1.32) describes Koble-Corrigan isotherm equation:

$$q_e = \frac{A_{KC} C_e^P}{1 + B_{KC} C_e^P} \tag{1.32}$$

Where A_k is Koble-Corrigan's isotherm constant, B_k is Koble-Corrigan's isotherm constant, and P is Koble-Corrigan's isotherm constant.

x) Sips adsorption isotherm

The Sips isotherm is a combined form of Langmuir and Freundlich models (Amrhar et al., 2015). At low adsorbate concentrations, this model is reduced effectively to the Freundlich isotherm and did not obey to the Henry's law. At high adsorbate concentrations, it predicts a monolayer sorption

capacity which is characteristic of the Langmuir isotherm. The Sips isotherm is a combination of the Langmuir and Freundlich isotherms and can be derived using either equilibrium or thermodynamic approach. The model can be written as the following:

$$q_e = \frac{Q_{max} b_s C_e^{1/n}}{\left(1 + K_s C_e^{1/n}\right)} \tag{1.33}$$

Where, Q_{max} (mg/g) is the sips maximum adsorption capacity, K_S (l/g) is the Sips model isotherm constant, and *1/n* is the sips model exponent. Where n is described as the surface heterogeneity and if it equals unity, the Sips isotherm returns to the Langmuir isotherm and predicts homogeneous adsorption. On the other hand, deviation of n value from the unity indicates heterogeneous surface. Alternatively, as either C_e or K_S approaches 0, this isotherm reduces to the Freundlich isotherm. This model is suitable for predicting adsorption on heterogeneous surfaces, thereby avoiding the limitation of increased adsorbate concentration normally associated with the Freundlich model. Therefore at low adsorbate concentration this model reduces to the Freundlich model, but at high concentration of adsorbate, it predicts the Langmuir model (monolayer adsorption). The parameters of the Sips isotherm model are pH, temperature, and concentration dependent and isotherm constants differ by linearization and nonlinear regression.

xi) Khan adsorption isotherm

The Khan Isotherm model is a general model for adsorption of adsorbate from pure dilute equations solutions (Ayawei et al., 2017). This isotherm model is expressed as follows

$$q_e = \frac{Q_{max} b_k C_e}{(1 + b_k C_e)^{a_k}} \tag{1.34}$$

Where a_k is Khan isotherm model exponent, b_k is Khan isotherm model constant, and Q_{max} is Khan isotherm maximum adsorption capacity (mg/g). Nonlinear methods have been applied by several researchers to obtain the Khan isotherm model parameters.

xii)Toth adsorption isotherm

The Toth isotherm (equation 1.35) is derived from the potential theory, and it is applicable for heterogeneous adsorption. This model assumes a quasi-Gaussian energy distribution, where most sites have sorption energy less than the mean value. The Toth isotherm (Srenscek-Nazzal et al., 2015) exponent is related to surface heterogeneity, usually less than or equal to unity. If t is equal to the unit this suggests that the process occurs on a homogenous surface. In the Toth equation is obvious that for t = 1 this isotherm reduces to the Langmuir sorption isotherm.

$$q_e = \frac{Q_t K_t C_e}{(1 + (K_t C_e)^t)^{1/t}} \tag{1.35}$$

Where, Q_t, K_t, and t are the Toth isotherm constants that could be written as a function of temperature.

xiii) Redlich-Peterson isotherm

Redlich-Peterson equation included three adjustable parameters into an empirical isotherm (Kumara et al., 2014). This equation is widely used as a compromise between Langmuir and Freundlich systems. The adsorption mechanism is unique and does not follow ideal monolayer adsorption characteristics. The equation for this model is

$$q_e = \frac{AC_e}{1 + BC_e^g} \tag{1.36}$$

In Redlich-Peterson's isotherm, A (L/g) and B $(L/mg)^g$ are Redlich-Peterson constants with g as heterogeneity factor. When the value of g is equal to 1, the above equation is reduced to the Langmuir isotherm, while it reduced to a Freundlich isotherm, in case the value of the parameter BCe^g is much bigger than 1. The ratio of A/B indicates the adsorption capacity. However, the accuracy of these interpretations strongly depends on the fitting method.

Generally, adsorption model parameters are obtained by the linear method due to the simple method used in the estimation. But linearization add to a specific deviation in the estimated data values of curved functions due to the inherent bias resulting from linearization. The optimization procedure depends on the selection of an error function, in order to fit experimental equilibrium data to the isotherm and kinetics models (Ho et al., 2005). In this study, three non-linear error functions were examined and model fitting was done using 'Solver', an add-in available in Microsoft Excel 2013 (Microsoft Corporation, USA). The sum of squared errors (SSE) was chosen as the objective function to be minimized. The best model was decided as the one having the least Residual Root Mean Square Error (RMSE) value and average relative error (ARE), in addition to coefficient of determination (R^2). The error functions employed were as follows:

$$SSE = \sum_{i=1}^{n} \left[q_{exp} - q_{model}\right]^2 \tag{1.37}$$

$$RMSE = \sqrt{\frac{1}{n-1}\sum_{i=1}^{n} \left(q_{exp} - q_{model}\right)^2} \tag{1.38}$$

$$ARE = \frac{100}{n}\sum_{i=1}^{n} \left|\frac{q_{exp} - q_{cal}}{q_{exp}}\right| i \tag{1.39}$$

Where, q_{exp} and q_{cal} dye uptake values observed experimentally and calculated using isotherm model, respectively.

1.2.3.3 Adsorption experiment

The amount of adsorbate adsorbed on polymer adsorbent was calculated based on the difference of dye concentrations in aqueous solution before and after adsorption experiment according to Eq. (1.40):

$$q_t = \frac{(C_o - C_t) \times V}{m} \tag{1.40}$$

Where, q_t is the amount of adsorbate adsorbed per unit weight of adsorbent (mg/g) at time t, C_o and C_t are the concentrations of adsorbate (mg/L) at initial time and at time t, respectively, V is the initial volume of solution (L) and m is the mass of adsorbent (g). When t is equal to the equilibrium time, $C_t = C_e$, $q_t = q_e$, then the amount of adsorbate adsorbed at equilibrium was calculated using the same eq. (1.40).

The removal percentage of mercury ions from aqueous solutions was calculated as follows:

$$Removal(\%) = \frac{(C_o - C_t)}{C_o} \times 100 \tag{1.41}$$

1.2.3.4 Desorption experiment

Desorption amount was calculated using eq. (1.42):

$$Desorption(\%) = \frac{(C_{des} \times V_{des})}{(C_o - C_e) \times V_{ads}} \times 100 \tag{1.42}$$

Where, V_{des} is the volume of desorbent used (50 mL), C_{des} is the final concentration of adsorbate in solution after desorption (mg/L), C_e is equilibrium adsorbate concentration after adsorption (mg/L), C_o is the initial adsorbate concentration before adsorption (mg/L) and V_{ads} is the volume of adsorbate solution used for adsorption experiment.

1.2.4 Knowledge gap for the adsorption of azo dyes removal and heavy metals from literature review

The literature review suggested that the adsorption of anionic azo dyes and heavy metals was the most sort after physicochemical technology, an important option in the integrated approach to waste water treatment. Hence, there is an imperative need to revise its effectiveness, efficiency, economic and environmentally safe startegies which minimize the azo dyes and heavy metal ion concentration from toxic to safe limits in environment. The effectiveness of the adsorption process for removal of pollutants strongly depends on the adsorbent used. Several commercially available adsorbents have high adsorption capability such as activated carbon. However, the main obstacles to using activated carbon as the adsorbent for wastewater treatment is its price. Therefore, there is a need to find an adsorbent that easily available, cost effective and highly efficient. In this regard polymeric adsorbents have gain much recognition in recent times due to its high efficiency and ability for regeneration and reuse for multiple times. Functional groups which are responsible for binding metal ions are amines, carboxylates, ethers etc. Coating silica, jute fiber, etc., with various polyamines is a cheap (one step) and ecological method. The use of an inorganic matrix, onto which a variety of functional groups can be chemically immobilized, has significant advantage over conventional organic supports. Advantages include a high surface area to enhance adsorption capacity, and greater physical and chemical robustness to withstand a variety of harsh environments alongwith the ease of regeneration has made the functionalized polymer an alternative adsorbents for removal of pollutants from wastewater treatment. Kumar et al., 2007a,b, 2008, 2009 successfully reported the removal of copper and chromium (trivalent and hexavalent) from aqueous solution by an amine based resinous polymer coated on silica gel (AFC-silica) and polyaniline coated on jute fiber (PANI-jute). These amine based polymers showed moderate

removal efficiency for Cu(II), Cr(III) and Cr(VI) adsorption from aqueous solution. But the polymers were resinous in nature which required support material for easy interaction between metal ions and the polymers. But the addition of support material makes the polymer synthesis more complex and during desorption process chances of detachment of the polymer from support material may take place.

It was also observed that limited research work was done on the supportless amine based polymers used as adsorbents. Therefore, effort was made to synthesize a supportless amine based polymer which could remove heavy metals from very dilute solution.

1.3 Objective of the research work

Based on the knowledge gap observed from literature review the present thesis work emphasis was given to synthesize a cost-effective modified amine based polymer adsorbent without using any supporting material to remove heavy metals from very dilute solution. Following are the main objective of the thesis work:

- Application of amine coated polymer (AFC-silica and PANI-jute) in the removal of anionic dyes from aqueous solution.
- Synthesis of amine based polymer of less resinous nature, that can be used without any supporting material and perform complete characterization of the polymer.
- Adsorption study with supportless polymer using toxic metals of dilute concentration and to check whether discharge limit can be met.
- Adsorption kinetics and isotherm studies with supportless polymer and dilute metals solution and to check the versatility of the supportless polymer on metal adsorption in multicomponent system.

CHAPTER 2

Adsorption of anionic azo dyes

2.1 Introduction

In textile industries, anionic azo dyes are largely used for high solubility, low cost and bright color and they remain unaffected in conventional treatment system (Moussavi and Mahmoudi, 2009; Liu et al., 2017;Chen et al., 2017; Konicki et al., 2017; Long et al., 2017). Anionic azo dyes consists of azo group (-N=N-) and are highly water soluble and give the dye molecule a negative charge. Their water solubility is due to sulphonic groups (SO_3^-) usually present as sodium salts and are characterized by highly toxic and recalcitrant organic molecules. Several amine based polymeric compounds were used for the removal of acid dyes. Amine based natural compounds like chitosan and crosslinked chitosan (Saha et al., 2005), ammonium chitosan derivative (Elwakeel et al., 2012) and synthetic polymers like MCM-41, polyaniline (PANI) were used for removals of sulfonated reactive and acid dyes (Donia et al., 2009; Mahanta et al., 2009; Ahmad and Kumar, 2010). In the present chapter two amine based polymers namely - AFC coated silica gel (AFC-silica), a chain polymer with amine group throughout the chain length whereas polyaniline coated on jute fiber (PANI-jute), another short chain polymer with terminal amine (–NH_2) group have been considered for the adsorption behavior on the removal of acid orange (AO8), acid violet 7 (AV7) and congo red (CR) as model acid azo dyes.

2.2 Materials

Commercial grade aniline ($C_6H_5NH_2$) was purified by distilling over KOH pellets at boiling point temperature of aniline (180°C). Analytical grade formaldehyde (HCHO) 37% v/v, isopropanol (C_3H_8O), NaOH pellets and concentrated HCl, H_2SO_4, HNO_3, ammonium peroxydisulfate [$(NH_4)_2S_2O_8$] and 1,4- phenylenediamine were used as received. Column chromatographic silica

gel (60–120 mesh) purchased from Merck was used as received. AO8, AV7 and CR dyes were purchased from Sigma-Aldrich, Bangalore and used as received. Both AO8 and AV7dyes were in powder form and sulfonated monoazo dyes whereas CR dye is a diazo dye. The physico-chemical properties of AO8, AV7 and CR dye is given in Table 2.1 and structure of dyes in Figure 2.1a.

Table 2.1: Physicochemical properties of AO8, AV7 and CR dye

Properties	AO8 dye	AV7 dye	CR dye
C.I. no.	15575	18055	22102
Characteristics	Anionic mono-azo dye, water soluble, red-orange color, contains one sulfonate group (SO_3^-).	Anionic mono-azo dye, water soluble, violet in color, contain two sulfonate group (SO_3^-)	Anionic di-azo dye, water soluble better in organic solvent, red in color, contain two sulfonate group (SO_3^-)
Formula	$C_{17}H_{13}N_2NaO_4S$	$C_{20}H_{16}N_4Na2O_9S$	$C_{32}H_{22}N_6Na_2O_6S_2$
M.W (g/mol)	364.35	566.47	696.66
λ_{max}	490 nm	520 nm	497 nm
Applications	Used for wool, silk, cotton, etc. dyeing	Used for wool, silk, cotton, paper, leather dyeing	Used to stain microscopic preparates, especially as a cytoplasm and erythrocyte stain, serve as acid-base indicator
Causes	Allergic dermatitis, skin irritation, carcinogen and mutagen	Genotoxic azo dye, harmful by ingestion, mutagenicity and carcinogenicity	Causes allergic reaction, induces drowsiness and respiratory problems, gastrointestinal irritant

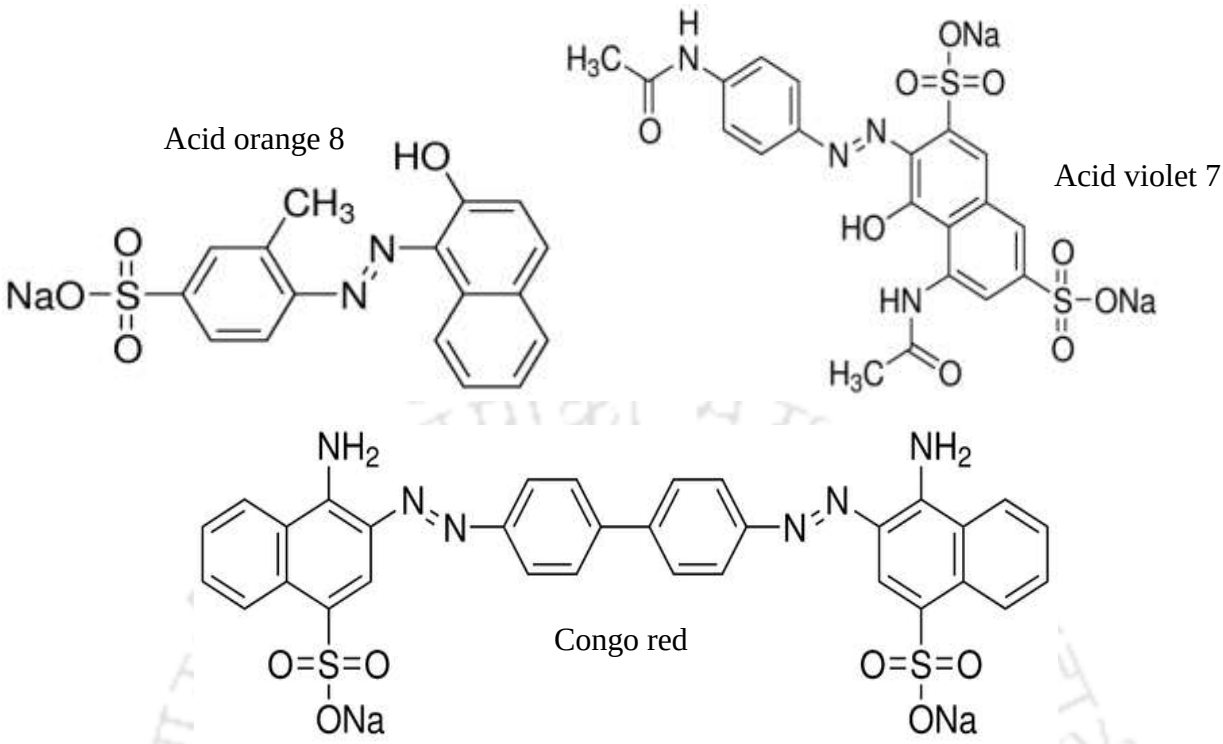

Figure 2.1a: Chemical structure of anionic azo dyes

2.2.1 Synthesis of AFC coated silica gel

AFC was synthesized by reacting formaldehyde (HCHO) with aniline ($C_6H_5NH_2$). Detailed procedure is given in previous published literatures (Kumar et al. 2007). In a 100 mL beaker, 10 mL of 37% formaldehyde (123 mmol) was added slowly to a mixture of 18.6 g of aniline (200 mmol) and 6 mL of concentrated HCl and kept in the water bath at 80 °C for 2 h with intermittent stirring. Synthesis scheme is shown in Figure 2.1b. Then it was neutralized with 8 mL of 30% NaOH and kept in the water bath for another 1 h at 60 °C temperature. Thereafter it was removed from the water bath and kept at room temperature for 12 h, then washed for three to four times with warm water to remove residual aniline and formaldehyde and dried by applying vacuum in a vacuum desiccator. AFC synthesized was of yellow color resinous material. In 25 mL methanol (CH_3OH) solution, 25–30 g resinous AFC polymer was dissolved at 40–45°C with stirring. Experimentally, it was observed that maximum 25 g of silica could be added in methanol–AFC

solution to completely soak the silica gel and permit mixing. After addition of 25 g silica gel in methanol – AFC mixture, manual stirring was applied for 5 min. Then excess liquid was removed by filtering and AFC coated on silica gel was air dried for 6 h. This AFC coated silica gel (Figure 2.1c) was used as the adsorbent for removal of acid dyes.

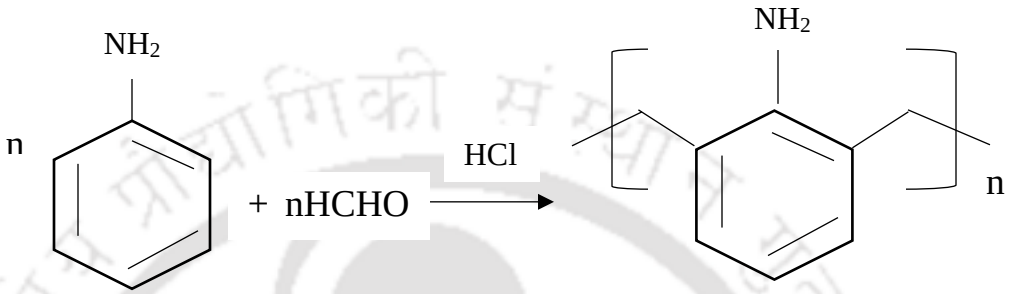

Figure 2.1b: Scheme synthesis of AFC-silica (Kumar et al., 2007)

Figure 2.1c: AFC coated silica gel

2.2.2 Synthesis of PANI coated jute fiber

Polyaniline was synthesized by oxidation of aniline ($C_6H_5NH_2$) in presence of 1,4-phenylenediamine, a chain terminator in acidic aqueous medium in presence of an oxidant, ammonium peroxydisulfate [$(NH_4)_2S_2O_8$] (Kumar et al., 2008). The synthesis scheme of PANI is shown in Figure 2.2a. Aniline (2.00 g, 21.5 mmol) and 1,4-phenylenediamine (0.330 g, 3.05 mmol) were dissolved in 66mL of 1M HCl (aq.). The mixture was cooled in iced bath to 0–5°C followed

by addition of 5g jute fibers and stirred for 5 min. The polymerization started by introduction of pre-cooled (5°C) solution of ammonium peroxydisulfate (1.62 g, 7.10 mmol) in 16mL of 1M HCl (aq.). The reaction mixture was kept at 5°C for 65 min and then kept for overnight at room temperature. Then the liquid was decanted from PANI-jute fiber. To ensure complete deprotonation of PANI-jute, alkali treatment was given by soaking PANI-jute in 1M NH_4OH for 5 min. The products were then washed with distilled water to adjust the solution to neutral pH. Finally, the blue black colored PANI-jute fiber was dried at 40°C in the oven (Figure 2.2b).

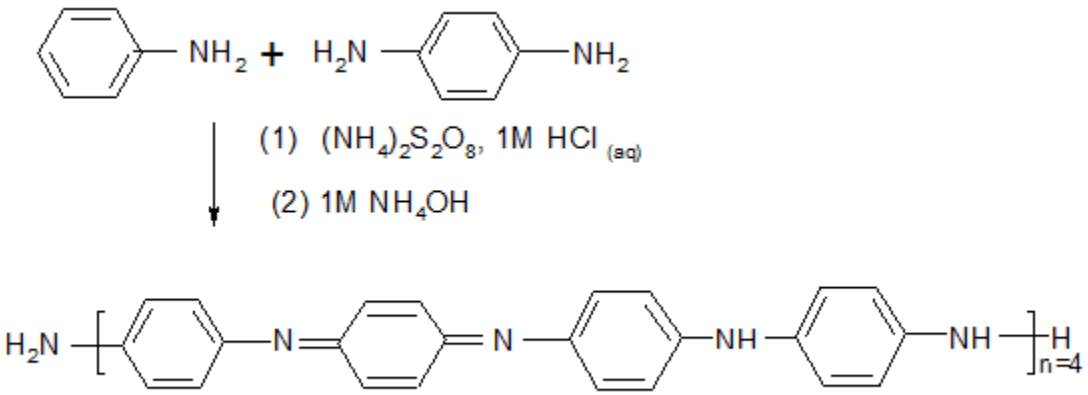

Figure 2.2a: Scheme synthesis of PANI coated jute fiber (Kumar et al., 2008)

Figure 2.2b: PANI coated jute polymer

2.2.3 Adsorption experiment

Initial solution pH, dose of adsorbent, temperature and initial concentration of dye were variable parameters for this study. Working solutions were obtained by diluting the stock solution with distilled water to the desired concentration. All experiments were carried out with 250 mL of dye solution in 500 mL plastic bottles. Predetermined quantities of adsorbent were added to the bottles and initial solution pH was adjusted using 0.1/1N HCl/NaOH at desired value and mixing was achieved in the horizontal incubator shaker at 150 rpm and 37°C temperature kept for 12 h without pH control. Adsorbent dose was varied from 0.5 to 12 g/L. In temperature study, temperature was varied from 10 to 50°C with a known amount of adsorbent for 12 h. For kinetic study, AO8, AV7 and CR dye solution with adsorbent was kept in horizontal shaker in different bottles and after regular time interval, each bottle was withdrawn from the shaker. After the experiment, adsorbent was separated from dye solution using centrifuge at 1000 rpm and after filtration with filter paper the residual concentration of dye and final pH was estimated. The amount of dye adsorbed on AFC-silca was calculated based on the difference of dye concentrations in aqueous solution before and after adsorption experiment according to Eq. (1.40). All experiments were done at least two times and average value of residual dye concentration was used in this study.

2.2.4 Desorption experiment

Desorption study was done using dye loaded adsorbent polymer with different strengths of NaOH (0.05–0.5N) as desorbing agent. Desorbent volume was 50 mL in each case and desorption experiments were performed in a horizontal shaker at 150 rpm for 6 h. Then the samples were centrifuged and analyzed for dye concentration in desorbent solution. Desorption amount was calculated using Eq. (1.42):

2.2.5 Analytical procedure

Zero point charge of adsorbent was estimated using immersion technique as described by (Fiol and Villaescusa 2009). Characterization of AFC was carried out using FTIR (Perkin Elmer, PE-RXI), FESEM (Hitachi 5500 FESEM), Particle size analyzer (Mastersizer 2000, Malvern) and BET surface area analysis (Autosorb-IQ MP) and experimental analysis was carried out by UV-visible spectrophotometer (Varian, model cary 100), pH meter (Thermoscientific, Orion 3 star benchtop), Hot air oven (ICT, Kolkata, India), Shaking incubator (Model; Labtech, India), and Electronic balance (Model: AW320, SHIMZADU).

For scanning, the standard solutions of dyes having concentrations of 5, 10, 15, 20, 30 and 40 mg/L were prepared and scanned through UV-Visible spectrophotometer between 400 nm to 800 nm and the wavelength at which maximum absorbance was achieved was identified. The maximum wavelengths were 490, 520, 497 and 504 nm respectively for AO8, AV7, CR and mixed dye. Effect of solution pH on absorbance of dye was determined by adjusting pH of dye solution from 1 to 10 using dye solution of concentration 20 mg/L. Absorbance was measured at each pH at wavelength of maximum absorbance and solution pH at which maximum absorbance was achieved was determined. Calibration curve (given in Appendix 1) was prepared by dissolving known amount of dye powder in distilled water and pH of solution was adjusted at desired value and absorbance was measured at selected wavelength. The absorbance values were plotted against these known concentrations and linear absorbance curve (given in Appendix 1) was obtained with correlation coefficient of 0.99. For AO8 dye, absorbance was measured at pH 3-8, for AV7 it was achieved at pH 5-8, for CR and mixed dye, maximum absorbance was achieved at pH 6-11 and 6-10, respectively.

2.3 Results and discussions

2.3.1 Characterization of AFC coated silica gel and PANI coated jute fiber

Field emission scanning electron microscopy (FESEM) is a primary and important tool for characterizing the surface morphology as well as identifying the fundamental physical properties of the adsorbent surface. It is also very helpful in determining the particle shape, porosity and appropriate size distribution of the adsorbent. The FESEM image given in Figure 2.3a of AFC coated silica gel before adsorption shows that the functionalized polymer is characterized by a relatively unevenly distributed surface with certain microstructures.

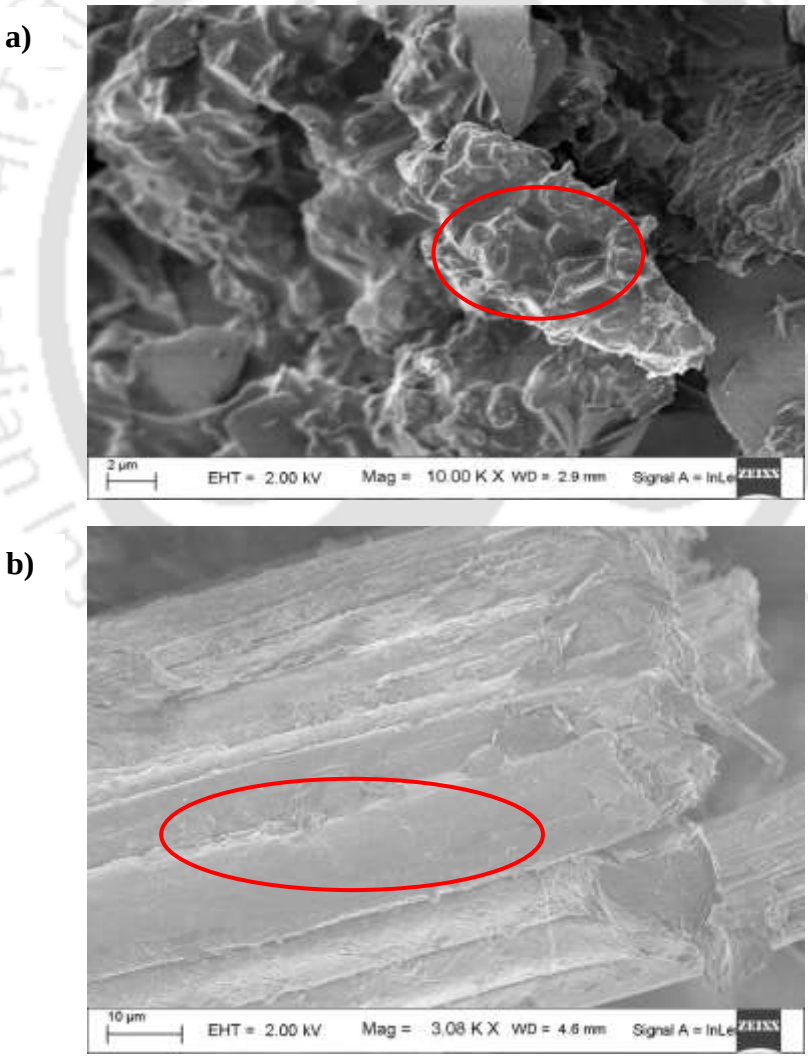

Figure 2.3: FESEM image of a) AFC coated silica gel and b) PANI coated jute fiber

Whereas the FESEM image of PANI-jute before adsorption given in Figure 2.3b suggested that the surface of the adsorbent consisted of a morphology that have almost uniformly distributed microstructures which are probably the functional groups attached to the coating materials mainly responsible for the adsorption of anionic dyes onto the surface of the amine based polymers. For further confirmation regarding the presence of functional groups in the polymer adsorbent, Fourier transform infrared spectrometer (FTIR) spectra of AFC-silica and PANI-jute polymer before and after adsorption of AO8, AV7 and CR dyes were performed and analyzed which is given in Figure 2.4a and b respectively. The FTIR spectra displayed a number of characteristic bands in the range 4000-400cm^{-1} were recorded before and after adsorption of anionic dyes (AO8, AV7 & CR dyes) with AFC coated silica gel and PAN coated jute fiber. In the case for AFC coated silica gel polymer before and after adsorption is given in Figure 2.4a. The broad peak at 3400–3500 and 1550 cm^{-1} were the characteristics peaks for NH_2 (Yang and Feng, 2010). The peaks at 500 and 1000 cm^{-1} are due to Si–O–Si asymmetric stretching vibration (Donia et al., 2009). After adsorption of dyes, the band at 3400–3500 and 1550 cm^{-1} diminished. After adsorption of the dyes (AO8, AV7 and CR dyes) the FTIR spectra showed similar characteristics as the AFC coated silica gel except for slight changes. The FTIR showed the characteristics peaks at 3300-3500 cm^{-1} suggested the presence of N-H group stretching, the peaks at 1626.32 cm^{-1}, 1650–1580 cm^{-1} due to N–H bend 1° amines and 910-665 cm^{-1} was due to N-H wag for 1°, 2° amines. For CR with AFC only the amine functional peaks were very prominent.

The peaks 3400.39 cm^{-1} are attributed to hydrogen bonded for normal polymeric OH stretch and aliphatic primary amine due to NH stretch, 1574 cm^{-1} attributed to secondary amine due to NH bend and 1170.34 cm^{-1} attributed to secondary or tertiary amine due to CN stretch. In case of PANI-jute adsorbent, the FTIR spectrum of the dyes (AO8, AV7 and CR dyes) before and after

adsorption indicates that the peaks have slightly shifted their position and the intensity has also got altered.

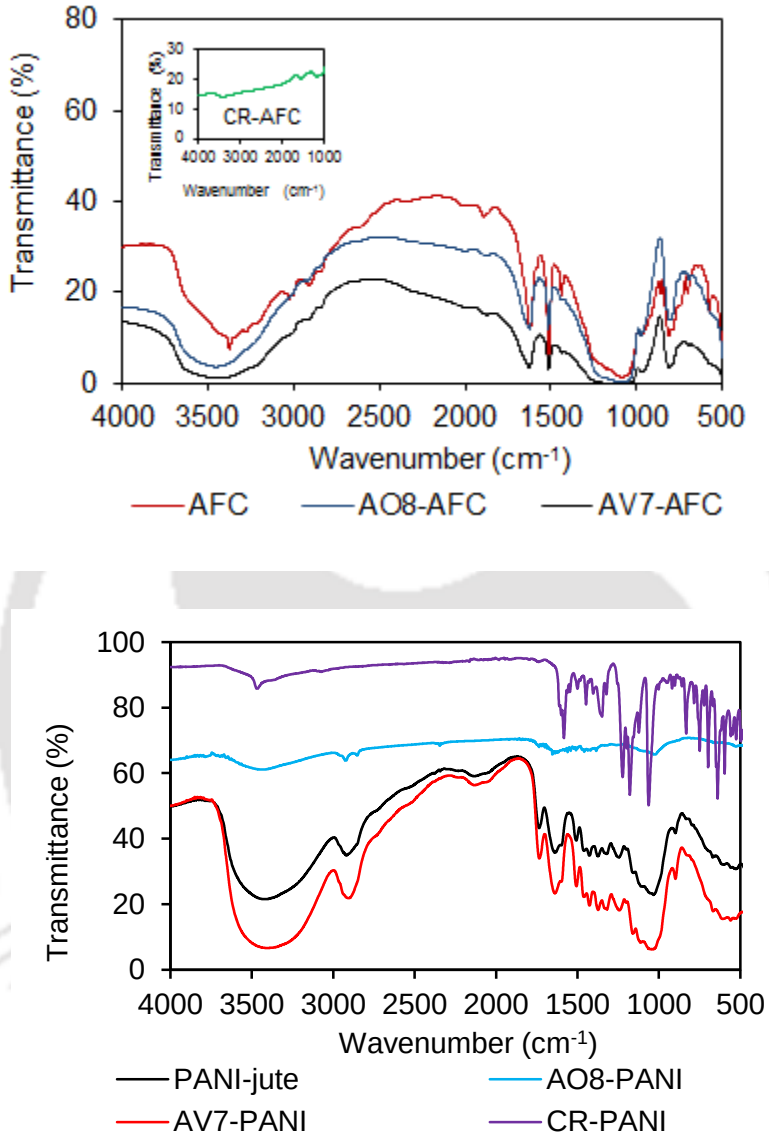

Figure 2.4: FTIR micrograph of a) AFC- silica and b) PANI-jute before and after adsorption of AO8, AV7 and CR dyes

The broad band at 3413.04 cm^{-1} and 2918.7cm^{-1} was due to stretching of NH_2 and NH group of polyaniline present in the adsorbent which a typical lignocellulosic material possess (Merlini et al., 2014). The peaks 1637.87 cm^{-1}, 1658.66 cm^{-1}, 1654.36 cm^{-1} attributed for the -NH_2 bending

vibration. Thus, both the polymer adsorbent – AFC coated silica and PANI coated jute fiber showed peak which were common characteristic peaks for amine based polymer. This indicates that the adsorption of the dyes occurred due to the amine functional groups present on the polymer adsorbent surface may be either electrostatic attraction or van der Waals forces. It should also be noted that the FTIR peaks of the adsorbed dyes showed prominent characteristics peaks of amine groups with good removal efficiency. BET analysis is also another very important parameter used in the characterization of an adsorbent because it gives a better knowledge about the adsorbent surface area, particle size distribution, porosity etc. During the adsorption–desorption cycle, capillary condensation in mesopores (larger than ~4 nm in diameter) occurs generally at a higher pressure of adsorbing gas then evaporation and thereby forming a hysteresis loop. The N_2 adsorption experiments were employed for the assessment of textural properties of the polymer adsorbent. On the basis of IUPAC classification, the pores of porous materials can be divided into micropore (size less than 2 nm), mesopore (size between 2 and 50 nm) and macropore (size greater than 50 nm). From Figure 2.5a shows the AFC coated silica gel adsorbent exhibits type-IV isotherm (Singh et al., 1985) with an apparent hysteresis loop of type H1, which suggested that the adsorbent comprises of mesoporous structures.

The specific surface area of AFC coated silica gel was estimated by the Brunauer- Emmett-Teller (BET) equation (Barret et al., 1951) and was found to be 20.850 m^2/g. The pore volume and pore radius of AFC was determined by analysis of the BJH pore size distribution curves was found to be 0.044 cc/g and pore diameter of 8.59 nm, suggesting mesoporous adsorbent. The other adsorbent – PANI coated jute fiber showed the same type of isotherm (type IV) which is typical of mesoporous materials (Figure 2.5a). PANI-jute polymer followed H3 hysteresis which is

usually observed for non- aggregates (loose assemblages) of plate-like particles forming slit-like pores.

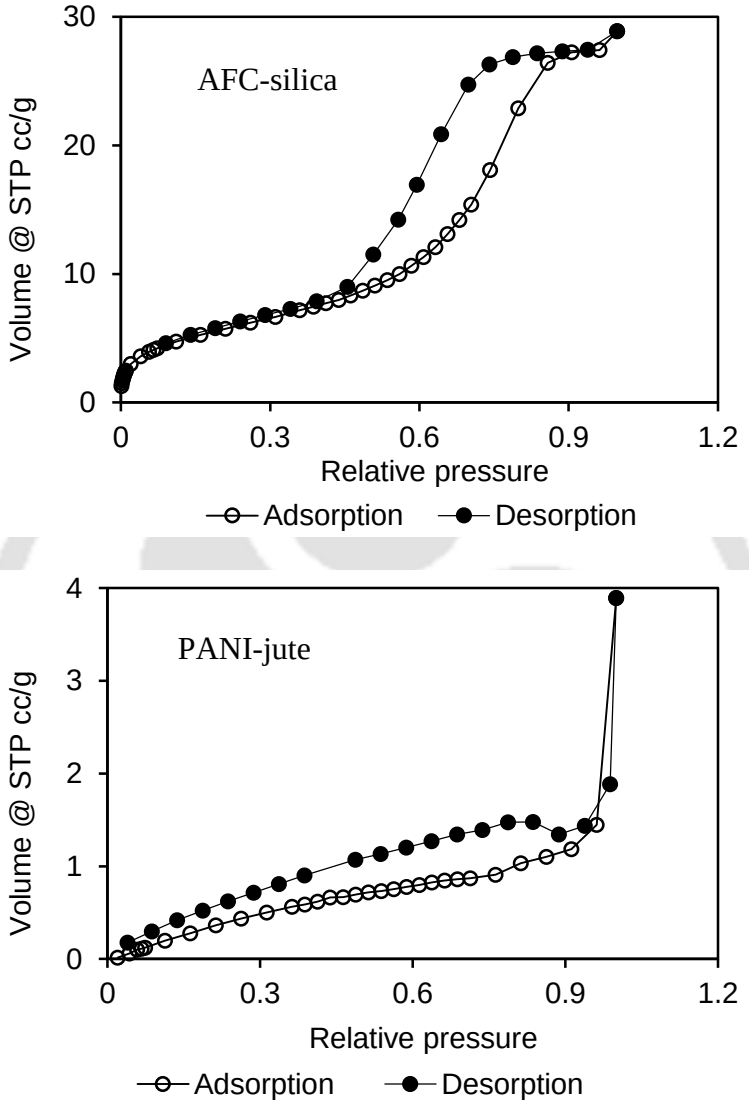

Figure 2.5a: N_2 adsorption-desorption isotherm of a) AFC-silica and b) PANI-jute

Similar type of isotherm was also observed by Fang et al., 2013 in the case of polyaniline/coconut shell–activated carbon composites. The N_2 sorption experiments employed for the assessment of textural properties of the adsorbents are given in Table 2.2.

Table 2.2: N_2 adsorption analysis

Adsorbent	BET surface area m^2/g	Total Pore volume (cc/g)	Average pore diameter (nm)
AFC coated silica gel	20.850	0.04477	8.58963
PANI coated jute fiber	2.738	0.006038	8.81921

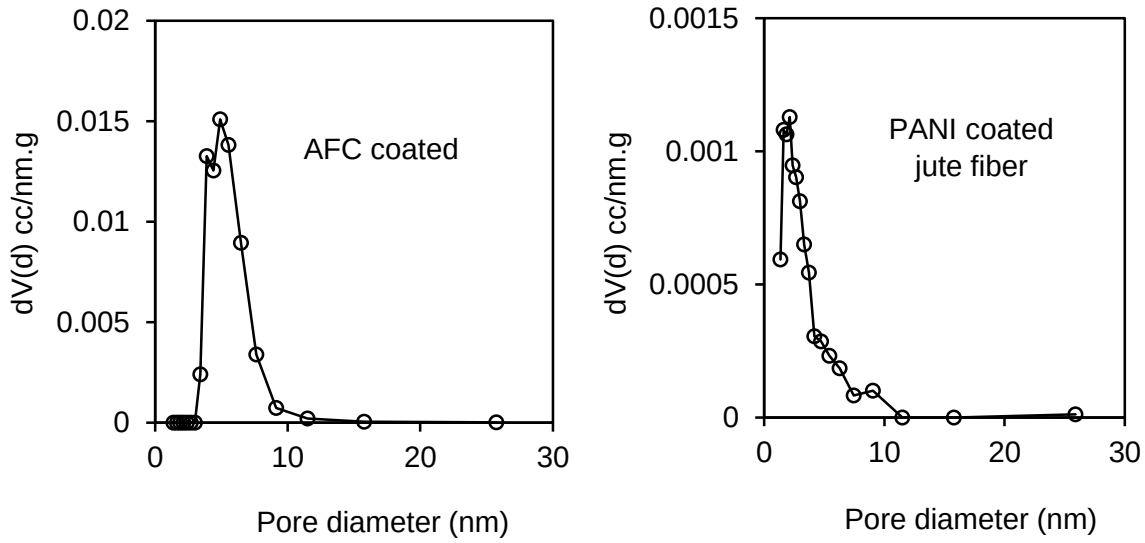

Figure 2.5b: Pore Size Distribution (PSD) of AFC coated silica gel and PANI coated jute fiber employing (BJH) analysis

From Figure 2.5b, pore volume distribution (BJH desorption) plot shows that both the polymer adsorbents exhibit a sharp pore size distribution with a maximum peak of 4.91 nm and 2.12 nm for AFC coated silica gel and PANI-jute respectively. Thus, the adsorbents contains mesoporous along with microporous structure.

The Particle size distribution is a mathematical function that defines the relative amounts of particles present, sorted according to size. Particle size distribution may be presented in

"cumulative" form in which the total of all sizes "retained" or "passed" by a single notional "sieve" is given for a range of size. In a Mavern Mastersizer, result analysis report of particle size analyzer the D50 is represented as D (0.50). D represents the diameter of powder particles and D50 means a cumulative 50 % point of dimeter (or 50 % pass particle size); D10 means a cumulative 10% point of dimeter; D50 is also called average particle size or median diameter; D (4,3) means volume mean diameter and D (3,2) means plane mean diameter. From Fig.2.6, the results obtained for AFC coated silica gel polymer adsorbent was found to be- D(0.1)-137.559µm, D(0.5) - 240.548µm and D(0.9) - 464.718µm for the particle size analysis based on the differential volume.

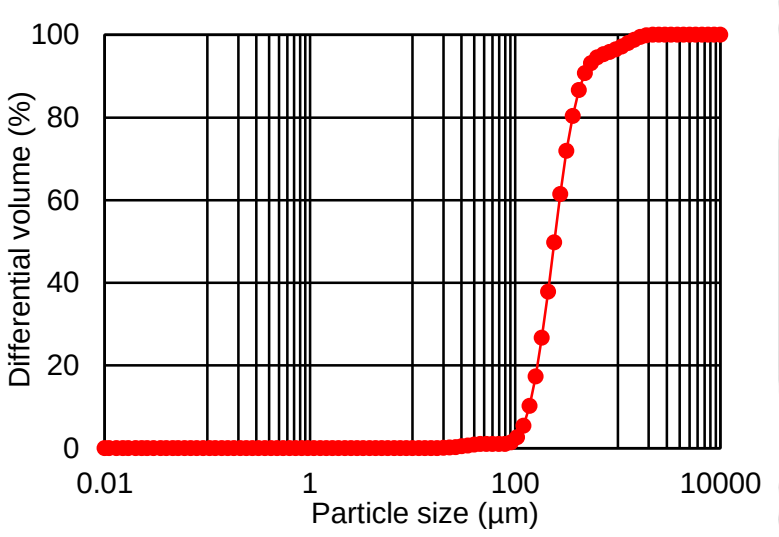

Figure 2.6: Particle size analyzer of AFC-silica

The size range was between 0.02 to 2000µm. The specific surface area was found to be 0.0281 m^2/g. The surface weighted mean D[3,2] was found to be 213.449µm whereas the volume weighted mean D[4,3] was found to be 306.632µm.

The determination and precision of surface characterization based on point of zero charge (pH_{zpc}) is an important factor used to describe the variable-charge surfaces well as very effective for adsorption (Appel et al., 2003; Kosmulski, 2002; Babić et al., 1999). The point of zero charge

(pH_{zpc}) is a concept relating to the phenomenon of adsorption, and it describes the condition when the electrical charge density on a surface is zero and in other terms the point of zero charge is the solution pH value where the net surface charge is zero. The knowledge of point of zero charge gives an idea on the ionization of functional groups and their interaction with any adsorbate in solution and also helps in understanding the surface chemistry and adsorption behavior versus pH of the aqueous medium. When, pH> pH_{pzc} the adsorbent surface is negatively charged and could interact with the adsorbate positive species and pH < pH_{pzc} the adsorbent surface is positively charged (Fiol et al., 2009). In immersion technique of pH_{zpc} determination, polymer dose of 25 g/L was kept for 24 h in 0.03 M KNO_3 solution and was adjusted at different pH values of 1–11 whereas the mass titration method was determined by varying the amount of polymer in the range 5–100 g/L in 0.03M KNO_3 solution for 24 h. The point of zero charge was determined and found out that the pH_{pzc} of the polymer adsorbent is given in Figure 2.7. The point of zero charge (pH_{zpc}) was determined from the change of pH. It can be seen that point of zero charge (pH_{zpc}) determined using immersion technique method was found to be pH 5.5 and by mass titration method was found to be pH 5.2 for AFC-silica whereas for PANI-jute it was at pH 5.2 and 5.6 respectively (Figure 2.7). It has been reported (Ingole et al., 2017; Gatabi et al., 2016), the adsorption of a positive charged adsorbate is favored when the pH of the solution is greater than the pH_{zpc} of the adsorbent, whereas the adsorption of negative charges, in turn, is favored at pH levels less than pH_{zpc}. Therefore, the adsorption of the anionic dyes is expected to be favored in solution the pH values less than the pH_{zpc} of the adsorbent.

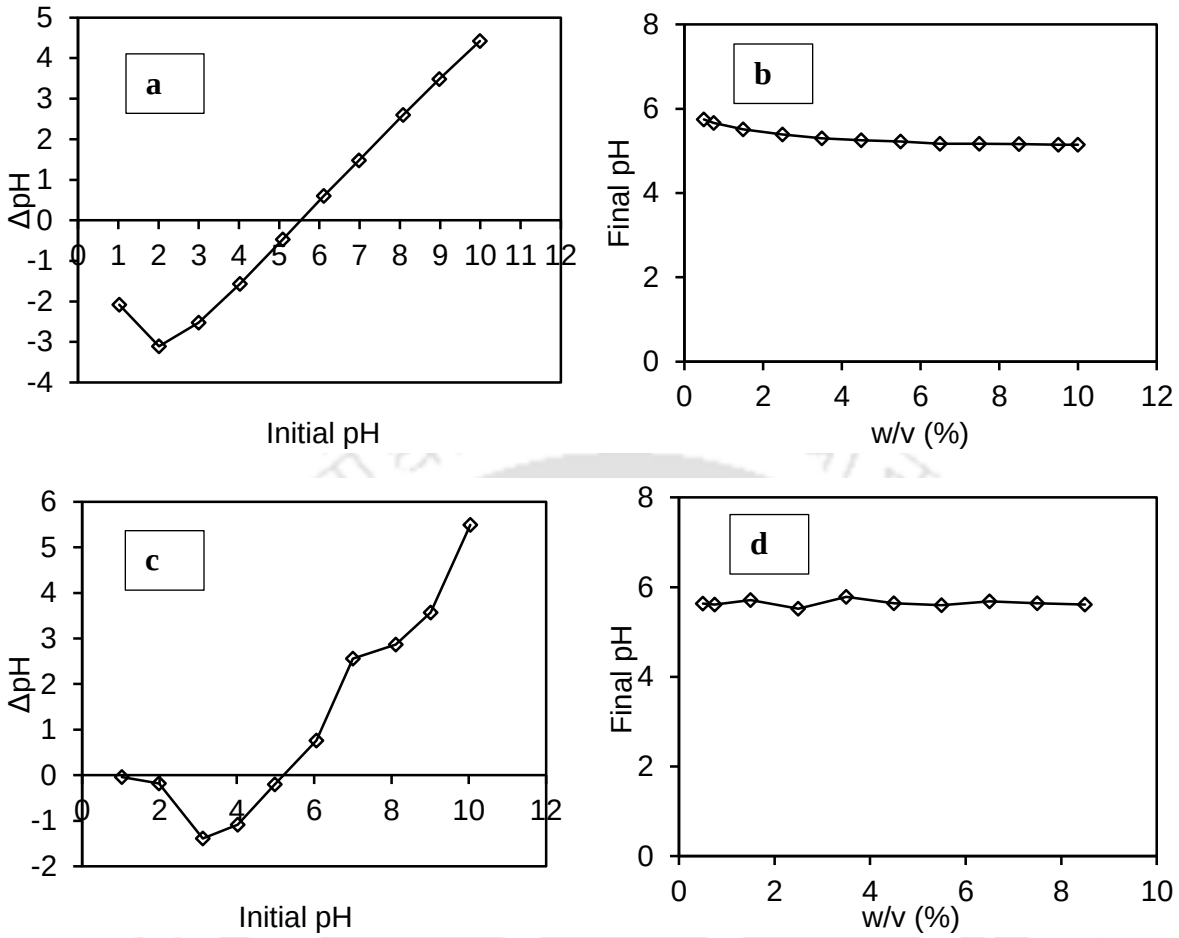

Figure 2.7: Point of zero charge of AFC-silica by a) immersion technique method, b) mass titration method and of PANI-jute by c) immersion technique, d) mass titration method

2.3.2 Removal of anionic dyes with AFC-silica

2.3.2.1 Effect of initial solution pH

The solution pH is an important parameter that determines the level of electrostatic or molecular interaction between the adsorbent and the adsorbate owing to the charge distribution on the materials (Chen et al., 2017; Zheng et al., 2018). The effect of initial solution pH was studied for three anionic azo dyes - acid orange 8 (AO8), acid violet 7 (AV7) and congo red (CR). The optimum pH for dye uptake was determined and results are shown in Figure 2.8. Acidic pH favored removals of AO8, AV7 and CR dyes. Maximum uptake was achieved at pH of 3 for AO8 and CR

while at pH of 2 for AV7 dye. The uncoated silica gel was used for the removal of AO8 and AV7 dye and it was observed that with 3 g/L dose of silica gel, dye removal was only 7% for AV7 and 8% for AO8 dyes. This indicates that removal of dyes mainly occurred by polymer. Final pH is shown in Fig. 2.8. Change in pH followed similar trends for all the three dyes. Increase in pH was observed, when initial pH was less than 6 and decreased when initial pH was higher than 6. The anionic dyes AO8 contains one sulfonic acid group (R-SO_3Na) whereas AV7 and CR contains two sulfonic groups(R-SO_3Na).

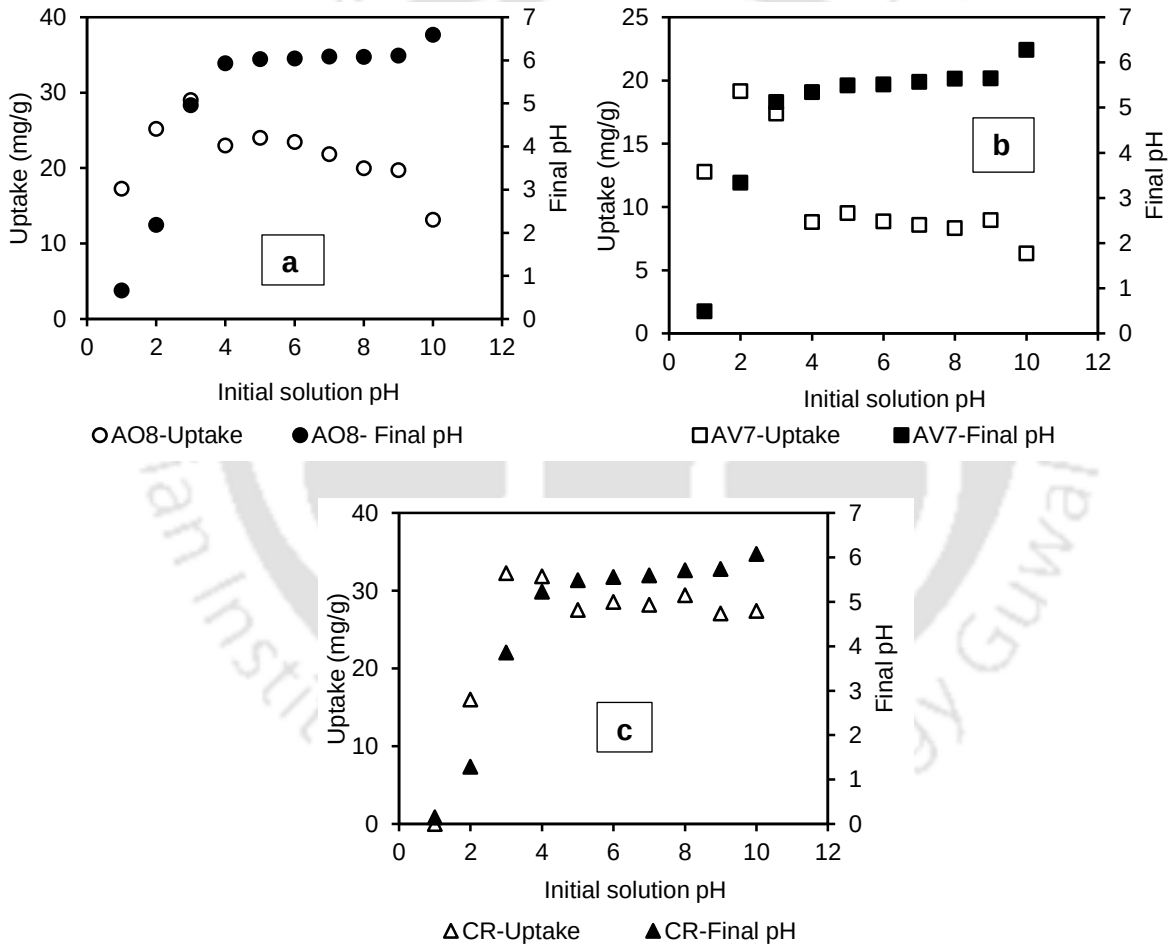

Figure 2.8: Effect of initial solution pH of a)AO8, b) AV7 and c) CR dyes with AFC-silica (C_o: 100 mg/L; dose: 3g/L; 12h; 150 rpm; 37°C)

In the aqueous solution, the sulfonate groups of the acid dyes ($R\text{-}SO_3Na$) were dissociated to sodium ions (Na^+) and converted to sulfonate anions (anionic dye ions) ($R\text{-}SO_3^-$). At acidic pH, the sulfonic groups of dye can be protonated to the neutral form ($R\text{-}SO_3H$); however, sulfonic groups exhibit negative charge even at higher acidic solutions due to their pKa values lower than zero (Konicki et al., 2017). Thus, in presence of excess protons and negatively charged sulfonic group or neutral form of sulfonic groups of dye are responsible of decrease in the adsorption of the dyes in pH 1-2 for AO8 and CR and pH 1 for AV7. Electrostatic attraction between amine (NH_3^+) and anionic dye molecule ($R\text{-}SO_3^-$) was responsible for higher uptakes of AO8 and CR at strong acidic pH (pH 3) whereas AV7 at pH 2. Many hydrogen ions were available in solution at lower pH and amine group ($–NH_2$) of AFC-silica accepted protons and remained in protonated form (NH_3^+) and solution pH increased. At neutral and alkaline pH, AFC-silica surface was in deprotonated form ($–NH_2$) and electrostatic attraction and dye uptake decreased. The pH_{zpc} of AFC-silica was observed as pH 5.5, suggesting that above this pH value, AFC-silica surface had negative charge and Figure 2.8 shows that some adsorption of dyes still occurred within pH range of 5.5–10. Electrostatic attraction could not be responsible for dye removals above pH 5.5. Hydrogen bond formation between nitrogen of amine group of polymers and OH group of dye, hydrophobic interaction between aromatic group of dye and polymers are other possible mechanisms of AO8 and AV7 dyes removal from solution (Figure 2.9). Similar mechanism for acid dye uptake by amine group of chitosan and crosslinked chitosan were suggested by previous researchers (Liu et al., 2015; Elwakeel et al., 2016a, b). Jin et al., 2015 found maximum removal of Acid red GR dye at pH 3.5. Chen et al. 2016 found maximum removal of anionic dyes (Alizarin red S, Methyl orange, Methyl blue, Sunset yellow FCF, Nuclear fast red, Alizarin green) with MPEI composites at pH 3.

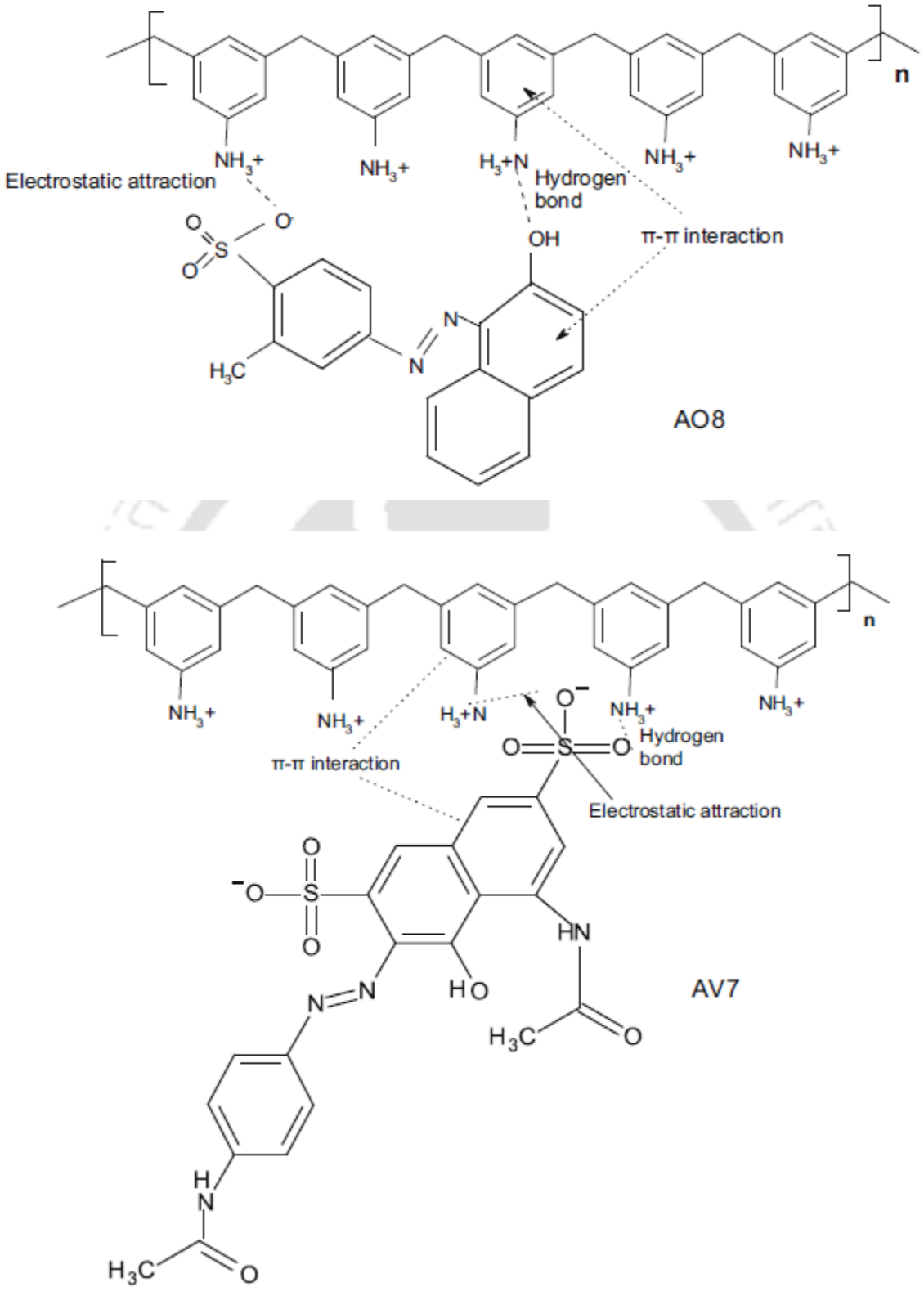

Figure 2.9: Scheme for the removal mechanism of AO8 and AV7 dye with AFC-silica

Pereira et al., 2017 also found the maximum removal of Remazol blue dye with CS and KSF-CTS composites at pH 3. Xu et al., 2016 during the adsorption of acid orange II with amino-functionalized magnetic nanoadsorbent, found maximum adsorption capacity at pH 2 and also by He et al. 2017 during adsorption of methyl orange by amine functionalized 3D porous organic polymer.

2.3.2.2 Effect of polymer dose

Dosage was varied from 0.5 to 12 g/L using 100 mg/L of AO8, AV7 and CR dyes at initial pH of pH 3. Initially with increase in adsorbent dose (0.5–12 g/L), removal of AO8 increased and the increase was substantial when the dose was increased from 0.5 to 2 mg/L (Figure 2.10). At adsorbent dose of 3.6 g/L, it achieved a plateau with 99% removal. In case of AV7 dye, removal increased up to a dose of 10 g/L with maximum removal of 75% whereas for CR dye removal increased from 96.87% to 99.42% with increase in the adsorbent dose. The maximum uptakes were 164 mg/g (0.45 mmol/g) for AO8, 68 mg/g (0.12 mmol/g) for AV7 and 226 mg/g (0.32mmol/g) for CR dye. Similar trend was observed for all the three dyes that the adsorption of dye increased with an increase in amount of adsorbent due to increased adsorbent surface area and availability of more adsorption sites. With the increase in adsorbent dose, the amount of dye adsorbed per unit mass of adsorbent is reduced, thus causing a decrease in q_e value (Bharathi et al. 2013). Ofomaja et al., 2007 reported that the increase in adsorbent dose at constant dye concentration and volume will lead to unsaturation of the adsorption sites through the adsorption process and secondly may be due to particulate interaction such as aggregation resulting from high adsorbent dose. Velmurugan et al., 2016 also reported similar observation during the removal of anionic dye congo red dye using amine-mesoporous hollow shells prepared from corn cob silica. Munagapati et al., 2017 during congo red dye adsorption using calcium alginate beads impregnated

with nano-goethite where he found that decrease in adsorption capacity with increasing adsorbent dosage and Zhang et al., 2018 during the adsorption of congo red dye from aqueous solution using ZnO-modified SiO_2 nanospheres with rough surfaces.

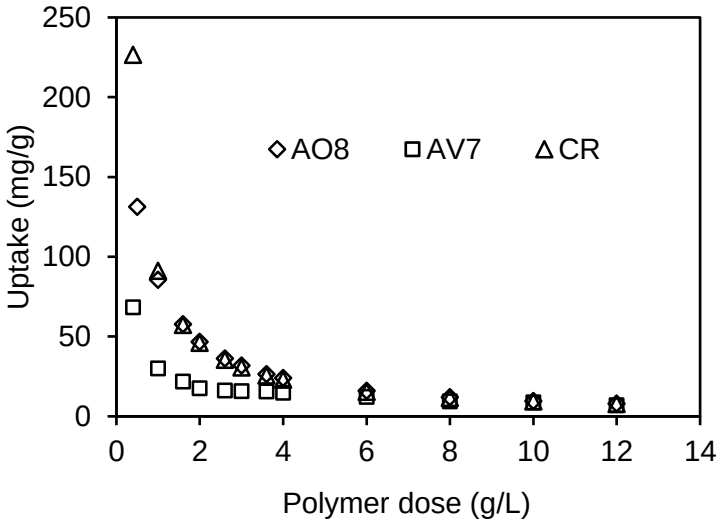

Figure 2.10: Effect of AFC-silica dose on dye uptake

2.3.2.3 Adsorption isotherm

The adsorption isotherm is defined as the relationship between the amount of substance adsorbed at constant temperature and its concentration in the equilibrium solution. Isotherm plots (q_e vs C_e) are shown in Figure 2.11. Isotherm shapes were convex type for AO8 dye whereas isotherm shapes was concave type for AV7 and CR dyes.

Based on isotherm classification provided by Giles et al., (1974a), AO8 adsorption on AFC-silica followed L2 type isotherm and based on another classification of IUPAC (Sing et al., 1985), AO8 isotherm was of Type I whereas for AV7 and CR adsorption on AFC-silica followed S1 type isotherm and based on another classification of IUPAC (Sing et al., 1985), AV7 and CR was of Type III isotherm. This suggest adsorption of solute on the adsorbent proceeds until a monolayer is established, with the formation of more than one layer not being possible (Al-Degs et al., 2007)

in case of AO8 whereas for AV7 and CR suggests that the adsorbate molecules tending to be adsorbed in rows or clusters (Terangpi et al., 2018).

Several other isotherm models were used to explain the behavior of dyes on AFC-silica polymer. Isotherm parameters were determined using nonlinear regression and experimental isotherm data were compared with modelled data in a plot. Isotherm parameters are given in Table 2.3. In Figure 2.11, experimental and modeled isotherm plots are shown for AO8 dye, both Langmuir and Freundlich models provided R^2 value of 0.99 was obtained. Adsorption isotherm of AV7 dye showed an upward curvature. Langmuir and Temkin models were unable to fit experimental data with low R^2 value (Table 2.3). Previous researchers observed that for this type of isotherm, Freundlich, BET models fit experimental data better (Hinz, 2001; Girods et al., 2009). Similar observation was seen in case of CR dye.

Figure 2.11 shows that experimental data followed Langmuir model (dotted line) pretty well. Hinz, 2001 suggested that L type isotherm can be described by Langmuir model. It is evident that AO8 adsorption on AFC-silica can be best described by Langmuir model with maximum monolayer uptake of 252 mg/g and affinity constant of 0.054 L/mg. Adsorption isotherm of AV7 and CR dye showed an upward curvature. Langmuir, Freundlich and Temkin models were unable to fit experimental data with low R^2 value and high ARE value (Table 2.3). In case of AV7 (Figure 2.11a), the experimental isotherm data of AV7 dye followed both BET and Freundlich models. However, Table 2.3 shows that Freundlich model provided higher R^2 value than BET model. Also, BET isotherm provided exceptionally high Q_m value, than observed in this study. Since, AV7 adsorption on AFC-silica followed Freundlich isotherm, the adsorption was heterogeneous and multilayer. The slope in Freundlich model, 1/n, was higher than 1, suggesting cooperative adsorption of AV7 adsorption on AFC-silica. For CR dyes (Figure 2.11b and Table 2.3), the results

indicated BET isotherm was favorable with high correlation coefficient (R^2) and very well fitted by the equation. CR dye adsorption on AFC-silica can be best described by BET model with maximum monolayer capacity of 119.78 mg/g and affinity constant of 0.0399 L/mg. The isotherm constants and regression coefficient (R^2) were evaluated with nonlinear regression of isotherm models using solver Microsoft Excel 2013.

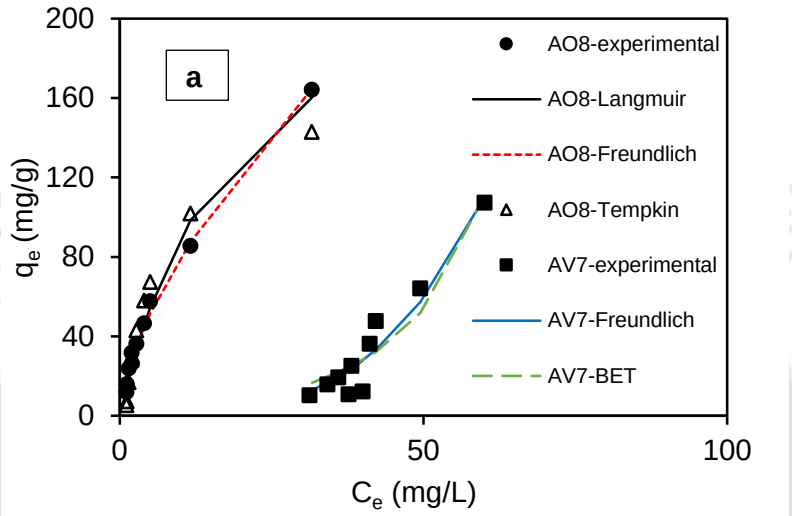

Figure 2.11a: Isotherm plots of AV7 and AO8 with AFC-silica

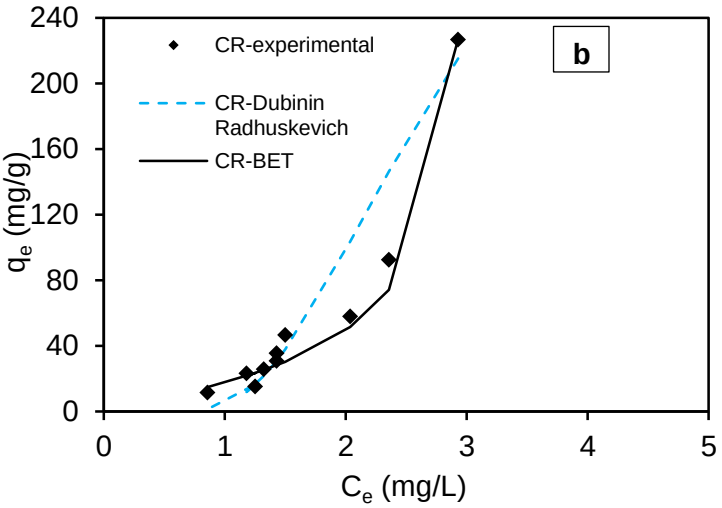

Figure 2.11b: Isotherm plots of CR dyes with AFC-silica

Table 2.3: Estimated isotherm parameters for adsorption of AO8, AV7 and CR dye on AFC-silica polymer at pH 3 and 37 °C

Isotherm models	Parameters	AO8	AV7	CR
Langmuir isotherm	Q_o (mg/g)	252.8	0.0002	-
	K_L (L/mg)	0.054	4392	-
	R_L	0.166	0.16	-
	R^2	0.99	0.92	-
	ARE(%)	11.02	95.94	-
Freundlich isotherm	1/n	1.58	3.37	-
	n	0.623	0.296	-
	K_f	18.58	0.0001	-
	R^2	0.99	0.96	-
	ARE(%)	13.33	8.43	-
Temkin isotherm	A_T (L/mg)	1.02	0.031	-
	b_T	61.32	16.24	-
	B	41.08	155.07	-
	R^2	0.97	0.93	-
	ARE(%)	25.34	103.35	-
Dubinin-Radhuskevich Isotherm	q_s (mg/g)	94.44	-	508.36
	K_{ad} (mol^2/kJ^2)	0.000001	-	0.000002
	E (kJ/mol)	0.707	-	0.5
	R^2	0.82	-	0.96
	ARE(%)	31.68	-	33.54
BET	Q_m (mg/g)	-	94.44	119.78
	C_s (mg/L)	-	18197.9	3.208
	B (L/mg)	-	0.0001	0.399
	R^2	-	0.85	0.99
	ARE(%)	-	92.6	20.83

2.3.2.4 Effect of temperature

Temperature was varied from 10 to 60 °C using initial dye concentration of 100 mg/L at initial pH of 3. With increase in temperature, uptake of AO8 increased, for AV7 decrease and CR increased initially but decreased at higher temperature (Figure 2.12). Thermodynamic parameters (given in Table 2.4) like enthalpy change (ΔH°) (J/mol) and entropy change (ΔS°) (J/mol K) were evaluated using van't Hoff equation (1.13) and the plot is shown in Figure 2.12 for all the three dyes.

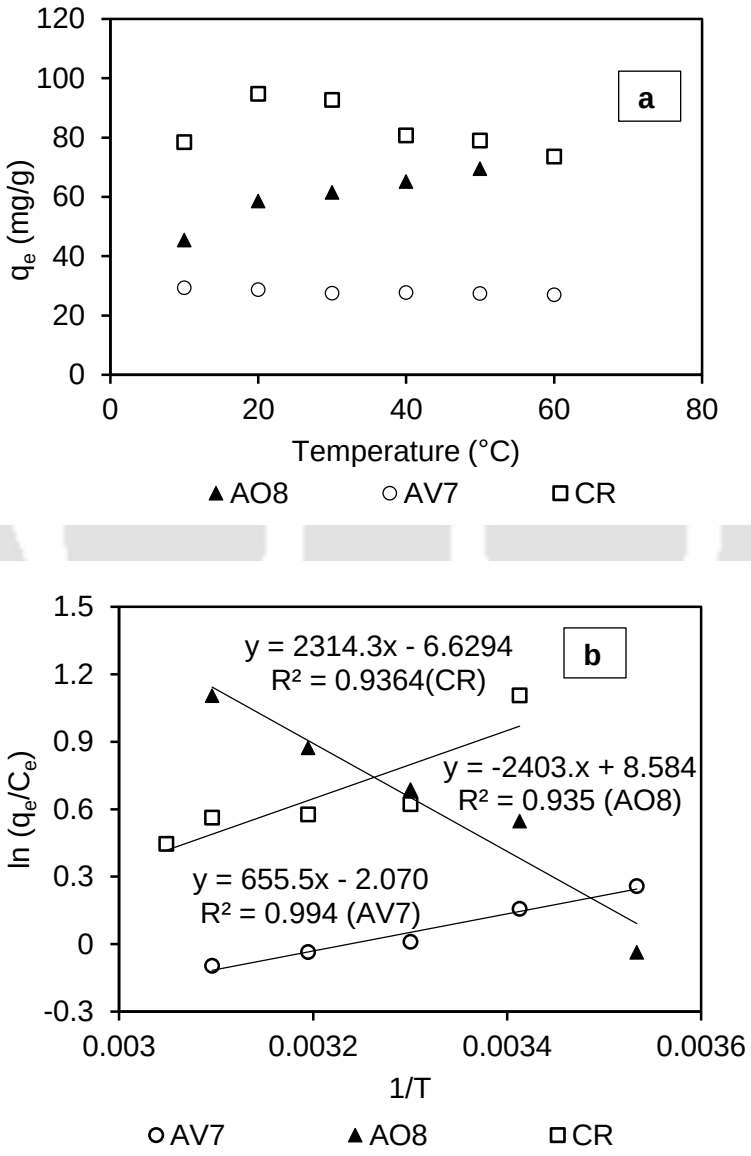

Figure 2.12: a) Effect of temperature on dye uptake and b) van't Hoff plot

AO8 removal was endothermic in nature. Enthalpy change was much higher for AO8 (19.97kJ/mol) and the heat of adsorption less than 20 kJ/mol suggests that AO8 adsorption processes were physical in nature (Liu et al., 2015). Entropy change was positive for AO8. Adsorption was spontaneous for AO8 for temperature ranging from 10 to 50°C.

Table 2.4: Thermodynamic parameters for AO8, AV7 and CR dyes on AFC-silica

Dyes	Temperature	ΔH°(kJ/mol)	ΔS° (J/mol K)	ΔG°(kJ/mol)	TΔS°(kJ/mol)
AO8	283	19.97	71.33	-0.21	20.18
	293			-0.92	20.90
	303			-1.64	21.61
	313			-2.35	22.32
	323			-3.06	23.39
AV7	283	-5.45	-17.21	-0.58	-4.87
	293			-0.40	-5.04
	303			-0.23	-5.21
	313			-0.063	-5.38
	323			0.108	-5.55
CR	283	-44.303	-126.913	-8.387	-35.916
	293			-7.118	-37.185
	303			-5.848	-38.454
	313			-4.579	-39.723
	323			-3.310	-40.992

AV7 was exothermic in nature for AFC-silica. Enthalpy change for AV7 and CR with AFC-silica was -5.45 kJ/mol and -44.3 kJ/mol respectively suggesting enthalpy governs the process. Similarly, for CR removal was exothermic in nature. Negative entropy change of AV7 and CR dye indicated decreased disorder at solid-solution interface. The heat of adsorption less than 20 kJ/mol suggests that AV7, AO8 and CR adsorption processes were physical in nature. Adsorption was spontaneous

for AO8 from 10 to 50 °C, for AV7 from 10 to 40 °C and for CR from 10 to 50 °C. Entropy change was positive for AO8 and negative for AV7 and CR dye.

2.3.2.5 Effect of initial concentration

The effect of initial dye concentration on dye adsorption capacity was investigated with respect to time at varying initial concentrations ranging from 20-150 mg/L for AO8 dye given in Figure 2.13a. At lower adsorbate concentration of 20 and 50 mg/L uptake was achieved at 6 mg/g and 14.6 mg/g respectively. But with the increase in initial dye concentration, the rate of uptakes was much higher value. Figure 2.13a shows that equilibrium time was 180 min for AO8 dye with initial concentration of 20-50 mg/L and increased to 600 min, at AO8 concentrations of 100 and 150 mg/L.

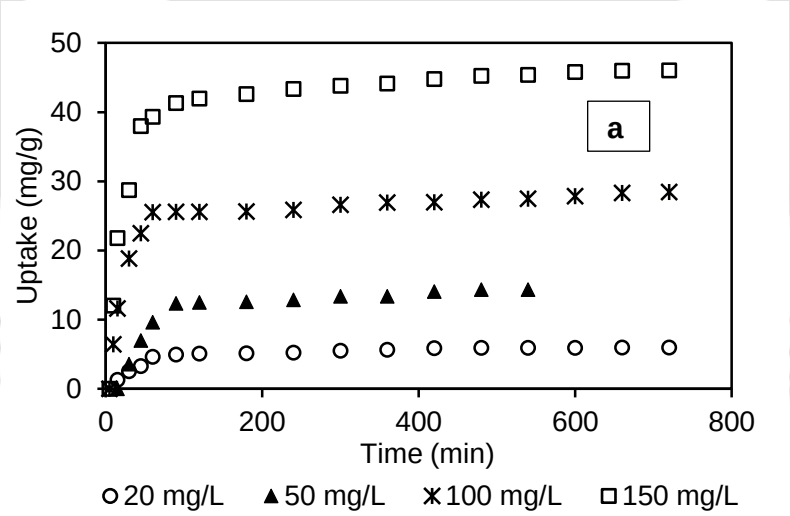

Figure 2.13a: Effect of initial concentration of AO8 with AFC-silica (C_o: 100 mg/L; pH 3; dose: 3g/L; 12h; 150 rpm; 37°C)

For AFC-silica adsorption of AV7, lower adsorbate concentration of 20 mg/L uptake was 5 mg/g whereas for 50 mg/L uptake was 14.2 mg/g. At higher initial concentration, for 100 mg/L uptake was 24.33 mg/g and for 200 mg/L uptake was 37.34 mg/g. Figure 2.13b shows the equilibrium

time 660–720 min at 20–50 mg/L concentration and increased to 1020 min at concentrations of 100 and 150 mg/L of AV7 with AFC-silica (Terangpi et al., 2018).

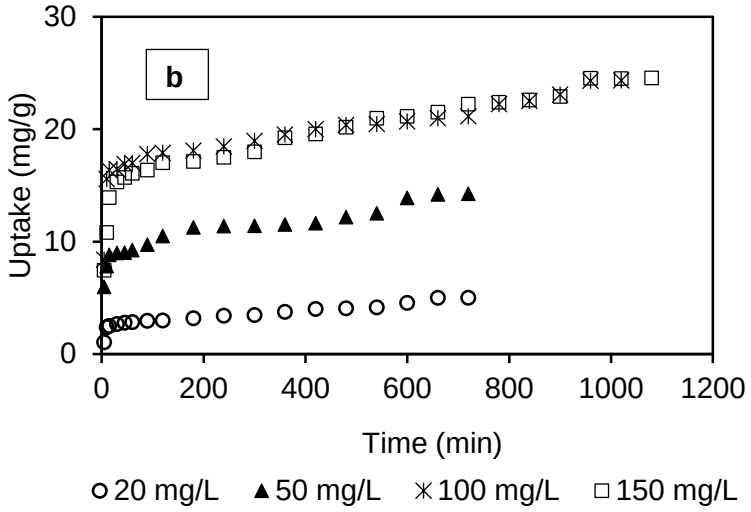

Figure 2.13b: Effect of initial concentration of AV7 with AFC-silica (C_o: 100 mg/L; pH 3; dose: 3g/L; 12h; 150 rpm; 37°C)

It was also observed that the adsorption of AO8 and AV7 onto AFC-silica was rapid in initial stages suggesting that adsorption takes place rapidly at the initial stage on the external surface of the adsorbent followed by a slower internal diffusion process, which may be the rate determining step. In addition, the fast adsorption at the initial stage also may be due to the fact that a large number of surface sites are available for adsorption but after a lapse of time, the remaining surface sites are difficult to be occupied. This creates a repulsive force between between the adsorbate onto the adsorbent surface and in bulk phase.

From the plot of time vs uptake (Figure 2.13) at varying concentrations showed that the rate of uptake (mg/g) increases with increase in initial concentration and after reaching equilibrium it becomes constant due to the driving force offered by the increased solute concentration which is sufficient enough to overcome the resistance to mass transfer between the solid and liquid phases.

Thus, the dye adsorption capacity increased with increase in initial dye concentration. This is due to the fact that high initial concentration enhances the driving force and thus in turn lowers the mass transfer resistance of the dye between the aqueous solution and the solid adsorbent. This results in higher adsorption efficiency. Similar observations of dye removal have been made by various researcher Fatiha et al., 2016 for methylene blue using natural clay; Naraghi et al., 2017 for acid orange 7 using Kenya tea pulps; Akazdam et al., 2017 using Resin Amberlite FPA-98; Magdalena et al., 2014 for acid orange using HDTMA-modified zeolite.

2.3.2.6 Adsorption kinetics

Adsorption kinetic study is very useful for predicting the rate of adsorption in order to obtain information for modelling the adsorption process system. There are several kinetic models available for analyzing experimental adsorption process – pseudo-first order, pseudo-second order, intraparticle diffusion and boyd model. The kinetic models were analyzed based on the regression coefficient (R^2).

From the Figure 2.14, it was observed that the plot of t/qt versus t gives a straight line for all the initial concentrations with high coefficient correlation (R^2) and the calculated and experimental q_e values match very well each other (Table 2.5) suggesting that the adsorption kinetic follows the pseudo-second order kinetic model and supports the assumption that the dye adsorption is due to chemisorption.

Intraparticle diffusion becomes the sole rate limiting step in adsorption, when intercept becomes zero. Plots are shown in Figure 2.15. It is evident that plots were straight lines but did not pass through origin, suggesting AO8 and AV7 adsorption on AFC-silica involved intraparticle diffusion, but it was not sole rate controlling step.

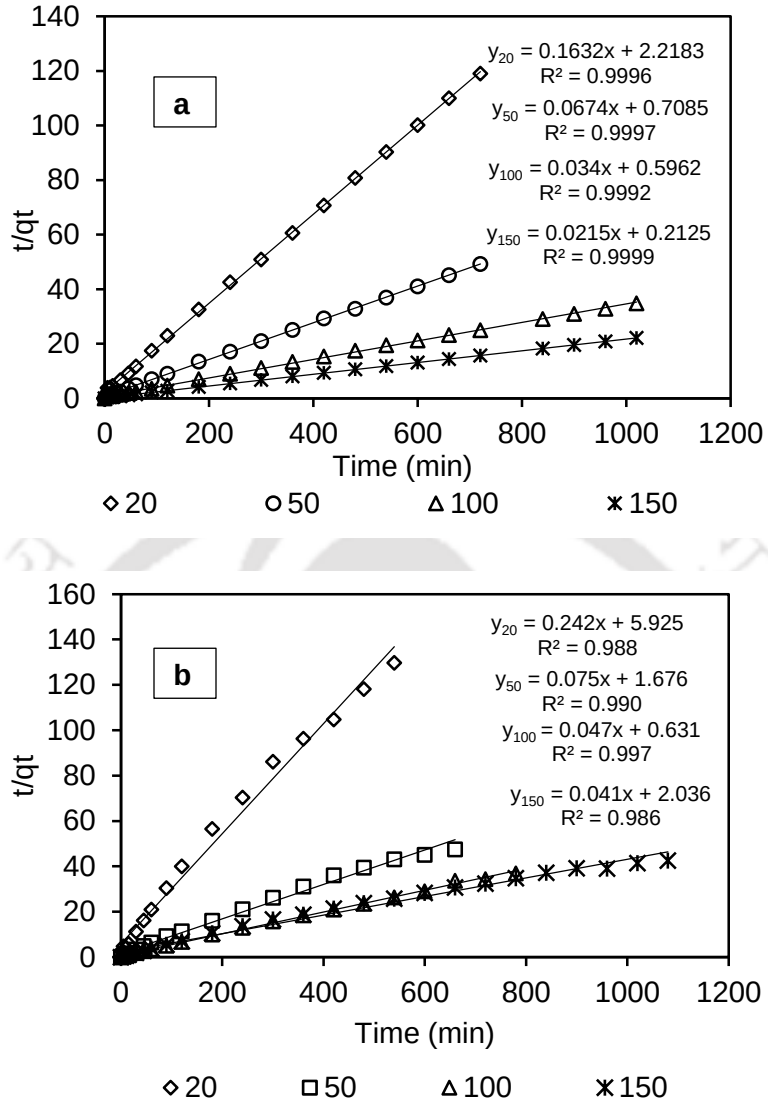

Figure 2.14: Pseudo-second order model of a) AO8 and b) AV7 with AFC-silica

Plots are shown in Figure 2.15 shows that the plots were straight lines but did not pass through the origin, suggesting AO8 and AV7 dye adsorption onto AFC-silica involved intraparticle diffusion, but it was not the sole rate controlling step. The slope of the plot of the linear part of the q_t against $t^{0.5}$ plot (here taken between 15 and 200–240 min) gives the values of diffusion rates (k_i). Values of diffusion rates (k_i) are given in Table 2.5.

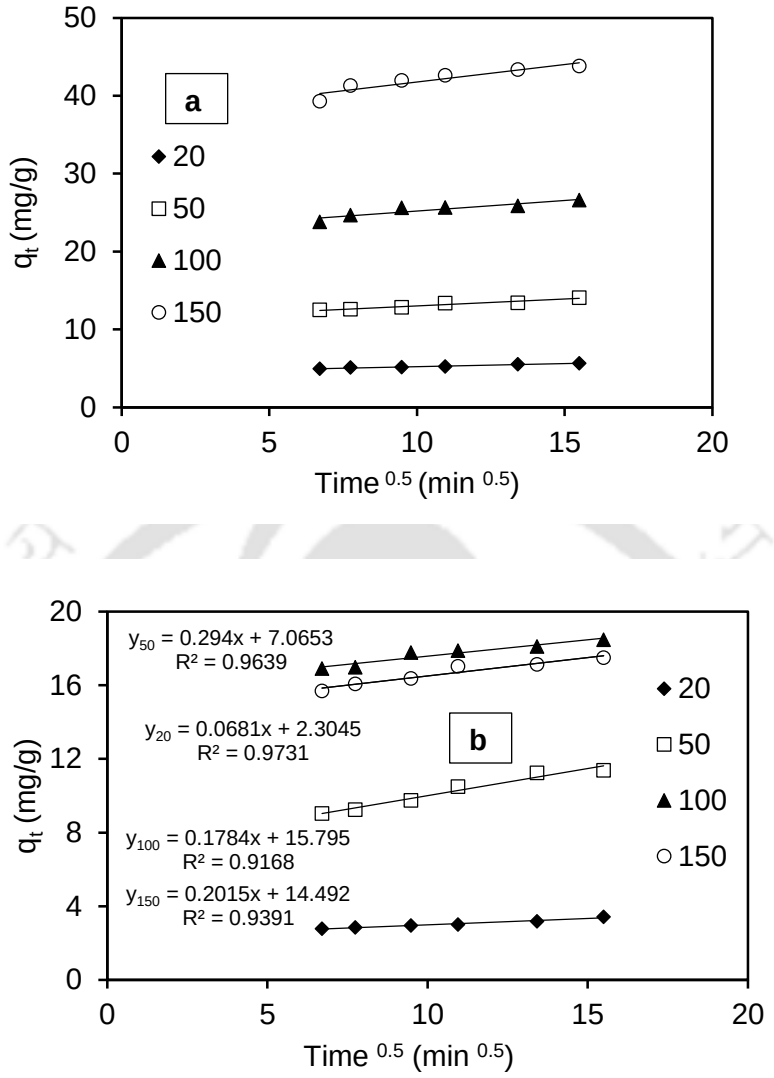

Figure 2.15: Intraparticle diffusion model of a) AO8 and b) AV7 with AFC-silica

Regression analysis showed initial internal adsorption rate with dye concentration followed by the following relation:

$$k_i = (-2.60)C_o^{0.012}(AO8)$$

$$k_i = (-2.73)C_0^{0.008}(AV7)$$

Reichenberg (1953) model was used to understand the role of external mass transfer/film diffusion on adsorption of acid dyes by AFC-silica (Eq. 11a). The plots of Bt vs. t (Boyd's plot) are shown

in Figure 2.16 for both dyes. The plots were nonlinear and did not pass through origin for both AO8 and AV7, suggesting that during initial 90–120 min, external resistance was strong and external mass transfer was controlling step in adsorption, though diffusion was also important in AO8 and AV7 adsorptions.

Table 2.5: Comparison of pseudo first and second order kinetic models for AO8 and AV7 adsorption by AFC-silica

Dyes	Initial conc. (mg/L)	q_e exp. (mg/g)	Pseudo-first order			Pseudo-second order			Intra-particle diffusion			Boyd model
			k_1 (min^{-1})	q_e (mg/g)	R^2	k_2 (g/mg/min)	q_e (mg/g)	R^2	K_i ($mg/g.min^{0.5}$)	C_d (mg/g)	R^2	R^2
AO8	20	6.05	0.160	5.283	0.94	0.0011	6.134	0.99	0.078	4.445	0.97	0.88
	50	14.62	1.085	12.73	0.93	0.0063	14.92	0.99	0.174	11.28	0.94	0.87
	100	29.27	0.175	25.87	0.97	0.0019	29.41	0.99	0.272	22.47	0.86	0.92
	150	46.02	0.199	42.14	0.99	0.0020	47.61	0.99	0.449	37.28	0.86	0.97
AV7	20	5.06	0.142	3.559	0.89	0.0098	4.132	0.99	0.0681	2.304	0.97	0.97
	50	14.27	0.312	11.04	0.75	0.0033	13.33	0.99	0.294	7.065	0.96	0.81
	100	21.15	0.493	18.40	0.75	0.0035	21.27	0.99	0.1784	15.79	0.91	0.98
	150	25.38	0.147	19.48	0.79	0.0082	24.39	0.99	0.2015	14.49	0.94	0.99

Mohan and Singh (2002) cited that low concentration of adsorbate, inadequate mixing, high affinity between adsorbate and adsorbent as reasons for film diffusion to be controlling step in adsorption. The lower initial dye concentration was probably responsible for adsorption controlled by external mass transfer/film diffusion.

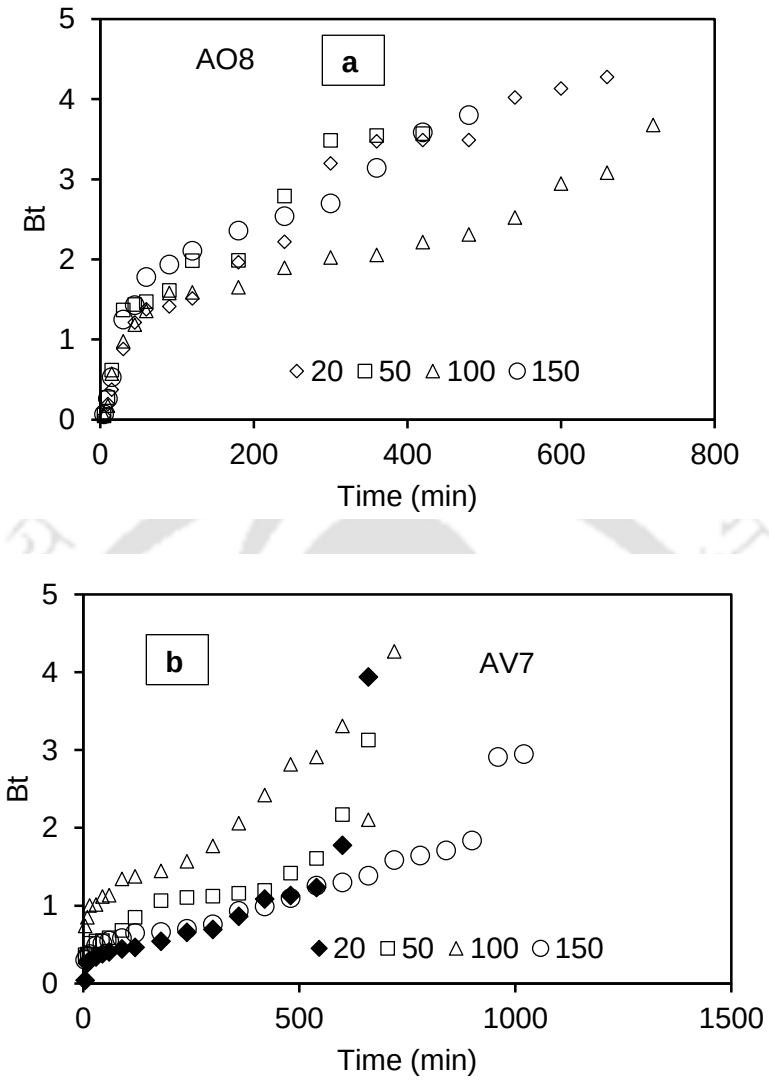

Figure 2.16: Boyd plot of a) AO8 and b) AV7 with AFC-silica

2.3.2.7 Desorption and reuse

The main aim of regeneration of a spent adsorbent is usually carried out in order to reuse it, avoiding the cost of a new acquisition and minimizing the amount of waste. Desorption of AO8 and AV7 dyes from AFC-silica surface was studied using varying strength of NaOH solution (0.0.5–0.5N). Maximum desorption of 49% and 88% only was achieved at NaOH strength of 0.1N for AO8 and AV7 respectively given in Figure 2.17a. According to Chiou and Li, 2004; Chen et

al., 2009, in basic solutions, the positively charged amino group is deprotonated such that the electrostatic interaction between adsorbent and dye becomes weaker and then the adsorbed dye leaves the adsorption site. But in this case low desorption was observed which reflects the existence of a strong chemical bond between AFC and AO8 dye during adsorption.

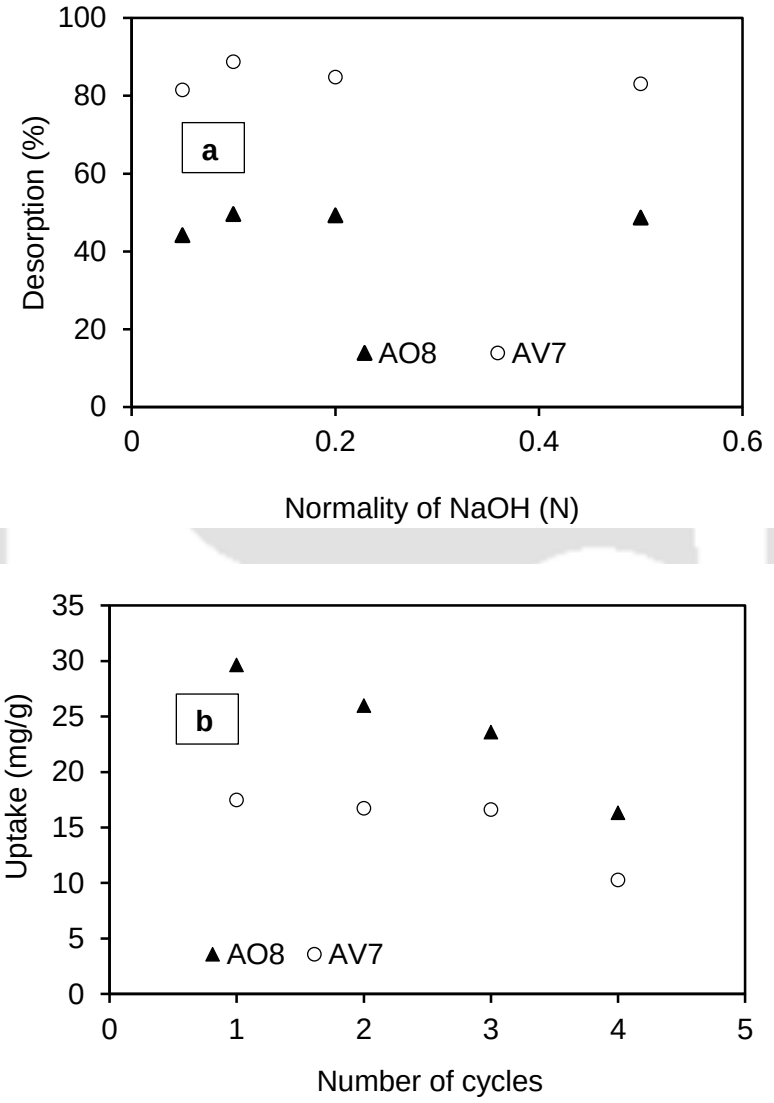

Figure 2.17: a) Desorption of AO8 and AV7 dye with NaOH and b) Resue of AFC-silica adsorbent

The resue of adsorbent (AFC-silica) was carried out by washing the adsorbent with distilled water after each adsorption experiment. The procedure was followed for each adsorption cycle. From Figure 2.17b, it was observed that the uptake decreased after each cycle. The uptake rate decreased from 29.6 mg/g to 16.3 mg/g for AO8 whereas 17.4 mg/g to 10.2 mg/g for AV7 with AFC-silica after four successive cycle. The decrease in uptake value after each cycle suggest that the washing with distilled water was unable to release to dye molecule from AFC-silica surface properly. Another reason may be that excessive washing could also cause some changes in the adsorbent surface and possibility of some dye molecule being washed out after each washing.

2.3.3 Removal of anionic dyes with PANI-jute

2.3.3.1 Effect of initial pH

The optimum pH for dye uptake was determined and results are shown in Figure 2.18. Acidic pH favored removal of AV7 dye and maximum uptake was observed at pH 2 for PANI-jute with AV7 dye. The plain jute fiber without any coating was used for the removal of AV7 dye and it was observed that with 3 g/L dose of plain jute fiber, dye removal was very negligible. This indicates that removal of dye mainly occurred by the polymer. Acid violet 7 dye showed a maximum removal of 62.31% and uptake of 19.15mg/g at pH 2 (Figure 2.18a). During adsorption a maximum removal of 83.58% with high uptake value of 32.59 mg/g at pH 2 and from pH 3-10 the removal percentage declined from 53.64-10.37%. Thus, the polymer adsorbent favored the adsorption acid violet 7 dye at acidic medium.

Effect of solution pH on the removal congo red dye (CR) with PANI-jute adsorbent was carried out and found out that at initial pH 2 maximum dye removal of 61.61% was achieved but very negligible removal about 9.77% at pH 3 (Figure 2.18b). Removal beyond pH 3 was extremely negligible. This may be due to the availability of negatively charged dye ions at low pH value. In

acidic solution, there will be excessive protons required to protonate the amine groups (-NH_2) present in the terminal end of the polymer adsorbent.

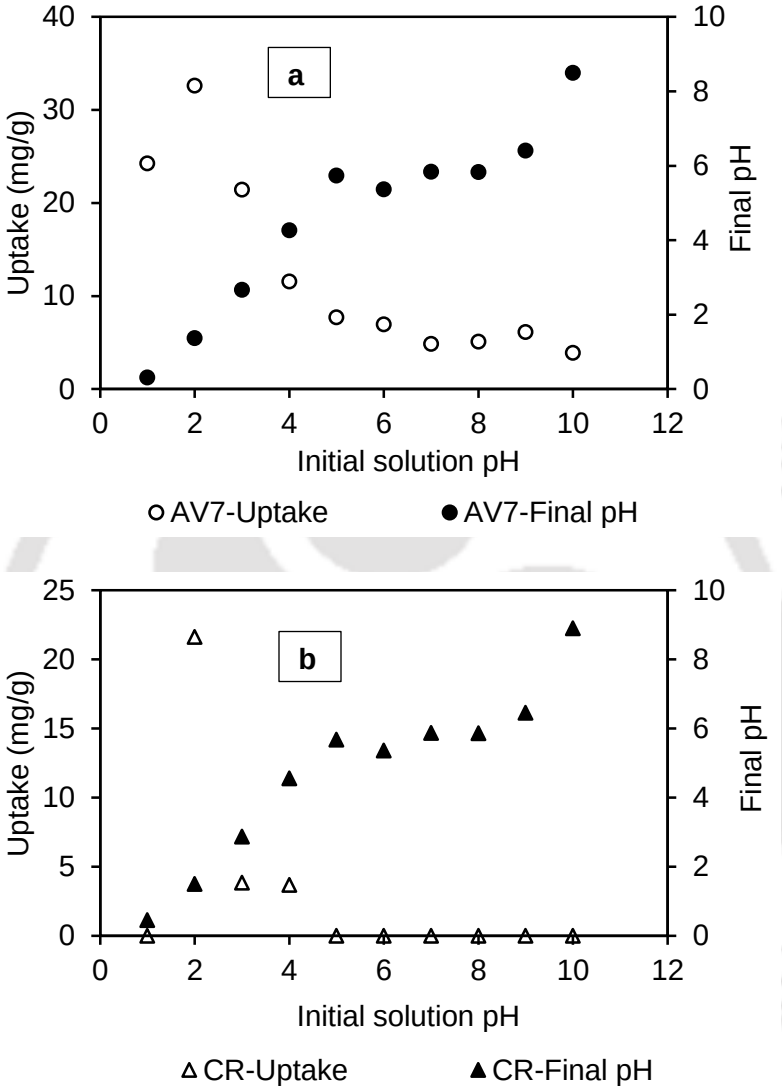

Figure 2.18: Effect of initial solution pH of a) AV7 and b) CR dye with PANI-jute (Co: 100 mg/L, dose: 3g/L, agitation rate: 150rpm, 12h)

Thus, the electrostatic attractive forces between the negatively charged sulfonic groups of CR dye molecules and the protonated sites of the polymer adsorbent, resulted in the high adsorption efficiency at lower pH. Hence, dye removal is favourable at low pH. Further, lower adsorption of

the CR in alkaline medium is also due to the competition between excess OH^- ions and the anionic CR dye molecule for the adsorption sites (Reddy et al., 2012). Similar observations was found by Xu et al., 2016 during the removal of acid orange II and reactive brilliant red X-3B with amino-functionalized magnetic nanoadsorbent and by Jain et al., 2017 during the removal of acid violet 17 dye with biosorbent obtained from NaOH and H_2SO_4 activation of fallen leaves of *Ficus racemose*. Wang et al., 2017 also found similar observations during the removal of acid orange 7 (AO-7), acid red 18 (AR-18) and acid black 1 (AB-1) on cationic gemini surfactant-modified flax shives (MFS) where maximum adsorption occurred at pH 2.

2.3.3.2 Effect of polymer dose

Effect of adsorbent dose on dye removal is shown in Figure 2.19. In case of PANI-jute (Figure 2.19) at initial pH of 2, dye uptake decreased from 56.15 mg/g to 6.7 mg/g with increase in the adsorbent dose from 0.5 to 10 g/L for AV7 whereas for CR dye adsorption the uptake decreased from 113.7 mg/g to 5.4 mg/g. It is evident that the adsorption capacities of both AV7 and CR dyes decreases with the increase in the adsorbent dosage (PANI-jute). This can be attributed due to the effect of concentration gradient between the dye molecules and PANI-jute and thereby decrease in the adsorbed amount of dye onto the adsorbent. Besides this in constant concentration the increase on adsorbent dose lead to particle interaction (aggregration) decreasing the total surface area of the adsorbent and increasing the diffusional path length (Kaur et al., 2015). The maximum uptakes were 56.15 mg/g (0.099 mmol/g) for AV7 and 113.7 mg/g (0.163 mmol/g) for CR.

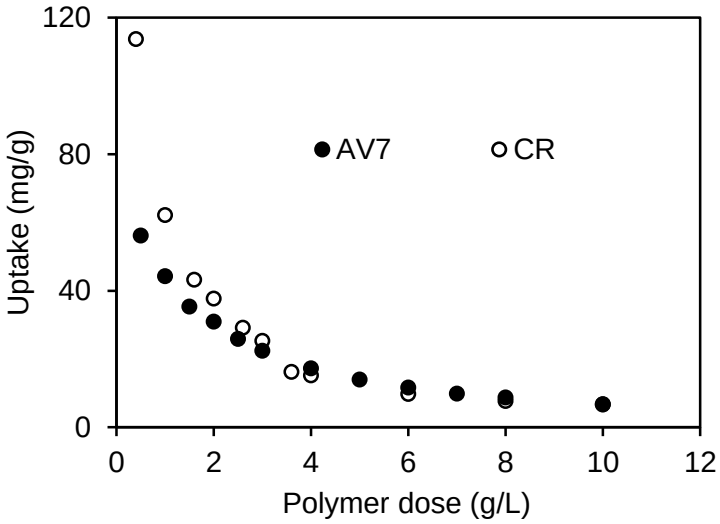

Figure 2.19: Effect of polymer dose on the uptake of a) AV7 and b) CR dye with PANI-jute (Co: 100 mg/L, dose: 3g/L, agitation rate: 150rpm, 12h

2.3.3.3 Adsorption isotherm

Data was plotted using linearized forms of Langmuir, Freundlich, Temkin and Dubinin-Radhuskevich isotherms for adsorption of AV7 with PANI-jute which was carried out using experimental data are shown in Table 2.6. Isotherm plots (q_e vs C_e) are shown in Figure 2.20a to compare with the experimental isotherm plot with various isotherm models as mentioned above (the comparison was made of q_e values calculated from various models to the experimental q_e values). It was observed that the Langmuir, Freundlich, Temkin and Dubinin-Radhuskevich isotherm models followed by best fitted with high correlation coefficient value closer to unity. The maximum adsorption capacity was found to be 232.6 mg/g. From Figure 2.20a, the isotherm plot of AV7 was found to slightly follow L-type or Langmuir isotherm which reflects a relatively high affinity between the adsorbate and the adsorbent and L type isotherm usually indicate chemisorption whereas for CR isotherm shape (Figure 2.20b) was of S-type suggesting multilayer

adsorption onto the heterogeneous active sites of PANI-jute (Giles et al., 1974a; Reddy et al., 2016).

AV7 dye followed both Langmuir and Freundlich isotherm but fitted very well in Freundlich isotherm model with high R^2 value and low ARE whereas for CR dye Freundlich isotherm model was favourable (Table 2.6).

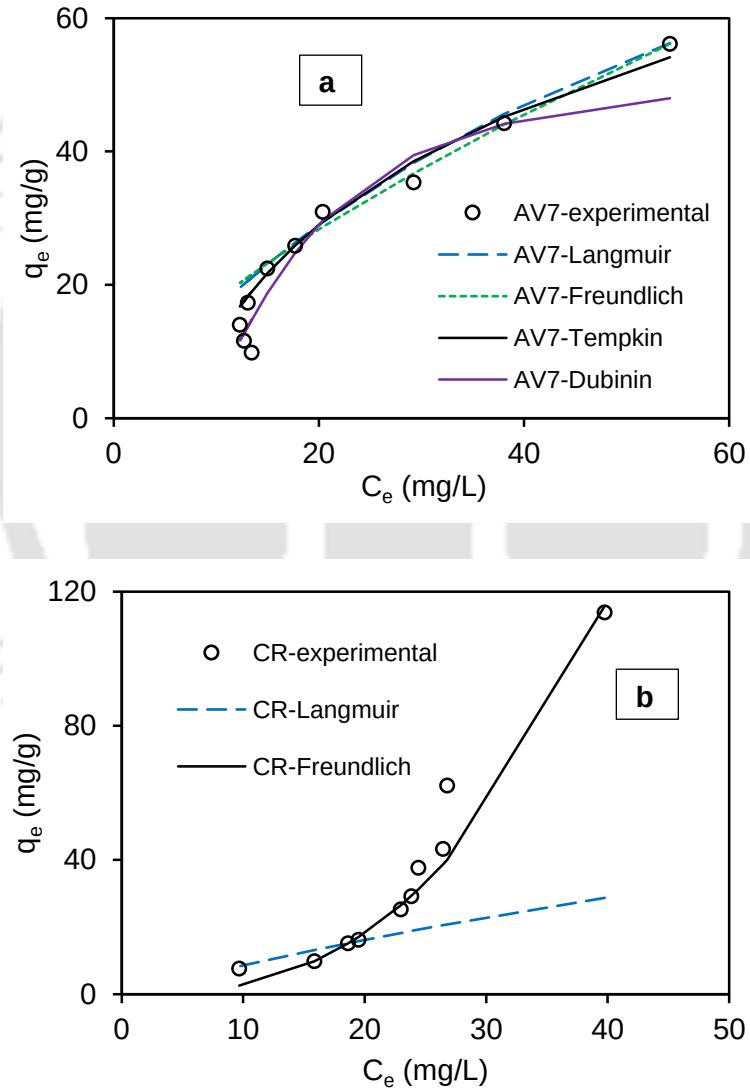

Figure 2.20: Isotherm plots of a) AV7 and b) CR dyes with PANI-jute

Table 2.6: Estimated isotherm parameters for adsorption of AV7 and CR dye on PANI-jute at pH 2 and 37°C

Isotherm models	Parameters	AV7	CR
Langmuir isotherm	Q_o (mg/g)	232.6	134.9
	K_L (L/mg)	0.0058	0.0067
	R_L	0.63	0.595
	R^2	0.96	0.89
	ARE(%)	18.71	35.17
Freundlich isotherm	1/n	0.219	0.835
	n	1.455	0.371
	K_f	3.61	0.0058
	R^2	0.97	0.97
	ARE(%)	28.01	14.16
Temkin isotherm	A_T (L/mg)	0.134	0.549
	b_T	90.06	386.256
	B	27.66	6.52
	R^2	0.98	0.82
	ARE(%)	14.63	43.71
Dubinin-Radhuskevich Isotherm	q_s (mg/g)	52.09	33.328
	K_{ad} (mol^2/kJ^2)	0.00004	0.000024
	E (kJ/mol)	0.1118	0.114
	R^2	0.97	0.67
	ARE(%)	14.79	38.79

2.3.3.4 Effect of temperature

Temperature was varied from 10 to 60°C using initial dye concentration of 100 mg/L at initial pH 2 for AV7 and CR dye adsorption onto PANI-jute. With increase in temperature from 10 to 60°C, uptake of AV7 increased from 37.5 mg/g to 67.75 mg/g (Figure 2.21a). Thermodynamic

parameters like enthalpy change (ΔH°) (J/mol) and entropy change (ΔS°) (J/mol.K) were given in Table 2.7 and the plot is shown in Fig. 2.21b. Removal of AV7 was endothermic in nature for PANI-jute. Enthalpy change for AV7 for PANI-jute was -18.49 kJ/mol. The ΔG° values of the adsorptions under various temperature was negative, suggesting that the dye adsorption was a spontaneous process and thermodynamically favorable processes at all the experimental temperatures.

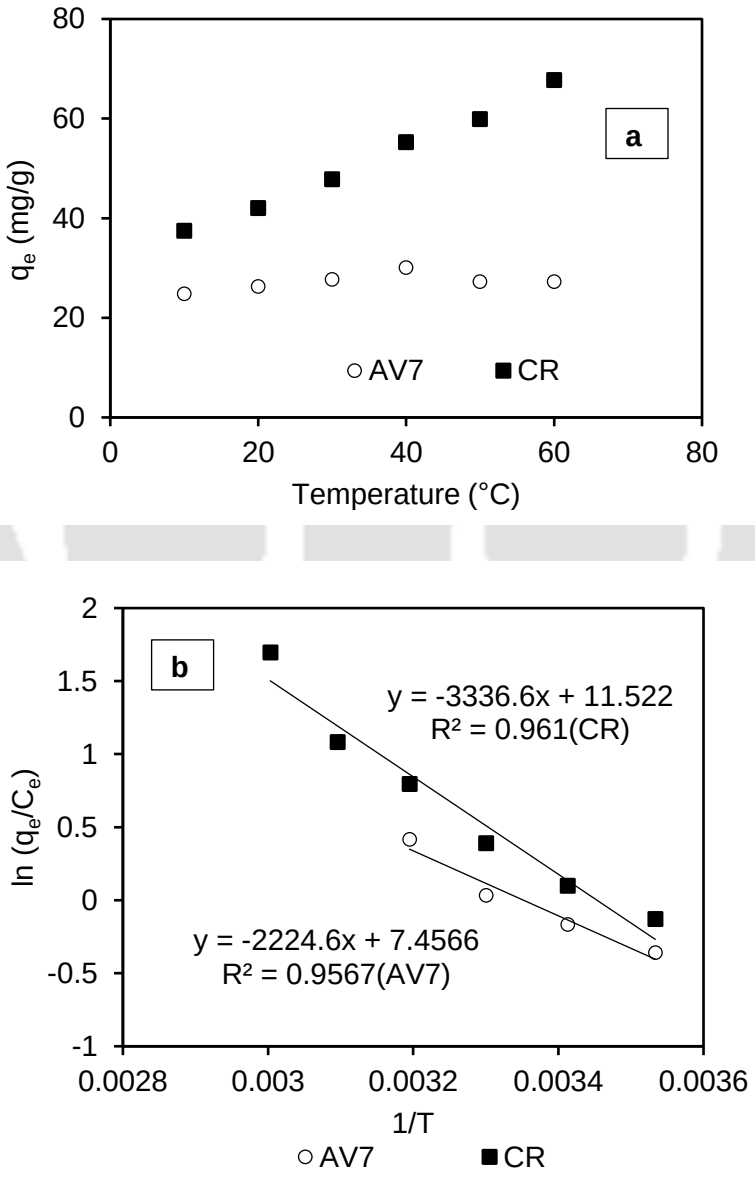

Figure 2.21: a) Effect of temperature on dye uptake and b) van't Hoff plot

In addition, the absolute ΔG° value increased with the increase of temperature, indicating that the adsorption tendency became stronger as temperature increased. The ΔH° of the AV7 adsorption by PANI-jute was 18.49 kJ/mol, indicating that the adsorption was physical in nature but enhanced by chemical effect, supported by the pseudo-second order kinetic model. The positive ΔS° value indicates the randomness and affinity towards the adsorbent.

Table 2.7: Thermodynamic parameters for AV7 and CR dyes on PANI-jute

Dyes	Temperature	ΔH°(kJ/mol)	ΔS° (J/mol K)	ΔG°(kJ/mol)	TΔS°(kJ/mol)
AV7	283	18.495	61.994	0.950	17.544
	293			0.331	18.164
	303			-0.288	18.784
	313			-0.908	19.404
	323			-1.528	20.024
CR	283	27.740	95.793	0.630	27.109
	293			-0.327	28.067
	303			-1.285	29.025
	313			-2.243	29.983
	323			-3.200	30.941

With increase in the temperature from 10°C to 60°C, the percentage of CR adsorption increased from 46.77% to 84.49% at 10°C and 60°C respectively (Figure 2.21a). The positive value of ΔH° suggest that the adsorption process was endothermic in nature and the value is 34.67 kJ/mol. The positive entropy ΔS° with value 95.79 kJ/(mol.K) suggests that the adsorption process involves an associative mechanism which indicated the increase in the degree of randomness at the solid-solution interface during the CR dye adsorption onto PANI-jute. The positive value of ΔG° (64.99 to 70.4 kJ/mol) indicates the spontaneous process from 20 to 50°C. Thus, with the increase in the

temperature the active sites of the PANI-jute adsorbent become more available for adsorption due to the increase in the mobility of the adsorbent and adsorbate molecules resulting in increase in removal percentage as well as uptake value.

2.3.3.5 Effect of initial concentration

Dye uptakes with time at varying initial concentrations (20–200 mg/L) for AV7 with PANI-jute is given in Figure 2.22. With PANI-jute adsorption, lower initial concentration 20 mg/L of AV7 dye gave uptake of about 14.87 mg/g and for 50 mg/L uptake was 34.68 mg/g, whereas for higher initial concentration 100 mg/L uptake was 44.81 mg/g and 200 mg/L uptake was 69.22 mg/g. This may be attributed to an increasing concentration gradient acting as an increasing driving force to overcome all mass transfer resistances of the dye molecules between the aqueous and solid phase, leading to an increasing equilibrium adsorption until saturation is achieved. Figure 2.26 shows the equilibrium time 30- 45 min and increased to 45 - 60 min.

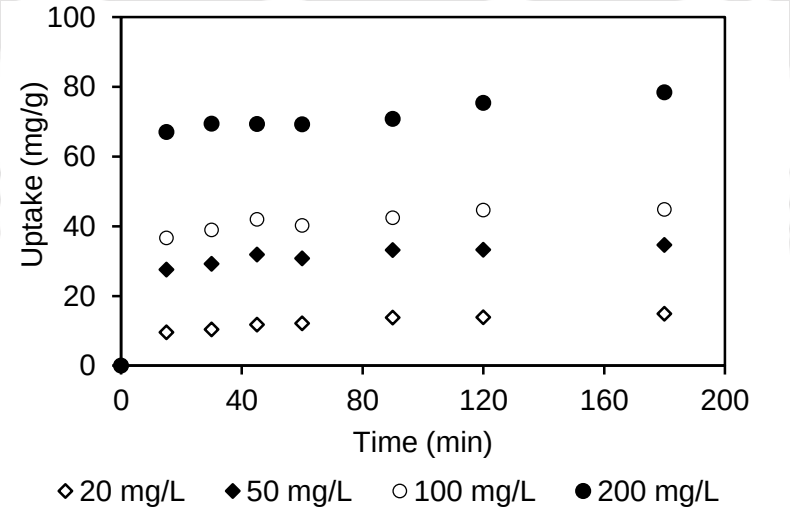

Figure 2.22: Effect of initial concentration of AV7 with PANI-jute (Co: 100 mg/L, dose: 1g/L, agitation rate: 1000rpm, 3h)

Thus, it was observed that PANI-jute showed higher uptake value and short equilibrium time during the adsorption of AV7 dye. Similar observation was reported by Taher et al., 2017 during the adsorption of congo red onto bentonite and Salman et al., 2015 during the removal of congo red dye from aqueous solution by using natural materials (Barnacles shells).

2.3.3.6 Adsorption kinetics

Several models were used in order to understand the mechanism of adsorption of AV7 dye onto the PANI-jute surface. The pseudo-first, second order model, intra-particle and boyd model were used for analyzing the mechanism involved during the adsorption process. The initial concentration range for study were considered as 20, 50, 100 and 200 mg/L. From the Table 2.8 and Figure 2.23a, it was observed that the adsorption process followed the pseudo-second order compared to pseudo-first order kinetic model with high correlation coefficient value (R^2-0.99) and the calculated q_e, and experimental, $q_e exp$ values were also very close to each other for all the studied concentrations.

Table 2.8: Comparison of pseudo first and second order kinetic models for AV7 adsorption by PANI-jute

AV7 conc. (mg/L)	q_e exp. (mg/g)	Pseudo-first order			Pseudo-second order			Intra-particle diffusion			Boyd model
		k_1 (min^{-1})	q_e (mg/g)	R^2	k_2 (g/mg/min)	q_e (mg/g)	R^2	K_i ($mg/g.min^{0.5}$)	C_d (mg/g)	R^2	R^2
20	14.872	0.11659	12.328	0.88	0.00674	15.290	0.99	0.0704	6.8283	0.97	0.95
								0.4351	9.1723	0.89	
50	34.681	0.23849	31.344	0.90	0.00659	34.965	0.99	0.9954	23.94	0.76	0.61
								0.6337	26.409	0.87	
100	44.818	0.05741	40.179	0.96	0.00579	45.454	0.99	1.1309	32.579	0.69	0.80
								0.815	34.58	0.84	
200	78.409	0.02499	65.256	0.88	0.00292	78.740	0.99	0.5938	65.251	0.76	0.78
								1.6823	56.036	0.95	

Figure 2.23b, shows that the plots of intraparticle diffusion for all the concentrations did not pass through the origin indicating some degree of control from the boundary layer and also other mechanisms in addition to the intra-particle diffusion were involved during the adsorption process.

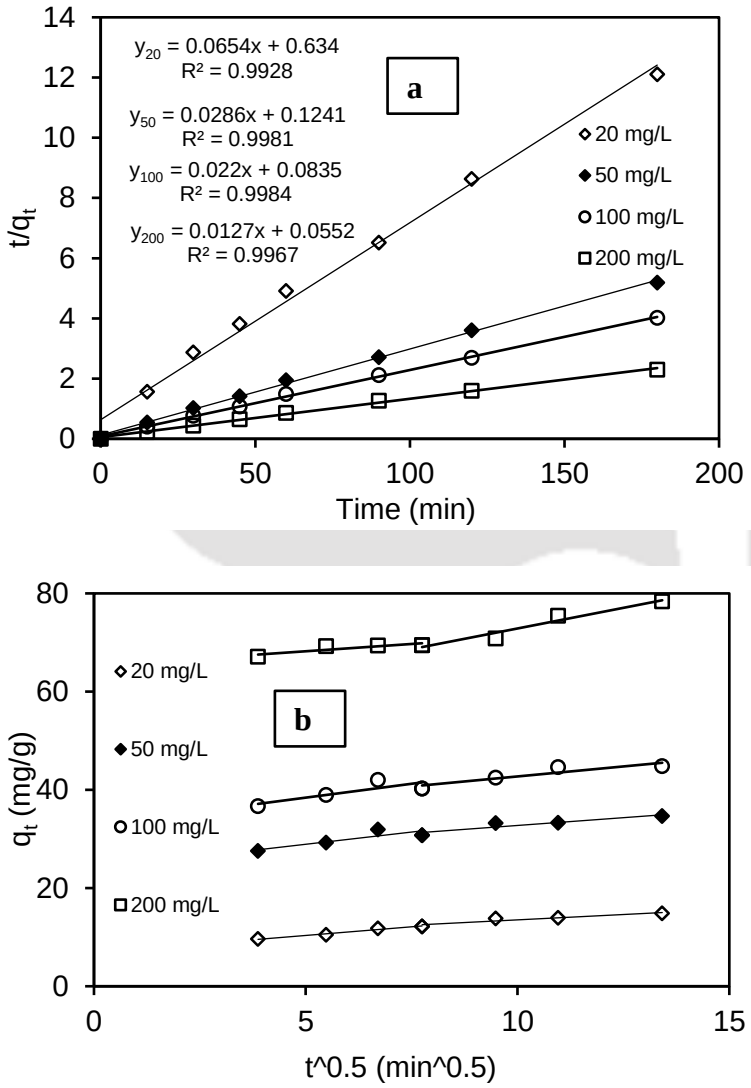

Figure 2.23: a) Pseudo-second order kinetic model and b) Intraparticle diffusion model

The boundary layer effect seems to increase with increasing initial concentration. The boyd model data from Table 2.8 and the presence of an intercept shows that diffusion is not the only the

observed mechanism of transfer. Thus the adsorption mechanism can explained in three steps of adsorption:

1) The adsorbate ions travel towards the external surface of the adsorbent (film diffusion)

2) Then the adsorbate ions travel within the pores of the adsorbent (intraparticle diffusion)

3) Finally, the adsorbate ions get adsorbed on the interior surface of the adsorbent (adsorption)

2.3.3.7 Desorption and reuse

To evaluate the economic feasibility of any adsorbent the first step involves the desorption efficiency of the adsorbent. The desorption efficiency gives a clear picture of an adsorbent whether it can regenerated and reuse making the adsorbent as an economically efficient adsorbent. During desorption study of AV7 dye with PANI-jute, the maximum desorption percentage of 96.89% was achieved by using 0.1N NaOH as desorbent (Figure 2.24a). The desorption percentage decreased with further increase in the desorbent (NaOH) strength. Thus, the results suggested that the PANI-jute adsorbent can economically feasible

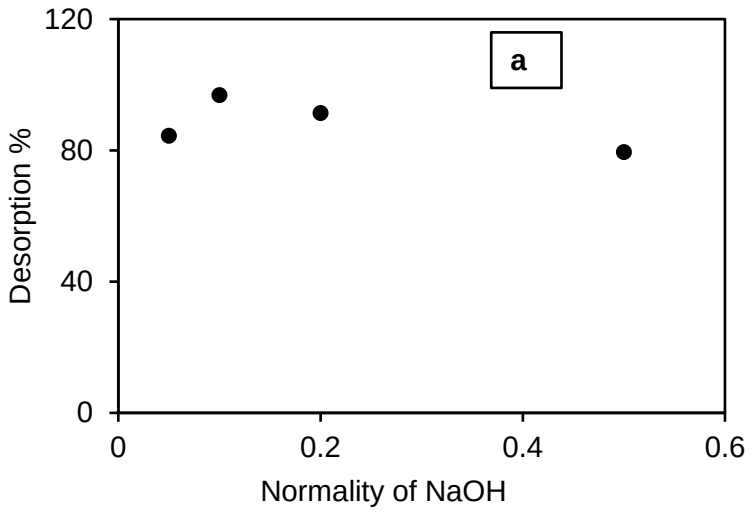

Figure 2.24a: Desorption of AV7 dye with NaOH

The reuse of PANI-jute adsorbent was carried out by washing with distilled water after each adsorption experiment. The uptake decreased from 17.48 mg/g to 9.46 mg/g from 1st cycle to 5th cycle (Figure 2.24b). This decrease in uptake may be described as either dye molecules were not completely washed out or exceesive washing may gave led some changes within the adsorbent surface.

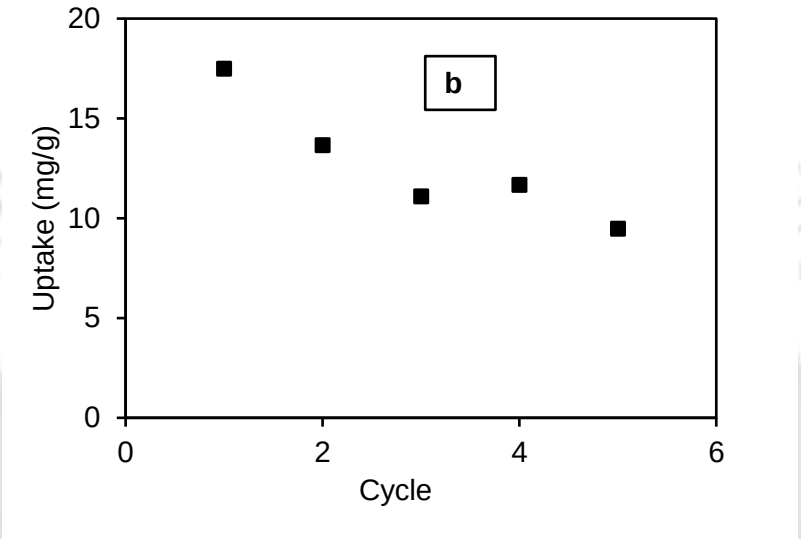

Figure 2.24b: Resue of PANI-jute adsorbent

Table 2.9: Comparison on the performance of the adsorbents on the removal efficiency anionic dyes (Conditions: C_o- 100 mg/L; dose-3g/L)

Adsorbent	Dyes	Optimum pH	Maximum removal (mg/g)
AFC-silica	AO8	3	31.78
	AV7		25.19
	CR		30.71
PANI-jute	AO8	2	32.66
	AV7		22.43
	CR		25.28

**AO8 removal with PANI-jute data was taken from Mallick, 2013*

From the above Table 2.9, it was found that under similar conditions, the removal efficiency of PANI-jute and AFC-silica for the adsorption anionic dyes (AO8, AV7 and CR) from aqueous solution were almost similar and therefore could be employed as an efficient adsorbent for industrial wastewater treatment.

2.4 Summary

In this chapter, the batch adsorption experiments - adsorption kinetics, thermodynamics and equilibrium behavior on anionic dyes – acid orange 8, acid violet 7, congo red onto amine based polymer – Aniline formaldehyde condensate coated silica gel (AFC-silica) and Polyaniline coated jute fiber (PANI-jute) were studied. The adsorption was found to befavourable in acidic medium. Electrostatic attraction between protonated amine group (NH_3^+) of AFC and anionic sulfonate group (SO_3^-) of dye molecule along with hydrogen bond formation and interaction between aromatic groups of the dyes was found to be the main mechanism responsible for the removal of dyes from aqueous solution. FTIR results revealed that amine functional groups may be responsible for anionic dyes adsorption. Kinetic studies demonstrated that the mechanism for adsorption followed the pseudo-second order model, which provided the best fit for the experimental data. The adsorption behavior of dyes in single system was very well ascribed by the various isotherm models- Langmuir, Freundlich, Temkin, Dubinin-Radhuskevich and BET isotherm models. A comparison on the adsorption of the dyes with the two adsorbents provides an insight of the amine polymer adsorbents to be a low cost adsorbents to remove anionic dyes from the aqueous solution.

CHAPTER 3

Synthesis and optimization of supportless AFC polymer adsorbent

3.1 Background

Aniline-formaldehyde polymer known as aniline formaldehyde condensate (AFC), is a rubbery thermoplastic and AFC contains free amines and exist in cationic form in acidic medium. The synthesis reaction is exothermic and usually results in sticky lump unsuitable for the most uses. Previously, AFC coated silica gel was shown to be effective in adsorption of hexavalent chromium from relatively concentrated aqueous solution in acidic medium. Studies revealed that the cationic form of the polymer functions as anion exchanger which is one of the main contributor in adsorption of hexavalent chromium in $HCrO_4^-$ form. Previously, Koner et al., 2008 chanced upon a method to control its morphology and physical properties by adding organic solvents during the reaction. In this chapter emphasis was giventhe main highlight of the research work was to improve the efficiency of the polymeric material new forms of polymer was prepared by modifying the synthesis without using any support material. Thus the careful investigation was carried out on the process systematically to isolate the factors that controls morphology and their relationship with the physical and chemical properties.

3.2 Materials

Commercial grade aniline ($C_6H_5NH_2$) was purified by distilling over KOH pellets at boiling point temperature of aniline (180°C). Analytical grade formaldehyde (HCHO) 37% v/v, isopropanol (C_3H_8O), potassium dichromate salt, NaOH pellets and concentrated HCl was used as recieved.

3.3 Analytical method

The apparatus used during the adsorption experiments are Electronic balance (Model: AW320, SHIMZADU), Cooling centrifuge (Model: 412 LAG, REMI), Spinix orbital shaker (Model: MC-02, Tarson), Ice flaker (Model: SLF-225A-Q), pH meter (Model: Thermoscientific, Orion 3 star benchtop) and pH meter (model-LT- 49, Microprocessor pH meter). The chromium metal ions were analyzed in AAS (Model: AA240, Varian, Australia) as total chromium using air-acetylene flame at 357.9 nm wavelength using slit width of 0.2 nm. At this condition measurement range of total chromium is 0.06-15 mg/L. Characterization of the polymer was carried out by BET surface area analysis (Autosorb –IQ MP Quantochrome), Particle size analyzer (Model: APA 5007, Mastersizer 2000 system), FTIR (Perkin Elmer PE-RXI)), CHNS analyzer (Eurovector EA3000), TGA (model-STA449F3A00), and zero point charge of adsorbent was estimated using the method described by Fiol and Villaescusa, 2009.

3.4 Synthesis of modified-AFC polymer adsorbent

Aniline in desired amount (in grams) was added to 7 mL conc. HCl and then the mixture was added to 15 mL isopropanol and cooled in ice bath. Now 15 mL 37% (w/v) formaldehyde was added to 15 mL isopropanol and kept on ice bath. This was then added to the pre-cooled aniline-acid solution with vigorous stirring to obtain a uniform homogeneous solution. The temperature was maintained at 0-5°C for 25 minutes and then kept at room temperature overnight. The solid was first washed with copious amount of 1N HCl to remove low molecular weight acid soluble polymer, followed by treating with 1N NaOH to form free amine form. The polymer was washed with distilled water until the filtrate pH reached neutrality. The solid chunk of polymers were dried under vacuum desiccator for over four days. The solid was grinded to fine micron size yellow colored light weight material. The ratio of aniline: HCHO: HCl was adjusted as required to check

the improvement in the characteristics of the polymer whereas isopropanol was used only for volume make up (given in Table 3.1).

Thereafter, these batches of polymer adsorbents were preliminary tested to identify which ratio of aniline: HCHO: HCl gives the best results yielding maximum removal efficiencyof total chromium. From Table 3.1 it was observed that the ratio 1:2:1 gives the best result whereas isopropanol volume plays no major role in the synthesis except for volume make up as discussed earlier.

Table 3.1: The batch wise preparation along with the preliminary evaluation performance test is given in the table below-

Batch	Aniline (g)	HCHO (mL)	HCl (mL)	Isopropanol (mL)	Ratio Aniline:HCHO:HCl	Total chromium removal (%)	Total chromium uptake (mg/g)
1	2	7.5	2.25	5	1:4.3:1	57.79	11.69
2	9	7.5	2.25	22.5	1:1:0.2	8.98	1.82
3	9	15	7	15	1:2:1	86.42	17.48
4	9	15	7	23	1:2:1	65.64	16.41

**Conditions: Initial concentration of chromium – 50 mg/L, Agitation rate – 270 rpm, time – 3h, pH 3, dose – 2g/L, room temperature*

After preparing the polymer adsorbents solubility test was performed and found out that:

1) All the five batches were insoluble in water
2) Insoluble in methanol
3) Insoluble 1M HCl with little color release
4) No significant change was observed at 80°C water bath.

5) Preliminary experiments were performed with all the batches of polymer and the third batch showed the best result for total chromium adsorption (given in Table 3.1) and named modified-AFC.

Again, modified-AFC was tested to cross-check its efficiency by varying chromium concentration. The stock solution of Cr(VI) of 1000 mg/L was prepared using required amount of potassium dichromate salt with pH adjusted water. All experiments were carried out in orbital shaker. The adsorption experiments were performed in triplicates and the best results were presented. It was observed that the under same conditions modified-AFC showed the best results and very good efficiency in chromium removal with concentration ranging from 10-100 mg/L given Table 3.2.

Table 3.2: Preliminary performance evaluation test by varying chromium initial concentration

Polymer adsorbent	Initial concentration (mg/L)	Removal (%)	Uptake (mg/g)
Modified-AFC	10	96.73	2.38
Modified-AFC	20	94.61	4.77
Modified-AFC	50	94.57	12.00
Modified-AFC	100	92.03	26.21

**Conditions: Agitation rate – 300 rpm, time – 3h, pH 3, dose – 4g/L, room temperature*

3.4.1 Mechanism of formation of Micron-sized clusters

The formation of polymer spheres usually requires use of amphiphilic additive which first form either a core micelle or a reverse micelle (Kim et al., 2001). The polymerization occurs on the surface of that core. In the present case, no such additive was used. The core formation may be due to the presence of anilinium salt having a polar head and a rather short aromatic tail formed a

reverse miceller arrangement in water/isopropanol mixture before the polymerization on the surface occurs (Kim et al., 2001). The aqueous solution of HCl and formaldehyde (HCHO) were the source of water.

Total volume of the solvent used was rather low which probably led to fusion of some of the miceller arrangement as the polymerization proceeded. A plausible mechanism of formation is shown in Figure 3.1a.

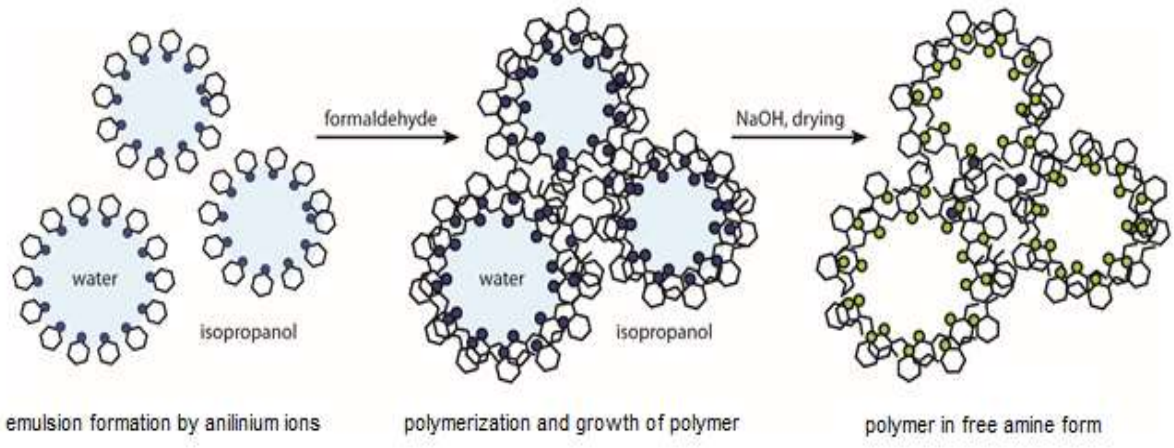

Figure 3.1a: Proposed way of formation of polymer globules

The remarkable part during the polymerization was observed that the simple addition of a non-polar solvent facilitates the formation of a mesoporous solid polymer. The absence of amphiphilic additive removes the additional steps necessary to remove the additive. Therefore, the formation of a mesoporous solid form of the AFC by simple addition of isopropanol during synthesis with little or no change in chemical formula was evident from the elemental analysis and FTIR.

3.5 Characterization of modified-AFC

The morphology of the polymer was checked with Field Emission Scanning Electron Microscope (FESEM) given in Figure 3.1b. The powder was a cluster of spherical shaped polymer particle

(Figure 3.1b).The diameter of the individual spheres was between 1-3µm. Clusters are consisting of partially fused spheres. The volume wise particle size distribution is rather broad with a mean particle diameter of 453µm. Thus the polymer can be best descried as random sized particles formed by partial fusion of 1-3µm diameter sized polymer spheres.

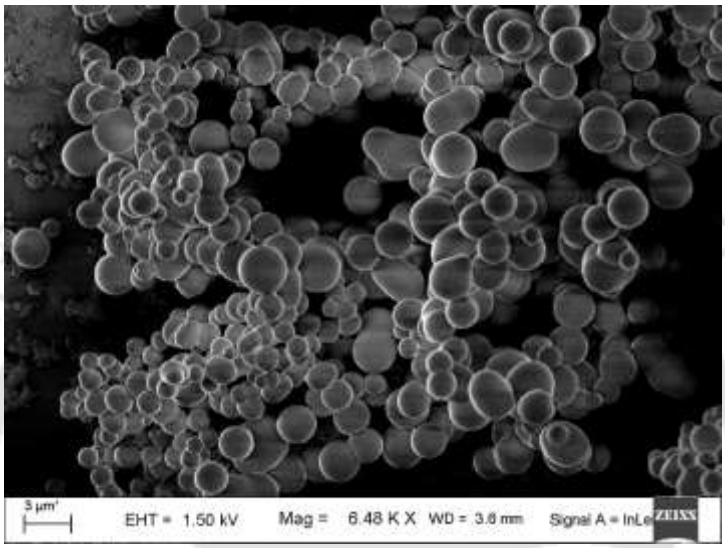

Figure 3.1b: FESEM micrograph of modified-AFC

The FTIR spectrum of the polymer showed sharp lines given in Figure 3.2. Some of the peaks were tentatively assigned by comparing with 2,6 dimethyl aniline and aniline. The 2,6 dimethyl aniline was chemically similar to the repeating unit of the polymer and FTIR spectrum of it was subjected to thorough analysis (Ojha et al., 2012). The expected peaks for primary amine (two N-H stretch expected) were under the broad envelope with a peak maximum at 3413 cm^{-1} due to H-bonding and water. Other characteristic peaks are 2924 cm^{-1}, 2853 cm^{-1} (C-H), 1613 cm^{-1} (very strong, N-H bending), 1517 cm^{-1} (Strongest, C-C stretching), 812 cm^{-1} (out of plane aromatic C-H). These assignments are broadly matching with previous reported assignments (Chandrasekaran et al. 2014). A peak at 1662 cm^{-1}, present in the current polymer, is assigned as C=N stretch arising due to possible imine formation between amine group of polymer and formaldehyde. As we have

used 2 mole equivalent of formaldehyde, formation of some amount of imine was possible. Elemental analysis were also investigated and found out that the absolute percentage values of elemental analysis of solid polymers specially the percentage value of hydrogen element was difficult to match with a formula as it was nearly impossible to control the amount of residual acid attached to amines or salts trapped within the solid and absorbed moisture (Koner et al., 2008).

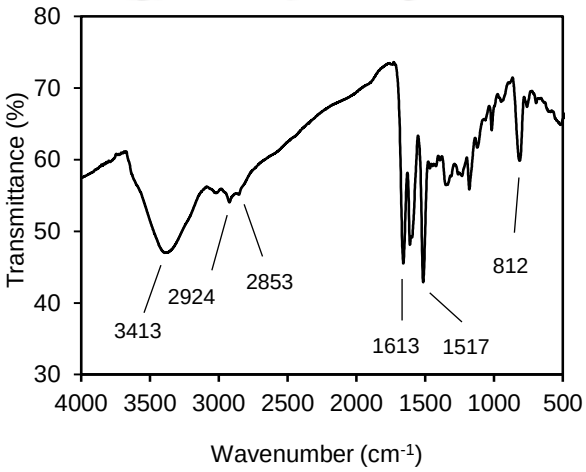

Figure 3.2: FTIR spectrum of polymer adsorbent

However, the mole ratio of C:N was a reliable indicator of composition as either of these elements cannot come from either salt or water or moisture. The C:H:N ratio for the polymer measured for two different batch are found to be 7.13:6.98:1 and 7.19:7.02:1.

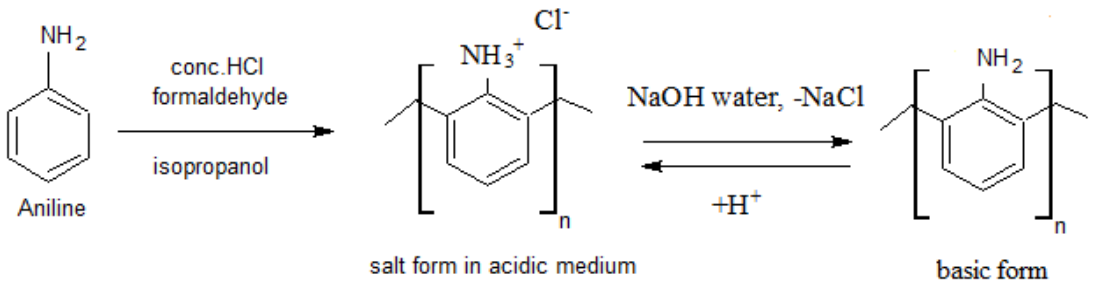

Figure 3.3: Scheme synthesis of modified-AFC

These values were close to expected ratio of 7:7:1 for the proposed formula (Figure 3.3) and they are found to be reproducible over different batches.

The surface area of the adsorbent was determined using standard nitrogen adsorption porosimetric technique employing the BET method (Can et al., 2017; Kishore et al., 2008). Surface area determined from Multi point fitting of BET was found to be 6.88 m^2/g with average pore diameter of 10.46 nm. However, the BET isotherm showed a complex hysteresis loop (Figure 3.4) without showing any limiting adsorption at high P/P_o similar to H3 type (Thommes, 2010). This behavior usually can be caused by the existence of non-rigid aggregates of plate-like particles or assemblages of slit-shaped pores and in principle should not be expected to provide a reliable assessment of either the pore size distribution or the total pore volume (Thommes, 2010).

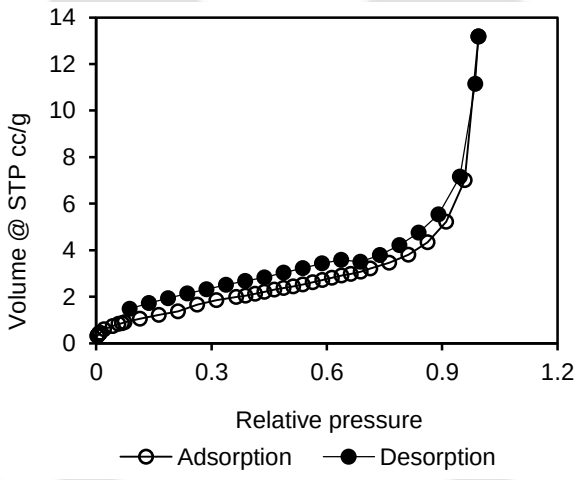

Figure 3.4: N_2 adsorption – desorption isotherm for modified-AFC

Further, the particle size measurements were carried out on the bulk polymer using Martersizer 2000 employing Mie scattering principle. In a Mavern Mastersizer, result analysis report of particle size analyzer the D50 is represented as D(0.50). D represents the diameter of powder particles and D50 means a cumulative 50% point of dimeter (or 50% pass particle size); D10 means a cumulative 10% point of dimeter; D50 is also called average particle size or median diameter; D (4,3) means

volume mean diameter and D (3,2) means plane mean diameter. The results obtained for modified –AFC polymer adsorbent was found to be- D(0.1)-49.234 µm, D(0.5) – 453.211 µm and D(0.9) – 1222.594µm (Figure 3.5). The size range was between 0.02 to 2000µm. The specific surface area was found to be 0.0647 m^2/g. The surface weighted mean D[3,2] was found to be 92.750µm whereas the volume weighted mean D[4,3] was found to be 554.196µm. Thus the polymer can be best descried as random sized particles formed by partial fusion of 1-3 µm diameter sized polymer spheres.

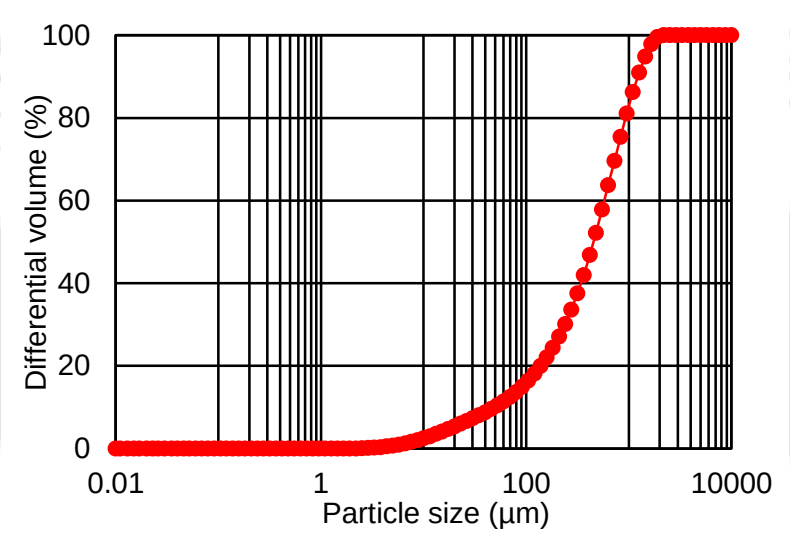

Figure 3.5: Particle size analyzer of modified-AFC

The point of zero charge (pH_{zpc}) was determined using two methods – mass titration method and immersion technique method. When pH_{zpc} was done by mass titration method by varying the amount of polymer in the range 5-100 g/L in 0.03M KNO_3 solution, after 24hrs, final pH became 4.7 for most of the amount of polymer dosage added to the solution given in Figure 3.6a. On the other hand, in immersion technique of pH_{zpc} determination, polymer dose of 25g/L was kept for 24 hrs in 0.03M KNO_3 solution and was adjusted at different pH values of 1-11 (Fiol et al., 2009). It was observed that when the initial pH was acidic to alkaline, (pH 5-11), final pH was decreased

to 3.9-4.5, this observation may be due to the reason that concentrated HCl was added during polymer synthesis and later polymer surface was deprotonated with 1N NaOH solution. Probably deprotonation was incomplete from all pores of polymer and HCl was released into solution when polymer was kept in KNO_3 solution for 24 hrs. The plot is shown in Figure 3.6b for initial pH vs ΔpH and the pH_{zpc} by immersion technique was found to be at pH 4.1.

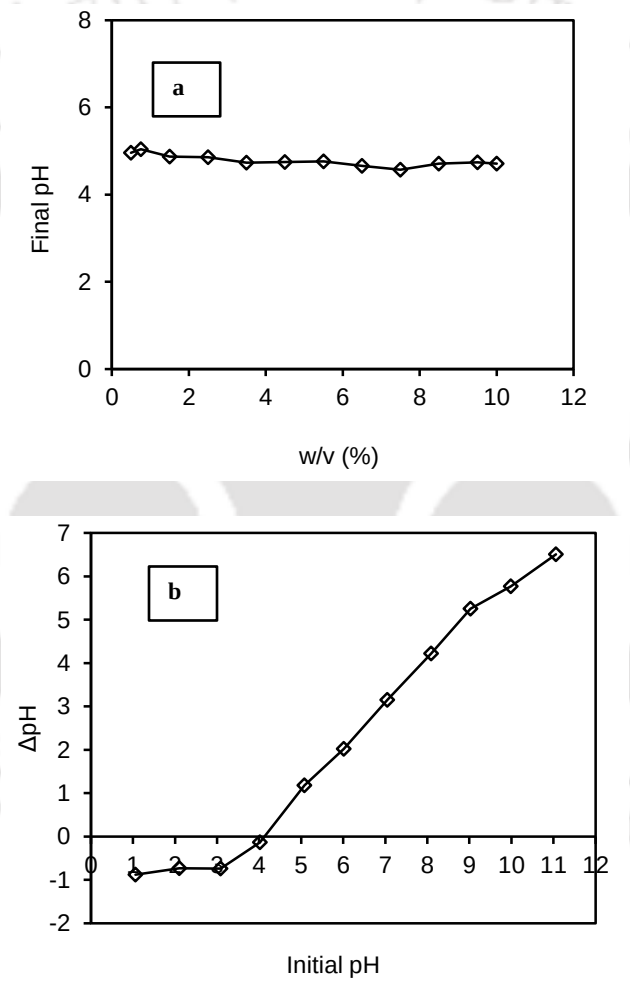

Figure 3.6: Determination of pHzpc of modified-AFC by (a) mass titration and (b) immersion technique

Thermal stability of the modified - AFC was evaluated by thermogravimetric analysis (TGA). As shown in Figure 3.7, the thermogravimetric profile of 6.840 mg of modified - AFC consists of two

degradation stages. The first stage extends from the beginning to about 125°C which may correspond to surface water loss (14.08 %) from the modified - AFC. The second regime from 155°C to 350°C indicates loss of 6.94 % probably due to thermal degradation of remaining material of the polymer adsorbent. A total mass loss of 21.96% was observed up to 350°C. This result reveals that the polymer can be used at ambient temperature and also at moderate temperature (250°C) which are suitable for application in industrial applications.

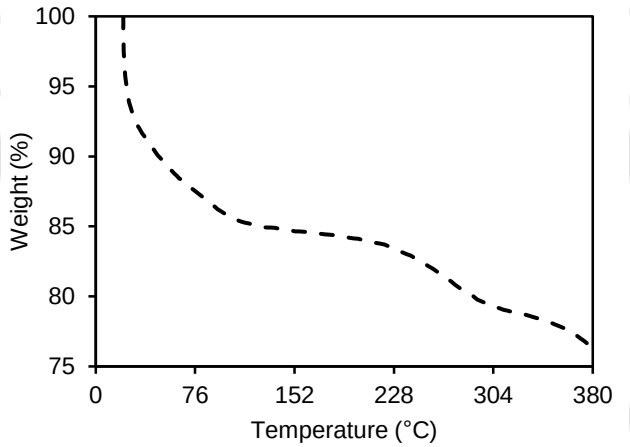

Figure 3.7: Thermogravimetric analysis

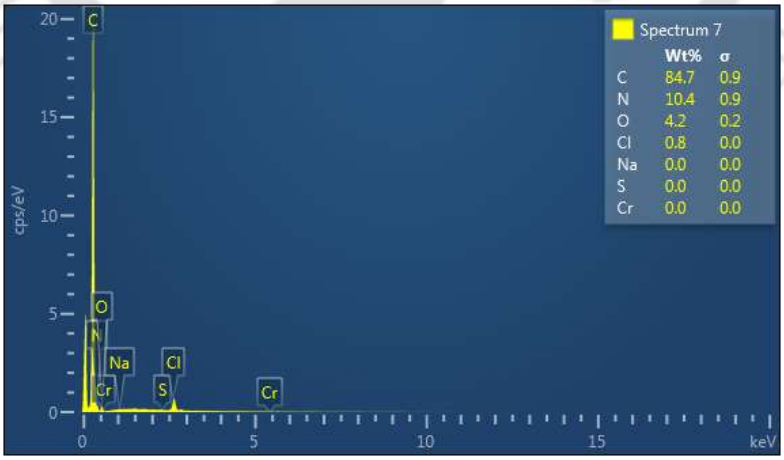

Figure 3.8: EDX micrograph of modified-AFC adsorbent before adsorption

Energy dispersive X-ray analysis was also performed to investigate the presence of any metals in the adsorbent prior to any adsorption experiment. As shown in Figure 3.8, presence of any metals prior to adsorption was found to be very negligible. Moreover, the EDX spectrum confirms that carbon dominates with a weight percentage of 84.7%, whereas N, O, Cl are in the decreasing order with 10.4%, 4.2% and 0.8% respectively.

3.6 Summary

The synthesis of AFC (aniline formaldehyde condensate) an amine based polymer in presence of isopropanol formed a micron sized particles instead of resinous form. Thus, this polymer do not require any supporting material for coating thereby making it cost effective and even reduces the extra weight of the polymer caused by the addition of supporting materials. Characterization of the polymer (modified-AFC) reveals that the polymer is a mesoporous solid polymer with a cluster of spherical shaped particles fused together. The point of zero charge was at pH 4.1 with particle size ranging from 0.02 to 2000 µm. The specific surface area from Multipoint fitting of BET was found to be 6.88 m^2/g with average pore diameter of 10.46 nm. Finally, the preliminary performance evaluation test performed on modified-AFC indicated the polymer to be very efficient from high concentration of Cr(VI) to even dilute concentration yielding high uptake value.

CHAPTER 4

Adsorption of Chromium by modified-AFC

4.1 Introduction

Paint, leather tanning, textile, electroplating, metal finishing industries generate wastewater containing chromium (Abdelhadi et al., 2017; Lee et al., 2018). A number of adsorbents used inactive support materials to increase the granularity and effective surface area such as silica gel, coconut husk, jute fiber etc. were used as support materials (Pakade et al., 2013; Fang et al., 2007; Gao et al., 2009; Bhaumik et al., 2012; Kumar et al., 2007a). Addition of support material increases the overall weight and volume which in turn reduces adsorbent capacity and increases difficulty in disposal of the used adsorbent. Thus, a support less solid polymer seems to be better suitable to address some of these issues mentioned above.

Relatively less literatures addressed Cr(VI) removal from very dilute solution upto the discharge limit (Pakade et al., 2013). As adsorption process is driven by concentration gradient and when initial concentration of adsorbate is higher in solution, higher uptake value is achieved. Adsorption process becomes really challenging to remove the adsorbate ion from very dilute solution due to poor concentration gradient. The objective of the present study was to optimize the removal condition of Cr(VI) from very dilute solution (10 mg/L) using modified-AFC polymer (detailed synthesis and characterization discussed in chapter 3).

4.2. Materials and methods

4.2.1 Materials

The stock solution of Cr(VI) of 1000 mg/L was prepared using required amount of potassium dichromate salt with pH adjusted water. This was diluted with pH adjusted water to get Cr(VI)

solution with concentration ranging from 2 to 10 mg/L. The pH of all the solutions before adsorbent added and after the adsorption experiment were measured and noted.

4.2.2 Adsorption experiment

Initial pH of solution, temperature, dose of adsorbent, initial concentration of Cr(VI) ion, effect of other ions were variable parameters for this study. All experiments were carried out at uncontrolled pH condition. In each experiment 100 mL solution of Cr(VI) (prepared with pH adjusted Millipore deionized water) was used in specimen tubes. Initial solution pH, dose of adsorbent was carried out at initial Cr(VI) of 10 mg/L. In pH variation study, initial pH of the solution was varied from pH 0.76 to pH 6.6 with polymer dose of 2 g/L for 3 h time period. Further experiments were carried out at initial pH of 4. Adsorbent dose was varied from 0.5 to 10 g/L for 12 h. Initial concentration of Cr(VI) was varied from 2 to 10 mg/L using 2 g/L of polymer dose and initial pH 4 for 12 h. All experiments were carried out in orbital shaker at 270 rpm. Effect of other ions on removal of Cr(VI) was studied in presence of chloride (Cl^-), nitrate (NO_3^-), sulphate (SO_4^{2-}), and phosphate (PO_4^{3-}), ions separately for varying concentration (0.002 to 5 mM/L). The respective salts used were: NaCl, KNO_3, Na_2SO_4, and KH_2PO_4. Initial Cr(VI) was 10 mg/L with 2 g/L polymer dose and initial solution pH of 4. Samples were filtered using Whatman filter paper (grade 1) and final pH and residual total chromium concentration were estimated in filtered samples. All experiments were conducted at room temperature and repeated twice to check the accuracy of the experimental results. The amount of total chromium adsorbed on polymer was calculated using Eq (1.40).

4.2.3 Desorption and reuse study

Desorption study was done using chromium loaded polymer with NaOH and HCl using 5 mL of desorbent. Desorption experiments were performed in the orbital shaker at 270 rpm for 3 h. Then

the samples were centrifuged and analyzed for total chromium concentration in desorbent solution. Desorption amount was calculated using Eq. (1.42).

Reusability of the polymer was studied in four consecutive cycles with each cycle consisting of adsorption-desorption. In the first cycle, 10 mg/L of Cr(VI) solution was used with 2g/L dose of polymer at pH 4 for 3 h of adsorption and after decanting the supernatant, the polymer was used for desorption experiment with 1N HCl solution for 3 h. Then the same polymer was used in similar way for another three cycles with fresh Cr(VI) solution of pH 4 and concentration 10 mg/L in every cycle. Residual total chromium concentration was estimated after each cycle of adsorption process and desorption process.

4.2.4 Analytical procedure

Zero-point charge of the polymer was estimated using immersion technique and mass titration method as described by (Fiol and Villaescusa, 2009). Characterization of polymer was carried out using FTIR (Perkin Elmer, PE-RXI), FESEM (Hitachi 5500 FESEM), Particle size analyzer (Mastersizer 2000, Malvern), CHNS analyzer (Eurovector EA3000) and BET surface area analysis (Autosorb-IQ MP). Chromium was analyzed as total Chromium in Atomic absorption spectrophotometer using air-acetylene flame at 357.9 nm wavelength using slit width of 0.2 nm. At this condition measurement range of total chromium is 0.06-15 mg/L. A calibration curve was prepared from 1 to 12 mg/L of Cr(VI) and it was observed that total chromium estimation curve was linear with correlation coefficient of 0.99.

4.2.5 Analysis of modified-AFC after adsorption

The FT-IR technique was used to determine the functional groups on the surface of modified-AFC, which are also responsible for chromium uptake. As shown in Figure 4.1a, there was very

negligible change in the FTIR spectra before and after chromium adsorption with broadly similar to shape as well as the intensity of the spectra. Thus, it can be concluded that the most active functional groups involved during the adsorption of chromium onto modified-AFC adsorbents was mainly the N-H groups followed by C-H and C=N groups. (The FTIR spectra of the adsorbent before adsorption was already discussed in chapter 3). From Figure 4.1b, the EDX spectra suggested the presence of chromium after adsorption.

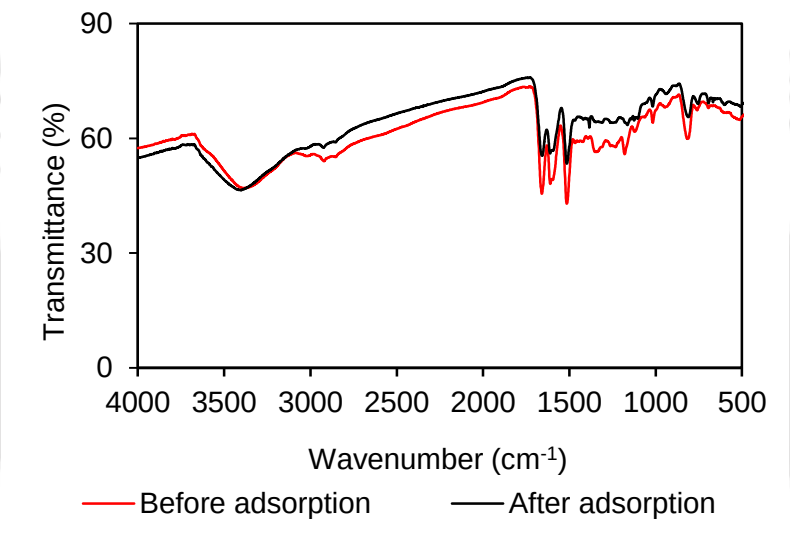

Figure 4.1a: FTIR spectra of modified-AFC

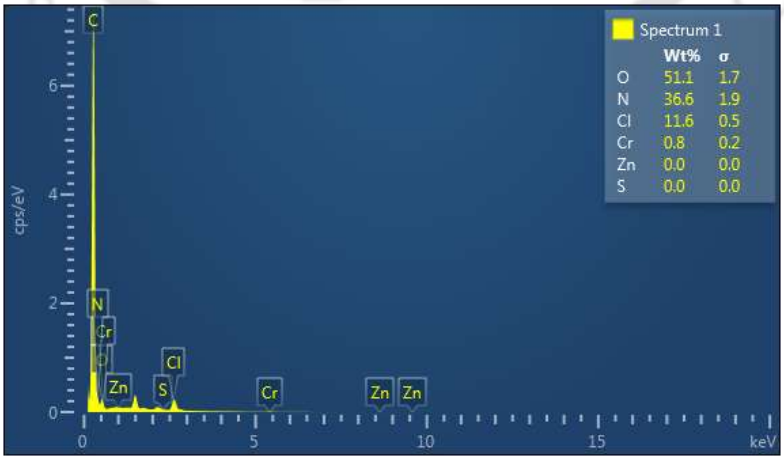

Figure 4.1b: EDX spectra of modified-AFC after chromium adsorption

4.3 Results and Discussion

4.3.1 Effect of initial solution pH and mechanism of removal

The effect of initial solution pH on total chromium uptake is shown in Figure 4.2. Uptake is very low at pH 1. It shows a sharp increase afterward and reaches a maximum at pH ~4, followed by gradual decrease up to pH 6. In order to understand the behavior, a comparison between the experimental result and the pH dependent distribution of the key species involved in the mixture was compared (Figure 4.2).

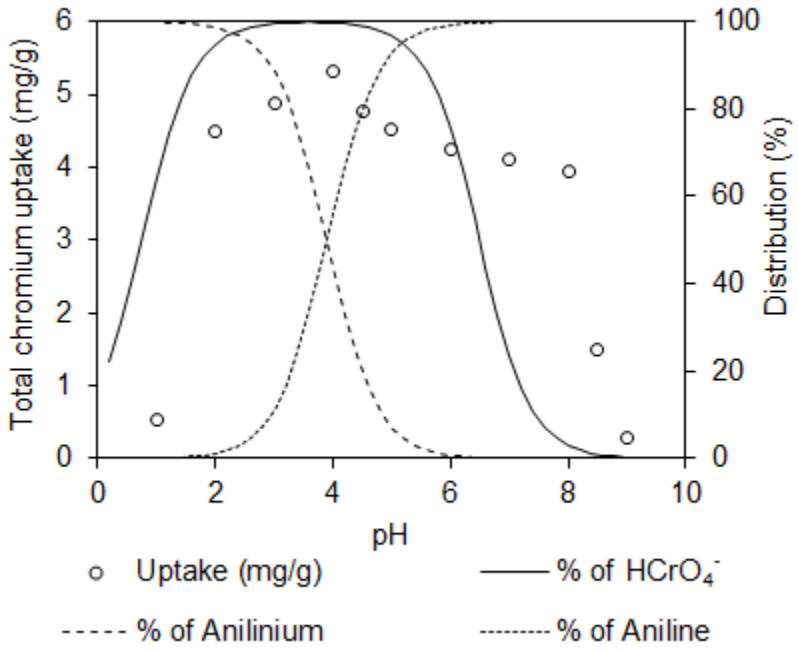

Figure 4.2: Effect of initial solution pH on total chromium removal and distribution of species

Distribution of $HCrO_4^-$ and amine functional group over a range of pH was calculated from the reported pKa values (Lide, 2004). The presence of dichromate ion was ruled out as it exists in higher concentration (above pCr of 1.5 or 0.03 M) (Gao et al., 2009). The species distribution of $HCrO_4^-$ showed sharp rise from pH 1 and remains the species up to ~6. On the other hand, the amine group of polymer is mostly in anilinium form between pH 1-4. Removal in this range closely

followed the concentration of $HCrO_4^-$ indicating removal through ion-exchange mechanism by the chloride counter ion of anilinium form of polymer. Anilinium form is less susceptible to oxidation than free amine form due to cationic nature. Thus, removal through redox mechanism [reduction of Cr(VI) and adsorption of Cr(III)] is less likely in this range. The slow drop after pH 4 where anilinium concentration decreased indicated decrease in ion-exchange. Decrease was not as rapid as decrease in anilinium, which indicates that removal by oxidation of amine somewhat compensates for lack of ion-exchange. Amine form is more susceptible to oxidation by $HCrO_4^-$ thus removal was likely to be through redox mechanism between pH 4-7. The drop in removal between pH 6 to 7 was consistent with the drop of $HCrO_4^-$ concentration. The value at pH 8 is expected to be lower as well but it did not. It is possible that this particular data may have some measurement problem. However, next two set at pH 8.5 and 9 shows the expected sharp drop due to the lack of oxidizer ($HCrO_4^-$). The CrO_4^{2-} ion, can neither ion exchange with amine form of amine or oxidize it as it is a weak oxidizer.

In previous study with AFC coated silica gel, initial Cr(VI) was 40 mg/L and with AFC dose of 8 g/L, maximum removal achieved at pH 3 (Kumar et al., 2007a). Experiments at pH 3 mean significant acid addition in the wastewater before adsorption process which is not desirable. Since uptake of total chromium in the present case is similar at initial pH of 3 and 4, further studies were carried out at pH 4.

4.3.2 Effect of adsorbent dose

Effect of polymer dose on removal and uptake of total chromium are shown in Figure 4.3. Uptake value decreased with increase in polymer dose, due to saturation of the adsorbent sites when adsorbate concentration remained constant.

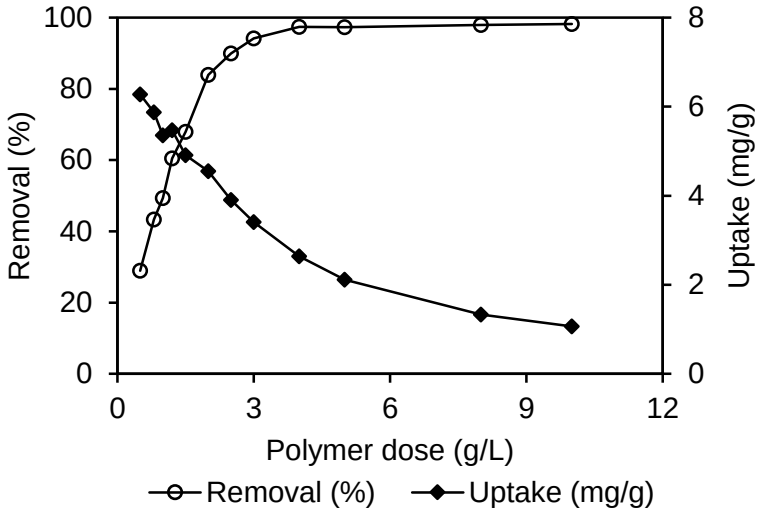

Figure 4.3: Effect of polymer dose on total chromium uptake and removal

In order to meet the discharge limit of 2 mg/L (IS) (Bhargava et al., 2018), minimum polymer dose required was 2 g/L for initial Cr(VI) of 10 mg/L and uptake value achieved was 4.55 mg/g. A comparison was compared with few other materials which was selected on the basis of similar pH and initial concentration range given in Table 4.1. Present polymer was found to be much better than our previously reported AFC on silica gel but closer to the polyaniline on jute. Uptake value was also comparable to commercially available ion exchanger Amberlite IRA-400 which contains quaternary amine functional group, and multiwall carbon nano tube despite having large available surface area. Higher uptake value alone does not ensure <1mg/L chromium residual concentration. In terms of percentage of removal, the present polymer reaches a balance between higher removals with a reasonably high uptake value compared to other materials listed in Table 4.1. In this regard, the cellulose based anion exchanger reported by Anirudhan et al. 2009 remains the best among all compared.

Table 4.1: Comparison of uptake and removal of various adsorbents at dilute concentration of Chromium

Adsorbent	pH	Dose (gm/L)	Adsorption capacity (mg/g)	Removal (%)	Surface area (m^2/gm)	Reference
Modified-AFC	4	2	4.5	85	6.9	This work
AFC on silica gel	3	8	0.62	43	49.6	Kumar et al. 2007a
Polyaniline on Jute	3	2	3.52	72	3.56	Kumar et al. 2008
Waste pumice	3	6	1.03	62	-	Sepehra et al. 2014
Surface modified pumice	3	6	1.31	78.6	-	Sepehra et al. 2014
Chitosan CDTA-GO nanocomposite	3.5	5	1.96	98	-	Ali et al. 2016
Cellulose based anion exchanger	3.5	2	4.99	99	-	Anirudhan et al. 2009
Activated carbon coated poly vinyl pyridine	4	1	6.76	75	-	Fang et al. 2007
Modified litchi peel	4	4	1.5	40	-	Yi et al. 2017
Activated charcoal	4	0.1	9.8	90	>1000	Jung et al. 2013
Single wall nanotube	4	0.1	7.5	80	>500	Jung et al. 2013
Multi wall nano tube	4	0.1	1.8	60	>500	Jung et al. 2013
Amberlite IRA-400	4	6	3	60	-	Kusku et al. 2014

4.3.3 Adsorption isotherm

Isotherm plot of total chromium uptake (q_e) and total chromium concentration (C_e) at equilibrium is shown in Figure 4.4. Isotherm shape was convex type without any plateau. Since this study was carried out at dilute concentration of Cr(VI), plateau could not be achieved.

According to isotherm classification it was of L1 type isotherm (Giles et al. 1974). Several isotherm models like Langmuir (eq. 1.17), Freundlich (eq. 1.19), Redlich-Peterson (eq. 1.36),

Langmuir-Freundlich (LF) (eq. 1.33) and Temkin (eq. 1.22) isotherm models were tested with experimental data (Hamdaoui et al., 2007).

Nonlinear regression was carried out to determine isotherm parameters. The fitness of the isotherm model with experimental data was verified from correlation coefficient (R^2) and average relative error (ARE) (eq. 1.39). Isotherm parameters are given in Table 4.2. In Figure 4.4, experimental and modeled isotherm plots are shown. It can be seen that Langmuir, Redlich- Peterson and Langmuir-Freundlich models showed more closeness to experimental data points than Freundlich and Temkin models. In Redlich-Peterson model, 'g' value of 1.08 (≈1), suggests, closeness to Langmuir model.

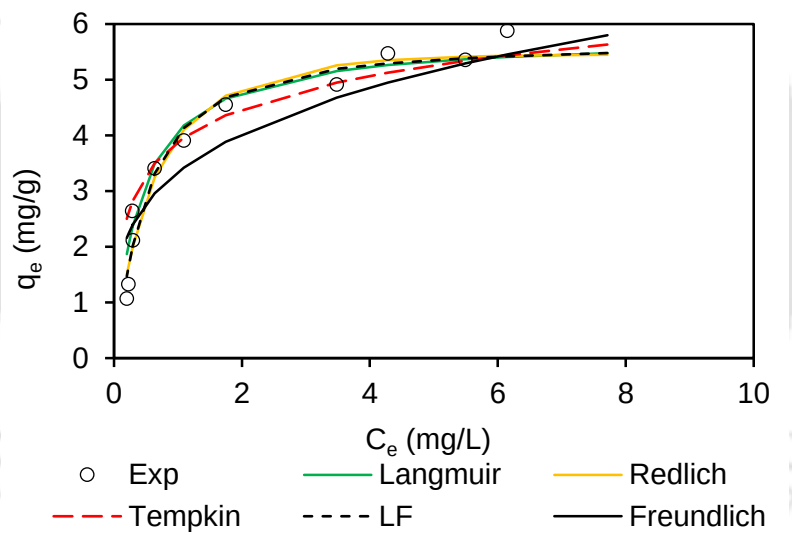

Figure 4.4: Isotherm plot of total chromium uptake by modified-AFC

Total chromium formed monolayer on polymer surface during adsorption process and maximum monolayer uptake achieved was 5.77 mg/g (0.11 mmol/g) and binding constant was 2.40 L/mg (124.8L/mmol). Fang et al., 2007 reported maximum uptake of 30.6 mg/g and binding constant of 0.214 L/mg, when poly(4-vinyl pyridine) coated activated carbon was used at pH 3.6 and initial Cr(VI) of 100 mg/L. Aniruddhan et al., 2009 reported binding constant of 18 L/mmol, when

tertiary amine loaded cellulose was used for Cr(VI) removal. The binding constant observed in this study was much higher than the reported values.

Table 4.2: Estimated isotherm parameters for adsorption of total chromium by modified-AFC at pH 4

Model	Model parameters		R^2	ARE (%)
Langmuir	Q_m (mg/g)	5.77	0.98	14.8
	b (L/mg)	2.40		
Freundlich	K_f	3.34	0.966	20.36
	1/n	3.70		
Redlich	A	9.28	0.975	10.61
	B	1.34		
	g	1.08		
LF	Q_m (mg/g)	5.67	0.978	9.96
	b (L/mg)	2.08		
	1/n	1.20		
Temkin	A	0.855	0.98	23.41
	ΔQ	61.32		

4.3.4 Effect of initial Cr(VI) concentration

The initial concentration of adsorbate provides an important driving force to overcome the mass transfer resistance during adsorption process. Initial Cr(VI) was varied from 1.9 to 9.9 mg/L and residual total chromium concentration with time is shown in Figure 4.5. From initial Cr(VI) of 1.9 mg/L, residual of 0.03 mg/L was achieved within initial 30 min at polymer dose of 2 g/L at pH 4. Chowdhury et al., 2010 reported an equilibrium time of 120 min and 90% removal from initial Cr(VI) of 2 mg/L by maghemite-magnetite nano size particles of dose 0.4 g/L.

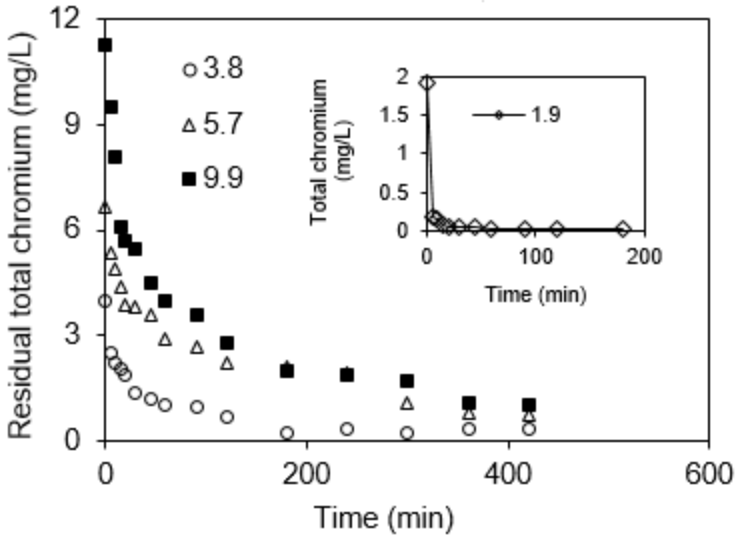

Figure 4.5: Kinetics of total chromium adsorption by modified-AFC

Total chromium uptake increased with increase in initial Cr(VI) concentration from 0.94 to 5.10 mg/g, due to higher driving force and higher chances of interaction between adsorbate and adsorbent molecules. Equilibrium time and removal decreased with increase in initial Cr(VI) concentration.

4.3.5 Adsorption kinetics

In order to find out the governing step of adsorption process, kinetic data of total chromium uptake by polymer was analyzed using intraparticle diffusion model (Jansson-Charrier et al., 1996) (eq. 1.18). Intraparticle diffusion plots as qt vs time$^{0.5}$ are shown in Figure 4.6. The plot shows three linear region for initial Cr(VI) of 3.8-9.9 mg/L and two linear portions for initial Cr(VI) of 1.9 mg/L. During initial 15-20 min, the slope was very high, which was due to external mass transfer resistance. Then slope became gradual upto 90-240 min and finally slope became flat, suggesting equilibrium stage. The intermediate portion was due to intraparticle diffusion. The slope of the plot of the linear part of the q_t against $t^{0.5}$ plot (here taken between 15 and 200-240 min) gives the

values of diffusion rates (k_i). Values of diffusion rates (k_i) are given in Table 4.3. As expected, diffusion rate increased with increase in initial Cr(VI) concentration due to higher driving force for adsorption process. Since external mass transfer and intraparticle diffusion both were involved in adsorption of total chromium, model proposed by Riechenberg, 1953 (eq. 1.11a and b) was tested to determine the rate limiting step of adsorption.

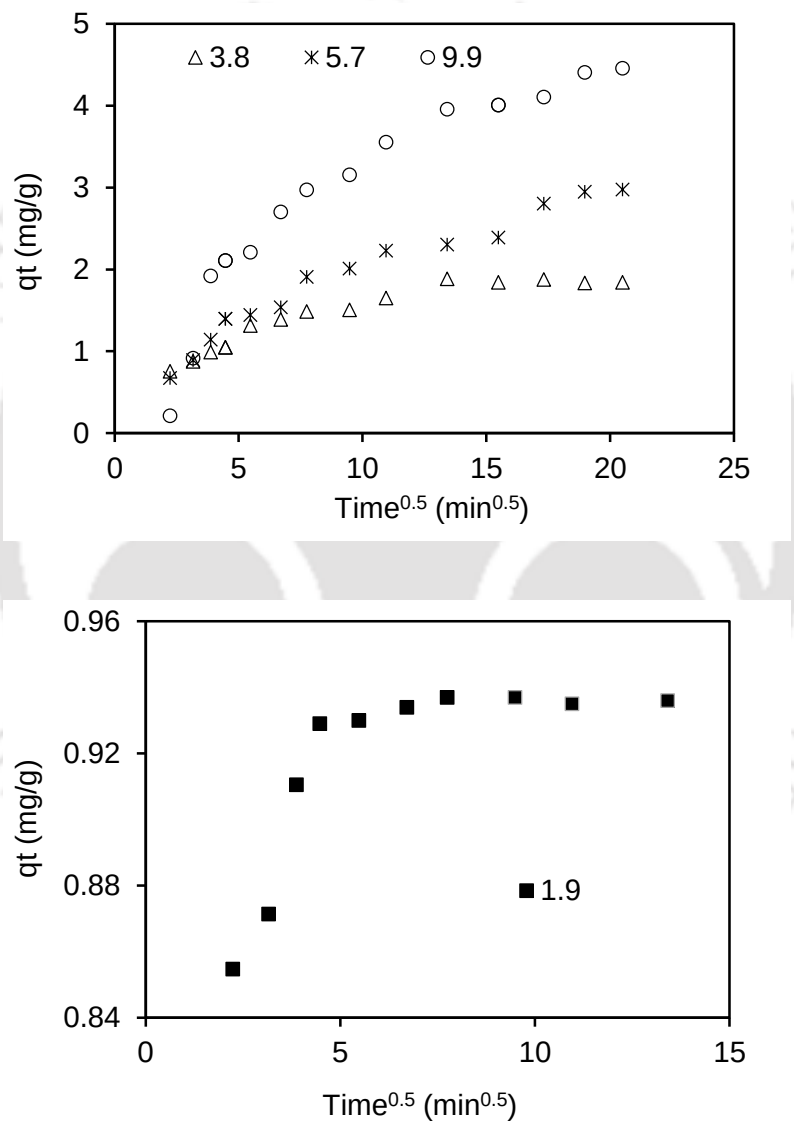

Figure 4.6: Intraparticle diffusion plots for total chromium uptake by modified-AFC

If the plot of Bt vs. t (Boyd's plot) is linear and passes through origin, it suggests that adsorption is governed by particle diffusion, otherwise it is controlled by film diffusion. Boyd's plots are shown in Figure 4.7.

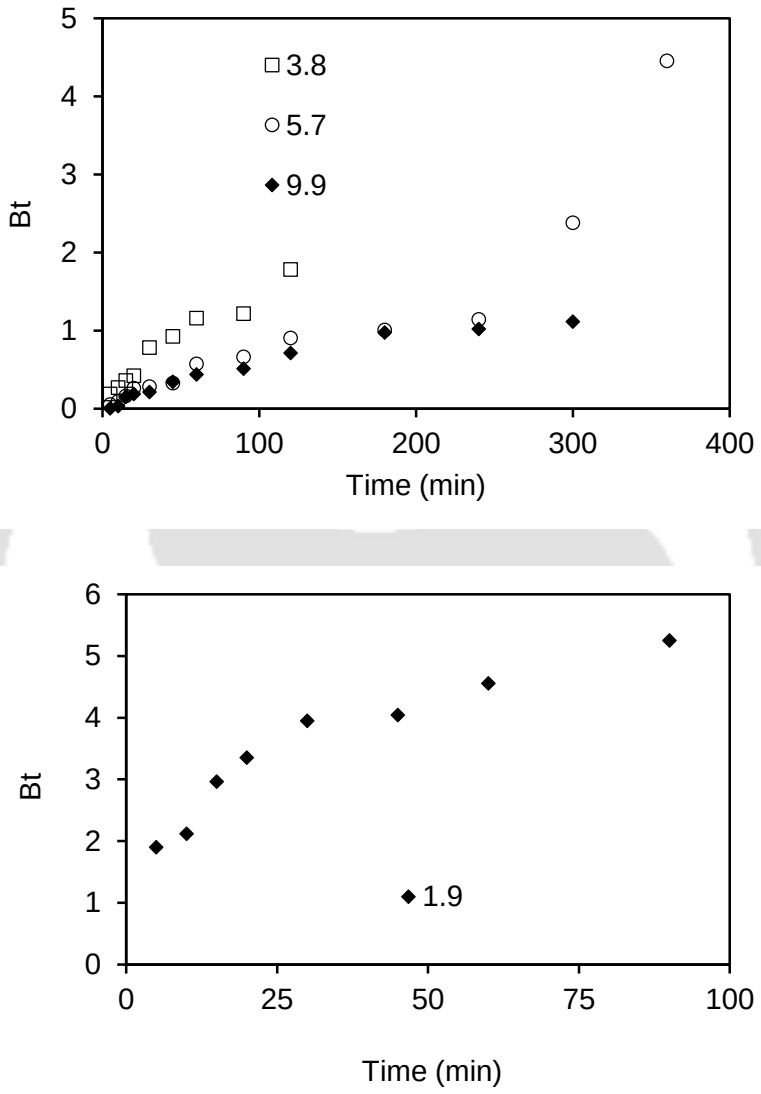

Figure 4.7: Boyd's plots for total chromium adsorption by modified-AFC

It can be seen that for initial Cr(VI) of 3.8-9.9 mg/L, the plots were linear upto 180-240 min and if extrapolated behind, passed through origin. However, for initial Cr(VI) of 1.9 mg/L, the plot did not pass through origin. This result suggests that total chromium adsorption by modified-AFC,

both diffusion and mass transfer were involved and mass transfer was dominating when initial Cr(VI) was 1.9 mg/L or less. Similar phenomenon was reported by previous researchers, when external mass transfer was dominating mechanism for Hg(II) adsorption by baggasse fly ash, when initial concentration of Hg(II) was lower than mM (Mohan and Singh, 2002).

External mass transfer coefficients were determined from "linear driving force" rate law given in eq. 4.1 (Cooney, 1999). This law states that the rate of adsorbate uptake by solid is equal to the rate of adsorbate disappearance from liquid (eq. 4.1) (Cooney, 1999).

$$-V\left(\frac{dc}{dt}\right) = k_f A_s (C - C_i) \qquad (4.1)$$

Where, V is liquid volume (250 mL); A_s is surface area of adsorbent (m^2) (1.611 x10^{-7} m^2, calculated from mean diameter of modified AFC as 453 µm); k_f is external mass transfer coefficient (m/min), C_i is the concentration of adsorbate on the surface of adsorbent. At t→0 (beginning of adsorption), C_i is very negligible and C= C_o (initial adsorbate concentration in solution). The slope of the plot of $\frac{C}{C_o}$ vs. t, near t→0 (here initial 20 min), is $\left(-\frac{k_f A_s}{V}\right)$. The value of k_f (m/min) is given in Table 4.3.

Table 4.3: Kinetic parameters of total chromium adsorption by modified-AFC

Initial Cr(VI) (mg/L)	Intraparticle diffusion		External mass transfer	
	R^2	k_i (mg/min$^{0.5}$)	R^2	k_f (m/min)
1.9	0.97	0.002	0.94	2.57x10^{-12}
3.8	0.94	0.078	0.98	6.44 x10^{-12}
5.7	0.86	0.136	0.99	9.02 x10^{-12}
9.9	0.86	0.183	0.94	14.82x10^{-12}

External mass transfer rate increased with increase in initial concentration of Cr(VI) ion and maximum value was observed $14.8x10^{-12}$ m/min at Cr(VI) concentration of 9.9 mg/L. Sag and Aktay, 2000 reported that external mass transfer coefficient of $6.78x10^{-4}$ m/min during adsorption on chitin, at initial Cr(VI) concentration of 27 mg/L and mass transfer rate increased with increase in initial Cr(VI) upto 102 mg/L. Probably extremely dilute concentration of Cr(VI) used in this study was responsible for lower mass transfer rate in our study.

4.3.6 Effect of other ions

Effect of competing anions on Cr(VI) adsorption was studied at pH of 4 and results are shown in Figure 4.8. Study was carried out separately using four anions of varying concentrations (0.002-5 mM/L) and constant concentration of Cr(VI) ion (0.19 mM/L). When Cr(VI) concentration was much higher than anion concentration, [Cr(VI): anion ratio of 95:1], phosphate and nitrate were responsible for decrease in uptake by 28-38%, but effect of sulphate and chloride on Cr(VI) uptake was negligible. With decrease in Cr(VI): anion ratio (1.9:1), more anions were available in solution and Cr(VI) uptake decreased further by 15% by sulphate, 38% by chloride, 53% by nitrate and 69% by phosphate. Higher the concentration of anion, more was inhibitory effect on chromium adsorption and inhibition was in the order of phosphate> nitrate> chloride > sulfate. Karthik et al., 2015 observed that except bicarbonate, sulphate, chloride, nitrate had no inhibitory effect during chromium adsorption by polyaniline-polyvinyl alcohol composite. Fang et al., 2007 reported that to hinder chromium adsorption by poly(4-vinyl pyridine), concentration of anions (sulphate, nitrate, phosphate) should be twenty six times higher than chromium concentration and inhibition was in the order of phosphate> nitrate> sulfate. In the present study, anions hindered chromium adsorption when present in solution half of chromium concentration, i.e. Cr(VI):ion ratio of 1.9:1. However, higher inhibitory effect of anions on Cr(VI) adsorption suggests that chromium

adsorption largely followed ion exchange type mechanism at pH 4 instead of chemical reduction as suggested by Lee et al., 2005 as well as the observation found during the investigation carried out during the adsorption experiment.

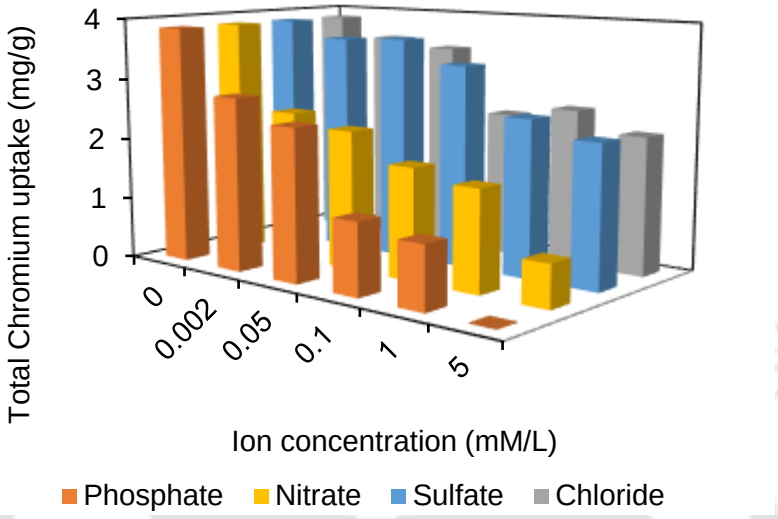

Figure 4.8: Effect of other anions on total chromium uptake by modified-AFC

4.3.7 Desorption and reuse of modified AFC

Chromium loaded modified AFC was treated with various desorbents and desorption efficiency is shown in Table 4.4. With NaOH, desorption was negligible (0.9-4%).

Table 4.4: Desorption of total chromium from modified-AFC

Desorbing agent	Desorption time (h)	Desorption efficiency (%)
0.5N NaOH	12	0.98
1 N NaOH	12	1.1
2N NaOH	12	4.0
0.5 N HCl	12	31
1N HCl	12	86
2N HCl	12	57

HCl of varying strength was used for desorption and maximum desorption 86% of total chromium was released in solution with 1 N HCl. This supports the ion exchange type mechanism being the major contributor in Cr(VI) removal at pH 4 along with minor contribution from redox based removal. Modified-AFC polymer was used for removal of Cr(VI) in four cycles of adsorption-desorption process with fresh Cr(VI) solution (10 mg/L and pH 4) in each cycle and results are shown in Figure 4.9. Total chromium uptake was 4.6 mg/g in the first cycle and decreased by 15%, 21% and 43% in second, third and fourth cycle, respectively.

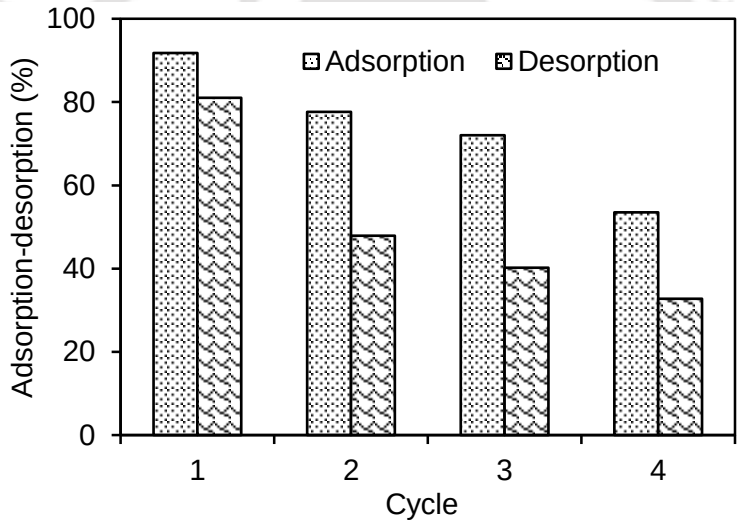

Figure 4.9: Adsorption-desorption of chromium from modified-AFC in several cycles

4.4 Summary

A support less microsized polymer clusters was synthesized by modifying the synthesis process of aniline formaldehyde condensate (AFC) polymer. Chemical analysis and characterization showed virtually no change in chemical composition from the unmodified one. Maximum adsorption was achieved at pH 3-4. Optimum polymer dose was observed to be 2 g/L for obtaining residual concentration of 1.74 mg/L which was found to be below the discharge limit of 2 mg/L from initial

concentration of 10 mg/L with uptake of 4.5 mg/g as total chromium. While AFC on silica gel showed only 30% removal with a dose of 8g/L, the present polymer showed 96% removal using 4g/L (85% removal using 2g/L dose), almost 8 fold increase in efficiency. Comparison showed that the present material is either at par or better than most of the materials compared including commercially available ion-exchanger (Table 4.1). Almost 86% desorption was possible with 1N HCl. All anions like phosphate, nitrate, sulfate and chloride were responsible for hindering total chromium adsorption and inhibition increased with increase in anion concentration. Phosphate and nitrate strongly inhibited total chromium uptake while effect of sulfate and chloride are less.

Ion-exchange mechanism by electrostatic attraction with protonated amine group of modified-AFC and acid chromate ion ($HCrO_4^-$) was found to be responsible for chromium uptake with some contribution from redox based removal. An additional benefit of using the amine form of polymer was that the final pH of the solution was in the neutral range due to consumption of proton by the polymer. This increases the usefulness of its use in the treatment of acidic Cr(VI) wastewater.

CHAPTER 5

Removal of anionic form of mercury(II) from dilute solution using modified-AFC

5.1 Introduction

Mercury [Hg(II)] is regarded as one of the most toxic pollutants due to its high toxicity and bioaccumulative properties (Shen et al., 2017, Liu et al., 2017). Almost all mercury species, inorganic ions or organomercury compounds are toxic (Yu et al., 2016; Attari et al., 2017; Bjørklund et al., 2017). The removal of mercury from dilute solution to reach permissible level in the ppb level still remains a challenging task. One interesting aspect of Hg(II) ion is that in presence of halide ions, Hg(II) tends to form either $[HgX_4]^{2-}$ (where $X = Cl^-, Br^-, I^-$) or one of the several other similar anionic species depending on the halide concentration and other conditions. In this condition, use of anion exchange resins instead of cation exchanger, might have advantages. Polymers with amine functional group can functions as anion exchangers in acidic pH. At higher pH, amine usually bind Hg(II) to form relatively less soluble mixture of HgO and amidate complex (Jeffery et al., 1989). There are very few reports of removal of Hg(II) using from very dilute solution polymers with amine functionality (Ma et al., 2009).

In this chapter, the same modified powdered form of the polymer was used to study the removal of dilute aqueous solution of $HgCl_2$.

5.2 Materials and methods

Mercuric chloride solution was used as the source of mercury (other materials already given in chapter 4).

5.2.1 Adsorption experiments

A stock solution of mercury chloride 1000 mg/L was prepared by dissolving in distilled water. The experimental procedure including the methodolody and apparatus used for adsorption experiments were almost similar to the procedure discussed in chapter 4. Adsorption experiments were carried with various parameters – pH, adsorbent doses, adsorbate concentrations and temperatures. Experimental solutions of the desired concentrations were obtained by successive dilutions with distilled water. The adsorption experiments were also carried out to determine the equilibrium time, the optimum pH, temperature and dosage of the adsorbent for maximum adsorption. Adsorption was performed in orbital shaker by adding 2g adsorbent in 1000 mL of Hg(II) aqueous solution and pH adjustments were done by adding acetate buffer (1M). All adsorption experiments were performed using 100 mL volume of Hg(II) solution. Acetate buffer of pH 4 was added about 1.5 mL in 100 mL total volume of mercury 10 mg/L solution. Adsorption was performed in orbital shaker after adding adsorbentThe amount of mercury ion adsorbed on modified-AFC was obtained using eq. 1.40. Effects of anions on Hg(II) adsorption was studied using four anions (chloride, sulphate, nitrate and phosphate) of varying concentrations (0.05, 0.1, 1.0 and 5.0 mM) in presence of Hg(II) of 10 mg/L at pH 4 for 3h. Potassium hydrogen phosphate anhydrous (K_2HPO_4), sodium sulfate (Na_2SO_4), sodium nitrate ($NaNO_3$) and sodium chloride (NaCl) was used as a source for phosphate, sulfate, nitrate and chloride, respectively.

5.2.2 Desorption experiment

To perform desorption different strengths of desorbent (HNO_3, HCl, H_2SO_4) were used. Desorbent volume of 30 mL was taken in 50 mL plastic vial and the experiment was performed in orbital shaker. The samples were drawn for analyzing final concentration. The desorption (%) was calculated by the equation (1.42).

For the adsorption-desorption cycle experiments were carried under the same conditions but for 60 mins agitation time and the adsorbent used in the next cycle was dried in room temperature for 12 h and then dried at 60°C for 1-2 h. The amount of mercury ions was determined after each adsorption-desorption cycle.

5.2.3 Analytical methods

Mercury was analyzed using cold vapor generation atomic absorption spectrometry (CVG-AAS) for lower concentration (standard ranging from 5 to 60 µg/L) and atomic absorption spectrometry (flame-AAS) (model-AA240, Varian) for higher concentration with wavelength of 253.7nm , slit width of 0.5nm, optimum working range between 2-400 mg/L for atomic absorption spectrometry (flame-AAS). All pH measurements were measured using pH meter (model-LT-49, Microprocessor pH meter). The elemental analysis was obtained from CHNS Elemental Analyzer (model- EA3000, Eurovector) and surface morphology was recorded in field emission scanning electron microscope (FESEM) (model-sigma, Zeiss). Thermogravimetric analysis was performed using TGA (model-STA449F3A00, Netzsch), BET surface area was analyzed using surface area and pore size analyzer and high pressure analyzer (model- Autosorb-IQ MP, Quantachrome).

5.3 Results and discussions

5.3.1 Analysis of modified-AFC after adsorption

The surface morphology of modified-AFC after examination was found to be a cluster of spheroid shaped uniformly distributed material shown in Figure 5.1, shows the morphology of the polymer after adsorption which clearly indicates the presence of the adsorbed pollutants i.e. significant amount of mercury on the surface of the polymer. This was resulted due to the fact that mercury ions were adsorbed chemically on the surface of the modified-AFC. (Detailed characterization of

modified-AFC was already discussed in chapter 3). The FTIR spectral analysis was carried to confirm the functional groups present in polymer. The FTIR spectra before and after adsorption shown in Figure 5.2a, suggested that no major change occurred during adsorption but indicates the presence of amine functional groups. The micrograph depicts the presence of amine group at the peak of 3413 cm^{-1} due to N-H stretching and at 1613 cm^{-1} due to N-H bend suggesting primary amines, 1517 cm^{-1} due to C-C stretching and 812 cm^{-1} due to C-H aromatic rings out of plane bending. As shown Figure 5.2b, the EDX spectra after mercury adsorption indicates the presence of mercury ions on the adsorbent. Presence of the chloride in both the EDX spectrum was because $HgCl_2$ was used as the source of mercury and the modified-AFC polymer also released chloride ion in aqueous solution (EDX spectra of blank polymer already discussed in chapter 3).

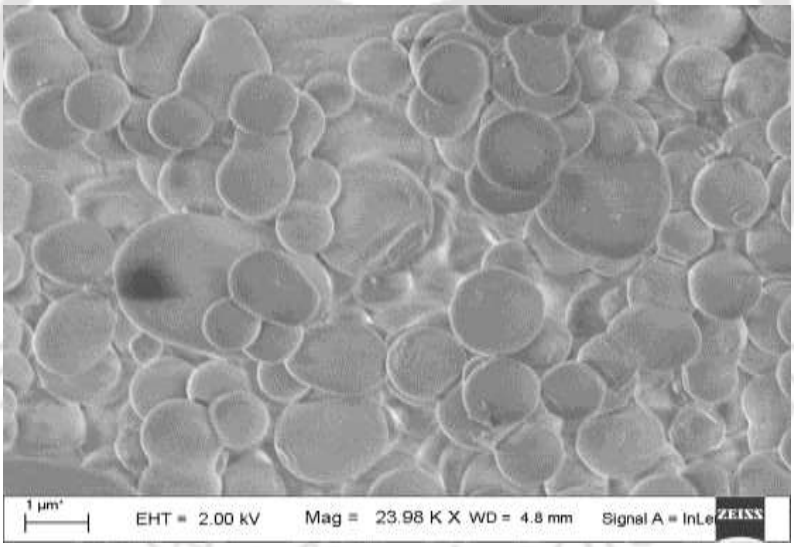

Figure 5.1: FESEM micrograph of modified-AFC after adsorption

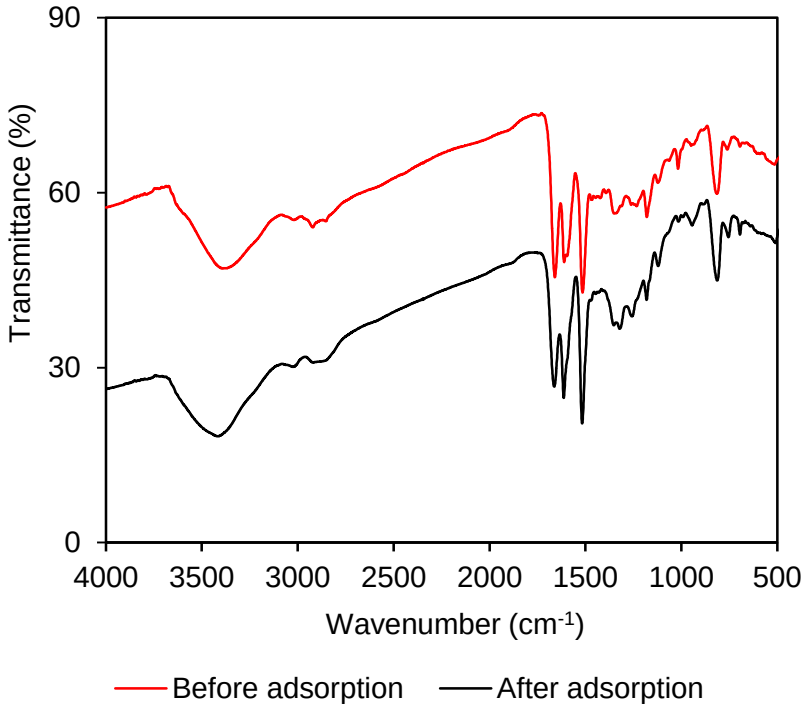

Figure 5.2a: FTIR spectra of modified-AFC before and after adsorption

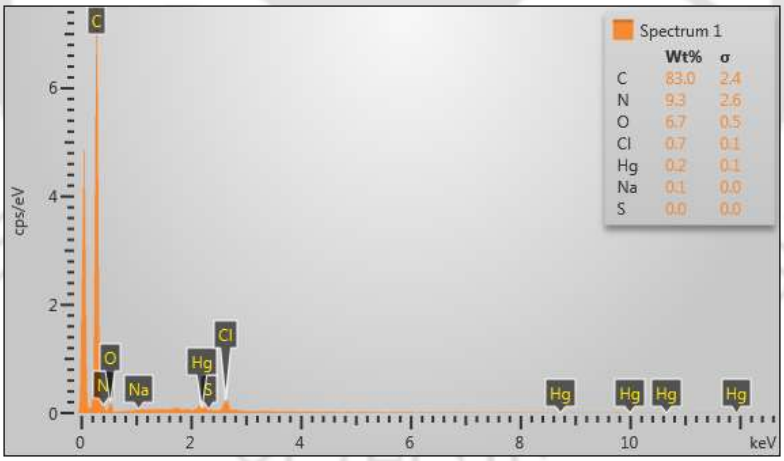

Figure 5.2b: EDX spectra of modified-AFC after mercury adsorption

5.3.2 Effect of pH

The influence of the solution pH on the removal efficiency was examined at initial Hg(II) concentration of 10 mg/L using 2g/L polymer dose. Initially, experiments were carried out at

uncontrolled pH condition (3-5) where the pH was adjusted using 1N HCl as shown in Figure 5.3. Equilibrium pH was 3.1-3.7, suggesting proton release at pH 4 and 5. Further experiments were carried out at constant pH using pH using acetate buffer. Experimental pH was varied from 3 to 5.5 to avoid any precipitation of mercury ions in higher pH range. From the results it can be seen that the addition of acetate buffer showed high removal efficiency with formation of a plateau within pH 3-4. A sharp decrease on the removal beyond pH 4 was then observed (Figure 5.4a). According to the Hard-Soft-Acid-Base (HSAB) theory, mercury is classified as a soft acid, with a high tendency to form strong covalent bonds with CN, -RS, -SH, $-NH_2$ groups. It is also known that the species of mercury are available in several soluble complex ions with chlorides, hydroxide and acetate like $HgCl^{+}_{(aq)}$, $HgCl_3^{-}{}_{(aq)}$, $Hg^{2+}{}_{(aq)}$, $HgCl_4^{2-}{}_{(aq)}$, $HgOH^{+}{}_{(aq)}$, $Hg(OH)_{2(aq)}$, $Hg(OH)_3^{-}{}_{(aq)}$, $HgOHCl_{(aq)}$, $HgAc^{+}{}_{(aq)}$, $HgAc_2{}^{0}$, $HgAc_3^{-}{}_{(aq)}$ and $Hg(Ac)_4^{2-}{}_{(aq)}$. It was experimentally observed that 2 g of polymer after dissolving in distilled water (1L), released chloride (Cl^{-}) ion of 3.98 g (0.112 M).

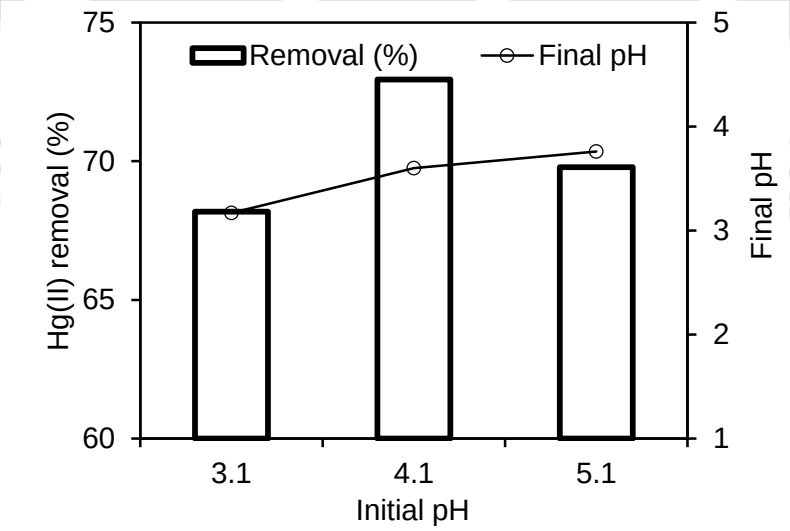

Figure 5.3: Effect of uncontrolled solution pH on the removal of Hg(II) with modified-AFC (C_o: 10mg/L, pH 4, dose: 2g/L, 3h)

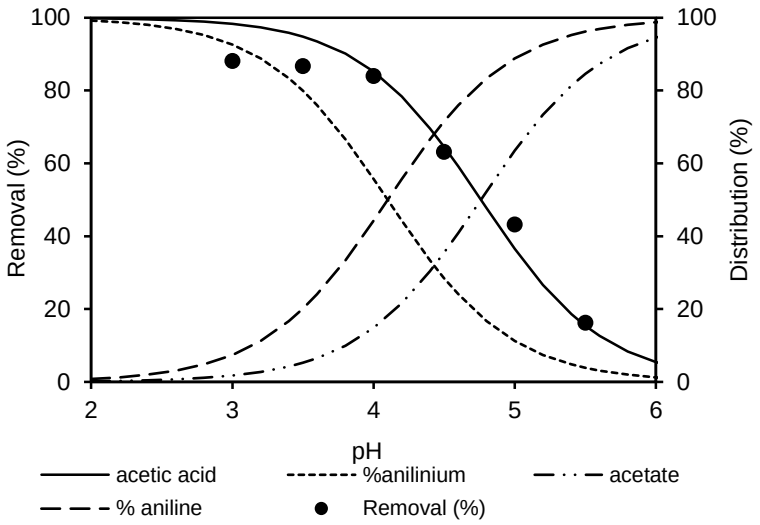

Figure 5.4a: Effect of controlled solution pH on the removal of Hg(II) with modified-AFC and species distribution (C_o: 10mg/L, pH 4, dose: 2g/L, 3h)

Mercury speciation diagram was constructed using this Cl^- ion and shown in Figure 5.4b. It is seen that $HgCl_3^-$ was the dominating specie, followed by $Hg(Ac)_4^{2-}{}_{(aq)}$, $Hg(Cl)_4^{2-}{}_{(aq)}$, $Hg(Ac)_3^-{}_{(aq)}$. From the Figure 5.4a, it was observed that the removal trend followed the acetic acid curve and not the anilinium curve. The percentage of anilinium form of the polymer and acetic acid (due to the presence of acetate buffer in the solution) were calculated using their respective pKa values. The anilinium form of the polymer is known to behave as anion exchanger for removal of chromate anion as was observed previously (Kumar et al., 2007a; discussed in chapter 4). Thus, if the removal of mercury is an anion removal process then it should have decreased after pH 3.5 following the anilinium form of the polymer concentration plot. However, presence of acetic acid protonated the polymer and extended the removal plateau till pH 4. Moreover, the pH_{zpc} of the polymer was 4.1, suggesting that above this pH, polymer surface was negatively charged. Therefore, as the acetic acid quantity decreased, the polymer started to lose the capacity of functioning as anion exchanger resulting in a sharp decrease of mercury removal.

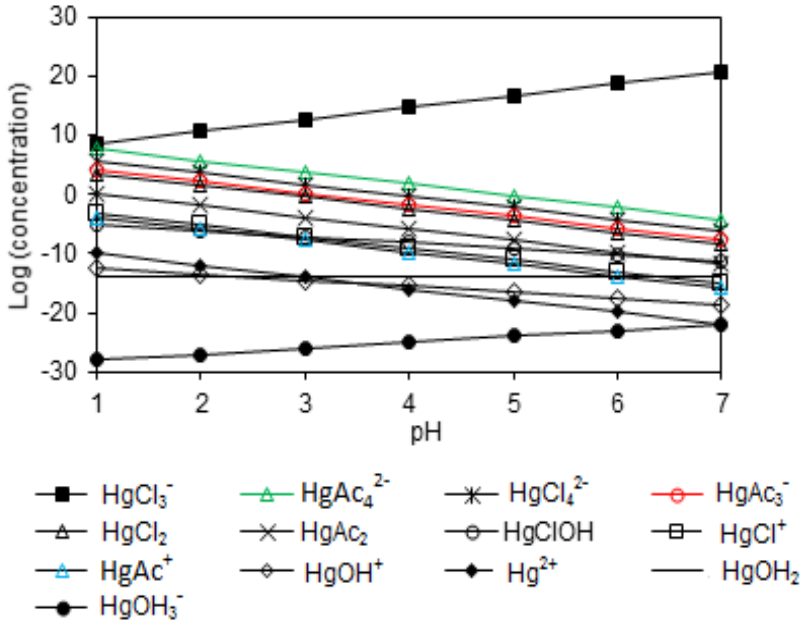

Figure 5.4b: Mercury speciation diagram

Thus, it can be attributed that the interaction between anionic form of Hg(II) and anilinium chloride salt form of polymer (cationic) was the main mechanism responsible for the removal of mercury from aqueous solution

5.3.3 Effect of adsorbent dosage

Figure 5.5 shows the effect of adsorbent dose on residual Hg(II) concentration in solution andHg(II) uptake by polymer. This study was carried out for 3h at constant pH 4 using acetate buffer 1M. Residual Hg(II) was estimated using vapour generation technique. The minimum concentration of residual Hg(II) achieved was 160 µg/L from initial concentration of 10 mg/L with removal efficiency of 98.5%, when polymer dose of 10 g/L was used. In order to achieved residual Hg(II) concentration of 1 mg/L, 2 g/L of polymer dose is needed with adsorption capacity of 4.93 mg/g. Table 5.3 shows a comparison of Hg(II) removal from initial concentration of 10 mg/L, in

terms of equilibrium time, adsorbent dose and final residual concentration of Hg(II) by various adsorbents.

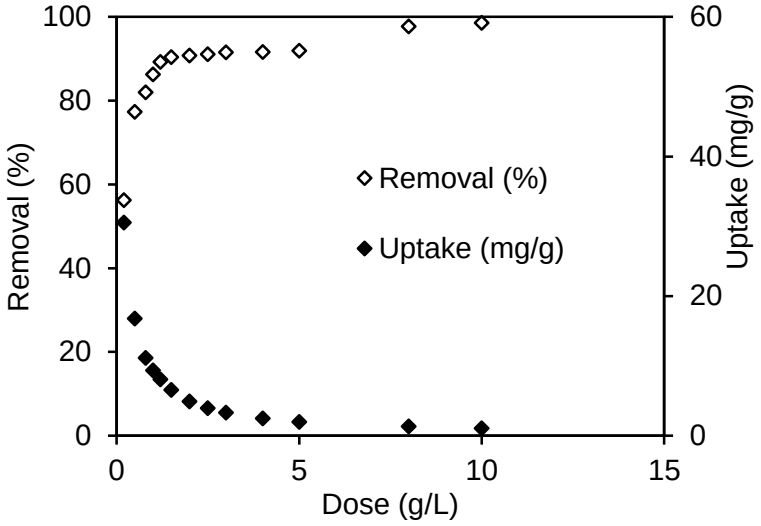

Figure 5.5: Effect of adsorbent dose on the removal of Hg(II)
(Co: 10 mg/L, pH 4, 3h)

It was found that modified-AFC was better than most adsorbents with adsorption capacity almost similar to activated carbon prepared from mango kernel and zea mays waste but ZnO:S adsorbent was seen to be best with very high adsorption capacity.

5.3.4 Effect of initial concentration

Initial Hg(II) was varied from 2 to 50 mg/L with polymer dose of 2g/L at pH 4. Figure 5.6, depicts residual Hg(II) concentrations with time. Equilibrium time was dependent on initial concentration of Hg(II) ion. When initial Hg(II) was 2-10 mg/L, equilibrium was achieved within 45 min. This study shows that present polymer was very fast to adsorb Hg(II) ion from a very dilute solution. In terms of Hg(II) removal efficiency, removals were > 90%, up to initial Hg(II) concentrations of 2-20 mg/L and 80% at Hg(II) of 50 mg/L. Residual Hg(II) concentration in solution were observed to be 0.13, 0.39, 0.94, 1.0 and 9.4 mg/L, from initial concentrations of 2, 5, 10, 20 and 50 mg/L,

respectively. When initial Hg(II) concentration was very low, positive charges on polymer greatly outnumbered Hg(II) ions. So, Hg(II) removal was faster and higher. With increase in Hg(II) concentrations, positive sites on polymer surface were exhausted and removal decreased.

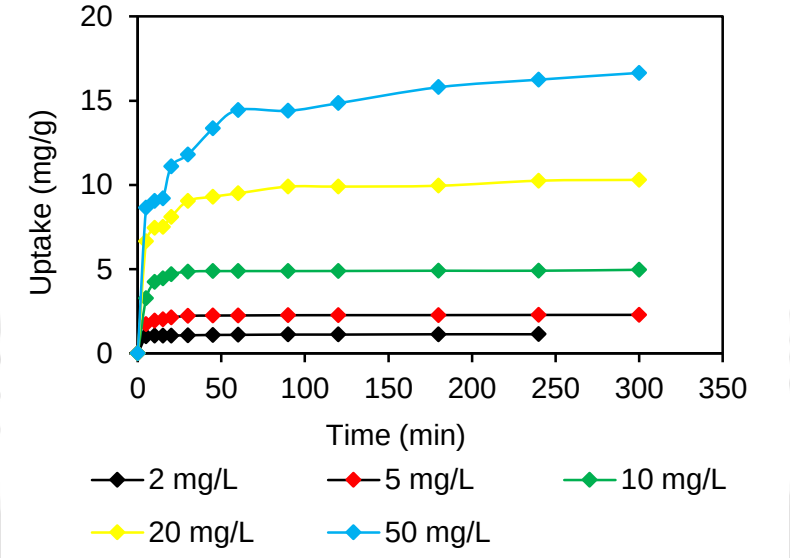

Figure 5.6: Effect of initial concentration on the uptake of Hg(II) (pH 4; dose- 2 g/L; 3 h)

Similar observation was found by Huang et al., 2016 during the removal of mercury from aqueous solution by poly(1-amino-5-chloroanthraquinone) nanofibrils were applied as novel nanoadsorbents.

5.3.5 Adsorption mechanism

Hg(II) adsorption kinetics by support less polymer was tested using pseudo first order, pseudo second order and intraparticle diffusion model. Pseudo first order (eq. 1.1) and second order (eq. 1.4) kinetic equations and their linear forms are given in eq. 1.2 and 1.7, respectively. Where, q_e is the Hg(II) uptake at equilibrium (mg/g), q_t is Hg(II) uptake at any time t and k_1 (1/min) and k_2 (g/mg.min) are first and second order rate constants. Liquid film diffusion model was also used to investigate the kinetics of the mercury ions adsorption whether the transport of mercury ions from

the liquid phase up to the solid phase boundary also plays a role in the adsorption process given in equation (5.1):

$$ln\left(1-\frac{q_t}{q_e}\right) = -k_{lf}t \qquad (5.1)$$

Where, q_t/q_e is the fractional attainment of equilibrium, k_{lf} is liquid film diffusion constant. A linear plot of $-\ln(1-q_t/q_e)$ versus t with zero intercept would suggest that the kinetics of the adsorption process was controlled by diffusion through the liquid surrounding the solid adsorbent. The plots of $\ln(1-q_t/q_e)$ against t (Figure 5.7), showed two linear regions for initial Hg(II) 5-50 mg/L and single plot for 2 mg/L. Similar observations were reported during methylene blue adsorption by sawdust and crushed bricks (Hamdaoui, 2006). The first linear portion was considered to determine first order rate constant as suggested by Ho and McKay, 1998. From the analysis the data (Table 5.1) reveals that the influence of the initial concentration of Hg(II) little persuade on the pseudo first order rate and very well fitted the pseudo second order plots (Figure 5.7a, show linear plots). The Kinetic constants and R^2 values are given in Table 5.1. Pseudo second order plots showed higher R^2 values than first order plots, suggesting Hg(II) adsorption by support less AFC can be better described by second order kinetic model. Pseudo-second-order kinetic model assumes that the adsorption rate is controlled by chemical adsorption through sharing or exchange of electrons between the adsorbate and adsorbent. Kinetics of Hg(II) adsorption was checked with intra-particle diffusion model (eq. 1.10). Plots of q_t vs. $t^{0.5}$ are shown in Figure 5.8b.

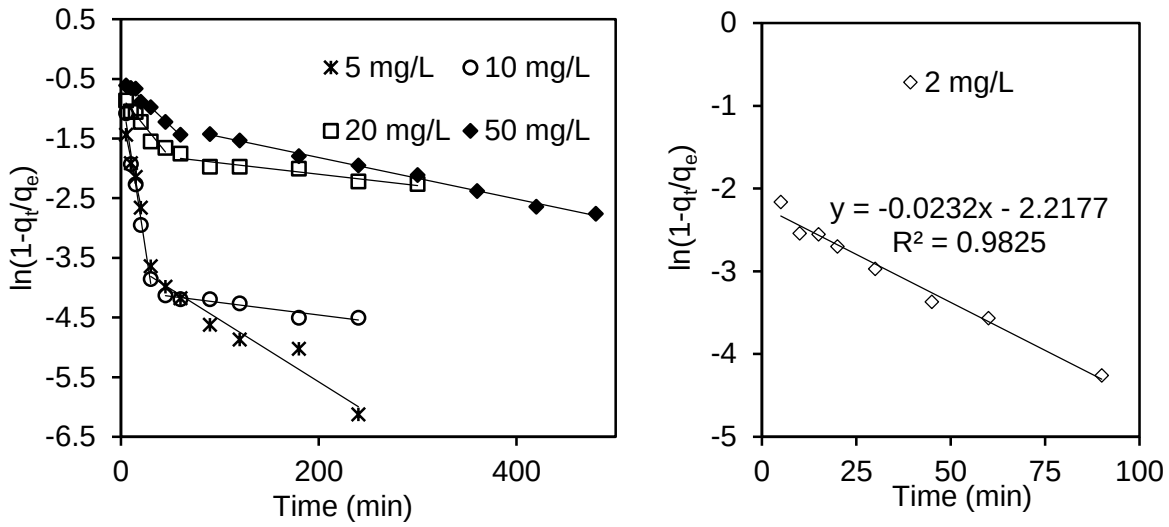

Figure 5.7: Liquid film diffusion model for various concentration of mercury adsorption

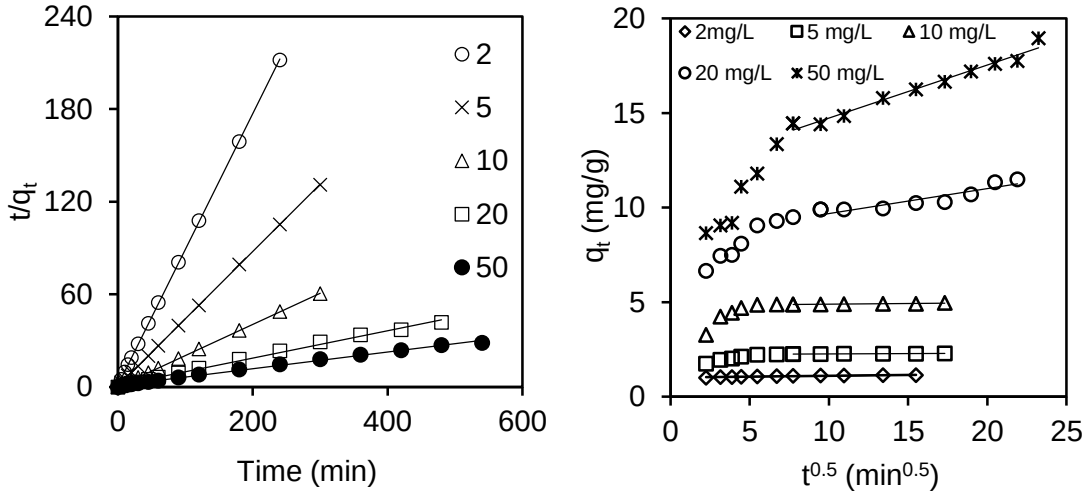

Figure 5.8: a) Pseudo-second order model and b) Intraparticle diffusion model

Plots showed two linear regions for initial Hg(II) of 5-50 mg/L and single linear plot for Hg(II) concentrations of 2 mg/L. The initial linear portion is attributed to the external mass transfer and the second linear portion represents intra particle diffusion. The plots do not pass through the origin, indicating that the intra-particle diffusion is involved in Hg(II) adsorption by modified-AFC, but it is not the sole rate controlling step.

Table 5.1: Summary of kinetic parameters of Hg(II) adsorption by modified-AFC

Type of model	Parameters	Initial conc. of Hg(II) (mg/L)								
		2	5		10		20		50	
	q_{exp} (mg/g)	1.13	2.05		4.55		11.5		18.95	
Pseudo-first order	q_e (mg/g)	1.082	2.167		4.68		9.556		14.697	
	k_1 (min^{-1})	5.706	1.832		1.193		0.409		0.015	
	R^2	0.77	0.95		0.98		0.96		0.98	
	χ^2	0.017	0.151		0.556		2.449		6.273	
	RMSE	0.118	0.478		1.153		4.623		9.629	
Pseudo-second order	q_e (mg/g)	1.136	2.293		4.958		11.274		18.45	
	k_2 (g/mg.min)	0.662	0.358		0.182		0.009		0.003	
	R^2	0.99	0.99		0.99		0.99		0.99	
	χ^2	0.014	0.015		0.128		3.356		6.314	
	RMSE	0.066	0.111		0.366		2.792		3.926	
Intraparticle diffusion	k_i ($mg/g.min^{0.5}$)	0.009	0.003		0.006		0.132		0.280	
	C_d (mg/g)	1.01	2.22		4.82		8.36		11.935	
	R^2	0.87	0.94		0.72		0.85		0.95	
Boyd model	R^2	0.93	0.79		0.58		0.82		0.95	
Liquid film diffusion model	k_{lf} (min^{-1})	-0.023	-0.078	-0.01	-0.108	-0.002	-0.02	-0.005	-0.015	-0.003
	Intercept	-2.217	-1.06	-3.49	-0.679	-4.038	-0.802	-1.243	0.505	-1.121
	R^2	0.98	0.98	0.95	0.98	0.91	0.94	0.68	0.98	0.99

5.3.6 Adsorption isotherm

Figure 5.9 shows the Hg(II) adsorption isotherm on modified-AFC as equilibrium uptake (q_e, mg/g) vs. residual Hg(II) concentration in solution at equilibrium (C_e, mg/L). When $C_e \leq 1$ mg/L, isotherm was of concave shape. Above $C_e > 1$ mg/L, isotherm showed an exponential increase to a concave shape. This change in slope of isotherm suggests change in adsorption mechanism at C_e

of 1 mg/L. The maximum equilibrium uptake was observed as 30 mg/g. According to Giles classification, Hg(II) adsorption isotherm was L3 type. Similar isotherm was observed during adsorption of Cu(II) by humin (Alvarez-Puebla et al., 2004). Langmuir and Freundlich isotherms were used separately for two regions of C_e. Langmuir isotherm equation is given (eq. 1.16) and linear form is given in eq. 1.17. Linear plots of Freundlich model are given in Figure 5.10c and 5.10d, respectively for $C_e \leq 1$ and $C_e > 1$. Langmuir plot showed negative intercept for $C_e \leq 1$, suggesting Langmuir model is unsuitable for Hg(II) adsorption by modified-AFC. It can be seen that Freundlich isotherm plots showed higher R^2 value than Langmuir plots for $C_e \leq 1$ and $C_e > 1$.

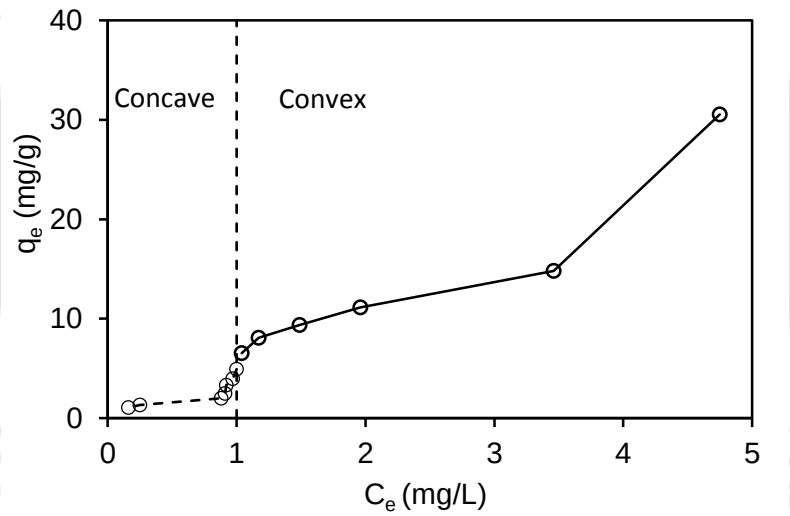

Figure 5.9: Equilibrium isotherm plot

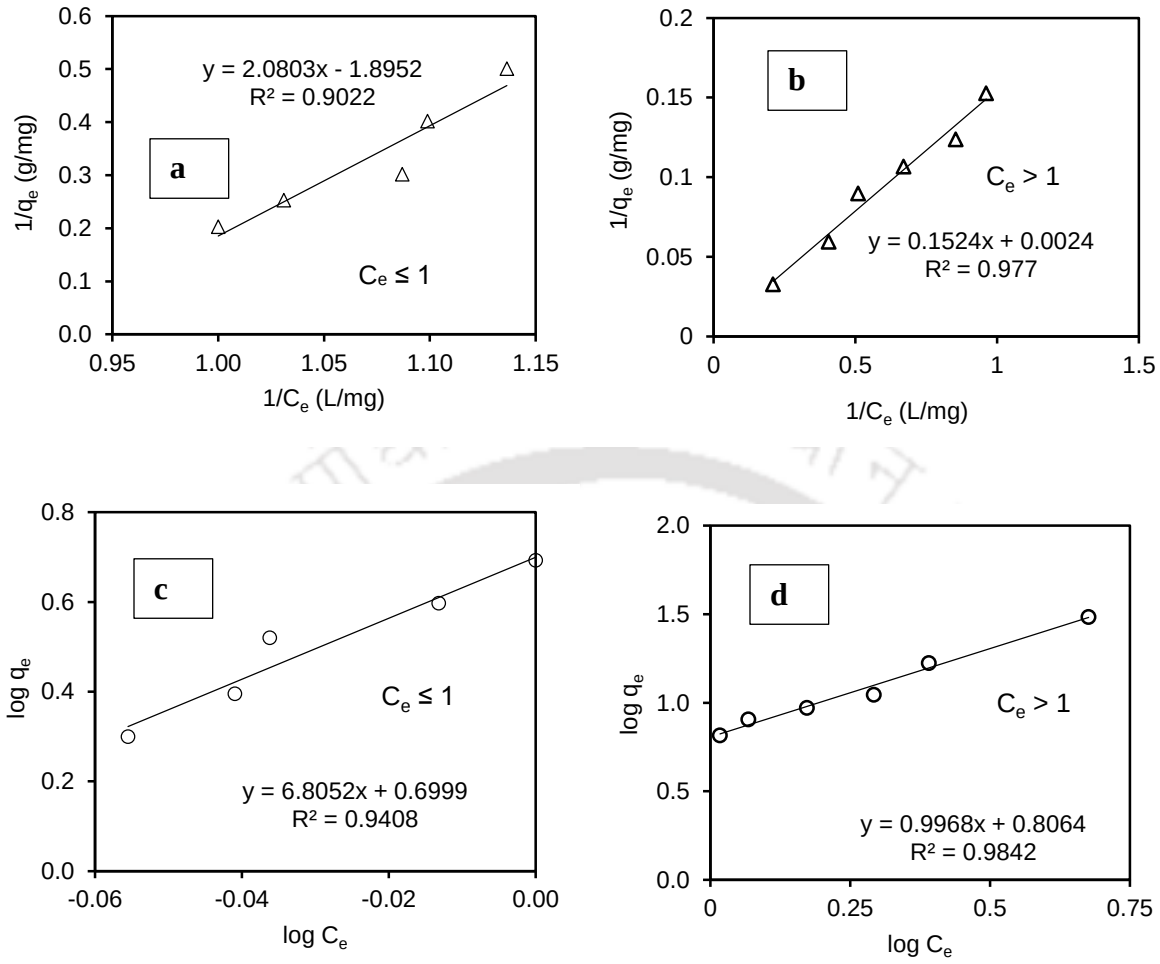

Figure 5.10: Linearized isotherm plot of different model a, b) Langmuir isotherm model and c, d) Freundlich isotherm mode

Isotherm constants are given in Table 5.2. When 1/n values are in the range 0.1 < 1/n <1, the adsorption process is favorable.

Table 5.2: Freundlich isotherm parameters for adsorption of Hg(II) on modified-AFC

Residual Hg(II) concentration at equilibrium (mg/L)	n	K_f (mg/g)	R^2
$C_e \leq 1$	0.146	5.00	0.94
$C_e > 1$	1.00	6.39	0.98

In this study the value of 1/n values were 6.8 ($C_e \leq 1$) and 0.996 ($C_e > 1$), suggesting that Hg(II) adsorption was favourable when equilibrium Hg(II) concentration was more than 1 mg/L.Comparing with various adsorbents (Table 5.3) it was found that modified-AFC was better than most adsorbents (fly ash, *aspergillus niger*, etc) and with adsorption capacity almost similar to activated carbon prepared from mango kernel and zea mays waste but ZnO:S adsorbent was seen to be best with very high adsorption capacity when 10 mg/L of Hg(II) was used.

Table 5.3: Comparison of removal of Hg(II) 10 mg/L by modified-AFC with other reported studies

Adsorbent	pH	Dose (g/L)	Adsorption capacity (mg/g)	Reaction time (min)	Final Hg(II) conc. (mg/L)	References
Modified-AFC	4	2	4.93	60	1	Present study
Synthetic terpolymer	4.5	5	53.48	180	0.095	Sangu et al., 2015
Fly ash	10	6	1.63	120	1	Verma et al., 2014
Aspergillus niger	7	20	0.75 0.8	90 180	4.93 8.93	Saritha et al., 2009
Activated carbon prepared from mango kernel	6.5	3	4.4	180	1	Somayajula et al., 2012
Modified Triplochytonscleroxylon sawdust	7	5	6.01	60	0.806	Kong et al., 2016
Nonviable *Bacillus* sp.	6	2	3.41	60	3.187	Green-Ruiz et al., 2006
Zea Mays waste	10	5	4.83	120	0.363	Jamil et al., 2009
Camel bone charcoal	2	0.3	28.24	30	0.917	Hassan et al., 2008
ZnO:S	2.5	0.08	101.01	30	0.5	Hassan et al., 2017

5.3.7 Effect of other ions

Adsorption performance depends on ionic strength of solution. It was found that the main removal mechanism was due to the anionic form of mercury so in order to understand the competitive effect of other anions present in the solution, Hg(II) adsorption was studied in presence of four anions: Cl^-, SO_4^{2-}, NO_3^- and PO_4^{2-} of varying concentrations (0.05-5 mM). Figure 5.11, shows the effect of other anions during the adsorption of Hg(II) ion of 10 mg/L at pH 4 with dose 2g/L of polymer. Hg(II) adsorption remained unaffected in presence of anions like sulfate, chloride and nitrate, only phosphate was responsible for lowering Hg(II) removal from 90% to 70%. This behavior could be attributed to the competitive effect between the mercury ions and phosphate ions for the active sites available thereby hindering the anion exchange mechanism involved during the adsorption process. Presence of phosphate ion affected the mercury removal efficiency which was also observed by Li et al., 2013 with aqueous mercury adsorption on activated coke by thiol-functionalization.

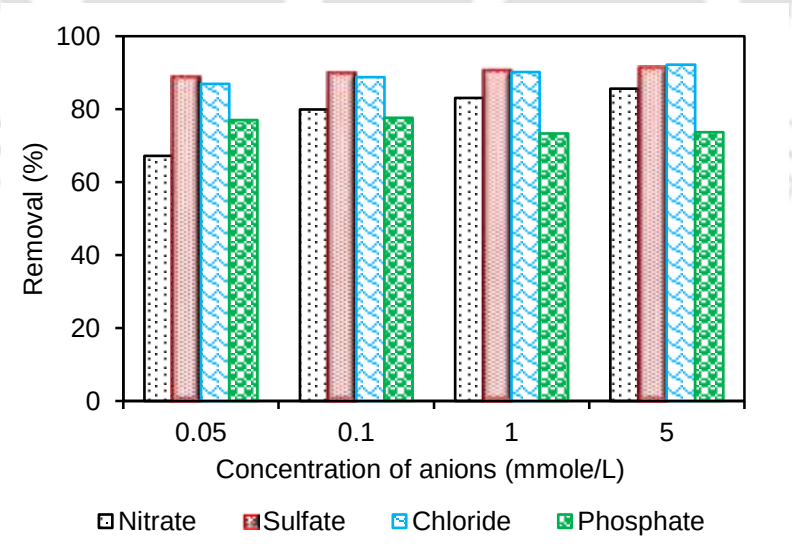

Figure 5.11: Effect of anions on the removal of mercury

5.3.8 Desorption and regeneration study

Desorption experiment were conducted to recover the Hg(II) ion adsorbed onto the surface of the from the adsorbent i.e. polymer using different strengths of acid such as HCl, H_2SO_4 and HNO_3. It was found that out of the three acids used, HNO_3 acid showed the best results with high desorption percentage of about 62.5% (Figure 5.12a). But after performing desorption kinetics it was found that HNO_3 acid with 1M strength solution caused release of about 90% of the mercury ion from the polymer adsorbent when agitated for 60 mins. The adsorption-desorption cycle was tested and found to be favourable till third cycle shown in Figure 5.12b.

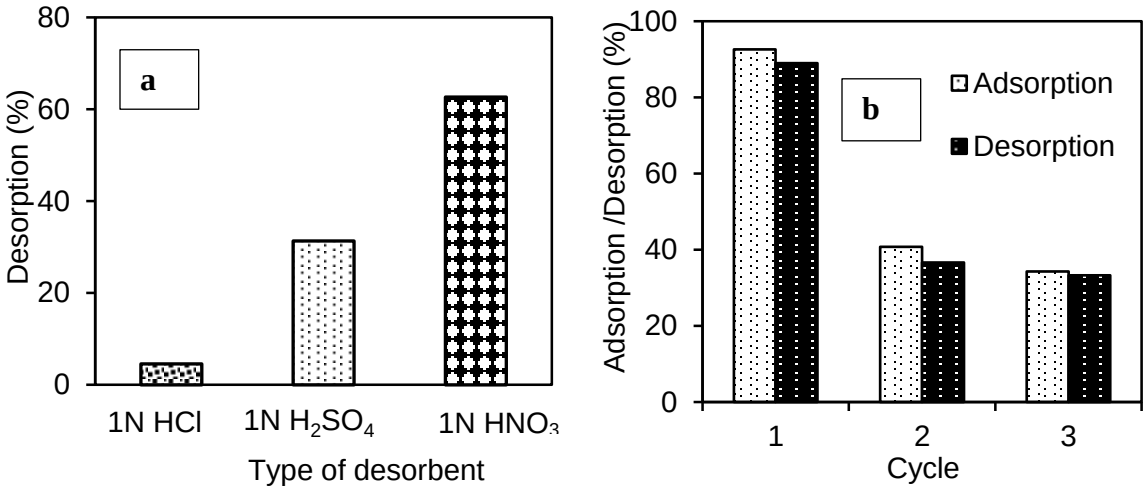

Figure 5.12: a) Effect of desorbents on mercury desorption (Agitation time 12 h) and b) Adsorption-desorption cycle (Agitation time 60 min)

5.3.9 Effect of temperature

Temperature plays an important role to identify the effects of adsorption process on the removal of mercury ions. Figure 5.13a shows the effect of temperature on the removal efficiency of mercury from aqueous solutions with modified-AFC at different temperatures ranging from 20°C to 50°C which indicates that the process is spontaneous and exothermic in nature (Table 5.4). Therefore, room temperature was selected as the optimum operational condition due to its high removal

efficiency at 20°C. Thus, the modified-AFC adsorbent was found applicable in industrial applications. Thermodynamic parameters, including the standard enthalpy change (ΔH°) (kJ/mol) and the standard entropy change (ΔS˚) (J/Kmol), were obtained using the van't Hoff equation (1.15). The values of ΔH° and ΔS° were obtained from the slope and intercept respectively, of the plot *ln* K_L vs *1/T* as shown in Figure 5.13b.

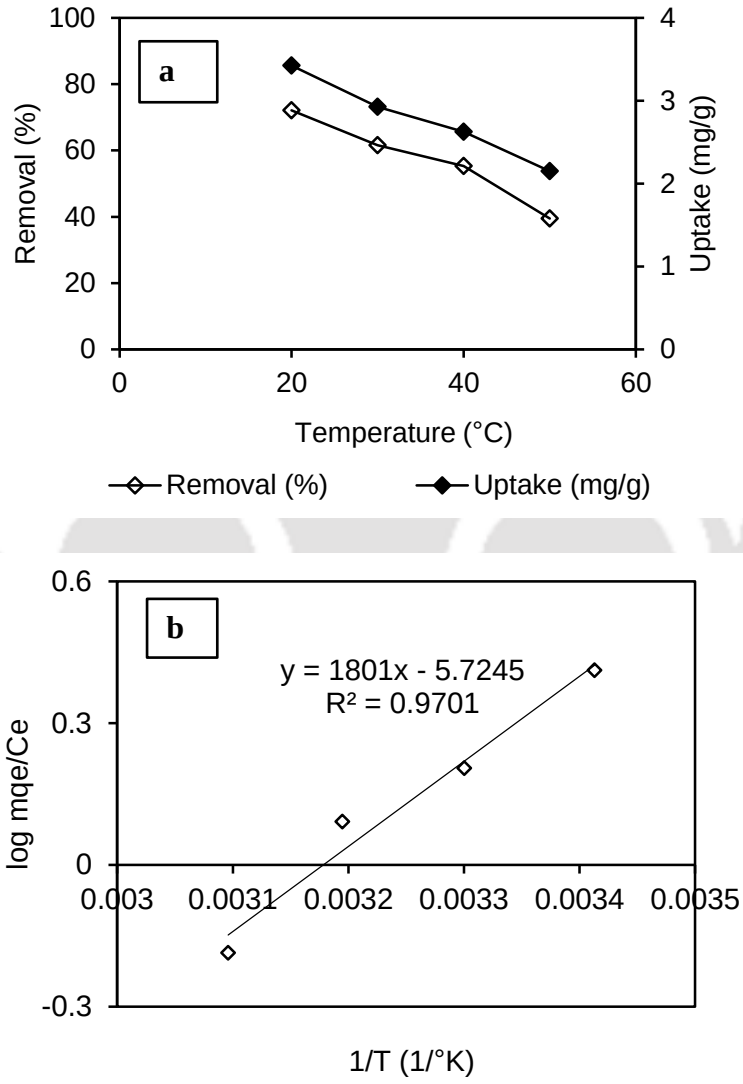

Figure 5.13: a) Effect of temperature and b) thermodynamic parameters on the removal of Hg(II) (C_o:10mg/L at pH 4 dose of 2g/L for 2 h)

The results in Table 5.4 indicates that mercury(II) and modified-AFC interactions were accompanied by an increase in Gibbs free energy which made the interactions spontaneous and suggests that the process is feasible at lower temperatures. The negative value of ΔH° was found to be -34.484 kJ/mol which suggest the process to be exothermic in nature and ΔS° was found to be -109.607 J.mol/K suggesting the adsorption process with a negative entropy change. The negative ΔG° suggested a feasible and spontaneous adsorption process. Decrease in the removal at higher temperature may be due to the increasing trend to desorption of Hg(II) from the interface to the solution or the distorted active sites on modified-AFC adsorbent. Similar observation was reported by Dawlet et al., 2013 during the removal of mercury from aqueous solution using sheep bone charcoal. Qing-Zhou Zhai, 2014 also reported similar observations during the adsorption of Hg(II) from water with α-Al_2O_3 for removal of Hg(II) from water.

Table 5.4: Thermodynamic parameters of Hg(II) adsorption onto modified-AFC at different temperatures.

T (K)	ΔG° (kJ/mol)	ΔH° (kJ/mol)	ΔS°(J.mol/K)	TΔS°(kJ/mol)
293	-2.368	-34.484	-109.607	-32.114
303	-1.272			-33.210
313	-0.176			-34.306
323	0.919			-35.403

5.4 Summary

In the present investigation, adsorption of Hg(II) was carried out using an amine based polymer synthesized using aniline, formaldehyde and isopropanol. The polymer (modified-AFC) was of powdered form and used as an adsorbent for removal of dilute concentration of Hg(II) as $HgCl_2$. The maximum removal was achieved at pH 4. The adsorption kinetics study demonstrated that the model of kinetics for removal of Hg(II) confirmed pseudo second-order equation. Adsorption isotherm was of concave shape at very dilute concentration of Hg(II) ion and changed to concave shape at higher concentration. Freundlich isotherm was appropriate in both regions. The nature of adsorption process was found to be spontaneous and exothermic. Desorption of the metal was successfully achieved which favored the adsorbent to be regenerated and reuse. The adsorption was found to be pH dependent and the main mechanism involved during the removal of Hg(II) from aqueous solution was governed by ion exchange between anionic form of Hg(II) and anilinium chloride salt form of polymer (cationic) besides other mechanisms.

CHAPTER 6

Competitive adsorption of Pb(II), Cu(II) and Cr(III) on modified-AFC: Kinetic and equilibrium studies

6.1 Introduction

Industries involving electroplating processes, i.e. surface treatments by chemical or electrolytic process, produce effluents rich in a wide variety of toxic metals, such as copper, zinc, silver, lead, chromium, cadmium etc., and petroleum refining which generates conversion catalysts is contaminated with nickel, vanadium, and chromium discharge as wastewater (Barakat et al., 2011). Textile industries produces wastewater containing heavy metals such as lead, copper, chromium and cadmium (Al-Khafaji et al., 2017; Halimoon et al., 2010). According to the World Health organization, the metals of most immediate concern are aluminium, chromium, cobalt, copper, cadmium, iron, lead, manganese, mercury and zinc (Moyib et al., 2017).

Therefore, it is of very significant and important concern to investigate the removal of heavy metals from wastewater consisting of multiple metals system. Binary and ternary adsorption studies may be highly complex but they best reflect the reality as the presence of only one metal is a rare condition in nature or wastewaters. Most of the adsorption works on heavy metal adsorption has considered only single metal system. Very few literatures reported the removal of metals in multicomponent system (Hernández-Hernández et al., 2017; Hayati et al., 2017; Mahmoud et al., 2010; Hadi et al., 2017). In previous chapters the performance of modified-AFC on removals of hexavalent chromium and mercury are reported. In this chapter, removal of lead [Pb(II)], copper [Cu(II)] and trivalent chromium [Cr(III)] by modified-AFC is presented. Adsorption study was carried out in single, binary and ternary system of these three metal ions to understand the adsorption mechanism involved during the adsorption process.

6.2 Materials and methods

6.2.1 Materials

Lead nitrate [$Pb(NO_3)_2$], copper sulfate pentahydrate [$Cu(SO_4).5H_2O$], chromium chloride hexahydrate [$CrCl_3.6H_2O$] were used as the source of lead, copper and chromium, respectively. Sodium acetate (CH_3COONa), acetic acid (CH_3COOH) were used for preparation of acetate buffer (1M strength and pH of 4).

6.2.2 Adsorption experiment

The initial concentration of each of the metals were milliequivalent per litre as the combination consisted of two bivalent cationic metals Pb(II) and Cu(II) and a trivalent cationic metal Cr(III). For single component system Pb(II), Cu(II) and Cr(III) initial concentration of each metal were taken as 0.24 meq/L (25 mg/L, 7.63 mg/g ad 4.56 mg/g of Pb(II), Cu(II) and Cr(III) respectively). For adsorption experiment in single system, 2g/L adsorbent dosage was added to adjusted pH 4 solution of 100 mL volume containing 0.24 meq/L concentration of total metal in each case and agitated for 3h at 270 rpm in room temperature. The pH was adjusted by adding 1M acetate buffer of about 6 mL, 1mL and 1.8 mL for Pb(II), Cu(II) and Cr(III) respectively in 100 mL solution. After adsorption, samples were centrifuged at 3000 rpm for 5 min and was filtered. All experiments were repeated twice to check the accuracy. The experimental contitions for single, binary and ternary system are described in Table 6.1.

Table 6.1: Experimental conditions for single and multicomponent metal system by modified-AFC

System	Metal ion	C_o (mg/L)	C_o (meq./L)	Experimental conditions
Single	Pb(II)	25	0.24	Total volume -500mL; pH 4; agiatated rate – 270 rpm; room temperature The amount of acetate buffer added to the total volume was 22 mL (lead), 9mL (copper) and 7mL (trivalent chromium). **For kinetics experiment:** Time – 0 to 420 min; dose- 2g/L. The samples were collected after every time interval. **For dose experiment:** Time- 3h, dose-0.5 to 10 g/L
	Cu(II)	7.6248	0.24	
	Cr(III)	4.159	0.24	
Binary	Pb(Pb-Cu)	12.432	0.12	All conditions was same as above (in single system) except acetate buffer of 16 mL was added to 500mL total volume.
	Cu(Pb-Cu)	3.8124	0.12	
	Pb(Pb-Cr)	12.432	0.12	Same as above conditions (Pb-Cu binary system)
	Cr(Pb-Cr)	2.0796	0.12	
	Cu(Cu-Cr)	3.8124	0.12	All conditions was same as above (in single system) except acetate buffer of 10 mL was added to 500mL total volume.
	Cr(Cu-Cr)	2.0796	0.12	
Ternary	Pb(II)	8.288	0.08	All conditions was same as above (in single system) except acetate buffer of 12 mL was added to 500mL total volume.
	Cu(II)	2.542	0.08	
	Cr(III)	1.386	0.08	

**Metals ratio of 1:1 and 1:1:1 was maintained in binary and ternary system respectively*

6.2.3 Analytical method

The metals [Pb(II), Cu(II) and Cr(III)] were analyzed using absorption spectrometry atomic absorption spectrometry (flame-AAS) (model-AA240, Varian). The working conditions in AAS for the heavy metals were i) Pb(II): wavelength (nm) = 283.3, slit width (nm) = 0.5, optimum working range = 0.5-50 mg/L, ii) Cu(II): wavelength (nm) = 217.9, slit width (nm) = 0.2, optimum

working range = 0.2-60 mg/L, and iii) Cr(III): wavelength (nm) = 357.9, slit width (nm) = 0.2, optimum working range = 0.06-15 mg/L.

6.3. Results and discussions

6.3.1 Analysis of modified-AFC after adsorption

The Fourier transform infrared spectroscopy (FT-IR) spectra of modified-AFC was already discussed in chapter 3 and after adsorption spectra given in Figure 6.1a showed no major changes and EDX spectra also confirmed the presence of metals on modified-AFC after adsorption process (Figure 6.1b).

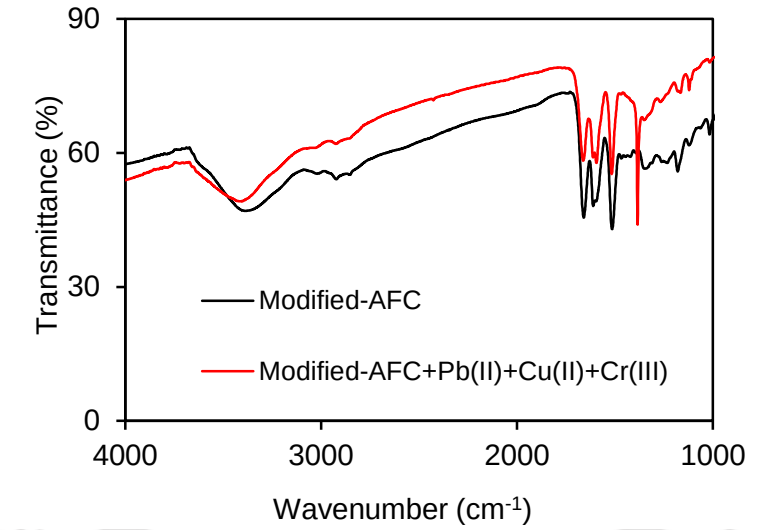

Figure 6.1a: FTIR spectra of modified-AFC before and adsorption of mixed metals

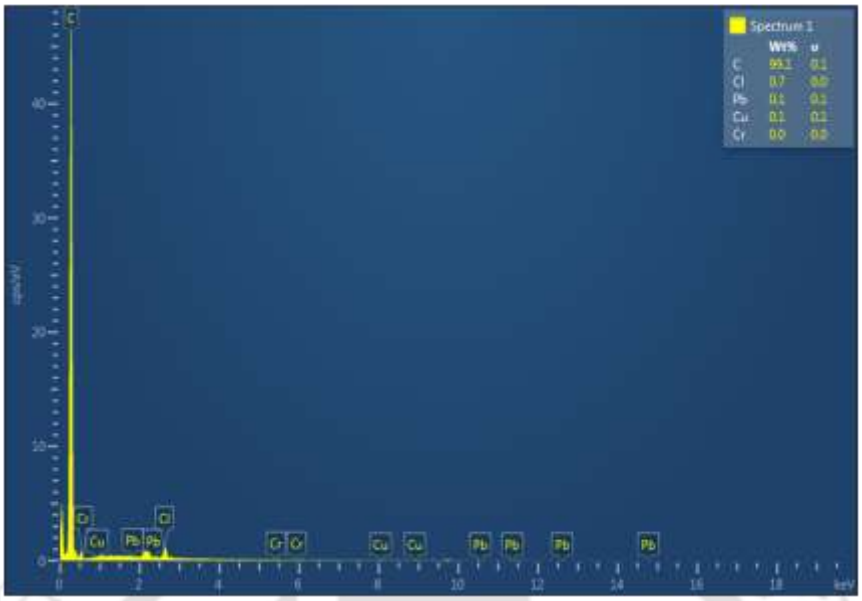

Figure 6.1b: EDX spectra of modified-AFC adsorption of mixed metals

6.3.2 Adsorption studies in mono and multi-component system

6.3.2.1 Adsorption study in single system

The adsorption experiments performed at controlled pH in the present study to identify the efficiency of metals removal is summarized in Table 6.2.

Table 6.2: Summary of adsorption Pb(II), Cu(II) and Cr(III) (single system) in controlled pH 4

Metals	Initial conc. (meq./L) and (mg/L)*	Removal (%)	Uptake (meq./g)	Dose (g/L)	pH
Lead [Pb(II)]	0.24 (25)	47.35	0.050	2	4
Copper [Cu(II)]	0.24 (7.63)	50.99	0.051	2	4
Chromium [Cr(III)]	0.24 (4.16)	60.2	0.073	2	4

Study was carried out at pH 4, to ensure that metal removal occurred by adsorption and not precipitation. The main mechanism of metal ion removal at pH 4 was due to formation of coordination bond between metal ions and nitrogen present in amine ($-NH_2$) group of modified – AFC. Modified-AFC showed maximum removal for Cr(III), followed by Cu(II) and then Pb(II). The probable reason for this behavior can be "hard-soft" theory of Pearson (Kumar et al., 2009). According to this theory, hard acids prefer to make bond with hard base and soft acid with soft base. Hard acids prefer hard bases and soft acids prefer soft bases. Cr(III) is a hard acid, Cu(II) a borderline hard acid and Pb(II) a soft acid. Amine ($–NH_2$) is considered a borderline hard base. Modified-AFC formed strong and stable complex with hard and borderline acids Cr(III) and Cu(II) as compared to soft acid Pb(II).

6.3.2.2 Effect of contact time

The experimental results in Figure 6.2, showed that the adsorption rate very fast. In single system the equilibrium time was established within 15 min in case of Pb(II) and Cu(II) but was not observed for Cr(III) even after 420 min but for Pb(II) and Cu(II) there was no significant change after 180 min upto 420 min.

In binary system, equilibrium time for Pb(II) and Cu(II) did not reached even after 540 min, and the uptake value of Pb(II) and Cu(II) reduced to half compared to single system. In case of Pb(II) and Cr(III) equilibrium was reached within 180 min for Pb(II) whereas desorption of Cr(III) metal ions started immediately after the initiation of adsorption. The uptake value of Pb(II) was reduced to 0.61 times of the single system. For Cu(II) and Cr(III) binary system, Cr(III) started desorption started from beginning whereas the equilibrium for Cu(II) did not reach even after 540 min. The uptake value of the both Cu(II) and Cr(III) was found to reduce compared to single system uptake value.

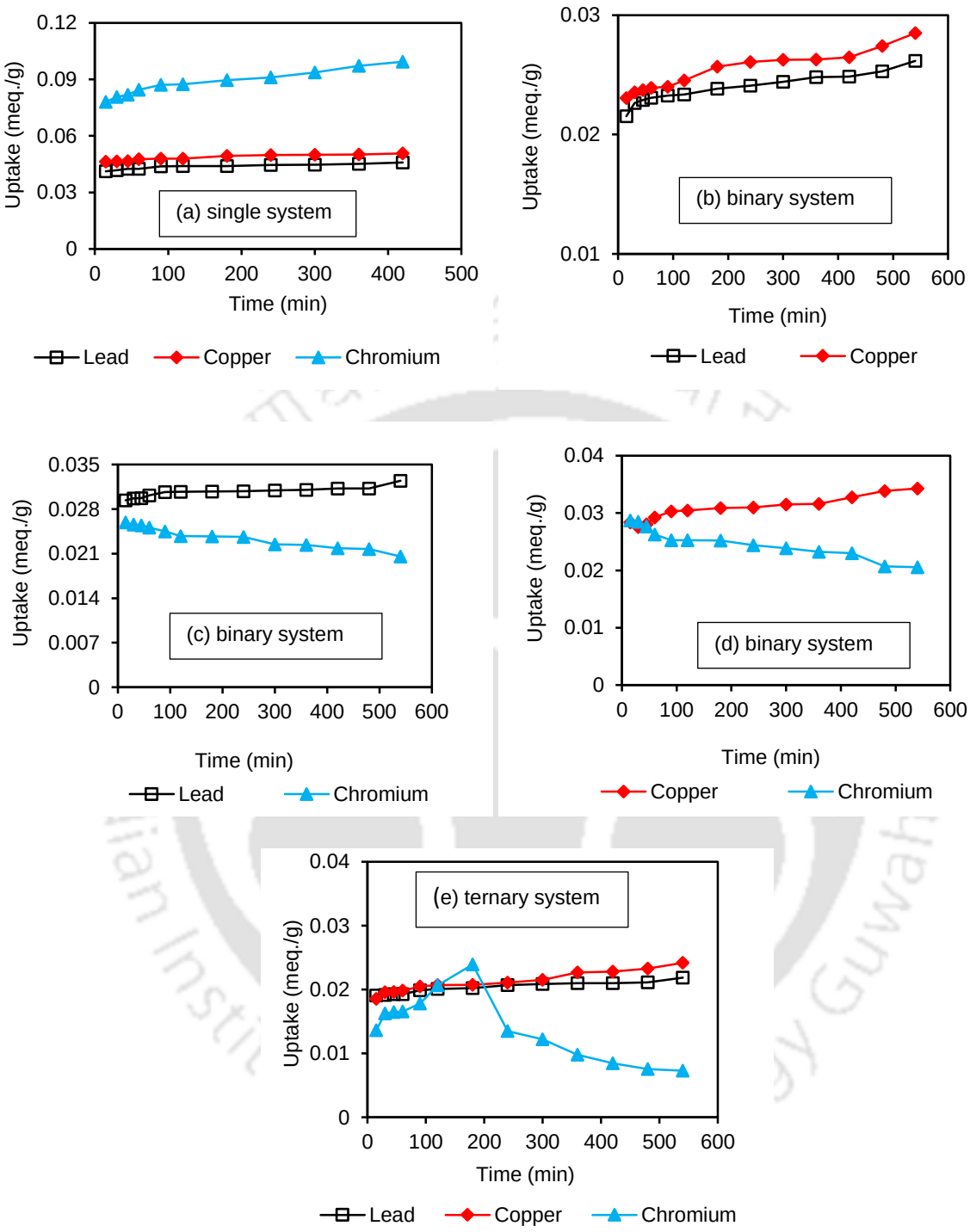

Figure 6.2: Effect of contact time on the uptake for a) lead-copper-chromium in single system, b) lead-copper, c) lead-chromium, d) copper-chromium in binary system and e) lead-copper-chromium in ternary system

For ternary system, Pb(II) reached equilibrium within 180 min and Cu(II) did not reach equilibrium even after 540 min but Cr(III) started desorption after 180 min which may be due to saturation. It may be noted that Cr(III) removal efficiency in single system was highest whereas in binary system and ternary system desorption was observed which suggested that it was greatly affected by the presence of other metal ions.

Similarly, the uptake values of were reduced compared to single system for all the three metals. It was also observed that within initial 15 min, significant metal uptake was achieved in single, binary and ternary system. Thus, it can be attributed that in multicomponent system the mesoporous surface of modified-AFC became saturated in the initial stage of adsorption which forces the metal ions to transfer further and deeper into the pores encountering much resistance which may be the reason for slow adsorption i.e. equilibrium was not achieved (Khalfa et al., 2016).

6.3.2.3 Adsorption kinetics

The experimental data was fitted into various kinetic models in order to evaluate the adsorption mechanism (equation 1.2; 1.7; 1.10; 1.11b). The values of k_1, R^2 and calculated uptake capacity q_e along with the RMS and $\chi 2$ (given in Table Appendix) suggested that the experimental data did not followed the pseudo-first order kinetic model. Whereas the values of k_2, R^2 and q_e for metal ions ion given in Table 6.3a and b shows that R^2 values are close to unity and the value of q_e obtained from the model was nearly equal with the experimental data. In view of these observations, it may be concluded that the pseudo-second order kinetic model provides a good fit for the adsorption of the metal ions onto modified AFC in comparison to the pseudo-first order kinetic model.

Figure 6.3 and Figure 6.4 shows the pseudo-second order model and intraparticle diffusion model respectively for the metal ions in mono and multicomponent system. Correlation coefficient value

was high in case of pseudo-second order followed by intra-particle and was followed by boyd model (Figure 6.5). It was observed that only chromium metal ion present in the multicomponent system did not follow any model which may be due to desorption of chromium ions from modified-AFC surface.

From the figures, it was clearly observed that the intraparticle diffusion plots (Figure 6.4) and boyd's plots (Figure 6.5) did not pass through the origin, so neither intra-particle nor film diffusion was not the only rate controlling step. This shows that the adsorption processes were not only influenced by the film diffusion but also intraparticle diffusion with some degree of boundary layer control. Moreover, the intraparticle diffusion plot consist of only one linear curve which suggest the completion of adsorption in one step except for chromium in ternary system involves two steps adsorption followed by desorption.

Table 6.3a shows, in one hand, that for all the studied metals, k_2 values (pseudo-second order rate constant) for lead in binary system decreased in presence of copper but increased in presence of chromium and also in ternary system. For copper in binary system increased presence of lead but decreased in presence of chromium and slightly increased in ternary system. Finally, for chromium the values decreased in all the system which may be due to the competition with other metal cations as well as with the active sites of the available in the adsorbent. With the same initial concentration in different metal system, k_2 values found for each metal ion decreased in the following order: Pb(II) $\geq$ Cu(II) >Cr(III). This suggest that in multicomponent system lead and copper were adsorbed fatser. It was observed from the Figure 6.5, the boyd plots were not completely linear and also did not pass through the origin, which can then be concluded that the limiting step is the film-diffusion or the chemical reaction.

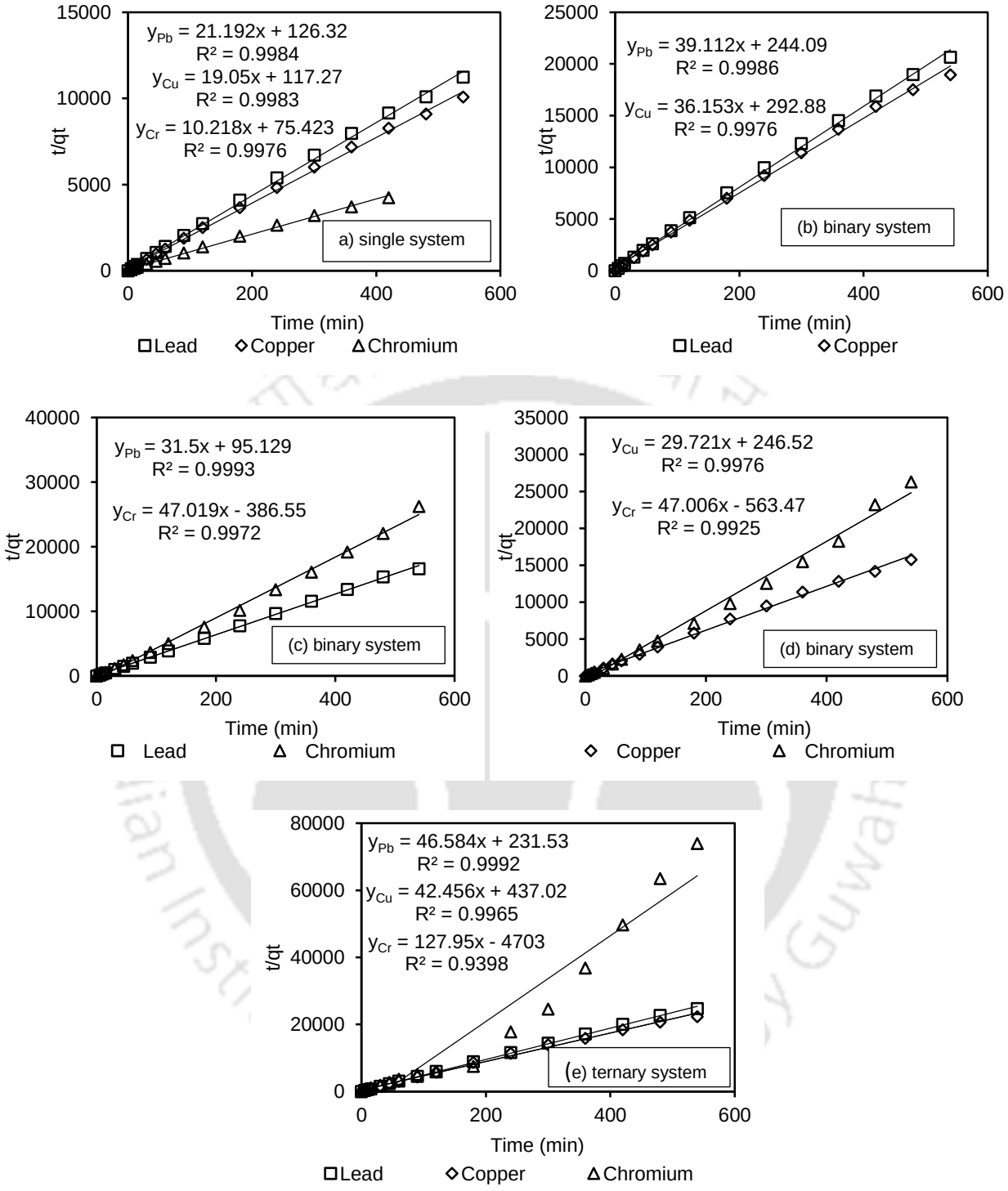

Figure 6.3: Pseudo-second order of a) lead, copper and chromium for mono-component system, b) lead-copper, c) lead-chromium, d) copper-chromium for binary system and e) lead-copper-chromium for ternary system

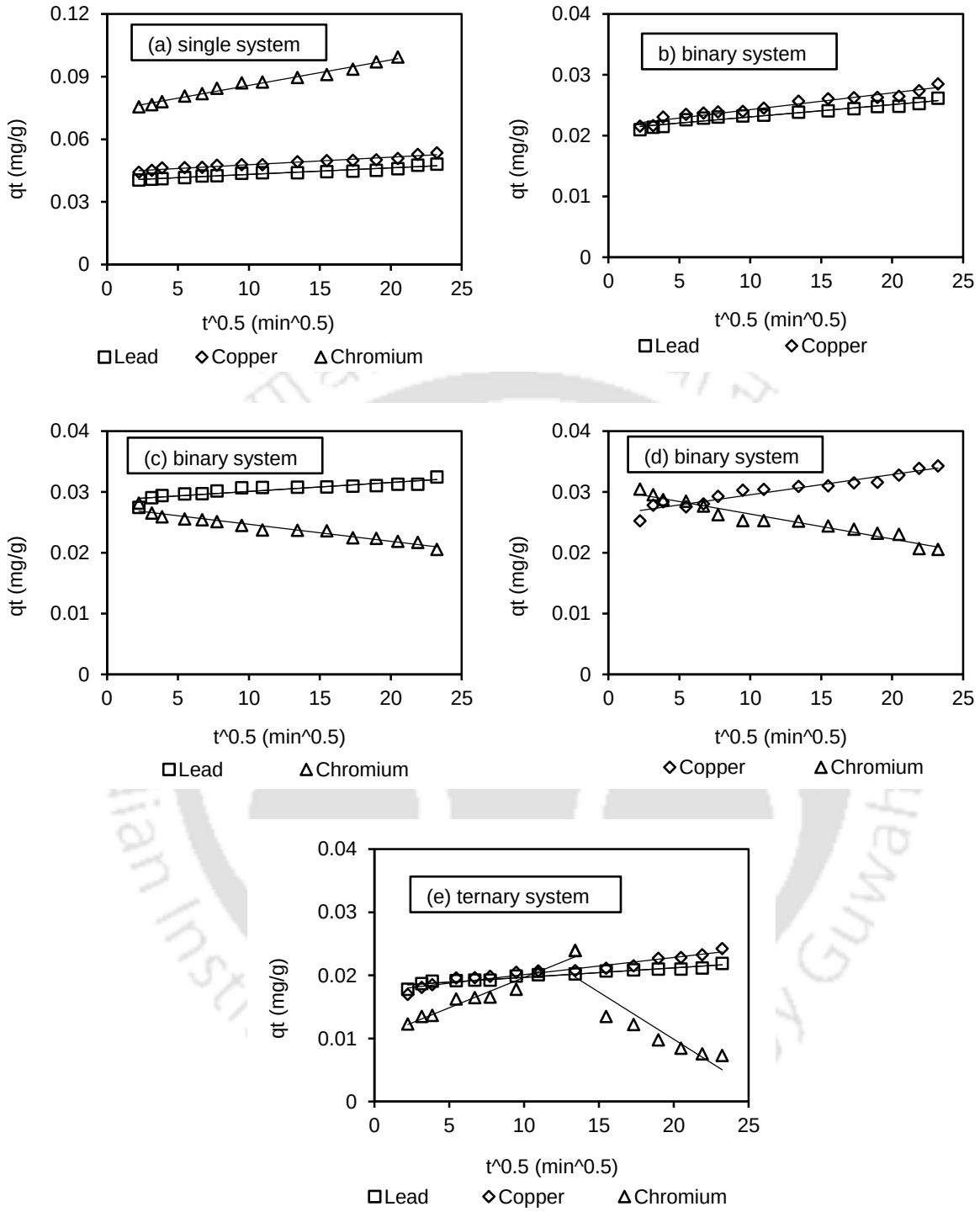

Figure 6.4: Intra-particle diffusion model for a) lead-copper-chromium for single system, b) lead-copper, c) lead – chromium, d) copper-chromium in binary system and e) lead-copper-chromium in ternary system

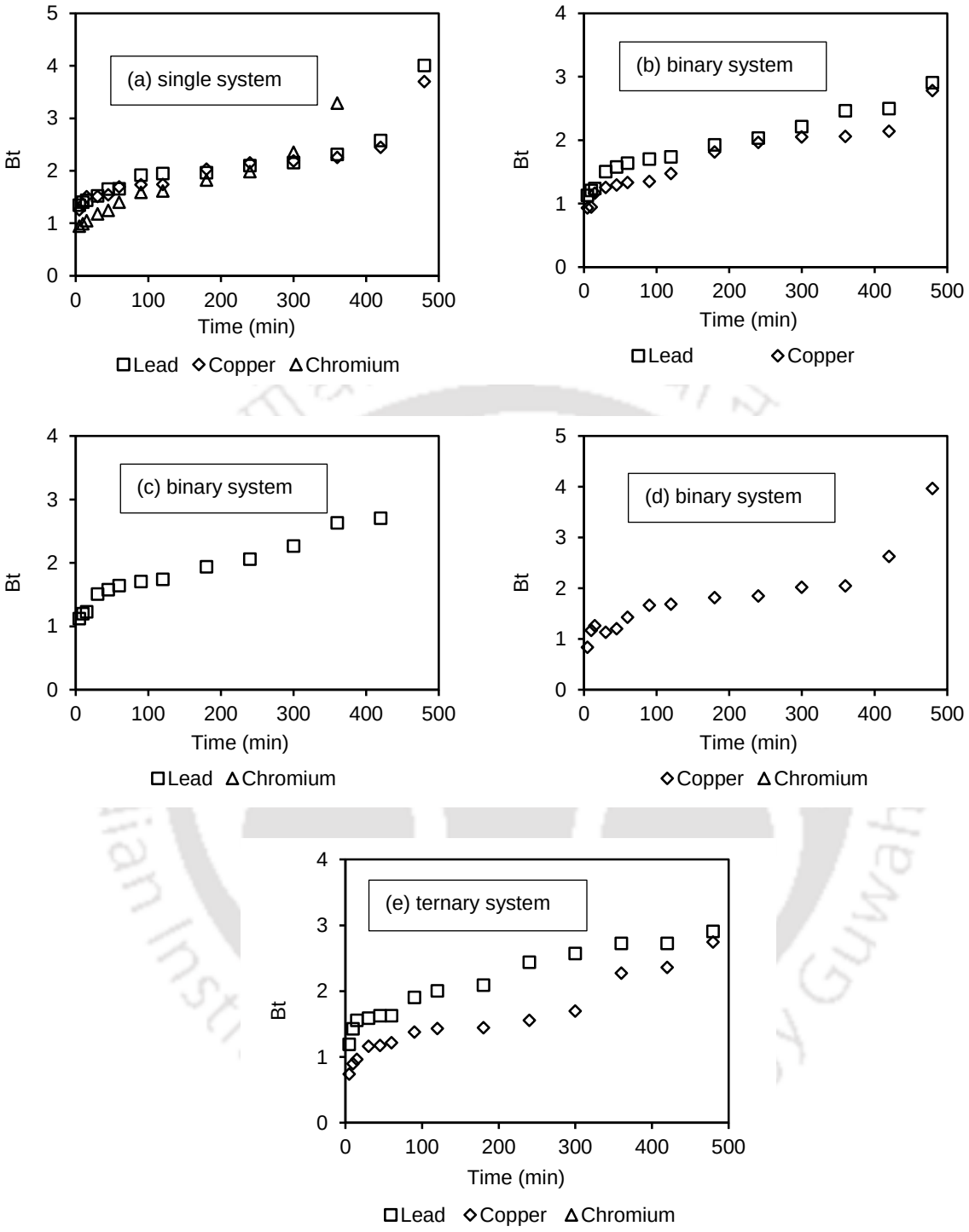

Figure 6.5: Boyd diffusion model for a) lead-copper-chromium for single system, b) lead-copper, c) lead – chromium, d) copper-chromium in binary system and e) lead-copper-chromium in ternary system

Table 6.3a: Pseudo-second order model kinetics parameters in single and multicomponent metal system

Single system		Experimental q_{eexp} (meq/g)	Pseudo-second order kinetic model Parameters				
			q_e (meq/g)	k_2 (g/meq.min)	R^2	χ^2	RMSE
Pb(II)		0.0481	0.046	6.756	0.99	0.06	0.002
Cu(II)		0.054	0.052	3.688	0.99	0.01	0.006
Cr(III)		0.099	0.098	1.188	0.99	0.161	0.56
Binary system							
Pb-Cu	Pb(II)	0.02361	0.026	6.06	0.99	0.008	0.011
	Cu(II)	0.0284	0.028	4.355	0.99	0.01	0.016
Pb-Cr	Pb(II)	0.0324	0.035	10.26	0.99	5.957	19.311
	Cr(III)	0.0205	0.021	-5.866	0.99	5.985	19.496
Cu-Cr	Cu(II)	0.0342	0.034	3.509	0.99	0.03	0.049
	Cr(III)	0.0205	0.021	-4.024	0.99	0.023	0.057
Ternary system							
Pb-Cu-Cr	Pb(II)	0.0218	0.021	9.794	0.99	0.017	0.012
	Cu(II)	0.0242	0.024	3.973	0.99	0.019	0.014
	Cr(III)	0.0072	0.008	-3.322	0.94	0.038	0.066

Table 6.3b: Intraparticle diffusion model and Boyd model parameters

Single system		Intraparticle diffusion model		
		k_i (meq/g.min$^{0.5}$)	C_d (meq/g)	R^2
Pb(II)		0.0003	0.04	0.94
Cu(II)		0.0004	0.0442	0.95
Cr(III)		0.0012	0.0736	0.98
Binary system				
Pb-Cu	Pb(II)	0.0002	0.0211	0.95
	Cu(II)	0.0003	0.0215	0.95
Pb-Cr	Pb(II)	0.0001	0.026	0.79
	Cr(III)	-	-	-
Cu-Cr	Cu(II)	0.0003	0.0262	0.91
	Cr(III)	-	-	-
Ternary system				
Pb-Cu-Cr	Pb(II)	0.0001	0.0182	0.94
	Cu(II)	0.0003	0.0174	0.94
	Cr(III)	-	-	-

6.3.2.4 Effect of polymer dosage

The study on the effect of dose on the removal of lead, copper and chromium was carried out by varying the amount of polymer dosage from 0.5g to 10g, while maintaining the same condition – lead, copper and chromium initial concentration 0.24meq/L, contact time 3h at 270rpm for pH 4 in room temperature for single, binary and ternary system given in Figure 6.6. In single system component Cu(II) and Cr(III) removal increased with increase in polymer dose whereas for Pb(II)

decreased above dose of 1.5 g/L (Figure 6.6a). The increase in the percentage removal of Cu(II) and Cr(III) could be due to an increase in the availability of more active sites on the surface of modified-AFC whereas for Pb(II) the case was opposite despite the available active sites removal was decreased which may be due to lead being a soft acid as discussed earlier in section 6.3.2.1.

In binary system of Pb(II)-Cu(II) (Figure 6.6b), removal of Cu(II) followed similar trend like single system but for Pb(II) was completely different than in single system. This may be that the presence of copper enhanced the adsorption of lead with the increase in available active sites. For Pb(II)-Cr(III) (Figure 6.6c) and Cu(II)-Cr(III) (Figure 6.6d) binary system, the removal decreased with increase in polymer dose suggesting that the presence of chromium hindered the adsorption process.

The ternary system for Pb(II)-Cu(II)-Cr(III) (Figure 6.6e) shows that removal of copper increased with polymer dose whereas lead and chromium decreased with increase in polymer dose. It may be noted that the copper was the least affected whereas lead and chromium was highly affected by the presence of other metal ions suggesting competitive adsorption.

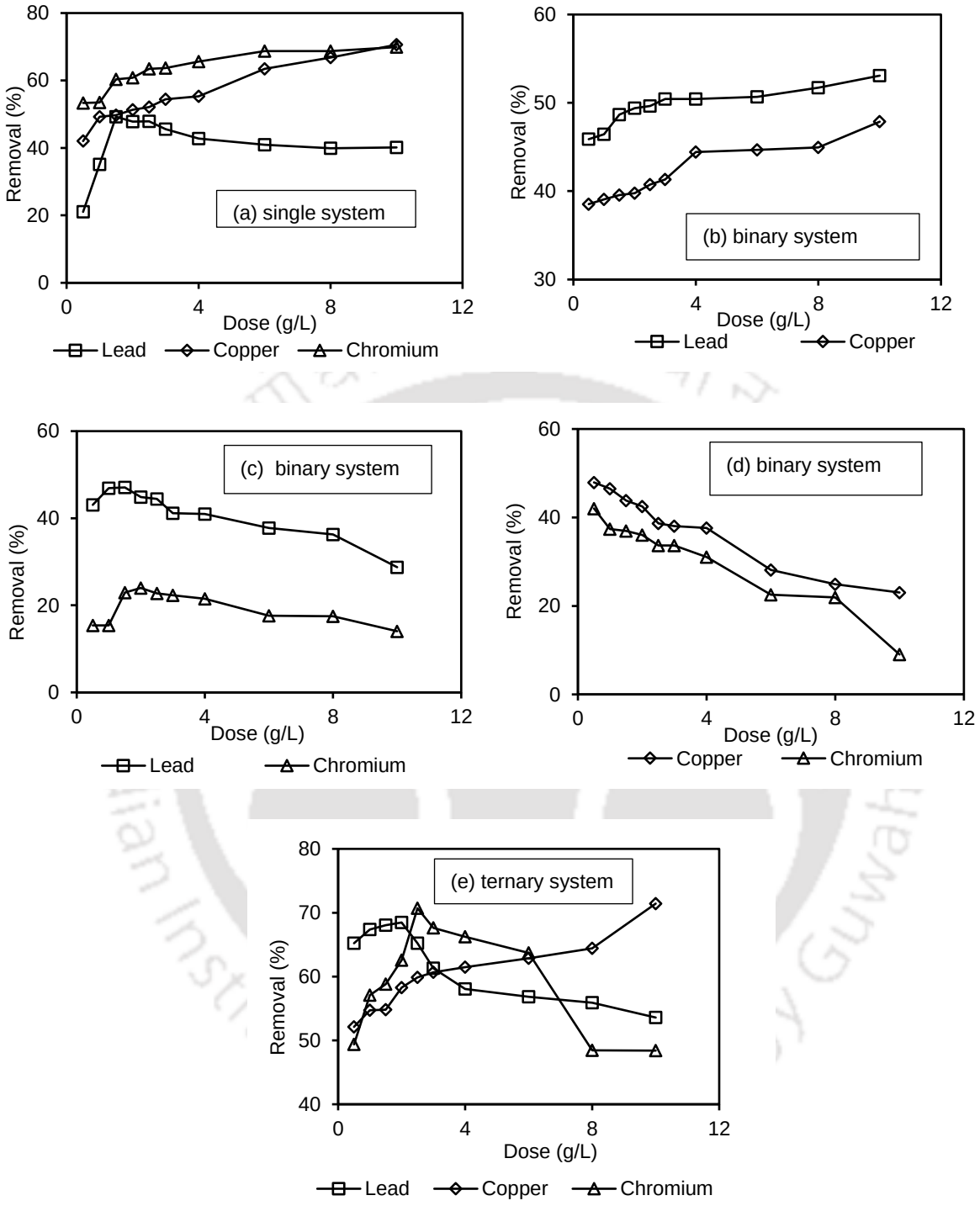

Figure 6.6: Effect of dose on the removal of a) lead-copper – chromium in single system, b) lead-copper, c) lead-chromium, d) copper-chromium in binary system and e) lead-copper-chromium in ternary system

6.3.2.5 Adsorption isotherm studies

To design an efficient adsorption system it is very important to determine the most accurate relationship from the adsorption equilibrium plots. Thus, different types of isotherm models were employed in order to explain the empirical data of the isotherms. In the present work, several types of isotherm models were used to describe the mono and multi component system including two and three parameters adsorption isotherm plot. According to Giles et al., 1974a, Figure 6.7a, showed that in single system Pb(II) lead isotherm could not be characterized while Cu(II) copper followed S1 type whereas Cr(III) chromium followed S3 type isotherm in which both the isotherm curves were concave shaped. Similar observation was found during the binary adsorption of Pb(II)-Cu(II) where the isotherm curves were almost same as the single system (Figure 6.7b).

From Figure 6.7c and d, both lead-chromium and copper-chromium in binary system followed reversible type III isotherm, the shape of the isotherm curve convex to the uptake value (Ng et al., 2017; Singh et al., 1985). And Figure 6.7e, in ternary system copper followed S1 type isotherm whereas lead followed reversible type III isotherm but for chromium it was observed that the shape of isotherm curve was difficult to characterize. Thus, it can be concluded that the isotherm curves are different for low initial concentrations and also different adsorption process involved in low and high concentration of metals with a tendency for available active sites present on the surface of an adsorbent.

Rearte et al., 2013 reported that for low initial concentration (<0.5mM) for Pb(II) and Cr(III) biosorption by *Schoenoplectus californicus*, the presence of both metals in solutions caused an effect of competence for active sites of sorption decreasing the sorption capacity compared to simple sorption. Rearte also suggested that in competitive sorption, the shapes of curves changed such that normal sorption isotherms were not detected.

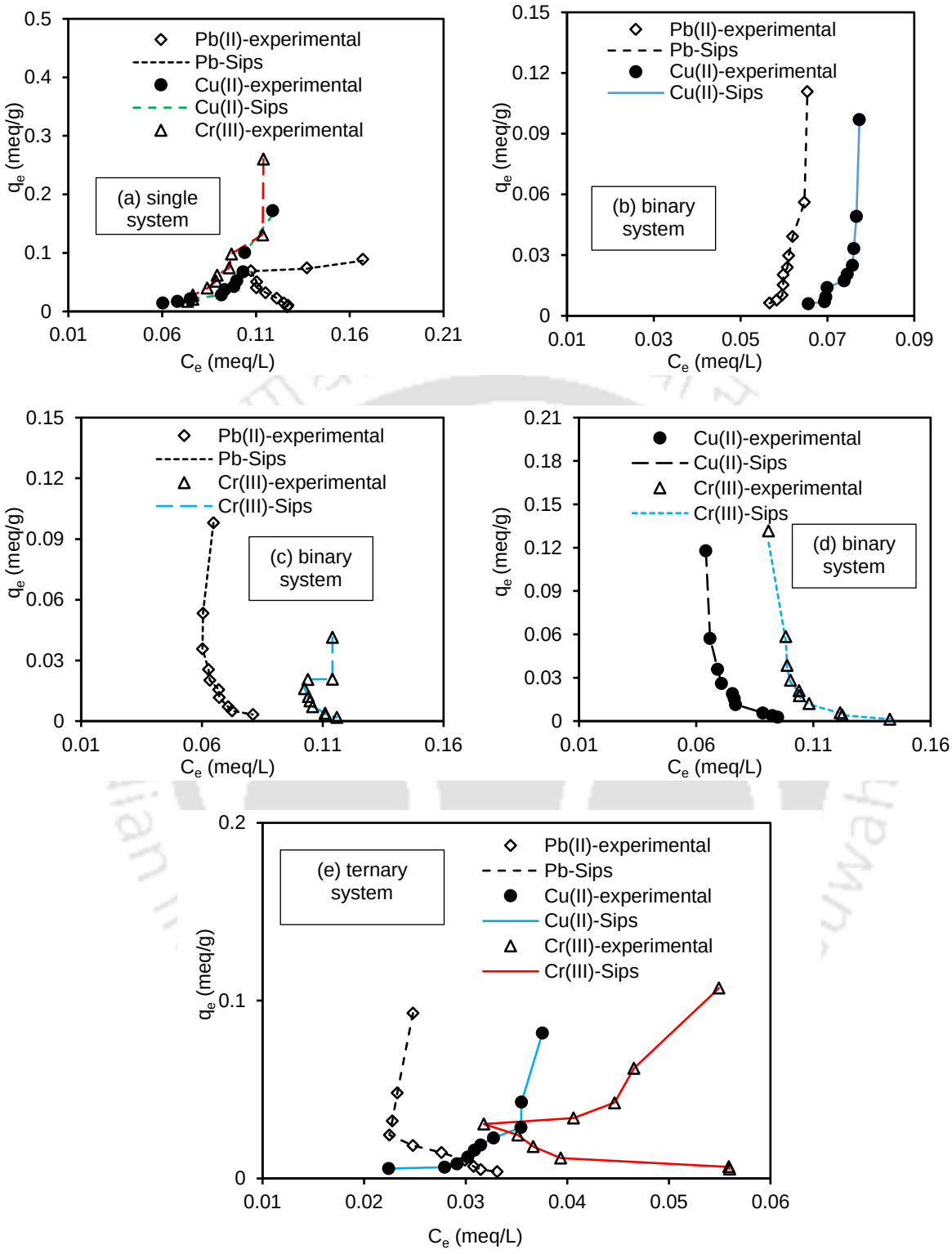

Figure 6.7: Experimental and Sips adsorption isotherm a) lead-copper-chromium in single system, b) lead-copper, c) lead-chromium and d) copper-chromium in binary system and e) lead-copper-chromium in ternary system

In order to relate the adsorption of metal ions onto modified-AFC, numerous isotherm models were considered – Halsay, Smith, Koble, Sips, Khan, Toth isotherm models (equation 1.29;1.31, 1..32;1.33;1.34;1.35). A mathematically rigorous nonlinear optimization routine was adopted to minimize the sum of squared error (SSE) and root mean square error (RMSE) between the experimental data and the modelled isotherms was determined. (A summary of the parameters of these isotherms obtained from fitting the experimental data given in Table A1 and A2 in Appendix 2). Figure 6.7, shows the experimental isotherm plot of C_e vs q_e for the metals in mono and multicomponent system isotherm. Sips isotherm model were applied to the experimental adsorption isotherm and the fitting results are listed in Table 6.4.

Table 6.4: Sips isotherm parameters of lead, copper and chromium adsorption onto modified-AFC (single, binary and ternary system component)

System	Metal ions	Parameters					
		Q_{max} (meq./g)	K_s (L/meq.)	1/n	R^2	SSE	RMSE
Single	Pb(II)	1.071	1.0300	1.0167	0.99	0.00095	0.000994
	Cu(II)	1.1162	1.1074	1.0555	0.99	0.003	0.002
	Cr(III)	6.21	0.1651	1.0107	0.99	0.0094	0.0094
Binary Pb(II)-Cu(II)	Pb(II)	1.0821	1.0807	1.0366	0.99	0.0012	0.0011
	Cu(II)	6.7252	0.1535	1.0075	0.99	0.00001	0.00004
Pb(II)-Cr(III)	Pb(II)	5.8537	0.1772	1.0087	0.99	0.00002	0.00005
	Cr(III)	3.6041	0.2863	1.0064	0.99	0.0000006	0.00001
Cu(II)-Cr(III)	Cu(II)	6.6225	0.1567	1.0091	0.99	0.00003	0.00006
	Cr(III)	6.14560	0.1569	1.0042	0.99	0.0034	0.00335
Ternary Pb(II)-Cu(II)-Cr(III)	Pb(II)	7.4209	0.1385	1.0064	0.99	0.00001	0.00004
	Cu(II)	4.8752	0.2131	1.0088	0.99	0.00001	0.00004
	Cr(III)	6.0916	0.1705	1.0095	0.99	0.00003	0.00006

To understand adsorption mechanism Sips isotherm model was analyzed which is obtained from combining the Langmuir and Freundlich isotherms for predicting the heterogeneous adsorption systems and avoiding the limitation of higher adsorbate concentration related with the Freundlich isotherm model. At low adsorbate concentrations, this model reduces to the Freundlich isotherm, while at high concentrations, it determines a monolayer adsorption capacity characteristic like the Langmuir isotherm.

Interaction of two-three components in multicomponent system could also be evaluated by the ratio of adsorption capacity of one component in the multicomponent (Q^M_{max}) to the same component when present in single system (Q^S_{max}) (Roy et al., 2013; Zhi-rong et al., 2010).

Therefore, in multicomponent system, there exist three types of effects, i.e., synergism, antagonism and non-interaction involve during the interaction of two-three components in an adsorption system. They are as follows:

1) Synergism ($Q^M_{max} / Q^S_{max} > 1$): effect of mixture of component in solution is greater than its individual effect.

2) Antagonism ($Q^M_{max} / Q^S_{max} < 1$): effect of mixture of component in solution is less than its individual effect.

3) Non-interaction ($Q^M_{max} / Q^S_{max} = 1$): effect of mixture of component in solution is neither less nor more than that of its individual effect.

In this work, the behavior of adsorption capacity was identified as a competitive effect of metal ions in the presence of chromium whereas lead and copper showed the opposite behavior given in Table 6.5. The adsorption capacities calculated from Sips isotherm model exhibited the trend, i.e. Cr(III)> Cu(II)> Pb, as observed for the equilibrium adsorption curves in single system.

Table 6.5: Experimental maximum adsorption capacities for single, binary and ternary component system onto modified-AFC

Metal ion	System	Q^S_{max} (meq/g) (single system)	Q^M_{max} (meq/g) (mixed system)	Ratio Q^S_{max} / Q^M_{max}	Interactive effect	Q_{total} (meq/g)
Pb(II)	Pb-Cu	1.071	1.0821	1.010	Synergism	7.8073
Cu(II)	Pb-Cu	1.1162	6.7252	6.025	Synergism	
Pb(II)	Pb-Cr	1.071	5.8537	5.465	Synergism	9.4578
Cr(III)	Pb-Cr	6.21	3.6041	0.580	Antagonism	
Cu(II)	Cu-Cr	1.1162	6.6225	5.933	Synergism	12.7675
Cr(III)	Cu-Cr	6.21	6.145	0.989	Antagonism	
Pb(II)	Pb-Cu-Cr	1.071	7.4209	6.928	Synergism	18.3877
Cu(II)	Pb-Cu-Cr	1.1162	4.8752	4.367	Synergism	
Cr(III)	Pb-Cu-Cr	6.21	6.0916	0.980	Antagonism	

**Antagonism – the adsorption is suppressed by the presence of other ions; Synergism- enhances the adsorption of other ions*; Q^M_{max} *is the maximum adsorption capacity in binary and ternary system whereas,* Q^S_{max} *is the maximum adsorption capacity in single system obtained from Sips isotherm model*

In binary system, Cu(II)>Pb(II), Pb(II)>Cr(III) and Cu(II)> Cr(III) and in ternary system was Pb(II)>Cr(III)> Cu(II) trend was observed which suggest competitive adsorption mechanism was involved as the isotherm adsorption curves were not similar to the single system (Goel et al., 2004). This difference in adsorption capacity may be explained by the results given in Table 6.5 where Pb(II) and Cu(II) showed synergistic behavior whereas Cr(III) showed antagonistic behavior in multicomponent system which could be due to the involvement of other factors such as- molecular weight, ionic radii, hydrated ionic radii, electronegativity etc., besides adsorption mechanism.

Finally, it can be attributed that the adsorption of multicomponent metal system is a combination of metal properties (electronegativity, molecular weight, etc.) and physicochemical properties of the adsorbent (morphology, surface area, functional groups, etc.) as well as the solution itself.

6.3.2.5 Comparison with other adsorbents

Most of the literatures reported competitive adsorption of metals with high initial concentration and very few was reported with low metal initial concentration. A comparison with other adsorbents at different conditions is listed in Table 6.6. Modified-AFC was found to be better than chitosan-immobilized on bentonite in ternary system, olive waste in binary system and floating aquatic macrophyte for Pb(II) removal in binary system. For Cu(II) removal modified-AFC was better in single system compared to other adsorbents and Cr(III) removal was found to be better than floating aquatic macrophyte in binary system. Thus, modified-AFC was found to be a good adsorbent for metal removal in single, binary and ternary system with low initial concentration.

Table 6.6: Comparison of maximum adsorption capacity of lead, copper and chromium adsorption capacity by various adsorbents

Adsorbent	conditions	Metals		Initial conc. (meq/L)	Uptake (meq/g)	Removal (%)	References
Natural meranti sawdust	single system pH-6, dose-5 g/L	Pb(II)		0.965	0.151	78	Rafatullah et al., 2009
		Cu(II)		3.147	0.507	80	
		Cr(III)		5.770	0.808	70	
		Ni(II)		3.407	0.518	76	
Olive waste	binary system pH-5,dose-10 g/L	Pb(II)		1.061	0.018	17.73	Hernáinz et al., 2009
		Cr(III)		6.347	0.069	10.91	
Chitosan-immobilized on bentonite	ternary system pH-4,dose-6.7 g/L	Pb(II)		0.241	0.028	80.4	Futulan et al., 2012
		Cu(II)		0.787	0.085	72.36	
		Ni(II)		0.852	0.072	56.28	
Dry Walnut shells	ternary system pH-6,dose-10 g/L	Pb(II)		0.482	0.028	60	Kamar et al., 2015
		Cu(II)		1.577	0.062	40	
		Cd(II)		0.889	0.017	20	
Floating aquatic macrophyte	binary system pH-4,dose-2 g/L	Pb(II)		0.224	0.050	16.61	Lima et al., 2015
		Cr(III)		1.799	0.149	44.64	
Modified-AFC	single system pH-4,dose-2 g/L	Pb(II)		0.24	0.051	47.83	Present study
		Cu(II)		0.24	0.052	51.31	
		Cr(III)		0.24	0.074	60.83	
	binary system pH-4,dose-2 g/L	Pb-Cu	Pb(II)	0.12	0.029	49.4	
			Cu(II)	0.12	0.025	39.78	
		Pb-Cr	Pb(II)	0.12	0.025	44.87	
			Cr(III)	0.12	0.016	23.98	
		Cu-Cr	Cu(II)	0.12	0.026	42.48	
			Cr(III)	0.12	0.028	36.07	
	ternary system pH-4,dose-2 g/L	Pb(II)		0.08	0.024	68.47	
		Cu(II)		0.08	0.022	58.27	
		Cr(III)		0.08	0.034	62.55	

*units converted to meq/L

6.4 Summary

The present study demonstrated the adsorption of capacity of modified-AFC for removals of lead, copper and trivalent chromium in single, binary and ternary system of metal ions. All studies were carried out using total metal ion concentration same (0.24 meq/L). Chromium was found to be highly affected by the presence of lead and copper showed antagonistic behaviour. It was also observed that within initial 15 min, significant metal uptake was achieved in single, binary and ternary system. Sips isotherm model fitted very well with the experimental data supporting a combination of Langmuir-Freundlich adsorption isotherm. In multicomponent system, chromium (antagonism) adsorption was highly affected by the presence of other ions lead and copper (synergism). Finally, it can be attributed that the adsorption of multicomponent metal system is a combination of factors such as metal properties and physicochemical properties of the adsorbent as well as the solution itself.

CHAPTER 7

7.1 Conclusion

The thesis was basically a research work with a combination of two main adsorbents – a) amine coated polymer and b) supportless amine polymer. Previous studies reported the successful application of amine coated polymer in the adsorption of heavy metals showing moderate to high removal efficiency. Therefore, in this thesis work the application of amine coated polymers (AFC coated silica gel and PANI coated jute fiber) were used for the adsorption studies of anionic azo dyes from aqueous solution. With the objective of achieving support less aniline formaldehyde condensate polymer after successive synthesis, it was found out that definitely supportless amine polymer was possible to synthesize and what made it more interesting was the fact that it could give better results during the adsorption of metals even in higher as well as in dilute concentration. Thus, based on the adsorption experiments the significant findings of the research work are as follows:

- Amine based coated polymers (AFC coated silica gel and PANI coated jute fiber) showed good results in removing anionic dyes from aqueous solution. The adsorbents were regenerated and reused.
- The synthesis of supportless amine polymer (mesoporous material) based on the ratios of aniline: HCl: formaldehyde ratio close to 1:2:1 and a solvent ratio close to 1: 1 (isopropanol: aqueous reagents) gave the best results.
- Ion exchange mechanism followed by minor redox mechanism was the main factor responsible for chromium removal. The optimum dose of modified-AFC was 2 g/L for total chromium removal from 10 g/L with residual concentration of 1.74 mg/L and uptake

of 4.55 mg/g which was lower than the discharge limit of 2mg/L. Desorption was 86% with 1N HCl and reuse of the modified AFC was possible for four cycles.

- Similarly, maximum Hg(II) removal was achieved at pH 3-4 by interaction between protonated amine group ($-NH_3^+$) and anionic specie mercury ($HgCl_3^-$). Desorption studies and the regeneration and reuse of the polymer and found to be favourable till third cycle.
- Removal of mixed metals in single, binary and ternary system for heavy metals Pb(II), Cr(III) and Cu(II) were carried out. Kinetic models data were adjusted to experimental data and pseudo-second order model presented the best fitting. Equilibrium isotherms were obtained for the adsorption of these metals in single, binary and ternary solutions. Presence of chromium metal ion hindered the adsorption process in mixed metal system.

7.2 Recommendation for future work

Based on the above conclusions the future scope of the polymer adsorbent may be as follows:

a) Desorption study of multicomponent with modified-AFC can be carried out.

b) Continuous mode study of the polymer adsorbent (modified-AFC) can be carried out.

c) Detailed adsorption experiments for other anionic dyes with modified-AFC can also be studied.

d) Similarly multicomponent system of anionic dyes removal with modified-AFC can also be carried out.

e) The modified-AFC polymer adsorbent can also be used to study the removal from real wastewater pollutants containing heavy metals and dyes combination.

References

1. Abdi, J., Bastani, D., Abdi, J., Mahmoodi, N. M., Shokrollahi, A., Mohammadi, A. H. **Assessment of competitive dye removal using a reliable method**. *Journal of Environmental Chemical Engineering*, 2 (**2014**) 1672–1683.
2. Abdelhadia, S. O., Dosoretz, C. G., Rytwo, G., Gerchman, Y., Azaizeh, H. **Production of biochar from olive mill solid waste for heavy metal removal**. *Bioresource Technology*, 244 (**2017**) 759–767.
3. Abou El-Reash, Y. G. **Magnetic chitosan modified with cysteine-glutaraldehyde as adsorbent for removal of heavy metals from water**. *Journal of Environmental Chemical Engineering*, 4 (**2016**) 3835–3847.
4. Abdelhadi, S. O., Dsoretz, C. G., Rytwo, G., Gerchman, Y., Azaizh, H. **Production of biochar from olive mill solid waste for heavy metal removal**. *Bioresource Technology*, 244 (2017) 759–767.
5. Abdolali, A., Ngo, H. H., Guo, W., Lu, S., Chen, S., Nguyen, N. C., Zhang, X., Wang, J., Wu, Y. **A breakthrough biosorbent in removing heavy metals: Equilibrium, kinetic, thermodynamic and mechanism analyses in a lab-scale study**. *Science of the Total Environment*, 542 (**2016**) 603–611.
6. Ahmad, R., Kumar, R. **Adsorptive removal of congo red dye from aqueous solution using bael shell carbon**. *Applied Surface Science*, 257 (**2010**) 1628–1633.
7. Akazdam, S., Chafi, M., Yassine, W., Gourich, B. **Removal of Acid Orange 7 Dye from Aqueous Solution Using the Exchange Resin Amberlite FPA-98 as an Efficient Adsorbent: Kinetics, Isotherms, and Thermodynamics Study**. *Journal of Materials and Environmental Sciences*, 8 (**2017**) 2993-3012.
8. Al-Degs, Y. S., Khraisheh, M. A. M., Allen, S. J., Ahmad, M. N. M. **Effect of carbon surface chemistry on the removal reactive dyes from textile effluent**.*Water Research*, 34(**2000**) 927-935.
9. Al-Khafaji, M. S., Al-Ani, F. H., Ibrahim, A. F. **Removal of Some Heavy Metals from Industrial Wastewater by Lemmna Minor**. *KSCE Journal of Civil Engineering*, (2017) 1-6.
10. Ali, S., Nisar, N., Hussain, T. **Dyeing properties of natural dyes extracted from eucalyptus**. *Journal of the Textile Institute*, 98 (**2007**) 559–562.

11. Aliabadi, R. S., Mahmoodi, N. O. **Synthesis and characterization of polypyrrole, polyaniline nanoparticles and their nanocomposite for removal of azo dyes; sunset yellow and Congo red**. *Journal of Cleaner Production*, 179 (**2018**) 235-245.
12. Ali, M. E. A. **Synthesis and adsorption properties of chitosan-CDTA-GO nanocomposite for removal of hexavalent chromium from aqueous solutions**. *Arabian Journal of Chemistry*, (2016) in press.
13. Ali, N. F., El-Mohamedy, R. S. R. **Microbial decolourization of textile waste water**. *Journal of Saudi Chemical Society*, 16 (**2012**) 117–123.
14. Ali, M. E. A. **Synthesis and adsorption properties of chitosan-CDTA-GO nanocomposite for removal of hexavalent chromium from aqueous solutions**. *Arabian Journal of Chemistry*, (2016) in press.
15. Alvarez-Puebla, R. A., Valenzuela-Calahorro, C., Garrido, J. J. **Modeling the adsorption and precipitation processes of Cu(II) on humin**. *Journal of Colloid and Interface Science*, 277 (**2004**) 55-61.
16. Amrhar, O., Nassali, H., Elyoubi, M. S. **Two and three-parameter isothermal modeling for adsorption of Crystal Violet dye onto Natural Illitic Clay: Nonlinear regression analysis**. *Journal of Chemical and Pharmaceutical Research*, 7 (**2015**) 892-903.
17. Amin, M. T., Alazba, A. A., Shafiq, M. **Adsorptive Removal of Reactive Black 5 from Wastewater Using Bentonite Clay: Isotherms, Kinetics and Thermodynamics**. *Sustainability*, 7 (**2015**) 15302-15318.
18. Anbia, M., Salehi, S. **Removal of acid dyes from aqueous media by adsorption onto amino-functionalized nanoporous silica SBA-3**. *Dyes and Pigments*, 94 (**2012**) 1-9.
19. Anastasi, A., Parato, B., Spina, F., Tigini, V., Prigione, V., Varese, G. C. **Decolourisation and detoxification in the fungal treatment of textile wastewaters from dyeing processes**. *New Biotechnology*, 29 (**2011**) 38-45.
20. Angelova, R., Baldikova, E., Pospiskova, K., Maderova, Z., Safarikova, M., Safarik, I. **Magnetically modified Sargassum horneri biomass as an adsorbent for organic dye removal**. *Journal of Cleaner Production*, 137 (**2016**) 189-194.
21. Anandkumar, A., Mandal, B. **Adsorption of chromium(VI) and Rhodamine B by surface modified tannery waste: Kinetic, mechanistic and thermodynamic studies**. *Journal of Hazardous Materials*, 186 (**2011**) 1088–1096.

22. Anirudhan, T. S., Jalajamony, S., Suchitra, P. S. **Improved performance of a cellulose based anion exchanger with tertiary amine functionality for the adsorption of chromium(VI) from aqueous solutions**. *Colloids and surfaces A: Physicochemical and Engineering Aspects*, 335 (**2009**) 107-113.
23. Appel, C., Mab, L. Q., Rhue, R. D., Kennelley, E. **Point of zero charge determination in soils and minerals via traditional methods and detection of electroacoustic mobility**. *Geoderma*, 113 (**2003**) 77 – 93.
24. Archna, Lokesh, K. N., Siva Kiran, R. R. **Biological methods of dye removal from textile effluents - A review**. *Journal of Biochemical Technology*, 3 (**2012**) S177-S180.
25. Attari, M., Bukhari, S. S., Kazemian, H., Rohani, S. **A low-cost adsorbent from coal fly ash for mercury removal from industrial wastewater**. *Journal of Environmental Chemical Engineering*, 5 (**2017**) 391–399.
26. Ayati, A., Shahrak, M. N., Tanhaei, B., Sillanpää, M. **Emerging adsorptive removal of azo dye by metal–organic frameworks**. *Chemosphere*, 160 (**2016**) 30-44.
27. Ayawei, N., Ebelegi, A. N., Wankasi, D. **Modelling and Interpretation of Adsorption Isotherms**. *Journal of Chemistry*, (**2017**) 1-11.
28. Babaei, A. A, Kakavandi, B., Rafiee, M., Kalantarhormizi, F., Purkaram, I., Ahmadi, E., Esmaeili, S. **Comparative treatment of textile wastewater by adsorption, Fenton, UV-Fenton and US-Fenton using magnetic nanoparticles-functionalized carbon (MNPs@C)**. *Journal of Industrial and Engineering Chemistry*, 56 (2017) 163–174.
29. Babic, B. M., Milonjic, S. K., Polovina, M. J., Kaludierovic, B.V. **Point of zero charge and intrinsic equilibrium constants of activated carbon cloth**. *Carbon*, 37 (**1999**) 477–481.
30. Barbusinski, K., Majewski, J. **Discoloration of Azo Dye acid Red18 by Fenton Reagent in the Presence of Iron Powder**. *Polish Journal of Environmental Studies*, 12 (**2003**) 151-155.
31. Ballesteros, F. C., Salcedo, A. F. S., Vilando, A. C., Huang, Y., Lu, M. **Removal of nickel by homogeneous granulation in a fluidized-bed reactor.** *Chemosphere*, 164 (**2016**) 59-67.
32. Barakat, M. A. **New trends in removing heavy metals from industrial wastewater**. *Arabian Journal of Chemistry*, 4 (**2011**) 361–377.
33. Barret, E. P., Joyner, L. G., Halenda, P. P. **The determination of pore volume and area distributions in porous substances. I. Computations from nitrogen isotherms**. *Journal of American Chemical Society*, 73 (**1951**) 373-380.

34. Bayramoglu, G., Akbulut, A., Liman, G., Arica, M. Y. **Removal of metal complexed azo dyes from aqueous solution using tris(2-aminoethyl)amine ligand modified magnetic p(GMA-EGDMA) cationic resin: Adsorption, isotherm and kinetic studies**. *Chemical Engineering Research and Design*, 124 (**2017**) 85-97.
35. Belbachir, I., Makhoukhi, B. **Adsorption of Bezathren dyes onto sodic bentonite from aqueous solutions**. *Journal of the Taiwan Institute of Chemical Engineers*, 75 (**2017**) 105–111.
36. Bharagava, R. N., Mishra, S. **Hexavalent chromium reduction potential of *Cellulosimicrobium sp.* Isolated from common effluent treatment plant of tannery industries**. *Ecotoxicology and Environmental Safety*, 147 (**2018**) 102–109.
37. Bhaumik, M., Maity, A., Srinivasu, V. V., Onyango, M. S. **Removal of hexavalent chromium from aqueous solution using polypyrrole-polyaniline nanofibers**. *Chemical Engineering Journal*, 181-182 (**2012**) 323-333.
38. Bjørklund, G., Dadar, M., Mutter, J., Aaseth, J. **The toxicology of mercury: Current research and emerging trends**. *Environmental Research*, 159 (**2017**) 545–554.
39. Bulut, M. O., Akar, E. **Ecological dyeing with some plant pulps on woolen yarn and cationized cotton fabric**. *Journal of Cleaner Production*, 32 (**2012**) 1-9.
40. Bureau of Indian Standards, Tolerance limits for industrial effluents prescribed by Indian Standards Institution, Indian Standards Institution, IS 2490, 1991 **(revised 2012)**.
41. Buthelezi, S. P., Olaniran, A. O., Pillay, B. **Textile Dye Removal from Wastewater Effluents Using Bioflocculants Produced by Indigenous Bacterial Isolates**. *Molecules*, 17 (**2012**) 14260-14274.
42. Can, M. **BET, thermal degradation, and FTIR spectras of triazine polyamine polymers**. *Data in Brief*, 11 (**2017**) 408-412.
43. Cataldo, S., Lazzara, G., Massaro, M., Muratore, N., Pettignano, A., Riela, S. **Functionalized halloysite nanotubes for enhanced removal of lead(II) ions from aqueous solutions**. *Applied Clay Science*, 156 (**2018**) 87–95.
44. Çetin, D., Dönmez, G. **Decolorization of reactive dyes by mixed cultures isolated from textile effluent under anaerobic conditions**. *Enzyme and Microbial Technology*, 38 (**2006**) 926–930.

45. Chanda, M., Rempel, G. L. **Polyethyleneimine gel-coat on silica. High uranium capacity and fast kinetics of gel-coated resin**. *Reactive Polymers*, 25 (**1995**) 25-36.
46. Chen, A., Chen, S. **Biosorption of azo dyes from aqueous solution by glutaraldehyde-crosslinked chitosans**. *Journal of Hazardous Material*, 172 (**2009**) 1111–1121.
47. Chen, Y., Ru, J., Geng, B., Wang, H., Tong, C., Dua, C., Wu, S., Liu, H. **Charge-functionalized and mechanically durable composite cryogels from Q-NFC and CS for highly selective removal of anionic dyes**. *Carbohydrate Polymers*, 174 (**2017**) 841–848.
48. Chen, K., Wu, J., Liou, D., Hwang, S. J. **Decolorization of the textile dyes by newly isolated bacterial strains**. *Journal of Biotechnology*, 101 **(2003**) 57-68.
49. Chiou, M., Ho, P., Li, H. **Adsorption of anionic dyes in acid solutions using chemically cross-linked chitosan beads.** *Dyes and Pigments*, 60 (**2004**) 69–84.
50. Chowdhury, S. R., Yanful, E. K. **Arsenic and chromium removal by mixed magnetic maghemite nanoparticles and the effect of phosphate on removal**. *Journal of Environmental Management*, 91 (**2010**) 2238-2247.
51. Conceiçã, D. S., Ferreira, D. P., Graça, V. C., Silva, C. R., Santos, P. F., Ferreira, L. F. V. **Photochemical studies of new benzothiazole- and benzoselenazole-derived aminosquarylium dyes**. *Tetrahedron*, 71 (**2015**) 967-976.
52. Cooney, D. O. **Adsorption design for wastewater treatment**. CRC Press, LLC, Florida, USA, (**1999**) pp. 66-74.
53. Constantin, M., Asmarandei, I., Harabagiua, V., Ghimici, L., Ascenzi, P., Fundueanu, G. **Removal of anionic dyes from aqueous solutions by an ion-exchanger based on pullulan microspheres**. *Carbohydrate Polymers*, 91 (**2013**) 74–84.
54. Crini, G. **Non-conventional low-cost adsorbents for dye removal: A review**. *Bioresource Technology*, 97 (**2006**) 1061–1085.
55. Cristian, P., Violeta, P., Anita-Lauraa, R., Ralucaa, I., Alexandrescu, E., Andrei, S., Daniela, I., Raluca, M. A., Cristina, M., Ioana, C. A. **Removal of zinc ions from model wastewater system usingbicopolymer membranes with fumed silica**. *Journal of Water Process Engineering*, 8 (**2015**) 1–10.
56. D. Andrade, P. R., Lemus, M. R., E. Pérez, C. C. Models of sorption isotherms for food: uses and limitations. *VITAE, REVISTA DE LA FACULTAD DE QUÕMICA FARMACUTICA*, 18 (**2011**) 325-334.

57. Dada, A.O., Olalekan, A. P., Olatunya, A. M., DADA, O. **Langmuir, Freundlich, Temkin and Dubinin–Radushkevich Isotherms Studies of Equilibrium Sorption of Zn^{2+} Unto Phosphoric Acid Modified Rice Husk**. *Journal of Applied Chemistry (IOSR-JAC)*, 3 (**2012**) 38-45.

58. da Fontoura, J. T., Rolima, G. S., Mela, B., Farenzana, M., Gutterres, M. **Defatted microalgal biomass as biosorbent for the removal of Acid Blue 161 dye from tannery effluent**. *Journal of Environmental Chemical Engineering*, 5 (**2017**) 5076-5084.

59. Dai, H., Peng, X., Yang, W., Hu, F., Qiu, Z., Xiang, Z. **Synthesis and characterization of graphitic magnetic mesoporous nanocomposite and its application in dye adsorption**. *Journal of Molecular Liquids*, **2018**.

60. Das, S., Dash, H. R. **Handbook of Metal-Microbe Interactions and Bioremediation**. CRC press, (**2017**).

61. Daoud, M., Benturki, O., Kecira, Z., Girods, P., Donnot, A. **Removal of reactive dye (BEZAKTIV Red S-MAX) from aqueous solution by adsorption onto activated carbons prepared from date palm rachis and jujube stones**. *Journal of Molecular Liquids*, 243 (**2017**) 799–809.

62. Dawood, S., Sen, T. K. **Review on Dye Removal from Its Aqueous Solution into Alternative Cost Effective and Non-Conventional Adsorbents**. *Journal of Chemical and Process Engineering*, 1 (**2014**) 1-4.

63. Delee, W., O' Neill C, Hakes E. R., Pinheiro, H. M. **Anaerobic treatment of textile effluent**. *Journal of Chemical Technology & Biotechnology*, 73 (**1998**) 323–335.

64. de Luna, M. S., Castaldo, R., Altobelli, R., Gioiella, L., Filipponea, G., Gentilec, G., Ambrogi, V. **Chitosan hydrogels embedding hyper-crosslinked polymer particles as reusable broad-spectrum adsorbents for dye removal**. *Carbohydrate Polymers*, 177 (**2017**) 347–354.

65. Desta, M. B. **Batch Sorption Experiments: Langmuir and Freundlich Isotherm Studies for the Adsorption of Textile Metal Ions onto Teff Straw (*Eragrostis tef*) Agricultural Waste**. *Journal of Thermodynamics*, 2013 (**2013**) 6.

66. Dincer, I., Colpan, C. O., Kizilkan, O., Eza, M. A. Progress in Clean Energy, Volume 1: Analysis and Modeling. *Springer International Publishing Switzerland*, (**2015**).

67. Dinker, M. K., Kulkarni, P. S. **Temperature based adsorption studies of Cr(VI) using p-toluidine formaldehyde resin coated silica material**. *Journal of Chemical & Engineering Data*, 39 (**2015**) 3687-3697.

68. Djilani, C., Zaghdoudi, R., Djazi, F., Bouchekima, B., Lallam, A., Modarressi, A., Rogalsk, M. **Adsorption of dyes on activated carbon prepared from apricot stones and commercial activated carbon**. *Journal of the Taiwan Institute of Chemical Engineers*, 53 (**2015**) 112–121.

69. Donia, M., Atia, A. M., Al-amrani, W. A., El-Nahas, A. M. **Effect of structural properties of acid dyes on their adsorption behaviour from aqueous solutions by amine modified silica**. *Journal of Hazardous Materials*, 161 (**2009**) 1544–1550.

70. El-Moselhy, M. M., Kamal, S. M. **Selective removal and preconcentration of methylene blue from polluted water using cation exchange polymeric material**. *Groundwater for Sustainable Deveperarment*, 6 (**2018**) 6–13.

71. Elwakeel, K. Z., El-Ghaffa, M. A. A., El-kousy, S. M., El-Shorbagy, H. G. **Synthesis of new ammonium chitosan derivatives and their application for dye removal from aqueous media**. *Chemical Engineering Journal*, 203 (**2012**) 458–468.

72. Elwakeel, K. Z, El-Bindary, A. A., El-Sonbatib, A. Z., Hawas, A. R. **Adsorption of toxic acidic dye from aqueous solution onto diethylenetriamine functionalized magnetic glycidyl methacrylate-N, N′-methylenebisacrylamide**. *RSC Advances*, 6 (**2016a**) 3350–3361.

73. Elwakeel, K. Z., El-Kousy, S., El-Shorbagy, H. G., Abd El-Ghaffard, M. A. (2016b) **Comparison between the removal of Reactive Black 5 from aqueous solutions by 3-amino-1,2,4 triazole,5-thiol and melamine grafted chitosan prepared through four different routes**. *Journal of Environmental Chemical Engineering*, 4 (**2016b**) 733–745.

74. Ertugay, N., Acar, F. N. **Removal of COD and color from Direct Blue 71 azo dye wastewater by Fenton's oxidation: Kinetic study**. *Arabian Journal of Chemistry*, 10 (**2017**) S1158–S1163.

75. Fabryantya, R., Valencia, C., Edi Soetaredjo, F. E., Putro, J. N., Santoso, S. P., Kurniawan, A., Ju, Y., Ismadji, S. **Removal of crystal violet dye by adsorption using bentonite – alginate composite**. *Journal of Environmental Chemical Engineering*, 5 (**2017**) 5677–5687.

76. Fajardo, A. S., Martins, R. C., Silva, D. R., Martínez-Huitle, C. A., Quinta-Ferreira, R. M. **Dye wastewaters treatment using batch and recirculation flow electrocoagulation systems**. *Journal of Electroanalytical Chemistry*, 801 (**2017**) 30–37.
77. Fan, H., Fan, X., Li, J., Guo, M., Zhang, D., Yan, F., Sun, T. **Selective Removal of Arsenic(V) from Aqueous Solution Using A Surface-Ion-Imprinted Amine-Functionalized Silica Gel Sorbent**. *Industrial & Engineering Chemistry Research*, 51 (**2012**) 5216−5223.
78. Fang, W., Wei, Y., Liu, J., Kosson, D. S., van der Sloot, H. A., Zhang, P. **Effects of aerobic and anaerobic biological processes on leaching of heavy metals from soil amended with sewage sludge compost**. *Waste Management*, 58 (**2016**) 324–334.
79. Fang, X., Xu, X., Wang, S., Dong Wang, D. **Adsorption Kinetics and Equilibrium of Cu(II) from Aqueous Solution by Polyaniline/Coconut Shell–Activated Carbon Composites**. *Journal of Environmental Eng*ineering, 139 (**2013**) 1279-1284.
80. Fang, J., Gu, Z., Liu, C., Ilton, E. S., Deng, B. **Cr(VI) removal from aqueous solution by activated carbon coated with quaternized poly (4-vinylpyridine)**. *Environmental Science & Technology*, 14 (**2007**) 4748-4753.
81. Fatiha, M., Belkacem, B. **Adsorption of methylene blue from aqueous solutions using natural clay**. *Journal of Materials and Environmental Sciences*, 7 (**2016**) 285-292.
82. Feng, Q., Wu, D., Zhao, Y., Wei, A., Wei, Q., Hao Fong, H. **Electrospun AOPAN/RC blend nanofiber membrane for efficient removal of heavy metal ions from water**. *Journal of Hazardous Materials*, 344 (**2018**) 819–828.
83. Ferreira, G. M. D., Ferreira, G. M. D., Hespanhol, M. C., Rezende, J, d., Pires, A. C. d. S., Gurgel, L. V. A., da Silva, L. H. M. **Adsorption of red azo dyes on multi-walled carbon nanotubes and activated carbon: A thermodynamic study**. *Colloids and Surfaces A*, 529 (2017) 531–540.
84. Fiol, N., Villaescusa, E. **Determination of sorbent point zero charge: usefulness in sorption studies**. *Environ. Chem. Lett*er, 7 (**2009**) 79–84.
85. Fosso-Kankeu, E., Mittal, H., Waanders, F., Ray, S. S. **Thermodynamic properties and adsorption behaviour of hydrogel nanocomposites for cadmium removal from mine effluents**. *Journal of Industrial and Engineering Chemistry*, 48 (**2017**) 151–161.

86. Frioui, S., Oumeddour, R., Lacour, S. **Highly selective extraction of metal ions from dilute solutions by hybrid electrodialysis technology**. *Separation and Purification Technology*, 174 (**2017**) 264–274.
87. Fu, F., Wang, Q. **Removal of heavy metal ions from wastewaters: A review**. *Journal of Environmental Management*, 92 (**2011**) 407-418.
88. Futalan, C, M., Tsai, W., Lin, S. **"Copper, nickel and lead adsorption from aqueous solution using chitosan-immobilized on bentonite in a ternary system"**. *Sustainable Environment Research*, 22 (**2012**) 345-355.
89. Gao, B., Chin, Y., Chen, Z. **Adsorption behavior of functional grafting particles based on polyethyleneimine for chromate ions**. *Chemical Engineering Journal*, 150 (**2009**) 337-343.
90. Gatabi, M. P., Moghaddam, H. M., Ghorbani, M. **Point of zero charge of maghemite decorated multiwalled carbon nanotubes fabricated by chemical precipitation method**. *Journal of Molecular Liquids*, 216 (**2016**) 117–125.
91. Ge, J., Xin-Geng, Dua, Y., Chena, J., Zhanga, L., Bai, D., Ji, D., Hu, Y., Li, Z. **Highly sensitive fluorescence detection of mercury (II) ions based on WS2 nanosheets and T7 exonuclease assisted cyclic enzymatic amplification**. *Sensors and Actuators B*, 249 (**2017**) 189–194.
92. Giannakoudakis, D. A., Kyzas,G. Z., Avranas, A., Lazaridis, N. K. **Multi-parametric adsorption effects of the reactive dye removal with commercial activated carbons**. *Journal of Molecular Liquids*, 213 (**2016**) 381-389.
93. Ghosh, A., Dastidar, M. G., Sreekrishnan, T. R**. Bioremediation of chromium complex dyes and treatment of sludge generated during the process**. *International Biodeterioration & Biodegradation*, 119 (**2017**) 448-460.
94. Giles, C. H., Smith, D., Huitson, A. **A general treatment and classification of the solute adsorption isotherm. I: theoretical**. *Journal of Colloid Interface Science*, 47 (**1974a**) 755–765.
95. Girods, P., Dufour, A., Fierro, V., Rogaume, Y., Rogaume, C., Zoulalin, A., Celzard, A. **Activated carbons prepared from wood particleboard wastes: characterisation and phenol adsorption capacities**. *Journal of Hazardous Materials*, 166 (**2009**) 491–501.

96. Gnanapragasam, G., Senthilkumar, M., Arutchelvan, V., Velayutham, T., Nagarajan, S. **Bio-kinetic analysis on treatment of textile dye wastewater using anaerobic batch reactor**. *Bioresource Technology*, 102 (**2011**) 627–632.
97. Goel, J., Kadirvelu, K., Rajagopal, C. **Competitive Sorption of Cu(II), Pb(II) and Hg(II) Ions from Aqueous Solution Using Coconut Shell-based Activated Carbon**. *Adsorption Science & Technology*, 22(**2004**) 3.
98. Green-Ruiz, C. **Mercury(II) removal from aqueous solutions by nonviable Bacillus sp. from a tropical estuary**. *Bioresource Technology*, 97 (**2006**) 1907–1911.
99. Goscianska, J., Fathy, N. A., Aboelenin, R. M. M. **Adsorption of solophenyl red 3BL polyazo dye onto amine-functionalized mesoporous carbons**. *Journal of Colloid and Interface Science*, 505 (**2017**) 593–604.
100. Gupta, V. K., Suhas. **Application of low-cost adsorbents for dye removal – A review**. *Journal of Environmental Management*, 90 (**2009**) 2313–2342.
101. Hadi, P., Barford, J., McKay, G. **"Selective toxic metal uptake using an e-waste-based novel sorbent–Single, binary and ternary systems".** *Journal of Environmental Chemical Engineering***,** 2 (**2017**) 332-339.
102. Halimoon, N., Yin, R. G. S. **Removal of Heavy Metals from Textile Wastewater using Zeolite**. *Environment Asia*, 3 (**2010**) 124-130.
103. Hamdaoui, O., Naffrechoux, E. **Modeling of adsorption isotherms of phenol and chlorophenols onto granular activated carbon Part I. Two-parameter models and equations allowing determination of thermodynamic parameters**. *Journal of Hazardous Materials*, 147 (**2007**) 381-394.
104. Hassan, S. S. M., Awwad, N. S., Aboterika, A. H. A. **Removal of mercury(II) from wastewater using camel bone charcoal**. *Journal of Hazardous Materials*, 154 (**2008**) 992–997.
105. Hassan, S. S. M., Kamel, A. K., Awwad, N. S., Aboterika, A. H. A., Yahia, I. S. **Adsorbent for efficient removal of mercury(II) from aqueous solution**. *European Chemical Bulletin*, 6 (**2017**) 558-563.
106. Hassaan, M. A., El Nemr, A., Madkour, F. F. **Testing the advanced oxidation processes on the degradation of Direct Blue 86 dye in wastewater**. *Egyptian Journal of Aquatic Research*, (**2017**) 43, 11–19.

107. Hayati, B., Maleki, A., Najafi, F., Daraei, H., McKay, G. "**Super high removal capacities of heavy metals (Pb^{2+} and Cu^{2+}) using CNT dendrimer".** *Journal of Hazardous Materials*, 336 (**2017**)146-157.

108. He, Y., Xu, T., Hu, T., Peng, C., Yang, Q., Wang, H., Liu, H. **Amine functionalized 3D porous organic polymer as an effective adsorbent for removing organic dyes and solvents**. *RSC Advances*, 7 (**2017**) 30500–30505.

109. Heraldy, E., Lestari, W. W., Permatasari, D., Arimurti, D. D. **Biosorbent from tomato waste and apple juice residue for lead removal**. *Journal of Environmental Chemical Engineering*, 6 (**2018**) 1201–1208.

110. Hernández-Hernández, L. E., Bonilla-Petriciolet, A., Mendoza-Castillo, D. I., Reynel-Ávila. H. E. **"Antagonistic binary adsorption of heavy metals using stratified bone char columns".** *Journal of Molecular Liquids*, 241 (**2017**) 334–346.

111. Hernáinz, F., Calero, M., Blázquez, G., Tenorio, Martín-Lara, M. A. **"Effect of the Presence of Chromium(III) on the Removal of Lead (II) from Aqueous Solutions by Agricultural Wastes".** *Journal of Environmental Engineering***,** 135 (**2009**) 1348-1356.

112. Hinz, C. **Description of sorption data with isotherm equations**. *Geoderma*, 99 (**2001**) 225–243.

113. Ho, Y. S., McKay, G. **The kinetics of sorption of basic dyes from aqueous solution by sphagnum moss peat**. *Can. J. Chem. Eng*., 76 (**1998**) 822-827.

114. Ho, Y., Chiu, W., Wang, C. **Regression analysis for the sorption isotherms of basic dyes on sugarcane dust**. *Bioresource Technology*, 96 (**2005**) 1285–1291.

115. Hu, H., Li, X., Huang, P., Zhang, Q., Yuan, W. **Efficient removal of copper from wastewater by using mechanically activated calcium carbonate**. *Journal of Environmental Management*, 203 (**2017**) 1-7.

116. Huang, Q., Liu, M., Deng, F., Wang, K., Huang, H., Xu, D., Zeng, G., Zhang, X., We, Y. **Mussel inspired preparation of amine-functionalized Kaolin for effective removal of heavy metal ions**. *Materials Chemistry and Physics*, 181 (**2016**) 116-125.

117. Huang, Y., Feng, F., Chen, Z., Wu, T., Wang, Z. **Green and efficient removal of cadmium from rice flour using natural deep eutectic solvents**. *Food Chemistry*, 244 (**2018**) 260–265.

118. Huang, S., Ma, C., Liao, Y., Min, C., Du, P., Jiang, Y. **Removal of Mercury(II) from Aqueous Solutions by Adsorption on Poly(1-amino-5-chloroanthraquinone)**

Nanofibrils: Equilibrium, Kinetics, and Mechanism Studies. *Journal of Nanomaterials*, (**2016**).

119. Ingole, R. S., Lataye, D. H., T. Dhorabe, P. T. **Adsorption of Phenol onto Banana Peels Activated Carbon**. *KSCE Journal of Civil Engineering*, 21 (**2017**) 100-110.
120. Inyinbor, A. A., Adekola, F. A., Olatunji, G. A. **Kinetics, isotherms and thermodynamic modeling of liquid phase adsorption of Rhodamine B dye onto *Raphia hookerie* fruit epicarp**. *Water Resources and Industry*, 15 (**2016**)14–27.
121. Jacob, J. M., Karthik, C., Saratale, G. R., Kumar, S. S., Prabakar, D., Kadirvelu, K., Pugazhendhi, A. **Biological approaches to tackle heavy metal pollution: A survey of literature**. *Journal of Environmental Management*, 217 (**2018**) 56-70.
122. Jain, S. N., Gogate, P. R. **Adsorptive removal of acid violet 17 dye from wastewater using biosorbent obtained from NaOH and H_2SO_4 activation of fallen leaves of Ficus racemose**. *Journal of Molecular Liquids*, 243 (**2017**) 132–143.
123. Jamil, N., Munawar, M. A., Badar, S., Sidra-Tul-Muntaha. **Biosorption of Hg(II) and Cd(II) from wastewater by using Zea Mays Waste**. *Journal of the Chemical Society of Pakistan*, 31 (**2009**) 3.
124. Janaki, V., Vijayaraghavan, K., Oh, B., Lee, K., Muthucheliand, K., Ramasamy, A. K., Kamala-Kannan, S. **Starch/polyaniline nanocomposite for enhanced removal of reactive dyes from synthetic effluent**. *Carbohydrate Polymers*, 90 (**2012**) 1437–1444.
125. Jansson-Charrier, M., Guibal, E., Roussy, J., Delanghe, B., Cloirec, P. **Vanadium (IV) sorption by chitosan: Kinetics and equilibrium**. *Water Resource*, 30 (**1996**) 465-475.
126. Jeffery, G. H., Basett, J., Mendham, J., Denny, R. C. **Vogel's Textbook of Quantitative Chemical Analysis**. *Longman Group UK Ltd., London*, 5th Ed., (**1989**).
127. Jia, Z., Li, Z., Ni, T., Li, S. **Adsorption of low-cost absorption materials based on biomass (*Cortaderia selloana* flower spikes) for dye removal: Kinetics, isotherms and thermodynamic studies**. *Journal of Molecular Liquids*, 229 (**2017**) 285-292.
128. Jiang, Y., Liu, B., Xu, J., Pan, K., Hou, H., Jingping Hu, J., Yang, J. **Cross-linked chitosan/β-cyclodextrin composite for selective removal of methyl orange: Adsorption performance and mechanism**. *Carbohydrate Polymers*, 182 (**2018**) 106–114.

129. Jin, L., Sun, Q., Xu, Q., Xu, Y. **Adsorptive removal of anionic dyes from aqueous solutions using microgel based on nanocellulose and polyvinylamine**. *Bioresource Technology*, 197 (**2015**) 348–355.

130. Jung, C., Heo, J., Han, J., Yoon, Y. **Hexavalent chromium removal by various adsorbents: Powdered activated carbon, chitosan, and single/multi-walled carbon nanotubes**. *Separation and Purification Technology*, 106 (**2013**) 63–71.

131. Kaith, B. S., Dhiman, J., Bhatia, J. K. **Preparation and application of grafted Holarrhena antidycentrica fiber as cation exchanger for adsorption of dye from aqueous solution**. *Journal of Environmental Chemical Engineering*, 3 (**2015**) 1038–1046.

132. Kamal, T., Ul-Islam, M., Khan, S. B., Asiri, A. M. **Adsorption and photocatalyst assisted dye removal and bactericidal performance of ZnO/chitosan coating layer**. *International Journal of Biological Macromolecules*, 81 (**2015**) 584–590.

133. Kamar, F, H., Nechifor, A, C., Alwan, G, M., Craciun, M, E. **"Comparative removal of lead, copper and cadmium ions from wastewater in single and ternary batch biosorption systems onto dry walnut shells"**. *Revista de Chimie -Bucharest,* 66, (**2015**) 8.

134. Kan, C., Ibe, A. H., Rivera, K. K. P., Arazo, R. O., de Luna, M. G. **Hexavalent chromium removal from aqueous solution by adsorbents synthesized from groundwater treatment residuals**. *Sustainable Environment Research*, 27 (**2017**) 163-171.

135. Karim, Z., Mathew, A. P., Grahn, M., Mouzon, J., Oksman, K. **Nanoporous membranes with cellulose nanocrystals as functional entity in chitosan: Removal of dyes from water**. *Carbohydrate Polymers*, 112 (**2014**) 668–676.

136. Kariyajjanavar, P., Jogttappa, N., Nayaka, Y. A. **Studies on degradation of reactive textile dyes solution by electrochemical method**. *Journal of Hazardous Materials*, 190 (**2011**) 952–961.

137. Katal, R., Zare, H., Rastegar, S. O., Mavaddat, P., Darzi, G. N. **Removal of dye and chemical oxygen demand (COD) reduction from textile industrial wastewater using hybrid bioreactors**. *Environmental Engineering and Management Journal*, 13 (**2014**) 43-50.

138. Kaur, S., Rani, S., Mahajan, R. K., Asif, M., Gupta, V. K. **Synthesis and adsorption properties of mesoporous material for the removal of dye safranin: Kinetics, equilibrium, and thermodynamics**. *Journal of Industrial and Engineering Chemistry*, 22 (**2015**) 19–27.

139. Kettum, W., Tran, T. T. V., Kongparakul, S., Reubroycharoen, P., Guan, G., Chanlek, N., Samart, C. **Heavy metal sequestration with a boronic acid-functionalized carbon-based adsorbent**. *Journal of Environmental Chemical Engineering*, **2018**.
140. Khalfa, L, Bagane, M., Cervera, M. L., Najjar, S. **Competitive Adsorption of Heavy Metals onto Natural and Activated Clay: Equilibrium, Kinetics and Modeling**. *International Journal of Chemical and Molecular Engineering*, 10 (2016) 5.
141. Khemila, B., Merzouka, B., Chouder, A., Zidelkhirb, R., Leclerc, J., Lapicque, F. **Removal of a textile dye using photovoltaic electrocoagulation**. *Sustainable Chemistry and Pharmacy*, 7 (**2018**) 27–35.
142. Khorram, A. G., Fallah, N. **Treatment of textile dyeing factory wastewater by electrocoagulation with low sludge settling time: Optimization of operating parameters by RSM**. *Journal of Environmental Chemical Engineering*, 6 (**2018**) 635–642.
143. Kim, N., Park, M., Park, D. **A new efficient forest biowaste as biosorbent for removal of cationic heavy metals**. *Bioresource Technology*, 175 (**2015**) 629–632.
144. Kim, B. J., Im, S. S., Oh, S. G. **Investigation on the Solubilization Locus of Aniline-HCl Salt in SDS Micelles with 1H NMR Spectroscopy**. *Langmuir*, 17 (**2001**) 565-566.
145. Kirby, N., McMullan, G., Marchant, R. **Bioremediation of textile industry wastewater by white-rot fungi**. *Studies in Environmental Science*, 66 (**1997**) 711-718.
146. Kirby, N., Marchant, R., McMullan, G. **Decolourisation of synthetic textile dyes by *Phlebia tremellosa***. *FEMS Microbiology Letters*, 188 (**2000**) 93-96.
147. Kishore, P. S., Viswanathan, B., Varadarajan, T. K. **Synthesis and Characterization of Metal Nanoparticle Embedded Conducting Polymer–Polyoxometalate Composites, Nanoscale**. *Nanoscale Research Letters*, 3 (**2008**) 14–20.
148. Koner, R. R., Kumar, P. A., Chakraborty, S., Ray, M. **Synthesis of morphologically different, metal absorbing aniline-formaldehdye polymers including micron-sized sphere using simple alcohols as morphology modifier**. *Journal of Applied Polymer Science*, 110 (**2008**) 1158-1164.
149. Kong S., Kamga E. T., Fossog V., Nanseu-Njiki C.P. **Removal of Mercury(II) from aqueous solution by modified Triplochytonscleroxylon sawdust**. *Journal of Chemical and Pharmaceutical Research*, 8 (**2016**) 342-353.

150. Kong, Y., Wei, J., Wang, Z., Sun, T., Yao, C., Zhidong Chen, Z. **Heavy Metals Removal from Solution by Polyaniline/Palygorskite Composite**. *Journal of Applied Polymer Science*, 122 (**2011**) 2054–2059.

151. Konicki, W., Aleksandrzak, M., Mijowska, E. **Equilibrium, kinetic and thermodynamic studies on adsorption of cationic dyes from aqueous solutions using graphene oxide**. *Chemical Engineering Research and Design*, 123 (**2017**) 35-49.

152. Kosmulski, M. **The pH-Dependent Surface Charging and the Points of Zero Charge**. *Journal of Colloid and Interface Science*, 253 (**2002**) 77–87.

153. Krishnan, J., Kishore, A. A., Suresh, A., Madhumeetha, B., Prakash, D. G. **Effect of pH, inoculum dose and initial dye concentration on the removal of azo dye mixture under aerobic conditions**. *International Biodeterioration & Biodegradation*, 119 (**2017**) 16-27.

154. Kumar, P. A., Chakraborty, S., Ray, M. **Hexavalent chromium removal from wastewater using aniline formaldehyde condensate coated silica gel**. *Journal of Hazardous Materials*, 143 (**2007a**) 24-32.

155. Kumar, G. P., Kumar, P. A., Chakraborty, S., Ray, M. **Uptake and desorption of copper ion using functionalized polymer coated silica gel in aqueous environment**. *Separation and Purification Technology*, 57 (**2007b**) 47-56.

156. Kumar, P. A., Chakraborty, S., Ray, M. **Removal and recovery of chromium from wastewater using short chain polyaniline synthesized on jute fiber**. *Chemical Engineering Journal*, 141 (**2008**) 130-140.

157. Kumar, P. A., Chakraborty, S., Ray, M. **Adsorption behaviour of trivalent chromium on amine-based polymer aniline formaldehyde condensate**. *Chemical Engineering Journal*, 149 (**2009**) 340-347.

158. Kumar, P. S., Senthamarai, C., Durgadevi, A. **Adsorption Kinetics, Mechanism, Isotherm, and Thermodynamic Analysis of Copper Ions onto the Surface Modified Agricultural Waste**. *Environmental Progress & Sustainable Energy*, 33 (**2012**) 1.

159. Kumar, P. S., Ramalingam, S., Senthamarai, C., Niranjanaa, M., Vijayalakshmi, P., Sivanesan, S. **Adsorption of dye from aqueous solution by cashew nut shell: Studies on equilibrium isotherm, kinetics and thermodynamics of interactions**. *Desalination*, 261 (**2010**) 52–60.

160. Kumara, N. T. R. N., Hamdan, N., Petra, M. I., Tennakoon, K. U., Ekanayake, P. **Equilibrium Isotherm Studies of Adsorption of Pigments Extracted from Kuduk-kuduk (*Melastoma malabathricum L.*) Pulp onto TiO_2 Nanoparticles**. *Journal of Chemistry*, (**2014**) 1-6.
161. Kunjadia, P. D., Sanghvi, G. V., Kunjadia, A. P., Mukhopadhyay,P. N., Dave, G. S. **Role of ligninolytic enzymes of white rot fungi (Pleurotus spp.) grown with azo dyes**. *SpringerPlus*, (**2016**) 5:1487.
162. Kuo, W. G. **Decolorizing dye wastewater with Fenton's reagent**. *Water Research*, 26 (**1992**) 881-886.
163. Kusku, O., Rivas, B. L., Urbano, B. F., Arda, M., Kabay, N., Bryjak, M. **A comparative study of removal of Cr(VI) by ion exchange resins bearing quaternary ammonium groups**. *Journal of Chemical Technology and Biotechnology*, 89 (**2014**) 851-857.
164. Lee, S., Choi, H. **Persimmon leaf bio-waste for adsorptive removal of heavy metals from aqueous solution**. *Journal of Environmental Management*, 209 (**2018**) 382-392.
165. Lee, M., Hong, K., Shin-Ya, Y., Kajiuchi, T. **Adsorption of Hexavalent Chromium by Chitosan-Based Polymeric Surfactants**. *Journal of Applied Polymer Science*, 96 (**2005**) 44-50.
166. Leitner, P., Fitz-Binder, C., Mahmud-Ali, A., Bechtold, T. **Production of a concentrated natural dye from Canadian Goldenrod (Solidago canadensis) extracts**. *Dyes and Pigments*, 93 (**2012**) 1416-1421.
167. Li, F., Li, Dong, Y., Kang, W., Cheng, B., Cui, G. **Enhanced removal of azo dye using modified PAN nanofibrous membrane Fe complexes with adsorption/visible-driven photocatalysis bifunctional roles**. *Applied Surface Science*, 404 (**2017**) 206–215.
168. Li, Z., Wua, L., Huijuan, L.W., Lan, H., Qu, J. **Improvement of aqueous mercury adsorption on activated coke by thiol-functionalization**. *Chemical Engineering Journal*, 228 (**2013**) 925–934.
169. Lide, D. R. **CRC handbook of chemistry and physics**. *Boca Raton*, (**2004**), CRC Press.
170. Lin, P., Liu, C., Li, J., Qi, J., Luo, R., Sun, X., Shen, J., Han, W., Wang, L. **Nanosized amine-rich spheres embedded polymeric beads for Cr (VI) removal**. *Journal of Colloid and Interface Science*, 508 (**2017**) 369–377.

171. Lima, L. K. S., Silva, M. G. C., Vieira, M. G. A. **"Study of binary and single biosorption by the floating aquatic macrophyte salvinia natans"**. *Brazilian. Journal of Chemical Engineering*, 33 (**2015**) 649 – 660.

172. Liu, C., Cheng, L., Zhao, Y., Zhu, L. **Interfacially crosslinked composite porous membranes for ultrafast removal of anionic dyes from water through permeating adsorption**. *Journal of Hazardous Materials*, 337 (**2017**) 217–225.

173. Liu, J., Wang, Z., Li, H., Hu, C., Raymer, P., Huang, Q. **Effect of solid state fermentation of peanut shell on its dye adsorption performance**. *Bioresource Technology*, 249 (**2018**) 307–314.

174. Liu, Q., Yang, B., Zhang, L., Huang, R. **Adsorption of an anionic azo dye by cross-linked chitosan/bentonite composite**. *International Journal of Biological Macromolecules*, 72 (**2015**)1129–1135.

175. Liu, C., Cheng, L., Zhao, Y., Zhu, L. **Interfacially crosslinked composite porous membranes for ultrafast removal of anionic dyes from water through permeating adsorption**. *Journal of Hazardous Materials*, 337 (**2017**) 217–225.

176. Liu, Y., Wang, X., Wu, H. **Reusable DNA-functionalized-graphene for ultrasensitive mercury (II) detection and removal**. *Biosensors and Bioelectronics*, 87 (**2017**)129-135.

177. Long, X., Pan, Q., Wang, C., Wang, H., Li, X. **Microbial fuel cell-photoelectrocatalytic cell combined system for the removal of azo dye wastewater**. *Bioresource Technology*, 244 (**2017**) 182–191.

178. Luo, J., Li, J., Yang, Z., Liu, X. **"Removal of chromium(III) from aqueous waste solution by predispersed solvent extraction"**. *Transactions of Nonferrous Metals Society of China*, 23 (**2013**)524-529.

179. Ma, N., Yang, Y., Chen, S., Zhang, Q. **Preparation of amine group-containing chelating fiber for thorough removal of mercury ions**. *Journal of Hazardous Materials*, 171 (**2009**) 288–293.

180. Magdalena, C. P., Fungaro, D. A. **Studies on Removal of Acid Orange 8 from Aqueous Solution Using HDTMA-Modified Zeolite from Coal Bottom Ash**. *International Journal of Advanced Research in Chemical Sciences*, 1 (**2014**) 23-33.

181. Magdy, Y. H., Altaher, H. **Kinetic analysis of the adsorption of dyes from high strength wastewater on cement kiln dust**. *Journal of Environmental Chemical Engineering*, 6 (**2018**) 834-841.

182. Mahanta, D., Madras, G., Radhakrishnan, S., Satish Patil, S. **Adsorption and Desorption Kinetics of Anionic Dyes on Doped Polyaniline**. *Journal of Physical Chemistry B*, 113 (**2009**) 2293–2299.

183. Mahanta, D., Madras, G., Radhakrishnan, S., Satish Patil, S. **Adsorption and Desorption Kinetics of Anionic Dyes on Doped Polyaniline**. *Journal of Physical Chemistry B*, 113 (**2009**) 2293–2299.

184. Mallick, S. K. **Removal of anionic azo dye acid orange 8 from wastewater using short chain polyaniline synthesizes on jute fiber**. *M. Tech thesis (Indian Institute of Technology Guwahati)*, (**2013**).

185. Malekia, A., Pajootan, E., Hayati, E. B. **Ethyl acrylate grafted chitosan for heavy metal removal from wastewater: Equilibrium, kinetic and thermodynamic studies**. *Journal of the Taiwan Institute of Chemical Engineers*, 51 (**2015**) 127–134.

186. Makhoukhi, B., Djab, M., Didi, M. A. **Adsorption of Telon dyes onto bis-imidazolium modified bentonite in aqueous solutions**. *Journal of Environmental Chemical Engineering*, 3 (**2015**) 1384–1392.

187. Mahmoodi, N. M., Khorramfar, S., Najafi, F. **Amine-functionalized silica nanoparticle: Preparation, characterization and anionic dye removal ability**. *Desalination*, 279 (**2011**) 61–68.

188. Mahmoodi, N. M., Najafib, F., Khorramfar, S., Amini, F., Arami, M. **Synthesis, characterization and dye removal ability of high capacity polymeric adsorbent: Polyaminoimide homopolymer**. *Journal of Hazardous Materials*, 198 (**2011**) 87–94.

189. Mahmoodi, N. M., Masrouri, O., Najafi, F. **Dye Removal Using Polymeric Adsorbent from Wastewater Containing Mixture of Two Dyes**. *Fibers and Polymers*, 15 (**2014**) 1656-1668.

190. Mahmoodi, N. M., Najafi, F., Neshat, A. **Poly (amidoamine-co-acrylic acid) copolymer: Synthesis, characterization and dye removal ability**. *Industrial Crops and Products*, 42 (**2013**) 119–125.

191. Mahmoud, M. E., Osman, M. M., Hafez, O. F., Elmelegy, E. **"Removal and preconcentration of lead (II), copper (II), chromium (III) and iron (III) from**

wastewaters by surface developed alumina adsorbents with immobilized 1-nitroso-2-naphthol". *Journal of Hazardous Materials*, 173 (**2010**) 349-357.

192. Majumdar, S. S., Das, S. K., Saha, T., Panda, G. C., Tarashankar Bandyopadhyoy, T., Guha, A. K. **Adsorption behavior of copper ions on *Mucor rouxii* biomass through microscopic and FTIR analysis**. *Colloids and Surfaces B: Biointerfaces*, 63 (**2008**) 138–145.
193. Maleki, A., Pajootan, E., Hayati, B. **Ethyl acrylate grafted chitosan for heavy metal removal from wastewater: Equilibrium, kinetic and thermodynamic studies**. *Journal of the Taiwan Institute of Chemical Engineers*, 51 (**2015**) 127–134.
194. Malinauskiene, L., Bruze, M., Ryberg, K., Zimerson, E., Isaksson, M. **Contact allergy from disperse dyes in textiles–a review**. *Contact Dermatitis*, 68 (**2012**) 65–75.
195. Mansourpanah, Y., Samimi, M. **Preparation and characterization of a low-pressure efficient polyamide multi-layer membrane for water treatment and dye removal**. *Journal of Industrial and Engineering Chemistry*, 53 (**2017**) 93–104.
196. Merlini, C., Barra, G. M. O., Schmitz, D. P., Ramôa, S. D. A. S., Silveira, A., Araujo, A. M., Pegoretti, A. **Polyaniline-coated coconut fibers: Structure, properties and their use as conductive additives in matrix of polyurethane derived from castor oil**. *Polymer Testing*, 38 (**2014**) 18-25.
197. Metcalf & Eddy. **Wastewater Engineering: Treatment and Reuse**. *4th Edition, McGraw-Hill, New York*, (**2003**).
198. Mezohegyi, G., van der Zee FP, Font, J., Fortuny, A., Fabregat, A. **Towards advanced aqueous dye removal processes: a short review on the versatile role of activated carbon**. *Journal of Environmental Management*, 102 (**2012**) 148-164.
199. Mishra, A., Kumar, S., Pandey, A. K. **Laccase production and simultaneous decolorization of synthetic dyes in unique inexpensive medium by new isolates of white rot fungus**. *International Biodeterioration & Biodegradation*, 65 (**2011**) 487-493.
200. Mohan, D., Singh, K. P. **Single- and multi-component adsorption of cadmium and zinc using activated carbon derived from bagasse an agricultural waste**. *Water Research*, 36 (**2002**) 2304-2318.
201. Mongkholrattanasit, R., Kryšt fek, J., Wiener, J. **Dyeing and Fastness Properties of Natural Dyes Extracted from Eucalyptus Leaves Using Padding Techniques**. *Fibers and Polymers*, 11 (**2010**) 346-350.

202. Mongkholrattanasit, R., Klaichoi, C., Rungruangkitkrai, N., Punrattanasin, N., Sriharuksa, K., Nakpathom, M. **Dyeing Studies with Eucalyptus, Quercetin, Rutin, and Tannin: A Research on Effect of Ferrous Sulfate Mordant**. *Journal of Textiles*, 2013 (**2013**) 1-7.
203. Moussavi, G., Mahmoudi, M. **Removal of azo and anthraquinone reactive dyes from industrial wastewaters using MgO nanoparticles**. *Journal of Hazardous Materials*, 168 (**2009**) 806-812.
204. Moyib, O. K., Ayedun, M. A., Awokoya, O. J. Omotola, O. E. **Waste printing paper as analogous adsorbents for heavy metals in aqueous solution**. *Nigerian Journal of Chemical Research*, 22 (**2017**) 1.
205. Mullai, P., Yogeswari, M. K., Vishali, S., Namboodiri, M. M. T., Gebrewold, B. D., Rene, E. R., Pakshirajan, K. **Aerobic Treatment of Effluents From Textile Industry**. *Biological Treatment of Industrial Effluents*, (**2017**) 3–34.
206. Munagapati, V. S., Kim, D. **Equilibrium isotherms, kinetics, and thermodynamics studies for congo red adsorption using calcium alginate beads impregnated with nano-goethite**. *Ecotoxicology and Environmental Safety*, 141 (**2017**) 226–234.
207. Munagapati, V. S., Yarramuthi, V., Kim, Y., Leea, K. M., Kim, D. **Removal of anionic dyes (Reactive Black 5 and Congo Red) from aqueous solutions using Banana Peel Powder as an adsorbent**. *Ecotoxicology and Environmental Safety*, 148 (**2018**) 601–607.
208. Muthukumar, M., Sargunamani, D., Selvakumar, N., Rao, J. V. **Optimisation of ozone treatment for colour and COD removal of acid dye effluent using central composite design experiment**. *Dyes and Pigments*, 63 (**2004**) 127–134.
209. Namieśnik, J., Rabajczyk, A. **The speciation and physico-chemical forms of metals in surface waters and sediments**. *Chemical Speciation and Bioavailability*, 22 (**2010**) 1.
210. Naraghi, B., Zabihi, F., Narooie, M. R., Saeidi, M., Biglari, H. **Removal of Acid Orange 7 dye from aqueous solutions by adsorption onto Kenya tea pulps; granulated shape**. *Electronic Physician*, 9 (**2017**) 4312-432.
211. Naz, S., Bhatti, I. A. **Dyeing properties of cotton fabric using un-irradiated and gamma irradiated extracts of *Eucalyptus camaldulensis* bark powder**. *Indian Journal of Fibre &Textile Research*, 36 (**2011**) 132-136.

212. Negin, G. **"A new approach to copper ion removal from water by polymeric nanocomposite membrane embedded with γ-alumina nanoparticles"**. *Applied Surface Science*, 364 (**2016**) 221–228.

213. Nethaji, S., Sivasamy, A., Mandal, A. B. **Adsorption isotherms, kinetics and mechanism for the adsorption of cationic and anionic dyes onto carbonaceous particles prepared from *Juglans regia* shell biomass**. *International Journal of Environmental Science & Technology*, 10 (**2013**) 231–242.

214. Ng, K. C., Burhan, M., Shahzad, M. W., Ismail, A. B. **A Universal Isotherm Model to Capture Adsorption Uptake and Energy Distribution of Porous Heterogeneous Surface**. *Scientific Reports*, 7 (**2017**) 10634.

215. Nidheesh, P. V., Zhou, M., Oturan, M. A. **An overview on the removal of synthetic dyes from water by electrochemical advanced oxidation processes**. *Chemosphere*, 197 (**2018**) 210-227.

216. Nouri, R., Tahmasebi, E., Morsali, A. **Capability of magnetic functional metal-organic nanocapsules for removal of mercury(II) ions**. *Materials Chemistry and Physics*, 198 (**2017**) 310-316.

217. Ofomaja, A. E., Ho, Y. **Equilibrium sorption of anionic dye from aqueous solution by palm kernel fibre as sorbent**. *Dyes and Pigments*, 74 (**2007**) 60-66.

218. Ojha, J. K., Reddy, B. V., Rao, G. R. **Vibrational analysis and valence force field for nitrotoluenes, dimethylanilines and some substituted methylbenzenes**. *Spectrochimica Acta Part A: Molecular and Biomolecular Spectroscopy*, 96 (**2012**) 632-643.

219. Olivo-Alanis, D., Garcia-Reyes, R. B., Alvarez, L. H., Garcia-Gonzalez, A. **Mechanism of anaerobic bio-reduction of azo dye assisted with lawsone-immobilized activated carbon**. *Journal of Hazardous Materials*, 347 (**2018**) 423–430.

220. Pakade. V, Chimka. L. **Polymeric sorbents for removal of Cr(VI) from environmental samples**. *Pure Applied Chemistry*, 85 (**2013**) 2145–2160.

221. Pajootan, E., Arami, M., Mahmoodi, N. M. **Binary system dye removal by electrocoagulation from synthetic and real colored wastewaters**. *Journal of the Taiwan Institute of Chemical Engineers*, 43 (**2012**) 282–290.

222. Panda, H., Tiadi, N., Mohanty, M., Mohanty, C. R. **"Studies on adsorption behavior of an industrial waste for removal of chromium from aqueous solution".** *South African Journal of Chemical Engineering*, 23 (**2017**) 132-138.

223. Pelegrini, R., Peralto-Zamora, P., de Andrade, A. R., Reyers, J., Duran, N. **Electrochemically assisted photocatalytic degradation of reactive dyes**. *Applied Catalysis B: Environmental*, 22 (**1999**) 83–90.

224. Peng, L., Liu, P., Feng, X., Wang, Z., Cheng, T., Liang, Y., Lin, Z., Shi, Z. **Kinetics of heavy metal adsorption and desorption in soil: Developing a unified model based on chemical speciation**. *Geochimica et Cosmochimica Acta*, 224 (**2018**) 282–300.

225. Peralta-Zamora, P., Kunz, A., de Moraes, S. G., Pelegrini, R., Molelro, R, d., Reyes, J., Duran, N. **Degradation of reactive dyes I. A comparative study of ozonation, enzymatic and photochemical processes**. *Chemosphere*, 38 (**1999**) 835-852.

226. Pereira, F. A. R., Sousa, Cavalcanti, G. R. S., França, D. B., Queiroga, L. N. F., Santos, I. M. G., Fonseca, M. G., Jaber, M. **Green biosorbents based on chitosan-montmorillonite beads for anionic dye removal**. *Journal of Environmental Chemical Engineering*, 5 (**2017**) 3309–3318.

227. Pirkarami, A., Olya, M. E. **Removal of dye from industrial wastewater with an emphasis on improving economic efficiency and degradation mechanism**. *Journal of Saudi Chemical Society*, 21 (**2017**) S179–S186.

228. Przystaś, W., Zabłocka-Godlewska, E., Grabińska-Sota, E. **Efficiency of decolorization of different dyes using fungal biomass immobilized on different solid supports**. *Brazilian Journal of Microbiology*, 49 (**2018**) 285-295.

229. Puspasari, T., Peinemann, K. **Application of thin film cellulose composite membrane for dye wastewater reuse.** *Journal of Water Process Engineering*, 13 (**2016**) 176–182.

230. Qing-Zhou Zhai. **Nano α-Al2O3 for removal of Hg(II) from water: Adsorption and desorption studies**. *Journal of Chemical and Pharmaceutical Research*, 6 (**2014**) 1310-1317.

231. Qureshi, U. A., Khatri, Z., Ahmed, F., Ibupoto, A. S., Khatri, M., Mahar, F. K., Brohi, R. Z., Kim, I. S. **Highly efficient and robust electrospun nanofibers for selective removal of acid dye**. *Journal of Molecular Liquids*, 244 (**2017**) 478–488.

232. Qureshi, U. A., Khatri, Z., Ahmed, F., Ibupoto, A. S., Khatri, M., Mahar, F. K., Brohi, R. Z., Kim, I. S. **Highly efficient and robust electrospun nanofibers for selective removal of acid dye**. *Journal of Molecular Liquids*, 244 (**2017**) 478–488.

233. Racho, P., Phalathip, P. **Modified Nylon Fibers with Amino Chelating Groups for Heavy Metal Removal**. *Energy Procedia*, 118 (**2017**) 195–200.

234. Rafatullaha, M., Sulaimana, O., Hashima, R., Ahmad, A. **"Adsorption of copper (II), chromium (III), nickel (II) and lead (II) ions from aqueous solutions by meranti sawdust".** *Journal of Hazardous Materials*, 170 **(2009)** 969–977.

235. Rahmani, Z., Kermani, M., Gholami, M., Jafari, A. J., Mahmoodi, N. M. **Effectiveness of photochemical and sonochemical processes in degradation of Basic Violet 16 (BV16) dye from aqueous solutions**. *Iranian Journal of Environmental Health Sciences & Engineering*, (**2012**) 9:14.

236. Rai, H, S., Bhattacharyya, M, S., Singh, J., Bansal, T. K., Vats, P., Banerjee, U. C. **Removal of Dyes from the Effluent of Textile and Dyestuff Manufacturing Industry: A Review of Emerging Techniques With Reference to Biological Treatment**. *Critical Reviews in Environmental Science and Technology*, 35 (**2005**) 219–238.

237. Rani, K. S., Srinivas, B., Naidu, K. G., Ramesh, K. V. **Removal of copper by adsorption on treated laterite**. *Materials Today: Proceedings*, 5 (**2018**) 463–469.

238. Raval, N. P., Shah, P. U., Shah, N. K. **Adsorptive removal of nickel(II) ions from aqueous environment: A review**. *Journal of Environmental Management*, 179 (**2016**) 1-20.

239. Rearte, T, A., Bozzano, P, B., Andrade, M, L., de Iorio, A, F. **"Biosorption of Cr(III) and Pb(II) by *Schoenoplectus californicus* and Insights into the Binding Mechanism"**. *ISRN Chemical Engineering*, (**2013**) Article ID 851602.

240. Reddy, T. V., Chauhan, S., Chakraborty, S. **Adsorption isotherm and kinetics analysis of hexavalent chromium and mercury on mustard oil cake**. *Environmental Engineering Research*, 22 (**2017**) 95-107.

241. Reddy, M. C. S., Sivaramakrishna, L., Reddy, A. V. **The use of an agricultural waste material, Jujuba seeds for the removal of anionic dye (Congo red) from aqueous medium**. *Journal of Hazardous Materials*, 203–204 (**2012**) 118-127.

242. Rehman, S., Khan, A. R., Sahiner, M., Sengel, S. B., Aktas, N., Siddiq, M., Sahiner, N. **Removal of arsenate and dichromate ions from different aqueous media by amine based p(TAEA-co-GDE) microgels**. *Journal of Environmental Management*, 197 (**2017**) 631-641.

243. Rahman Bhuiyan, M. A., Mizanur Rahman, M., Shaid, A., Khan, M. A. **Decolorization of textile wastewater by gamma irradiation and its reuse in dyeing process**. *Desalination and Water Treatment*, 54 (**2015**) 2848–2855.

244. Reichenberg, D. **Properties of ion-exchange resins in relation to their structure. III, Kinetics of exchange**. *Journal of American Chemical Society*, 75 (**1953**) 589–597.

245. Roy, A., Bhattacharya, J. **"A binary and ternary adsorption study of wastewater Cd(II), Ni(II) and Co(II) by γ-Fe_2O_3 nanotubes".** *Separation and Purification Technology***,** 115 (**2013)** 172-179.

246. Sadeek, S. A., Negm, N. A., Hefni, H. H. H., Wahab, M. M. A. **Metal adsorption by agricultural biosorbents: Adsorption isotherm, kinetic and biosorbents chemical structures**. *International Journal of Biological Macromolecules*, 81 (**2015**) 400–409.

247. Sag, Y., Aktay, Y. **Mass transfer and equilibrium studies for the sorption of chromium ions onto chitin**. *Process Biochem*, 36 (**2000**) 157-173.

248. Saha, T. K., Karmaker, S., Ichikawa, H., Fukumori, Y. **Mechanism and kinetics of trisodium 2-hydroxy-1,1′-azonaphthalene-3,4′,6-trisulfonate adsorption onto chitosan**. *Journal of Colloid Interface and Science*, 286 (**2005**) 433–439.

249. Salam, H. M., Zaki, T. **Removal of hazardous cationic organic dyes from water using nickelbased metal-organic frameworks**. *Inorganica Chimica Acta*, 471 (**2018**) 203–210.

250. Salarirad, M. M., Behnamfard, A. **Modeling of equilibrium data for free cyanide adsorption onto activated carbon by linear and non-linear regression methods**. *2011 International Conference on Environment and Industrial Innovation IPCBEE*, 12 (**2011**).

251. Salleh, M. A. M., Mahmoud, D. K., Karim, W. A. W. A., Idris, A. **Cationic and anionic dye adsorption by agricultural solid wastes: A comprehensive review**. *Desalination*, 280 (**2011**) 1–13.

252. Salman, J. M., Amrin, A. R., Hassan, F. M., Jouda, S. A. **Removal of congo red dye from aqueous solution by using natural materials**. *Mesopotamia Environmental Journal*, 1 (**2015**) 82-89.

253. Salzano de Luna, M., Castaldo, R., Altobelli, R., Gioiella, L., Filippone, G., Gentile, G., Ambrogi, V. **Chitosan hydrogels embedding hyper-crosslinked polymer particles as reusable broad-spectrum adsorbents for dye removal**. *Carbohydrate Polymers*, 177 (**2017**) 347–354.

254. Samadi, N., Ansari, R., Khodavirdilo, B. **"Removal of Copper ions from aqueous solutions using polymer derivations of poly (styrene-alt-maleic anhydride)"**. *Egyptian Journal of Petroleum*, 26 (**2017**) 375–389.

255. Sangu V., Kannan V., Srinivasan K. **Removal of mercury(II) ion from aqueous solution using a synthetic terpolymer**. *Indian Journal of Chemical Technology*, 22 (**2014**) 219-226.

256. Sani, A. H., Ahmad, B., Hussein, M. Z., Ibrahim, N.A., Saleh, T. **"Nanocomposite of ZnO with montmorillonite for removal of lead and copper ions from aqueous solutions".** *Process Safety and Environmental Protection*, 109 (**2017**) 97-105.

257. Saritha E, Anand R, Suja S, Uma Devi P., Swaminathan K. **Bio adsorption of mercury using *Aspergillus niger***. *Asian Journal of Environmental Science*, 3 (**2009**) 111-116.

258. Sarkar, C., Basu, J. K., Samanta, A. N. **Synthesis of mesoporous geopolymeric powder from LD slag as superior adsorbent for Zinc (II) removal**. *Advanced Powder Technology*, (**2018**).

259. Saruchi, Kumar, V. **Adsorption kinetics and isotherms for the removal of rhodamine B dye and Pb^{+2} ions from aqueous solutions by a hybrid ion-exchanger**. *Arabian Journal of Chemistry*, (**2016**).

260. Sarvajitha, M., Reddy, G. K. K., Nancharaiah, Y. V. **Textile dye biodecolourization and ammonium removal over nitrite in aerobic granular sludge sequencing batch reactors**. *Journal of Hazardous Materials*, 342 (**2018**) 536–543.

261. Sedman, R. M., Beaumont, J., Mcdonald, T. A., Reynolds, S., Krowech, G., Howd, R. **Review of the evidence regarding the carcinogenicity of hexavalent chromium in drinking water**. *Journal of Environmental Science and Health Part C*, 24 (**2016**) 155-182.

262. Seow, T. W., Lim, C. K. **Removal of Dye by Adsorption: A Review**. *International Journal of Applied Engineering Research*, 11 (**2016**) 2675-2679.

263. Sepehra, M. N., Amrane, A., Karimainian, K. A., Zarrabi, M., Ghaffari, R. **Potential of waste pumice and surface modified pumice for hexavalent chromium removal:**

Characterization, equilibrium, thermodynamic and kinetic study. *Journal of the Taiwan Institute of Chemical Engineers*, 45 (**2014**) 635-647.

264. Sham, A. Y. W., Notley, S. M. **Adsorption of organic dyes from aqueous solutions using surfactant exfoliated graphene**. *Journal of Environmental Chemical Engineering*, 6 (**2018**) 495–504.
265. Sharma, V., Rekha, P., Mohanty, P. **Nanoporous hypercrosslinked polyaniline: An efficient adsorbent for the adsorptive removal of cationic and anionic dyes**. *Journal of Molecular Liquids*, 222 (**2016**) 1091–1100.
266. Sharma, V., Rekha, P., Mohanty, P. **Nanoporous hypercrosslinked polyaniline: An efficient adsorbent for the adsorptive removal of cationic and anionic dyes**. *Journal of Molecular Liquids*, 222 (**2016**) 1091–1100.
267. Shahid-ul-Islam, Mohammad, F. **Recent advancements in natural dye applications: a review**. *Journal of Cleaner Production*, 53 (**2013**) 310-331.
268. Shawaqfah, M., Al Momanib, F. A., Al-Anber, Z. A. **Ozone treatment of aqueous solutions containing commercial dyes**. *Afinidad –Barcelona*, 69 (**2012**) 229-234.
269. Shen, B., Tian, L., Fukuan, Li., Zhang, X., Xu, H., Singh, S. **Elemental mercury removal by the modified bio-char from waste tea**. *Fuel*, 187 (**2017**) 189-196.
270. Singh, S., Lien Lo, S. L., Srivastava, V. C., Hiwarkar, A. D. **Comparative study of electrochemical oxidation for dye degradation: Parametric optimization and mechanism identification**. *Journal of Environmental Chemical Engineering*, 4 (**2016**) 2911–2921.
271. Sing, K. S. W., Everett, D. H., Haul, R. A. W., Moscou, L., Pierotti, R. A., Rouquerol, J., Siemieniewska, T. **REPORTING PHYSISORPTION DATA FOR GAS/SOLID SYSTEMS with Special Reference to the Determination of Surface Area and Porosity**. *International Union Of Pure And Applied Chemistry*, 57 (**1985**) 603—619.
272. Sinha, K., Saha, P. D., Datta, S. **Extraction of natural dye from petals of Flame of forest (Butea monosperma) flower: Process optimization using response surface methodology (RSM)**. *Dyes and Pigments*, 94 (**2012**) 212-216.
273. Slokar, Y. M., Le Marechal, A. M. **Methods of Decoloration of Textile Wastewaters**. *Dyes and Pigments*, 37 (**1998**) 335-356.
274. Soares, P. A., Souza, R., Soler, J., Silva, T. F. C. V., Souza, S. M. A. G. U., Boaventura, R. A. R., Vilar, V. J. P. **Remediation of a synthetic textile wastewater from polyester-cotton**

dyeing combining biological and photochemical oxidation processes. *Separation and Purification Technology*, 172 (**2017**) 450–462.

275. Sohrabi, M. R., Khavaran, A., Shariati, S., Shariati, S. **Removal of Carmoisine edible dye by Fenton and photo Fenton processes using Taguchi orthogonal array design**. *Arabian Journal of Chemistry*, 10 (**2017**) S3523–S3531.
276. Somayajula. A., AzrinaAbd Aziz. S., Saravanan. P., Matheswaran. M. **Adsorption of mercury (II) ion from aqueous solution using low-cost activated carbon prepared from mango kernel**. *Asia-Pacific Journal of Chemical Engineering*, (**2012**).
277. Son, G., Kim, D., Lee, J. S., Kim, H., Lee, C., Kim, S., Lee, H. **Synchronized methylene blue removal using Fenton-like reaction induced by phosphorous oxoanion and submerged plasma irradiation process**. *Journal of Environmental Management*, 206 (**2018**) 77-84.
278. Srenscek-Nazzal, J., Narkiewicz, U., A. W., Wrobel, R. J., Michalkiewicz, B. **Comparison of Optimized Isotherm Models and Error Functions for Carbon Dioxide Adsorption on Activated Carbon**. *Journal of Chemical and Engineering Data*, 60 (**2015**) 3148−3158.
279. Srihari, V., Babu, S. M., Das, A. **Kinetics of Phenol-sorption by Raw Agro-wastes**. *Journal of Applied Sciences*, 6 (**2005**) 47-50.
280. Srivastava, N. K., Majumder, C. B. **Novel biofiltration methods for the treatment of heavy metals from industrial wastewater**. *Journal of Hazardous Materials*, 151 (**2008**) 1–8.
281. Subramani S.E., Thinakaran N. **Isotherm, kinetic and thermodynamic studies on the adsorption behaviour of textile dyes onto chitosan**. *Process Safety and Environmental Protection*, 106 (**2017**) 1-10.
282. Sumithra, S., Arivoli, S., Hema, M. **Kinetics, thermodynamics and isotherm analysis on the removal of Cr(VI) ion onto PONC**. *World Journal of Pharmacy and Pharmaceutical Sciences*, 6 (**2018**) 483-503.
283. Sun, J., Wu, L., Li, Yunhua. **"Removal of lead ions from polyether sulfone/Pb(II)-imprinted multi-walled carbon nanotubes mixed matrix membrane".** *Journal of the Taiwan Institute of Chemical Engineers*, 78 (**2017**) 219–229.
284. Tahar, L. B., Oueslati, M. H., Abualreish, M. J. A. **Synthesis of magnetite derivatives nanoparticles and their application for the removal of chromium (VI) from aqueous solutions**. *Journal of Colloid and Interface Science*, 512 (**2018**) 115–126.

285. Taher, T., Rohendi, D., Mohadi, R., Lesbani, A. **Kinetic and Thermodynamic Adsorption Studies of Congo Red On Bentonite**. *International Conference on Chemistry, Chemical Process and Engineering (IC3PE)* (**2017**).

286. Tavakoli, O., Goodarzi, V., Saeb, M. R., Mahmoodi, N. M., Borja, R. **Competitive removal of heavy metal ions from squid oil under isothermal condition by CR11 chelate ion exchanger**. *Journal of Hazardous Materials*, 334 (**2017**) 256–266.

287. Terangpi, P., Chakraborty, S**. Adsorption kinetics and equilibrium studies for removal of acid azo dyes by aniline formaldehyde condensate**. *Applied Water Science*, 7 **(2018)** 3661-3671.

288. Thasilu, K., Karthikeyan, J. **Removal of color and COD from C. I. Acid Red 52 aqueous solution by NaOCl and H_2O_2 oxidation processes**. *International Journal of Civil Engineering and Technology*, 7 (**2016**) 47-59.

289. Thommes, M. **Physical adsorption characterization of nanoporous materials**. *Chemie Ingenieur Technik*, 82 (**2010**) 1059-1073.

290. Tran, T., Chiu, K., Lin, C., Leu, H. **Electrochemical treatment of wastewater: Selectivity of the heavy metals removal process**. *International Journal of hydrogen energy*, 42 (**2017**) 27741-27748.

291. Umukoro, E. H., Madyibi, S. S., Peleyeju, M. G., Tshwenya, L., Viljoen, E. H., Ngila, J. C., Arotiba, O. A. **Photocatalytic application of Pd-ZnO-exfoliated graphite nanocomposite for the enhanced removal of acid orange 7 dye in water**. *Solid State Sciences*, 74 (**2017**) 118-124.

292. Velmurugan, P., Shim, J., Oh, B. **Removal of anionic dye using amine-functionalized mesoporous hollow shells prepared from corn cob silica**. *Res Chem Intermed*, 42 (**2016**) 5937–5950.

293. Venkatesh, S., Venkatesh, K., Quaff, A. R. **Dye decomposition by combined ozonation and anaerobic treatment: Cost effective technology**. *Journal of Applied Research and Technology*, 15 (**2017**) 340–345.

294. Verma V. K, Tripathi I. N. **Kinetic study on the removal of mercury by fly ash**. *Global NEST Journal*, 16 (**2014**) 385-392.

295. Vieira, M. G. A., Neto, A. F. A., Gimenes, M. L., da Silva, M. G. C. **Removal of nickel on Bofe bentonite calcined clay in porous bed**. *Journal of Hazardous Materials*, 176 (**2010**) 109–118.

296. Volesky, B. **Advances in biosorption of metals: Selection of biomass types**. *FEMS Microbiology Reviews*, 14 (**1994**) 291-302.

297. von Burg, R., Liu, D. **Chromium and hexavalent chromium**. *Journal of Applied Toxicology*, 13 (**1993**) 225-230.

298. Vunain, E., Mishra, A. K., Mamba, B. B. **Dendrimers, mesoporous silicas and chitosan-based nanosorbents for the removal of heavy-metal ions: A review**. *International Journal of Biological Macromolecules*, 86 (**2016**) 570–586.

299. Wang, W., Huang, G., An, C., Zhang, P. **Adsorption of Anionic Azo Dyes from Aqueous Solution on Cationic Gemini Surfactant-Modified Flax Shives: Synchrotron Infrared, Optimization and Modeling Studies**. *Journal of Cleaner Production*, 172 (**2017**)1986-1997.

300. Wang, Y., Xie, Y., Zhang, Y., Tang, S., Guo, C., Wu, J., Lau, R. **Anionic and cationic dyes adsorption on porous poly-melamine-formaldehyde polymer**. *Chemical Engineering Research and Design*, 114 (**2016**) 258-267.

301. Wang, H., Li, Q., He, N., Wang, Y., Sun, D., Shao, W., Yang, K., Lu, Y. **Removal of anthraquinone reactive dye from wastewater by batch hydrolytic–aerobic recycling process**. *Separation and Purification Technology*, 67 (**2009**) 180–186.

302. Wang, J., Qin, L., Lin, J., Zhu, J., Zhang, Y., Liu, J., Bruggen, B. V. **Enzymatic construction of antibacterial ultrathin membranes for dyes removal**. *Chemical Engineering Journal*, 323 (**2017**) 56–63.

303. Wang, J., Zheng, S., Shao, Y., Liu, J., Xu, Z., Zhu, D. **Amino-functionalized Fe_3O_4@SiO_2 core–shell magnetic nanomaterial as a novel adsorbent for aqueous heavy metals removal**. *Journal of Colloid and Interface Science*, 349 (**2010**) 293–299.

304. Wang, D., Sun, W., Xu, Y., Tang, H., Gregory, J. **Speciation stability of inorganic polymer flocculant–PACl**. *Colloids and Surfaces A: Physicochemical and Engineering Aspects*, 243 (**2004**) 1–10.

305. Wang, Y., Feng, Y., Zhang, X., Zhang, X., Jiang, J., Yao, J. **Alginate-based attapulgite foams as efficient and recyclable adsorbents for the removal of heavy metals**. *Journal of Colloid and Interface Science*, 514 (**2018**) 190–198.

306. Wahyuni, E. T., Aprilita, N. H., Hatimah, H., Wulandari, A. M., Mudasir, M. **Removal of Toxic Metal Ions in Water by Photocatalytic Method**. *American Chemical Science Journal*, 5 (**201**5) 194-201.

307. Wasti, A., Awan, M. A. **Adsorption of textile dye onto modified immobilized activated alumina**. *Journal of the Association of Arab Universities for Basic and Applied Sciences*, 20 (**2016**) 26–31.

308. Wawrzkiewicza, M., Bartczak, P., Teofil Jesionowski, T. **Enhanced removal of hazardous dye form aqueous solutions and realtextile wastewater using bifunctional chitin/lignin biosorbent**. *International Journal of Biological Macromolecules*, 99 (**2017**) 754–764.

309. Wei, M., Wang, K., Huang, C., Chiang, C., Chang, T., Lee, S., Chang, S. **Improvement of textile dye removal by electrocoagulation with low-cost steel wool cathode reactor**. *Chemical Engineering Journal*, 192 (**2012**) 37–44.

310. **WHO**, **Guidelines for Drinking-Water Quality**. *World Health Organization*, *Geneva* (**2004**).

311. Wijannarong, S., Aroonsrimorakot, S., Thavipoke, P., Acharaporn Kumsopa, A., Sangjan, S. **Removal of Reactive Dyes from Textile Dyeing Industrial Effluent by Ozonation Process**. *APCBEE Procedia*, 5 (**2013**) 279 – 282.

312. Wu, S., Dai, X., Kan, J., Shilong, F., Zhu, M. **Fabrication of carboxymethyl chitosan–hemicellulose resin for adsorptive removal of heavy metals from wastewater**. *Chinese Chemical Letters*, 28 (**2017**) 625–632.

313. Xiao, X., Li, T., Lu, X., Feng, X., Han, X., Li, W., Li, Q., Yu, H. **A simple method for assaying anaerobic biodegradation of dyes**. *Bioresource Technology*, 251 (**2018**) 204–209.

314. Xu, X., Gao, B., Tan, X., Yue, Q., Zhong, Q., Li, Q. **Characteristics of amine-crosslinked wheat straw and its adsorption mechanisms for phosphate and chromium (VI) removal from aqueous solution**. *Carbohydrate Polymers*, 84 (**2011**) 1054–1060.

315. Xu, Z., Li, W., Xiong, Z., Fang, J., Li, Y., Wang, Q., Zeng, Q. **Removal of anionic dyes from aqueous solution by adsorption onto amino-functionalized magnetic nanoadsorbent**. *Desalination and Water Treatment*, 57 (**2016**) 7054–7065.

316. Xu, L., Cao, G., Xu, X., Liu, S., Duan, Z., He, C., Wang, Y., Huang, Q. **Simultaneous removal of cadmium, zinc and manganese using electrocoagulation: Influence of**

operating parameters and electrolyte nature. *Journal of Environmental Management*, 204 (**2017**) 394-403.

317. Xu, Z., Li, W., Xiong, Z., Fang, J., Li, Y., Wanga, Q., Zeng, Q. **Removal of anionic dyes from aqueous solution by adsorption onto amino-functionalized magnetic nanoadsorbent**. *Desalination and Water Treatment*, 57 (**2016**) 7054–7065.
318. Ya, V., Martina, N., Chou, Y., Chen, Y., Choo, K., Chen, S., Li, C. **Electrochemical treatment for simultaneous removal of heavy metals and organics from surface finishing wastewater using sacrificial iron anode**. *Journal of the Taiwan Institute of Chemical Engineers*, 83 (**2018**) 107–114.
319. Yagub, M. T., Sen, T., Afroze, S., Ang, H. M. **Dye and its removal from aqueous solution by adsorption: a review**. *Advances in Colloid and Interface Science*, 209 (**2014**) 172–184.
320. Yang, H., Feng, Q. **Characterization of pore-expanded amino-functionalized mesoporous silicas directly synthesized with dimethyldecylamine and its application for decolorization of sulphonated azo dyes**. *Journal of Hazardous Materials*, 180 (**2010**) 106–114.
321. Yao, W., Wang, J., Wang, P., Wang, X., Yu, S., Zou, Y., Hou, J., Hayat, T., Alsaedi, A., Wang, X. **Synergistic coagulation of GO and secondary adsorption of heavy metal ions on Ca/Al layered double hydroxides**. *Environmental Pollution*, 229 (**2017**) 827-836.
322. Yi, Y., Lv, J., Liu, Y., Wu, G. **Synthesis and application of modified Litchi peel for removal of hexavalent chromium from aqueous solutions**. *Journal of Molecular Liquids*, 225 (**2017**) 28.
323. Yin, H., He, B., Peng, H., Ye, J., Yang, F., Zhang, N. **Removal of Cr(VI) and Ni(II) from aqueous solution by fused yeast: Study of cations release and biosorption mechanism**. *Journal of Hazardous Materials*, 158 (**2008**) 568–576.
324. Yoo, J., Lee, C., Lee, J., Baek, K. **Simultaneous application of chemical oxidation and extraction processes is effective at remediating soil Co-contaminated with petroleum and heavy metals**. *Journal of Environmental Management*, 186 (**2017**) 314-319.
325. Yousef, N. S., Farouq, R., Hazzaa, R. **Adsorption kinetics and isotherms for the removal of nickel ions from aqueous solutions by an ion-exchange resin: application of two and three isotherm models**. *Desalination and Water Treatment*, 57 (**2016**) 21925–21938.

326. Yu, J., Yue, B., Wu, X., Liu, Q., Jiao, F., Jiang, X., Chen, X. **Removal of mercury by adsorption: a review**. *Environmental Science and Pollution Research*, 23 (**2016**) 5056–5076.

327. Zanina, E., Scapinello, J., de Oliveira, M., Rambo, C. L., Franscescon, F., Freitas, L., de Mello, J. M. M., Fiori, M. A., Oliveira, J. V., Magro, J. D. **Adsorption of heavy metals from wastewater graphic industry using clinoptilolite zeolite as adsorbent**. *Process Safety and Environmental Protection*, 105 (**2017**) 194-200.

328. Zhang, X., Song, L., Zeng, X., Li, M. **Effects of Electron Donors on the TiO2 Photocatalytic Reduction of Heavy Metal Ions under Visible Light**. *Energy Procedia*, 17 (**2012**) 422 – 428.

329. Zhang, J., Yan, X., Hu, M., Hu, X., Zhou, M. **Adsorption of Congo red fromaqueous solution using ZnO-modified SiO_2 nanospheres with rough surfaces**. *Journal of Molecular Liquids*, 249 (**2018**) 772–778.

330. Zhang, X., Huang, Q., Liu, M., Tian, J., Zeng, G., Zhen Li, Z., Wang, K., Zhang, Q., Wan, Q., Denga, F., We, Y. **Preparation of amine functionalized carbon nanotubes via a bioinspired strategy and their application in Cu^{2+} removal**. *Applied Surface Science*, 343 (**2015**) 19–27.

331. Zhao, Y., Chen, Y., Zhao, J., Tong, Z., Jin, S. **Preparation of SA-g-(PAA-co-PDMC) polyampholytic superabsorbent polymer and its application to the anionic dye adsorption removal from effluents**. *Separation and Purification Technology*, 188 (**2017**) 329–340.

332. Zhi-rong, L., Shao-qi, Z. **"Adsorption of copper and nickel on Na-bentonite".** *Pro*cess *Safety and Environmental Protection*, 88 (**2010**) 62-66.

333. Zhou, S., Wang, J., Gan, L., Han, X., Fan, H., Mei, L., Huang, J., Liu, Y. **Individual and simultaneous electrochemical detection toward heavy metal ions based on L-cysteine modified mesoporous $MnFe_2O_4$ nanocrystal clusters**. *Journal of Alloys and Compounds*, 721 (**2017**) 492-500.

334. Zhu, J., Yang, J., Deng, B. **Enhanced mercury ion adsorption by amine-modified activated carbon**. *Journal of Hazardous Materials*, 166 (**2009**) 866–872.

335. Zuorro, A., Maffei, G., Lavecchia, R. **Kinetic modeling of azo dye adsorption on non-living cells of *Nannochloropsis oceanica***. *Journal of Environmental Chemical Engineering*, 5 (**2017**) 4121–4127.

Appendix 1

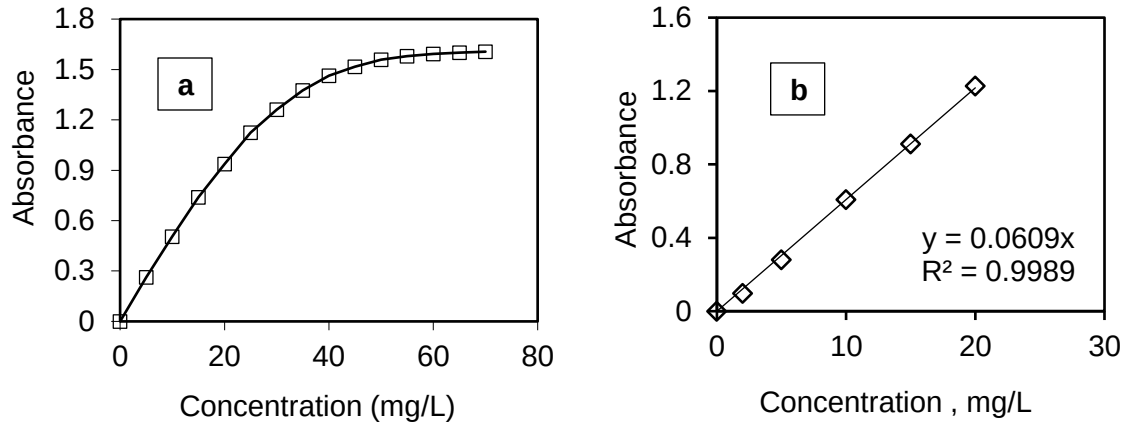

Figure A1.1: a) Effect of solution pH on the absorbance and b) Linear calibration curve of AO8 dye at 490 nm wavelength

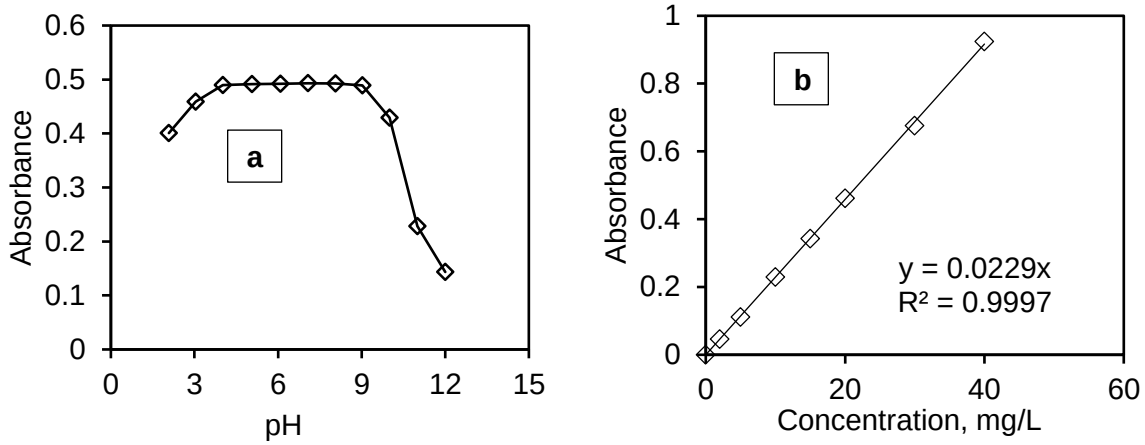

Figure A1.2: a) Effect of solution pH on the absorbance and b) Linear calibration curve of AV7 dye at 520 nm wavelength

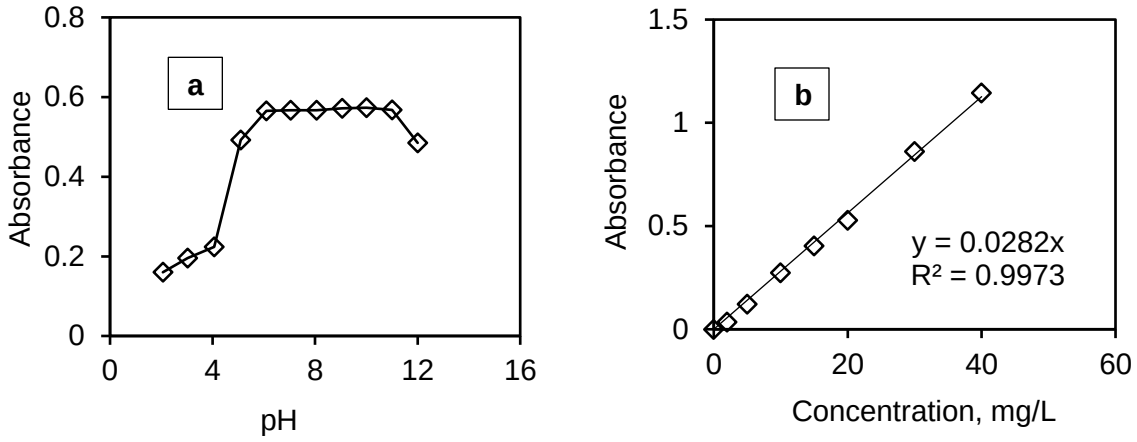

Figure A1.3: a) Effect of solution pH on the absorbance and b) Linear calibration curve of CR dye at 497 nm wavelength

APPENDIX 2

Table A2.1: Isotherm parameters of lead, copper and chromium adsorption onto modified-AFC (single system component)

Isotherm model	Formula	Parameters	Pb(II)	Cu(II)	Cr(III)
Halsay	$q_e = \mathrm{Exp}(\frac{\ln K_{HA} - \ln C_e}{n_{HA}})$	n_{HA}	-	-	-
		K_{HA} (meq./L)	-	-	-
		SSE	-	-	-
		RMSE	-	-	-
		R^2	-	-	-
Smith	$q_e = W_b - W\ln(1 - C_e)$	W	-	0.01	-0.448
		W_b	-	0.633	5.365
		SSE	-	0.044	0.0454
		RMSE	-	0.044	0.0454
		R^2	-	0.250	0.66
Koble	$q_e = \frac{A_{KC} C_e^P}{1 + B_{KC} C_e^P}$	A_{KC}(meq./g)(L/meq.)$^{-P}$	0.85	0.298	0.3
		B_{KC} (L/meq.)^P	0.12	0.199	0.1996
		P	1.2	0.563	0.5920
		SSE	0.16	0.026	0.0515
		RMSE	0.028	0.027	0.0522
		R^2	0.99	0.99	0.99
Hill	$q_e = \frac{Q_H C_e n_H}{KD + C_e n_H}$	Q_H	1.326	1.256	1.2819
		n_H	1.012	1.041	1.0271
		KD	1.393	1.472	1.4400
		SSE	5.44	5.420	5.3880
		RMSE	5.44	5.437	5.4289
		R^2	0.99	0.99	0.98
Sips	$q_e = \frac{Q_{max} b_S C_e^{1/n}}{(1 + K_S C_e^{1/n})}$	Q_S (meq./g)	1.0821	1.1162	6.3611
		K_s (L/meq.)	1.0807	1.1074	0.1687
		1/n	1.0366	1.0555	1.0224
		SSE	0.0005	0.003	0.0001
		RMSE	0.0006	0.002	0.0003
		R^2	0.99	0.99	0.99
Khan	$q_e = \frac{Q_{max} b_k C_e}{(1 + b_k C_e)^{a_k}}$	Q_K(meq./g)	0.0810	0.097	0.2591
		a_k	0.0100	13.624	14.8693
		b_k	8.3057	0.0100	3.1438
		SSE	0.0305	0.0453	0.071
		RMSE	0.0285	0.0423	0.067
		R^2	0.137	0.33	0.26
Toth	$q_e = \frac{Q_t K_t C_e}{(1 + (K_t C_e)^t)^{1/t}}$	Q_t (meq./g)	4.8191	7.6540	4.8915
		K_t	0.8652	52.2321	24.9201
		1/t	3.825	8.510	6.9204
		SSE	0.0294	0.0289	0.0393
		RMSE	0.0272	0.0268	0.0363
		R^2	0.23	0.53	0.56

Table A2.2: Isotherm parameters of lead, copper and chromium adsorption onto modified-AFC (multicomponent system)

Isotherm model	Parameters	Pb(II)+Cu(II)		Pb(II)+Cr(III)		Cu(II)+Cr(III)		Pb(II)+Cu(II)+Cr(III)		
		Pb(II)	Cu(II)	Pb(II)	Cr(IIII)	Cu(II)	Cr(III)	Pb(II)	Cu(II)	Cr(III)
Halsay	n_{HA}	-0.0589	-0.0294	0.1508	-0.1398	0.0695	0.0736	0.608	-0.136	-0.404
	K_{HA} (meq./L)	0.0752	0.0833	0.0381	0.2009	0.0549	0.0783	0.018	0.054	0.186
	SSE	0.0108	0.0110	0.0264	0.0130	0.0082	0.0054	0.001	0.007	0.033
	RMSE	0.0108	0.0110	0.0264	0.0130	0.0082	0.0054	0.001	0.007	0.0337
	R^2	0.89	0.85	0.27	-0.06	0.95	0.98	0.96	0.90	-0.05
Smith	W	12.947	18.1300	-0.5190	1.2823	-6.177	-7.688	-1.988	8.175	2.6501
	W_b	-0.7807	-1.3472	0.1126	-0.1341	0.5278	0.9210	0.308	-0.238	-0.089
	SSE	0.0174	0.0644	0.0018	0.0142	0.0559	0.1183	0.033	0.024	0.0375
	RMSE	0.0174	0.0644	0.0018	0.0142	0.0559	0.1183	0.033	0.024	0.0375
	R^2	0.73	-3.823	0.96	-0.2686	-1.230	-7.097	-12.00	0.008	-0.306
Koble	A_{KC}(meq./g) $(L/meq.)^{-P}$	0.2898	1.0321	1.0323	1.0323	1.0363	0.9917	1.031	1.029	1.0291
	B_{KC} $(L/meq.)^{P}$	0.1996	0.1534	0.1539	0.15390	0.1505	0.2001	0.154	0.158	0.1583
	P	0.5920	1.0074	1.0075	1.0075	1.0088	0.9886	1.007	1.006	1.0065
	SSE	0.0136	0.0000138	0.000017	0.000023	0.000017	0.0005	$1.4*10^{-05}$	$1.1*10^{-05}$	0.0001
	RMSE	0.0148	$4.7*10^{-05}$	$5.0*10^{-05}$	$4.3*10^{-05}$	$6.6*10^{-05}$	0.0008	$4.5*10^{-05}$	$3.5*10^{-05}$	0.0001
	R^2	0.99	0.99	0.99	0.99	0.99	0.99	0.99	0.99	0.99
Hill	Q_H	7.3383	7.3515	7.1585	7.2068	8.8594	8.8488	6.8368	1.2000	7.8024
	n_H	1.0078	1.0066	1.0069	1.0031	1.0066	1.0074	1.0271	0.9000	1.0072
	KD	7.5748	7.5607	7.3699	7.3189	9.1010	9.1122	6.6344	1.0000	8.0328
	SSE	5.4543	5.4601	5.4606	5.4803	5.4576	5.454	5.46328	5.4652	5.4511
	RMSE	5.4494	5.4509	5.4523	5.4570	5.4527	5.4522	5.45296	5.45227	5.4484
	R^2	0.99	0.99	0.99	0.99	0.99	0.99	0.99	0.85	0.99
Sips	Q_S (meq./g)	1.0821	6.7252	5.8537	5.8039	6.6225	6.6345	7.4209	4.8752	6.0916
	K_s (L/meq.)	1.0807	0.1535	0.1772	0.1757	0.1567	0.1569	0.1385	0.2131	0.1705
	1/n	1.0366	1.0075	1.0087	1.0040	1.0091	1.0102	1.0064	1.0088	1.0095
	SSE	0.0012	$1.4*10^{-05}$	$2.8*10^{-05}$	$4.3*10^{-06}$	$3.0*10^{-05}$	$2.0*10^{-05}$	$1.8*10^{-05}$	$1.9*10^{-05}$	$3.1*10^{-05}$
	RMSE	0.0011	$4.7*10^{-05}$	$5.8*10^{-05}$	$1.08*10^{-05}$	$6.9*10^{-05}$	$7.9*10^{-05}$	$4.09*10^{-05}$	$4.7*10^{-05}$	$6.6*10^{-05}$
	R^2	0.99	0.99	0.99	0.99	0.99	0.99	0.99	0.99	0.99
Khan	Q_K(meq./g)	0.1168	0.1350	0.0503	0.0503	6.4505	0.3101	0.0506	0.2666	0.8010
	a_k	13.163	8.0229	247.6698	247.6698	15.531	18.895	95.5180	6.9806	0.4240
	b_k	4.6516	2.9255	14.9693	14.9693	20.645	11.196	36.5730	3.1346	1.2560
	SSE	0.0345	0.0301	0.0236	0.0212	0.0088	0.0056	0.022604	0.0232	0.0342
	RMSE	0.0322	0.0281	0.0220	0.0198	0.0082	0.0052	0.021144	0.0217	0.0320
	R^2	0.086	0.085	0.49	-1.439	0.95	0.98	0.47	0.2197	0.0603
Toth	Q_t (meq./g)	5.0263	0.5761	4.6892	3.8666	0.0198	0.0209	5.3410	2.4340	2.5000
	K_t	0.9024	0.4965	0.8418	0.6942	32778	317496	0.9589	0.2527	0.2527
	1/t	0.2835	5.6017	0.2597	0.2089	2.3601	1.8551	0.3213	2.8468	3.5000
	SSE	0.0179	0.0151	0.0207	0.0086	0.0205	0.0214	0.0195	0.0117	0.02375
	RMSE	0.0827	0.0140	0.0192	0.0080	0.0190	0.0198	0.0181	0.0108	0.02199
	R^2	0.49	0.52	0.25	0.35	0.40	0.43	0.20	0.61	0.24

List of publications:

1. Praisy Terangpi and Saswati Chakraborty. **"Adsorption kinetics and equilibrium studies for removal of acid azo dyes by aniline formaldehyde condensate"**. *Applied Water Science*, 7(2017), 3661-3671. (Published) [Chapter 2].
2. Praisy Terangpi, Saswati Chakraborty and Manabendra Ray. **"Improved removal of hexavalent chromium from 10 mg/L solution by micron sized polymer clusters of aniline formaldehyde condensate"**. *Chemical Engineering Journal*, 350 (2018), 599–607. (Published) [Chapter 4].

Conference attended

1. **Praisy Terangpi**, Saswati Chakraborty and Manabendra Ray (2012). "Application of amine based polymers in wastewater treatment". Poster presentation at One day Symposium on "Environment and Us" held in Centre for the Environment, Indian Institute of Technology Guwahati, Guwahati, during 5th June 2012.
2. **Praisy Terangpi**, Saswati Chakraborty and Manabendra Ray (2014). "Removal of Acid violet 7 using amine based polymer adsorbent". Poster presentation at First symposium on advances in sustainable polymers (ASP-14) held in Department of Chemical Engineering at Indian Institute of Technology Guwahati, Guwahati, during 10-11st January 2014.
3. **Praisy Terangpi**, Saswati Chakraborty and Manabendra Ray (2014). "A review on the removal of heavy metals and anionic azo dyes using amine based polymer adsorbent". Poster presentation at International conference on Harnessing Natural Resources for Sustainable Development: Global Trends, held at Cotton College, Guwahati, during 29-31st January 2014.
4. **Praisy Terangpi**, Saswati Chakraborty and Manabendra Ray (2014) "A study on the removal of anionic azo dyes using amine based polymer". Oral presentation at National conference on Sustainable Development of Environmental Systems held in Centre for the Environment, Indian Institute of Technology Guwahati, Guwahati, during 20-21st June 2014.
5. **Praisy Terangpi,** Saswati Chakraborty and Manabendra Ray (2015). Presented a poster titled "Removal of acid orange 8 dye using aniline formaldehyde condensate (AFC) polymer as an adsorbent" at National conference on challenges in Environmental Research

at Center for the Environment, Indian Institute of Technology Guwahati, Guwahati held from 4-6th June 2015.

6. **Praisy Terangpi**, Saswati Chakraborty and Manabendra Ray (2016). "Removal of Acid violet 7 using polymer coated adsorbent". Oral presentation at National conference on research advancements in environmental research held on June 4-5th, 2016 by Centre for the Environment, Indian Institute of Technology Guwahati, Guwahati.